Ocean Engineering & Oceanography 2

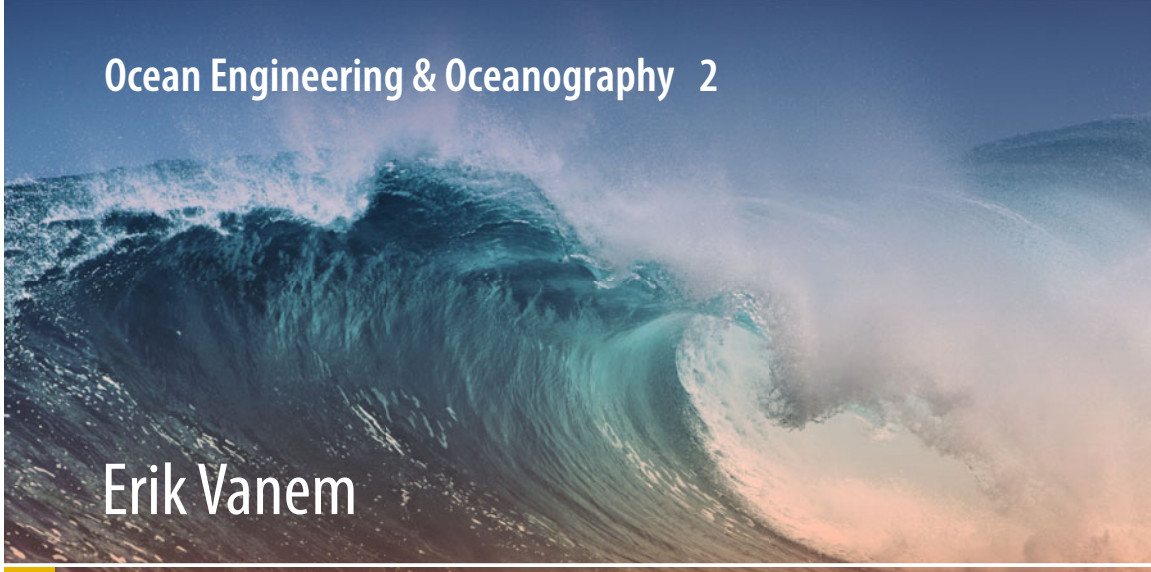

Erik Vanem

Bayesian Hierarchical Space–Time Models with Application to Significant Wave Height

Springer

Ocean Engineering & Oceanography

Volume 2

For further volumes:
http://www.springer.com/series/10524

Erik Vanem

Bayesian Hierarchical Space–Time Models with Application to Significant Wave Height

Springer

Author
Erik Vanem
Department of Mathematics
University of Oslo
Oslo
Norway

Foreword by
Elzbieta Maria Bitner-Gregersen
Det Norske Veritas
Høvik
Norway

Christopher K. Wikle
Department of Statistics
University of Missouri
Columbia, MO
USA

ISSN 2194-6396 ISSN 2194-640X (electronic)
ISBN 978-3-642-30252-7 ISBN 978-3-642-30253-4 (eBook)
DOI 10.1007/978-3-642-30253-4
Springer Heidelberg New York Dordrecht London

Library of Congress Control Number: 2013941499

Mathematics Subject Classification (2010): 62P12, 60K40, 86A32, 60H30, 60G15

Printed on acid-free paper

Springer is part of Springer Science+Business Media (www.springer.com)

Foreword

Marine safety is one of the main concerns of shipping and offshore industry in general and classification societies as well as oil companies in particular. The importance of including the state-of-the-art knowledge about meteorological (temperature, pressure, wind) and oceanographic (waves, current) conditions in ship and offshore standards have been discussed increasingly by industry and academia in the last decades in several international forums. There are potential safety, economic, and environmental advantages in utilizing the recent knowledge about meteorological and oceanographic (met-ocean) conditions and investigating its implication for design and operation of marine structures.

The ongoing debate around the observed and projected climate change has confronted the shipping and offshore industry with two important questions: is it likely that marine structures will experience higher environmental loads; will Classification Societies' Rules and Offshore Standards need to be updated? Although the climate system is very complex and its mechanism is still not fully understood, observed, and projected climate changes indicate that changes in met-ocean conditions can be expected which have impact on marine structure design.

Observed and projected changes in wave and wind climate are expected to have the largest impact on marine structure design in comparison to other environmental phenomena. Changes in sea level combined with storm surge have little potential to affect ship design directly but may impact offshore and coastal installations, depending on how significant they are. Secondary effects, such as changes in sea level range, harbor depths and offloading heights may need to be taken into account in future design of marine structures. The predicted increase in marine growth may increase loads on marine structures in some ocean regions, e.g., the Baltic Sea.

To be able to design for climate change, time-dependent statistical descriptions need to be adopted. Statistical extreme value analysis, as currently used in the met-ocean community, has to be upgraded to take into account the nonstationary character of current climate, in terms of both climate change trends and natural variability cycles. These changes need to be incorporated in the risk-based approach used currently in design.

The adaptation process to climate change has already been initiated by the shipping and offshore industry. It includes studies investigating potential impact of

climate change on design of marine structures. The Bayesian hierarchical models in space and time provide very valuable contribution to the adaptation process. They allow predicting climate changes in met-ocean conditions based on historical data while avoiding running climate models. The input from the models can be easily in-cooperated in joint met-ocean description used currently in design.

Jar, March 2012 Elzbieta Maria Bitner-Gregersen

Foreword

Spatio-temporal processes are ubiquitous in the environment. These processes are complex, with multiple scales of spatial and temporal variability and internal excitations that vary considerably depending on the type of forcing applied to the system. The interaction of these processes (e.g., the wind driven forcing of the ocean circulation) can lead to interesting behavior that is typically scale dependent. Although we know that there is inherent complex variability and interaction of the system components, there is substantial uncertainty associated with our detailed understanding of these processes (particularly the interactions between processes and across scales) as well as the data that are collected on the system. Often there is a tradeoff between high resolution, yet incomplete observations over the spatial domain (such as from satellite observation platforms) and fairly high resolution in time, yet sparse in space in situ observations (such as from buoys or ships). In both cases, the actual data collected may just be a proxy for the state variables of actual interest. In addition, the level of resolution associated with these observations in time and space may not agree with the level of resolution for which we want to gain understanding. Thus, it is fair to say that environmental systems are complex and our understanding of the processes and data that make up the systems is, to various degrees, uncertain.

Starting in the mid-1990s, statisticians began to consider a coherent paradigm to partition both variability and uncertainty into a series of models that are formally linked through fundamental rules of probability. The first stage of this hierarchical modeling framework allows one to consider the observations conditioned on the true process of interest and parameters that control the distributional difference between the observations and process. This so-called data model distribution is then multiplied by a distribution describing the true process itself, conditioned on parameters (i.e., the process model). Finally, and in many ways most critically, one specifies distributions for the parameters that were conditioned upon in the previous stages (i.e., the parameter models). Such a simple framework leads to a powerful modeling paradigm because it allows the scientist and statistician to consider separately the effect of observation uncertainty, process uncertainty, and parameter uncertainty. Yet, the true complexity of the system comes through when one integrates over the effects of the parameter and process variability. This complexity is almost impossible to specify directly in classical likelihood-based

models for complex multivariate spatio-temporal environmental processes with multiple sources of information.

Although the hierarchical framework is conceptually quite simple, the individual component models can themselves be quite complicated, accounting for spatio-temporal variability and uncertainty at each stage (data, process, and parameter). The issue then becomes how to do inference and prediction in this framework. Such analysis would not have been possible on high-dimensional complex environmental systems before the early 1990s, when it was realized that Markov Chain Monte Carlo (MCMC) methods, which had been developed much earlier in statistical physics, could be used in the context of Bayesian inference to deal with the very high-dimensional integrals that make up the normalizing constant in Bayes rule. Indeed, the key to this was that one needs not have to work out those integrals analytically, nor even with standard numerical integration, but rather could use an iterative method that generated dependent samples from the posterior distribution of interest without having to actually calculate the normalizing constant. This methodology revolutionized Bayesian statistics and made the large-scale application of the hierarchical modeling paradigm practical for very complex problems. Early applications of this approach to environmental problems associated with the atmosphere and ocean were very successful.

This monograph provides a wonderful example of how these methods can be applied to an extremely complicated problem of great practical importance. Without a doubt, this is the most complete statistical modeling study that has been done on wave height, and illustrates very clearly how scientific and empirical knowledge can be used to partition uncertainty and variability across the data, process, and parameter models that describe the system. The manuscript also provides fundamental and essential background material related to the statistical methods as well as the science governing the problem. As such, this monograph provides a complete and thorough reference to the analysis of wave height data, but perhaps more critically, a framework for researchers to analyze other complex environmental processes. In a world where there is increasing interest in the economic and social costs associated with the climate-induced changes to environmental processes, this monograph serves as a shining example of how one can approach such problems in a unified way while accommodating realistic sources of uncertainty.

Columbia, Missouri, USA, March 2013 Christopher K. Wikle

Preface

Within the history of shipping, there are numerous examples of ships that have been lost at sea as a consequence of bad weather, but also in cases where bad weather is not the main cause of accident, severe weather impedes rescue operations and leads to escalation of events. Tragic accidents such as the sinking of the passenger ship Estonia in 1994 and the breaking up of the oil tanker Erika in 1999 easily comes to mind. Both these maritime disasters occurred in rough weather and resulted in severe consequences in terms of human fatalities or environmental damage; 852 lives were lost in the Estonia accident and thousands of tons of oil were released into the sea in the Erika accident, killing marine life, polluting nearby shores, and making it one of the greatest environmental disasters to ever hit France. Furthermore, several thousand containers are lost at sea each and every year during maritime transportation and rough seas are often to blame.

These are merely examples of how heavy weather may contribute to maritime accidents but there are numerous others with catastrophic consequences in terms of lives lost, severe environmental damage and property loss; they serve to illustrate the influence of the ocean wave climate on maritime safety. Obviously, a roughening of the ocean wave climate also has the potential to severely impact other areas of society as well, related to maritime, offshore, and coastal activities. Combined with sea level rise and other possible effects of climate change, coastal areas throughout the globe may be seriously affected.

Ships and other marine structures are constantly exposed to the wave and wind forces of its environment, and extreme ocean climate represents a great risk to marine operations, as illustrated by the examples above. According to maritime casualty statistics, bad weather is a major cause of ship accidents, and this stresses the importance of taking extreme sea state conditions adequately into account in ship design. This is important to ensure that the ships can withstand the environmental forces they are expected to encounter throughout their lifetime. Hence, a correct and thorough understanding of meteorological and oceanographic conditions, most notably the extreme values of relevant wave and wind parameters, such as the significant wave height (H_s) is of paramount importance to maritime safety, and there is a need for appropriate statistical models to describe the variability of these phenomena.

With the climate change that the globe is currently experiencing the future ocean wave climate may change and it may no longer be sufficient to base design codes and safety standards on current knowledge about the past and present ocean environment. The implicit assumption that the future will be like the past may no longer be even approximately valid and there is a need to consider how wave parameters are expected to change in the future, as a consequence of climate change. Thus, there is a need for time-dependent statistical models that can take the long-term time-dependency of integrated wave parameters properly into account. Furthermore, there is a need for methods to take potential impacts of such long-term trends on the environmental loads of ships and other marine structures into account.

The models presented in this monograph are stochastic models, probabilistic counterparts to physical models that are more deterministic, with treatment of uncertainties as an integral part of the models. In a historic perspective, it is noted that for a long time following the scientific revolution in the sixteenth century, the predominant world-view was deterministic. It was believed that if exact knowledge of initial conditions and causal laws governing a system were available, the exact state of the system could be determined at any later point in time. In such a mechanistic world, randomness would not exist and failure to precisely predict future events would be entirely due to incomplete knowledge of initial states and universal laws. However, in the late nineteenth and early twentieth century, new scientific discoveries cast serious doubts on a strictly deterministic world-view. Chaos theory explained how even an infinitesimally small perturbation of initial conditions of a purely deterministic non-linear system can lead to large changes in the development of the system (the butterfly effect). Furthermore, the development of quantum mechanics and the formulation of the Heisenberg uncertainty principle demonstrated that reality, at least at atomic scales, does not seem to be absolutely deterministic, suggesting a more probabilistic understanding of the world.

Regardless of whether the world is fundamentally probabilistic or if it is deterministic but with uncertain knowledge of the underlying physical laws, physical environmental processes inevitably display some seemingly causal relationships along with a considerable degree of randomness. Hence, it is argued that it would make sense to describe such phenomena probabilistically, i.e., using probability theory and statistics to model physical processes as stochastic processes, where there are several possible ways for a system to evolve. Notwithstanding, the probabilistic modeling approach presented in this monograph is presented as a complementary alternative to more geophysics-based deterministic wave and climate models. Physical models remain the primary approach for investigating the impacts of climate change, but it is believed that the results obtained from probabilistic models can be used to complement such models and yield increased insight into these complicated processes.

One of the more practical advantages of using a stochastic model is that estimates of the uncertainties are given explicitly. These are important when future projections are to be incorporated in risk analyses or utilized in probabilistic load calculations as illustrated by an example herein. The case study reveals that the effect of the predicted trend in the ocean wave climate on environmental loads of ships are far from being negligible, and that this may need to be taken into account in design and construction of ships.

This monograph presents recent research on the statistical modeling of ocean wave climate in space and time, with a particular interest in the modeling of long-term trends, possibly as a result of climate change. The research was mainly carried out at the Statistics Department at the Mathematical Institute of University of Oslo, Norway as a part of my Ph.D. thesis in statistics [2]. The material presented in this monograph summarizes and is to a large degree based on seven recent publications in various academic journals. The literature survey presented in Chap. 2 was first published in [1]. Chapter 3 which outlines the main Bayesian hierarchical space–time model for H_s is based on the paper published in [5], but contains some additional results pertaining to monthly maximum data, previously presented at the Geostat 2012 conference [7]. The work on including a logarithmic transform of the data was originally published in [6], but again Chap. 4 is extended with results for monthly maximum data [7]. Chapter 5, which extends the base model with a CO_2-regression component is based on [8] and Chap. 7 concerning the potential impact on ship's environmental loads and structural responses is an extension of [3], where also the trends estimated from the models with CO_2-regression are considered. Finally, the case study in Chap. 8 where the model is applied to different ocean areas worldwide, is based on [9]. An additional chapter, Chap. 6 which is based on [4], is included where the modeling framework is applied to oceanic surface wind speeds over the same area.

Some appendices are included at the end of this book, where some important concepts and general results that have been utilized in the research are briefly outlined. Appendix A contains a brief introduction of Markov chain Monte Carlo (MCMC) methods, which has been used in the implementation of the model. In particular, the main ideas behind the Gibbs sampler and the Metropolis–Hastings algorithm are described. Appendix B introduces some of the most common methods of modeling extreme values, i.e., the block maxima approach and the peaks over threshold approach, and some basic results pertaining to Markov Random Fields are briefly introduced in appendix C. In appendix D, the derivation of the full conditionals of the Bayesian hierarchical space–time model is presented, which have been used in the MCMC simulations. Finally, appendix E presents a straightforward method for obtaining samples from an arbitrary multi-normal distribution based on independent samples of the univariate standard normal distribution which has been exploited in the simulations of the model.

It is believed that this research monograph should be of interest to anyone with an interest in stochastic modeling in general and to those with a special interest in environmental research and effects of climate change in particular. Furthermore, the research has practical applications related to ocean and coastal engineering and should be of interest to various stakeholders within the maritime industries such as designers, classification societies, ship owners and operators, flag states, and intergovernmental agencies such as the IMO. The intended audience for this publication includes, but is not limited to, statisticians, environmental researchers, climate researchers, ocean and coastal engineers, naval architects, oceanographers, meteorologists, maritime policy makers, and risk analysts.

References

1. Vanem, E.: Long-term time-dependent stochastic modelling of extreme waves. Stoch. Environ. Res. Risk Assess. **25**, 185–209 (2011)
2. Vanem, E.: Bayesian hierarchical space–time models for significant wave height data. Ph.D. dissertation, University of Oslo (2012)
3. Vanem, E., Bitner-Gregersen, E.: Stochastic modelling of long-term trends in the wave climate and its potential impact on ship structural loads. Appl. Ocean Res. **37**, 235–248 (2012)
4. Vanem, E., Breivik, O.N.: Bayesian hierarchical modelling of North Atlantic windiness. Nat. Hazards Earth Syst. Sci. **13**, 545–557 (2013)
5. Vanem, E., Huseby, A.B., Natvig, B.: A bayesian hierarchical spatio-temporal model for significant wave height in the North Atlantic. Stoch. Environ. Res. Risk Assess. **26**, 609–632 (2012)
6. Vanem, E., Huseby, A.B., Natvig, B.: Modeling ocean wave climate with a Bayesian hierarchical space–time model and a log-transform of the data. Ocean Dyn. **62**, 355–375 (2012)
7. Vanem, E., Huseby, A.B., Natvig, B.: A stochastic model in space and time for monthly maximum significant wave height. In: Abrahamsen, P., Haugen, R., Kolbjørnsen, O. (eds.) Geostatistics, pp. 505–517 Springer, Oslo (2012)
8. Vanem, E., Huseby, A.B., Natvig, B.: Bayesian hierarchical spatio-temporal modelling of trends and future projections in the ocean wave climate with a CO_2 regression component. Environmental and Ecological Statistics (2013, in press)
9. Vanem, E., Natvig, B., Huseby, A.B.: Modelling the effect of climate change on the wave climate of the world's oceans. Ocean Sci. J. **47**, 123–145 (2012)

Acknowledgments

The author wishes to acknowledge the valuable support and contributions to the work presented in this monograph from Prof. Bent Natvig, University of Oslo, Prof. Arne Bang Huseby, University of Oslo and Dr. Elzbieta Maria Bitner-Gregersen, Det Norske Veritas. They have all been very supportive of me and my research project and have always been available for fruitful discussions and help whenever called upon. Bent has been an extremely patient discussion partner, sharing his knowledge and long experience in Bayesian hierarchical modeling which has been greatly appreciated, and a very dedicated proofreader of my work. Arne has been of great help, especially in getting started with the implementation of the MCMC simulations in Java. Elzbieta has shared her great knowledge of met-ocean modeling and its applications related to ship structures. In particular, she contributed to this monograph with the loads and structural calculations in Chap. 7. The work presented herein could not have been possible without the help and support from these mentors. Thanks also to Ph.D. student Olav Nikolai Breivik for carrying out the simulations on wind data reported in Chap. 6.

The author further wants to express his thanks to Dr. Andreas Sterl at KNMI for kindly providing the significant wave height data used in this analysis and for clarifying some issues discovered when investigating the data. Thanks also to Dr. Pieter Tans for kind permission to use the NOAA ESRL CO_2-data. The data on future projections of atmospheric concentration of CO_2 were obtained from the IPCC and the $ERA_{Interim}$ data was provided by the Norwegian Meteorological Institute.

Oslo, Norway, February 2013 Erik Vanem

Contents

Acronyms

AIC	Akaike Information Criterion
BIC	Bayesian Information Criterion
BME	Bayesian Maximum Entropy
BVN	BiVariate Normal distribution
C-ERA-40	Corrected dataset of significant wave height from the ERA-40 project
CMA	Conditional Modeling Approach
DIC	Deviance Information Criterion
DLM	Dynamic Linear Models
DNV	Det Norske Veritas
ECMWF	European Centre for Medium-Range Weather Forecasts
ECP	Extended Concentration Pathway
EM	Expectation Maximization
EP	Equatorial Pacific
ERA	ECMWF Reanalysis
ERA-40	ECMWF 40 Year Reanalysis
ERS	European Remote Sensing
ESRL	Earth System Research Laboratory
FORM	First-Order Reliability Method
FVN	Four-Variate Normal distribution
GDP	Gross Domestic Product
GEV	Generalized Extreme Value
GHG	Green House Gases
GoM	Gulf of Mexico
GPD	Generalized Pareto Distribution
$H_{1/3}$	Significant Wave Height
H_s	Significant Wave Height
IFORM	Inverse First-Order Reliability Method
IG	Inverse Gamma distribution
IID	Independent and Identically Distributed
INLA	Integrated Nested Laplace Approximations
IO	Indian Ocean
IPCC	Intergovernmental Panel of Climate Change
ISAM	Integrated Science Assessment Model

KNMI	Royal Netherlands Meteorological Institute
LMC	Linear Models of Coregionalization
MA	Mid Atlantic
MCMC	Markov Chain Monte Carlo
MENU	MEan Number of Up-crossings
MLE	Maximum Likelihood Estimation
MLM	Maximum Likelihood Model
MPa	Mega Pascal
MRF	Markov Random Field
MS	Mediterranean Sea
MVN	MultiVariate Normal distribution
N	Normal distribution
NA	North Atlantic
NAO	North Atlantic Oscillation
NCAR	National Center for Atmospheric Research
NCEP	National Centers for Environmental Prediction
NEP	North East Pacific
NOAA	National Oceanic and Atmospheric Administration
NPP	Nonhomogeneous Poisson Process
NS-GEV	Nonstationary Generalized Extreme Value
NWP	North West Pacific
PDF	Probability Density Function
PM	Particulate Matter
POT	Peaks Over Threshold
PPM	Parts Per Million
PWM	Probability Weighted Moments
QMLE	Quasi Maximum Likelihood Estimator
RCP	Representative Concentration Pathway
SD	Standard Deviation
SORM	Second-Order Reliability Method
SP	South Pacific
SWH	Significant Wave Height
SWH_x	x-year Significant Wave Height
T_r	Response period
T_z	Zero up-crossing period
TS	Tasmanian Sea
VOS	Voluntary Observing Ship
WAfr	West Africa
WAust	Western Australia
WAM	WAve prediction Model
WASS	Wave Acquisition Stereo System

Chapter 1
Introduction and Background

This book is concerned with stochastic models in space and time for describing the variability and possible long-term trends in the ocean wave climate. Such stochastic models constitute an alternative to more physics-based climate and wave models for describing the statistics of the sea surface and for projecting future ocean wave climate. The ocean wave climate has important implications on maritime, offshore, and coastal activities. In particular, the wave climate is important to marine safety and this is the main motivation for this research.

The research presented in this monograph could to some extent be regarded as interdisciplinary and it can be related to different scientific traditions and communities. It is a contribution to the important ongoing debate about climate change, perhaps one of the most crucial research areas of our times and also a major political, economic, and moral question for our generation. Furthermore, it is intimately related to current research areas within physical oceanography, meteorology, marine engineering, and risk assessment. Nevertheless, this monograph has its main foundation in the statistical research tradition and is first and foremost a book in applied statistics and stochastic modeling. Therefore, the presentation in this monograph aims at communicating the research to a mixed audience with different backgrounds, and it is believed that readers of different backgrounds might find it comprehensible and of interest.

In the following, a brief introduction to the sciences of climate change, ocean waves, and maritime safety as well as statistical modeling of environmental processes will be given. In this way it is believed that the most important contexts within the main research traditions the material presented in this book is related to will be made clear.

The main research question that this monograph tries to address can be formulated as follows: "To what extent will the ocean wave climate be expected to change in the future as a result of climate change, what are the uncertainties and how may this affect the structural safety of ocean-going ships?" More specifically, the task of establishing long-term, time-dependent statistical models for significant wave height was identified as a possible approach to address this question.

E. Vanem, *Bayesian Hierarchical Space-Time Models with Application to Significant Wave Height*, Ocean Engineering & Oceanography 2,
DOI: 10.1007/978-3-642-30253-4_1, © Springer-Verlag Berlin Heidelberg 2013

The high-level problem description was proposed by Det Norske Veritas (DNV), a classification society genuinely concerned with the safety at sea and responsible for developing class rules and standards for ships and offshore structures. Hence, the research presented in this book addresses a real-life problem of genuine interest to the stakeholders within the maritime and offshore industries and DNV has been involved as an industrial partner in the research project. Indeed, a recent report on the effect of climate change on marine structural design identified the need for an improved methodology for time-dependent statistics and modeling of the long-term variations in wave parameters due to climate change [3]. Hence, the development of such models in both space and time is interesting from an academic point of view, but is also a response to genuine needs within the industry with real and practical applications [4]. Hence, the research presented in this monograph is essentially applied research more than fundamental theoretical research.

1.1 Climate Change

This section will give a very brief introduction to the science of climate change. There are numerous information sources for more details and an excellent introduction to the science of modern climate change can be found in e.g. the recent textbook by Dessler [9].

1.1.1 Weather and Climate

Before discussing climate change, it is important to have a clear understanding of what is meant by *climate*, as opposed to *weather*. Whereas weather usually refers to the actual state of the weather system and the atmosphere, climate is used for a long-term statistical description of weather over time. Typically, climate can be thought of as average weather as well as the variability of weather and contains information of the likely range of conditions at a particular location and time. One way to look at it is to consider the climate to be the distribution of weather at a particular time and location and the actual weather as one realization from that distribution. However, there is natural climate variability at different timescales such as daily, seasonal, decadal, and centurial variations. Short term variations are obvious: night is different from day and the winter climate is different from the summer climate, but there is considerably more uncertainty associated with the natural long-term variability of the climate and its causes.

It is important to distinguish between natural climate change and anthropogenic—or man-made—climate change. Over the ages, the climate has experienced dramatic changes at various time scales, with oscillations between cold periods of planetary glaciation and warmer interglacial periods. Such changes have occurred throughout the history of the planet with ice ages typically lasting about 100,000 years and the

interglacial periods typically lasting 10,000–30,000 years. By anthropogenic climate change, on the other hand, is meant the currently experienced climate change that can be ascribed to human activities and in particular to human emissions of greenhouse gases and aerosols. One crucial difference between natural and anthropogenic climate change is that the latter occurs much faster, making it difficult for the species, including humans, and entire ecosystems to adapt.

1.1.2 A Brief History of Climatic Research

There is a long scientific tradition for studying the climate and climate change; climate change has been scientifically studied since the early nineteenth century. The discovery of the natural greenhouse effect is often ascribed to the French scientist Joseph Fourier who published papers on the terrestrial temperatures in the 1820s. He basically suggested that a planet's atmosphere is able to trap heat and increase the temperature of the surface of the planet. This idea was further strengthened in the 1830s by the works of Claude Pouillet and later in the 1850s by the works of John Tyndall. At about the same time, in the 1830s, evidence of a widespread ice age in northern Europe was first recognized by geologist Louis Agassiz among others, indicating that the climate could change: the climate had evidently changed in the past, suggesting that it could certainly change again in the future. Prior to this discovery it was commonly assumed that the climate was unchanging and was as it had always been, but this discovery was an important motivation for the further scientific study of climate over the next decades.

Towards the end of the nineteenth century it was first argued that human emissions of greenhouse gases could change the climate of the planet. In 1896, Swedish scientist Svante Arrhenius tried to calculate how changes in atmospheric levels of CO_2 could change the surface temperature of the earth in a theory to explain the ice ages [1]. Although not explicitly referring to burning of fossil fuel, his works mark the beginning of the theory of man-induced climatic change. During the first decades of the twentieth century the temperature was rising and by the 1930s it was apparent that the planet was warming. In 1938, Guy Steward Callendar suggested that this warming was a result of human emissions of CO_2 [5]. From 1957 to 1958 the International Geophysical Year, an international scientific project for coordinating observations of the earth from pole to pole in order to make progress in the understanding of fundamental geophysical processes governing the environment, greatly improved the understanding of the earth. This initiative also started measurements of atmospheric carbon dioxide, and the continuous record of atmospheric CO_2 measurements utilized in this book was actually initiated in March 1958 with equipment for remote observatories acquired with funding from international geophysical year grants.

Over the twentieth century, scientists became increasingly convinced that greenhouse gases were influential in most climate changes and that human emissions were contributing seriously to global warming. Currently, the authoritative scientific

view on climate change is the one held by the Intergovernmental Panel on Climate Change (IPCC),[1] which was established in 1988 by the United Nations Environmental Programme (UNEP) and the World Meteorological Organization (WMO). This is a scientific body that reviews and assesses the most recent scientific information about climate change and thousands of scientists from all over the world contribute on a voluntary basis. Hence, reports from the IPCC can be construed as the most balanced and accurate scientific knowledge on climate change, see e.g., [15–17].

Regularly, the IPCC prepares assessment reports on the science of climate change. The first assessment report was released in 1990 and this suggested that the size of the observed global warming was consistent with predictions from climate models, but also that the changes were within the range of natural variability [13]. Hence, by 1990 the scientific community could not confidently establish whether the observed warming was due to natural or anthropogenic causes. However, the second assessment report which was released in 1996 [14] stated that the balance of evidence now suggested that there was a discernible human influence on the global climate and that most of the recent studies showed that the observed warming trend was unlikely to be entirely natural in origin. The third assessment report released in 2001 went further and concluded that there was now new and stronger evidence that most of the warming observed over the last 50 years is likely attributable to human activities [15], where likely refers to a chance of 2 out of 3. So far the fourth assessment report from 2007 is the most recent, and this concludes that most of the observed increase in globally averaged temperatures since the mid-twentieth century is very likely due to observed increase in anthropogenic greenhouse gas emissions [16], where now very likely should be construed to mean with a probability of 90 % of being true. Since the last assessment report, there has also been released a special report with focus on extreme events and climate change adaptation [17].

Hence, although the current climate change must obviously be a combination of natural and anthropogenic climate change, the current debate on climate change is mostly concerned with anthropogenic climate change, and often *climate change* in the media and the literature should be construed as anthropogenic climate change. The introduction to modern climate change, found in the book by Dessler [9] is completely in line with the view of the IPCC.

The physical mechanisms behind climate change are today well understood for the most part, and there is no longer any notable disagreement in the scientific community of whether the climate is currently warming; the IPCC states that the current warming of the climate system is unequivocal. Furthermore, there is little uncertainty to the fact that human activities are responsible for a significant part of the currently observed climate change; IPCC concludes that most of the observed increase in global average temperatures since the mid-twentieth century is very likely[2] due to the observed increase in anthropogenic greenhouse gas concentrations [16]. Hence, some of the currently most important questions in the climate change debate are to what extent the climate will continue to change in the future (not *if* it will change), what can be

[1] website: http://www.ipcc.ch/

[2] The words *very likely* are defined to mean *with a 90 % probability of being true*.

done to mitigate future climate change, what will be the impacts of climate change, and how can we adopt to a changing climate. It is basically one aspect of the two latter of these questions that is addressed in this book. More specifically, the potential impact of climate change on the ocean wave climate is investigated, and consequently the impact of changes in the ocean wave climate on the structural safety of ocean going ships. One way of adapting to this particular aspect of climate change could then be to take such potential impacts into account in structural ship design.

1.1.3 The Physical Mechanisms of Anthropogenic Global Warming

The physical mechanisms responsible for anthropogenic global warming are often referred to as the *greenhouse effect*. As was outlined above, this effect has been known for a long time and the overall mechanisms are fairly well understood. In short, it relates the temperature of the surface of the earth, or indeed of any planet, to the extent and composition of the atmosphere. In this section, a very short qualitative description of the greenhouse effect will be given.

The ultimate source of energy for our planet is the sun with energy input in the form of solar radiation. In order to explain the temperature of the planet, one can set up an energy or heat budget taking energy coming in to and going out from the planet into account. In a simple model, incoming energy is the solar radiation that is absorbed and outgoing energy are black-body radiation from the planet back into space. For the black-body radiation, it is known that both the wave length and the total emitted power of the radiation depend on the temperature of the object, with warmer objects emitting at shorter wave lengths (higher frequencies) and more power than cooler objects. Hence, the difference in the radiation from the sun and the earth is important for explaining the greenhouse effect. The temperature of the sun is about 6000 K and this means that most of the energy of the emitted radiation is within the visible range (0.39–0.75 μm), whereas most of the radiation from the earth is above 3 μm, in the infrared part of the spectrum (0.75–300 μm). A simple energy budget for the earth without any atmosphere shows that energy balance is achieved with much lower temperatures than what is observed on the planet, and the atmosphere is needed to explain why the temperature is not much lower.

The atmosphere is transparent to the visible photons emitted by the sun so most of these reach the surface of the earth. However, the atmosphere is opaque to infra-red photons emitted by the surface of the earth so that these are absorbed by the atmosphere, increasing the energy and thereby the temperature of the atmosphere. The atmosphere also behaves as a black body and will emit energy by way of photons based on its temperature. About half of this energy is emitted in the upward direction and this energy escapes the earth into space but the other half is emitted towards the surface where it will be absorbed and increase the temperature. This is a what is referred to as the greenhouse effect, which is very important for life to exist on earth.

It turns out, however, that only a few components of the atmosphere actually absorb infra-red radiation and these are the gases referred to as *greenhouse gases* (GHG).

The other constituents do not contribute to warm the planet. The most abundant and most important greenhouse gas in the atmosphere is water vapour, mainly coming from evaporation from the oceans. The second most important greenhouse gas is carbon dioxide (CO_2), although just making up about 390 ppm[3] (or 0.039 %) of the atmosphere. Other important greenhouse gases are methane (CH_4) at about 1.8 ppm, nitrous oxide (N_2O) at about 0.3 ppm, various halocarbons at concentration of a few parts per billion (ppb) and ozone (O_3) with concentrations varying between 10 ppb and 10 ppm. *Aerosols* are small particles in the atmosphere that can interact with both incoming and outgoing radiation. Hence, the net effect of aerosols is opposite that of greenhouse gases, with a negative net *radiative forcings* from aerosols. Radiative forcing is often referred to as the change in the difference between energy input and output, $\Delta(E_{\text{in}} - E_{\text{out}})$ to and from the earth, and positive radiative forcings correspond to changes that warm the climate.

Increasing the abundance of greenhouse gases in the atmosphere does not change the energy input from solar radiation since this is not absorbed in the atmosphere, but will decrease the net energy being carried away as black body radiation and will consequently represent a positive radiative forcing. There are many aspects of the changes in atmospheric concentration of greenhouse gases that will be omitted here, such as the carbon cycle and how carbon is exchanged between the atmosphere and the land biosphere, oceans and rock, various feedback mechanisms and climate sensibility. Reference is made to e.g., [9] for a comprehensible overview, and it is simply stated that human activities related to burning of fossil fuels release greenhouse gases into the atmosphere, which have resulted in unprecedented concentrations and have consequently contributed to warm the planet due to the mechanisms of the greenhouse effect as briefly outlined above. The extent of future climate change is thus dependent on future emissions of greenhouse gases, and this is explored in different emission scenarios.

1.1.4 Emission Scenarios

Some of the factors influencing the climate of the planet are the solar radiation from the sun, the earth's orbit around the sun and the obliquity of the earth, the planetary albedo, internal variability, and the level of greenhouse gases in the atmosphere. It is the latter that is influenced by human emissions, and future projections of climate change are based on various emission scenarios.

It is generally acknowledged that the emission of greenhouse gas from a society is proportional to the gross domestic product, GDP. This can again be broken down to the product of the following four factors: the population of the society, the affluence of the population (GDP per person), the energy intensity (average energy required to generate a monetary unit of goods and services) and carbon intensity (amount of greenhouse gas emitted per unit of energy generated). Hence, future emission sce-

[3] parts per million.

narios can be established based on socio-economic scenarios of how the population, economics, and technology will develop in the future. An increase in population will increase emissions, economic growth will increase emissions and technology developments may reduce the energy intensity of goods and services production and reduce the carbon intensity of energy production. Developments in agriculture, land use, and energy supply will also affect the future emission scenarios.

It is difficult to make a single prediction of how the factors that control emissions will evolve in the future, but alternative emission scenarios have been constructed that are regarded as equally plausible, each representing an internally consistent vision of how the world may evolve in the future. These emission scenarios are then fed into carbon-cycle models that calculate how much of the emitted carbon dioxide that is absorbed in ocean and land reservoirs, to convert the emission scenarios into atmospheric concentrations of greenhouse gases.

The IPCC has constructed four main families of socio-economic scenarios over the twenty-first century, denoted as A1, A2, B1, and B2, as follows, with corresponding projections of future atmospheric concentrations of greenhouse gases [15, 16, 22]:

A1: This scenario describes a world of rapid economic growth for both rich and poor societies, leading to a reduction in the wealth gap and a reduction in poverty. Because of the wealth gain by the poor, population growth diminishes with a global population peak in the mid-century and a decline thereafter. There is also a rapid introduction of new and more efficient technologies.

A2: This scenario describes a world of high economic growth, but unevenly distributed in favour of the rich. Poverty remains high and consequently the global birth rates remain high resulting in a continuously increasing population throughout the century. The technological development is slower with introduction of new technology primarily in the richer parts of the world.

B1: This scenario describes a world where economic growth is evenly distributed, but slower than in the A1 scenario due to an emphasis on sustainable growth and environmental protection. This scenario has the same mid-century peak in population as scenario A1. The global economy shifts toward a less energy intensive service and information economy, and clean and resource-efficient technologies are introduced.

B2: This scenario again describes a world of unevenly distributed economic growth. The population increases continuously, but with a slower rate than the A2 scenario. The technological development is less rapid and more diverse than in the A1 and B1 scenarios. Sustainability and environmental protection are the focus at local and regional levels.

The A1 family contains three additional scenarios A1T, A1FI, and A1B, where A1T assumes a shift towards non-carbon energy sources (*T* denotes technology), A1FI assumes a shift toward coal (*FI* denotes fossil intensive) and A1B assumes a balance between energy sources (*B* denotes balance, i.e., not relying too heavily on one particular energy source).

Future projections of atmospheric concentration of CO_2 corresponding to these emission scenarios and based on two different carbon cycle models are provided

by the IPCC Data Distribution Centre, and these projections have been assumed in some of the work in this book, where atmospheric CO_2 levels have been introduced as covariates (Chaps. 5 and 8).

More recently, a set of four *representative concentration pathways* (RCP) has been developed to describe possible projections of radiative forcings towards the year 2100 [21, 31]. These pathways represent internally consistent scenarios containing trajectories of various emissions, concentrations, and land use and are based on underlying socio-economic scenarios. The pathways have been extended to the year 2300 by a set of extended concentration pathways based on simple extension rules [19].

1.1.5 Impacts: The Ocean Wave Climate

The impacts of global warming may be many and some of the most debated are sea level rise, diminishing availability of fresh water, increase in drought, and flooding events, increased frequency of heat waves, ocean acidification, loss of ecosystems, melting of the permafrost and ice, increased disease risk and decline in food production. In addition, there is the possibility of abrupt climate changes, where the climate system undergoes a large and rapid shift to an entirely different climate state within a few decades. The possibility of such abrupt climate changes is deemed low, but if they were to occur it could be an irreversible catastrophe.

The possible impact of climate change on the ocean wave climate has perhaps been less studied, but a number of studies have been published in the literature with future projections of the ocean wave climate. A thorough review of such research is presented in Chap. 2 and will not be repeated herein, but it is noted that different studies get different results. Hence, even though most studies indicate that the future ocean wave climate will tend to be rougher than the current and historic wave climate, the uncertainty of the future ocean wave climate must be considered large. For example, in the recent special report from IPCC [17], it is stated that, even though there are strong linkages between wave height and winds and storminess, due to insufficient literature there is low confidence[4] that there has been an anthropogenic influence on extreme wave heights and that there is overall low confidence in wave height projections because of the small number of studies, the lack of consistency of the different wind projections and limitations in the ability to simulate extreme winds. It is partly in this scientific discussion this book is meant to contribute, with an alternative model for long-term time-dependent description of the ocean wave climate.

[4] About 20 % chance of being correct.

1.1.5.1 Ocean Waves, Sea States, and the Wave Climate

Just as the distinction between *weather* and *climate* emphasized above, it is useful to make a clear distinction between waves, sea states, and wave climate and define what we understand by the wave climate. *Waves* are movements of the sea surface or changes in the sea surface elevation, and just as the weather is constantly changing, the sea surface elevation at an arbitrary point is constantly changing. An individual wave is often described by its wave height, wave crest, wave period, wave length, and wave direction and a physical wave is a superimposition of different wave components. In order to avoid contributions from small capillary waves and ripples on the sea surface, a wave height is normally defined as the distance from the maximum and minimum sea surface elevation where it crosses the zero-level (mean level). The zero-crossing wave period is defined as the time between two zero-upcrossings (or zero-downcrossings). The arrival of consecutive crests (crest period) at a stationary point can also be used. The wave direction is the direction of the wave propagation. More details on waves can be found in standard textbooks on physical oceanography such as [28].

The physical mechanisms behind wave generation are complex and not completely understood, but basically ocean waves are generated by wind forces or wind friction on the sea surface. However, there are also waves generated by other mechanisms such as tidal waves and tsunamis. Waves generated by local winds are normally referred to as wind-sea whereas swell is used to refer to waves that remain after the wind has died out and that can propagate considerable distances. Waves of many different wave frequencies and directions are present in the open ocean and wave fields are therefore often described by wave spectra. These often display two distinctive frequency modes associated with wind-sea and swell (bimodal wave spectrum). A multi-modal wave spectrum may have several swell components present.

The sea surface on the open ocean is constantly changing and is characterized by randomness. It would therefore not be very practical to give a long-term description of individual waves or the instantaneous states of the sea surface, but for a limited period of time and in a particular geographical region met-ocean conditions vary in a stationary way referred to as the *sea state*. Sea states are characterized by a set of integrated sea state parameters, which may be averages over certain periods of time. Examples of such integrated sea state parameters are significant wave height, mean wave period, and mean wave direction. Of these, the significant wave height, often referred to as H_s or SWH, is perhaps the most important parameter for describing the severity of a sea state and this is the parameter that has been studied in the research presented in this book.

The significant wave height is defined as the average of the 1/3 of the highest individual waves measured over a specified period of time, and it is a measure of the sea state. It is implicitly assumed that the sea state is stationary over the measurement period, which can typically be in the order of 20 min up to a few hours. As was mentioned above, ocean waves are generated by wind forces, and the significant wave height is typically a result of wind speed, wind duration (how long time the wind has blown), and fetch (the length of the area the wind is blowing over). Given

a certain sea state, there are also statistical models for the distribution of individual waves, and one common assumption is that the distribution of wave heights in a sea state approximately follows the Rayleigh distribution [18] (under the assumption that the sea surface is Gaussian and narrow-banded). This is a one-parameter distribution where the parameter can be directly related to the significant wave height. Using such assumptions, short-term statistics of individual waves and long-term statistics of sea states may be combined to provide long-term distributions of individual waves.

Finally, the *ocean wave climate* could be construed as the statistics or distribution of sea states, just as sea states are statistics of individual waves. Typically, the interest will be in averages or extremes of ocean sea states, and the variability of those, and trends in the ocean wave climate can be trends in either of such statistics. In this book, it is the distribution, in space and time, of the significant wave height that is investigated. Furthermore, long-term trends in the distribution of significant wave height have been analysed.

1.1.5.2 Long Term Trends and Changes in the Ocean Wave Climate

The oceans are highly dynamic systems, with sea states and wave climate varying constantly in both space and time. In one sense, however, some of the average and extreme properties of the sea state can be regarded as stationary if the overall average boundary conditions do not change. In spite of the continuous variations of sea states over time, the averages such as seasonal average wave heights and return periods for extreme waves can be considered as stationary if the average boundary conditions (e.g., average atmospheric pressure, average wind, average temperatures, etc) remain stationary.

However, in recent years it has become increasingly apparent that the climate system overall is not stationary and that the climate will change in the near future. In fact it has been observed that the climate is already undergoing a change with a global long-term trend towards higher temperatures and more frequent and intense severe weather events, although local and regional trends may differ from this global trend. These climate changes—man-made or not—will thus change the overall boundary conditions for the sea, and the assumption that the average sea states can be regarded as stationary ceases to be valid.

One approach for investigating the impacts of climate change on the ocean wave climate is to use physical wave models in conjunction with wind fields or sea level pressure fields, since winds are generating the waves and winds are generated by pressure gradients. A significant amount of research has gone into the development of sophisticated wave models [11] which can be fed by output from global circulation models. Future projections of the ocean wave climate can then be obtained based on projections of wind or pressure fields. Ensemble studies can be carried out in order to quantify uncertainties, as for example reported in [10], with different climate models or small perturbations of the initial conditions yielding different results. However, it has been increasingly acknowledged that there are notable statistical challenges in projecting future climate from such ensemble studies, see e.g., [6, 26, 29].

The research presented in this book represents an alternative approach to modeling the impacts of climate change on the wave climate. It is a stochastic approach rather than a geophysical approach, and it should rather be seen as a complement to the efforts made in developing physical wave models than a competitor to such models. It is believed that by developing a statistical model, trends in observed wave climate may be identified in order to assess the impacts of climate change. Furthermore, such trends can be extrapolated, or regression on projections of relevant covariates can be used in order to make projections of future impacts of future climate change. It is noted that a number of statistical models for investigating the impact of climate change on the ocean wave climate have been reported in the literature, and a comprehensive literature review is presented in Chap. 2 of this book.

1.1.6 Ocean Waves and Maritime Safety

Ships and other marine structures operate at sea and are continuously exposed to the environmental forces from waves and wind. Failure to withstand such forces may lead to severe consequences, and ocean waves are obviously important for maritime safety and for marine safety in general. Possible impacts of climate change may be a roughening of the wave climate, which could lead to increased risk to maritime transportation. In fact, changes in the ocean wave climate may have serious implications on maritime, offshore and coastal activities and combined with sea level rise, coastal areas throughout the globe may be seriously affected.

Maritime accident databases reveal that bad weather account for a great number of ship losses and accidents, and there are several failure modes that are related to the wave forces. Wave-induced forces will impact both global and local loads on a ship structure. If extreme global loads exceed the structural capacity, breaking in two may occur in extreme sagging conditions. Such failure modes are mostly related to the extreme environmental conditions, and possible changes in the ocean wave climate may increase the extreme loads a ship is expected to experience throughout its lifetime. Another failure mode directly related to wave motion is fatigue. In this case, also the average wave conditions are important, and trends in both extreme as well as low and moderated wave conditions may have an impact on ship safety. Other failure modes that are directly related to the waves are parametric roll, capsize, sloshing of tanks and cargo shift, breaking of windows, and loss of containers. In addition, wave forces may influence ship stability and manoeuvrability, and thereby increase the risk of grounding and impede handling operations.

When designing and constructing ocean going ships, severe sea states are taken into account. In order to do this, there is a need for a description of the variability of various sea state parameters such as the significant wave height, the mean wave period and other relevant parameters. Typically, a number of design sea states are defined based on their return periods and exceedance probabilities and ships are designed to withstand the environmental loads they are likely to encounter throughout their lifetimes. One way of defining structural requirements is by the so-called inverse first

order reliability method (I-FORM), using environmental contour lines as discussed in [12]. Such environmental contour lines may be established from the joint distributions of relevant sea-state parameters such as significant wave height and mean wave period.

If there are long-term trends in the wave climate, be it due to climate change or not, these would need to be taken into account in the structural dimensioning of ships in order to ensure that ships are safe in a future environment. One way to do this, is to estimate the possible changes in the ocean wave climate, e.g., the significant wave height and mean wave period, and update their joint distribution. In such a way, modified environmental contours can be obtained that incorporates possible future changes in the wave climate due to climate change. This will enable ship designers to assess the impact of climate change on wave induced loads and responses, and consequently allow for adaptation by adequately strengthening the ship structures.

The Bayesian hierarchical space-time models presented in this book are models for significant wave height, and results from these models provide estimates of how the marginal distribution of significant wave height might change in the future due to climate change. In order to obtain the joint distribution of significant wave height and mean wave period, one may assume a conditional model, where the distribution of wave period is conditional on the significant wave height and where the conditional distribution for wave period remains unaffected by the climate change (although the marginal distribution of wave period obviously will be affected). Hence, the results from the models for significant wave height can be used to modify environmental contour lines used in structural design. This can be used to assess the impact of climate change on wave-induced loads and responses on ships and consequently to propose how to update design rules for ships, as illustrated in Chap. 7 of this book.

1.2 Stochastic Modeling of Environmental Processes

As explained in the previous section, the statistics of the present and future ocean sea states, i.e., the wave climate, is of great interest to the maritime industries, and this monograph is concerned with developing stochastic models of significant wave height as a way of exploring this. This is seen as an alternative to more geophysics based models for describing the statistics of oceanic sea states.

1.2.1 Probabilistics Versus Deterministics

Statistics, with its foundation in probability theory, is a relatively new science, even though the concept of probability is ancient. Currently, probability theory is often used to describe the underlying mechanics and regularities of complex systems, but for a long time following the scientific revolution of the sixteenth century, the predominant world-view was deterministic. It was believed that if exact knowledge

of the initial conditions of a system and of the causal laws governing the system were available, the exact state of the system could be determined at any later point in time.

A number of new discoveries made many scientists believe in determinism, i.e., that causality implies that any state of a system is completely determined by its prior states just like clockwork. Thomas Hobbes (1588–1679) was one of the earlier exponents of such a world-view and in his political philosophy, he basically regarded humans as being matter and motion, obeying the same physical laws as other matter and motion. The great success of Isaac Newton (1642–1727) and his formulation of Newtonian physics was also important for promoting a mechanistic, deterministic world-view. Suddenly, the motions of all the physical matter of the universe, be it celestial bodies or earthly objects, were obeying the same universal laws and could be explained by a few mechanical principles. Other influential scientists and philosophers of this era that expressed their support for different versions of a deterministic world were René Descartes (1596–1650), Baruch Spinoza (1632–1677), Gottfried Leibniz (1646–1716) and David Hume (1711–1776).

The mechanical and deterministic world-view is perhaps best expressed by Pierre-Simon Laplace (1749–1827) as follows, in the first articulation of causal or scientific determinism:

> We may regard the present state of the universe as the effect of its past and the cause of its future. An intellect which at a certain moment would know all forces that set nature in motion, and all positions of all items of which nature is composed, if this intellect were also vast enough to submit these data to analysis, it would embrace in a single formula the movements of the greatest bodies of the universe and those of the tiniest atom; for such an intellect nothing would be uncertain and the future just like the past would be present before its eyes.

In such a world, randomness would not exist and if it would be possible to have complete knowledge of all physical matter and all of the laws governing that matter at any one time, then it would be theoretically possible to compute the time and place of every event that will ever occur. Moreover, any failure to precisely predict future events would be due to incomplete understanding of the universal laws and incomplete knowledge of the exact state of the universe.

However, in the late nineteenth and early twentieth century, new scientific discoveries started to cast serious doubts on a strictly deterministic world-view. Chaos theory and the associated butterfly effect predicted the sensitive dependence upon the development of a system on the initial conditions; even an infinitesimally small perturbation of initial conditions of a deterministic nonlinear system can lead to large changes at a later stage. Hence, even if the world is strictly deterministic, future events cannot be precisely predicted if there are even small errors in the knowledge of initial conditions, and a purely deterministic description of the world would be impractical. The development of quantum mechanics in the beginning of the twentieth century and the formulation of the Heisenberg uncertainty principle further questioned whether the fundamental laws of the universe could be considered deterministic. The reality according to quantum physics does not seem to be absolutely deterministic, at least at atomic scales, suggesting a more probabilistic understanding of the world. Further

arguments for a probabilistic word-view are presented in [24], based on descriptions of non-equilibrium thermodynamics and time irreversible processes.

Regardless of whether the world is fundamentally probabilistic or deterministic but with uncertain knowledge of the underlying physical laws, physical environmental processes inevitably displays some seemingly causal relationships along with a considerable degree of randomness. Hence, it is argued that it would make sense to describe such phenomena probabilistically, i.e., using probability theory and statistics to model physical processes.

The foundation of probability theory goes back to the sixteenth century and the elementary probability rules formulated by Girolamo Cardano (1501–1576) and to the works of Pierre de Fermat (1601–1665) and Blaise Pascal (1623–1662) in the seventeenth century. In the nineteenth century, Pierre-Simon Laplace established many of the fundamental results in classical statistics and probability theory (the very same as referred to above for having expressed a deterministic world-view), and in the twentieth century, Andrey Kolmogorov (1903–1987) formulated a set of axioms for probability theory and introduced the notion of probability space that became the foundations of modern probability theory.

In probability theory, a stochastic process (or a random process) is a set of random variables defined on a state space that is often used to describe the evolution of a complex system over time. It is a probabilistic counterpart to a deterministic process, where there are several possible ways for the system to evolve from an initial state. Stochastic processes, with their foundations in probability theory and a probabilistic world-view are often used to describe complex environmental systems, and have been utilized in this book to describe the statistics of ocean sea states. It represents an alternative to describing the ocean wave climate as fundamentally deterministic processes by more physics-based wave models.

1.2.1.1 Bayesian Statistics

Statistics is normally thought of as all aspects of collection, organization, analysis, interpretation, and presentation of data. Bayesian statistics is a branch of statistics relying on Bayes' theorem, named after Thomas Bayes (1701–1761) who first used it. Pierre-Simon Laplace later stated the theorem in a more general form in 1812. Basically, it expresses how a subjective degree of belief should rationally change in light of evidence or data. Hence, it involves a prior belief, evidence or data, and a posterior belief or posterior probability that has been updated based on the evidence. Mathematically, Bayes' theorem can be expressed as

$$P(A|X) = \frac{P(X|A)P(A)}{P(X)} = \frac{P(X|A)P(A)}{\sum_{A'} P(X|A')P(A')} \propto P(X|A)P(A)$$

where $P(A)$ denotes the prior degree of belief of event A, $P(X|A)$ denotes the probability of the evidence X conditioned on event A, often referred to as the likelihood of A, $P(X)$ is the unconditional probability of X and $P(A|X)$ is the updated degree

of belief of event A in light of the evidence X, often referred to as the posterior probability of A. In Bayesian statistical modeling, A would typically represent the model parameters and X would represent the data.

In Bayesian statistical models, the formulation of prior degree of belief, typically expressed as prior distributions for any unknown parameters, is therefore an extra requirement. The parameters of such prior distributions are often called hyperparameters. Bayesian inference uses Bayes' theorem to update the probability distributions of model parameters as additional evidence or data is gathered, and such Bayesian updating is particularly important in dynamic analysis of sequences of data, see e.g., [32]. The basic concepts and theory of Bayesian statistics are thoroughly covered in e.g., [2], including foundations, modeling and inference in Bayesian statistics.

1.2.2 Bayesian Hierarchical Space-Time Models

In this monograph, the aim has been to develop sensible stochastic models for the ocean wave climate. The first steps comprised of a literature survey in order to appreciate the state of the art and what type of models had previously been used to model the evolution of the ocean wave climate. Subsequently, a review of stochastic models for describing other relevant processes was performed. These initial literature surveys are reported in Chap. 2 of this book and will not be repeated in this introduction, but the outcome of these initial steps was that a type of models referred to as Bayesian hierarchical space-time models was identified as a promising framework for modeling the ocean wave climate. Hence, such models have been developed in this book, as presented in Chaps. 3, 4, 5 and 6 and have also been applied in Chaps. 7 and 8.

The framework of Bayesian hierarchical space-time models have successfully been applied to model a number of different environmental and other processes in the past [34]. For example, in [35], a Bayesian hierarchical space-time model was applied to atmospheric data of monthly maximum temperature and in [36] a similar model was used to model tropical ocean surface winds. Much inspired by these models, [23] presents a related model for earthquake data. A similar framework was used for modeling the population of house finch in [33]. Such stochastic models include the physics of the studied phenomena through data as well as various terms reflecting spatial, temporal, and spatial-temporal processes. The success of such models in describing different sets of environmental data in space and time inspired the development of similar models for the ocean wave climate.

Some of the main features of such stochastic models are that they are hierarchical in nature, with an observation model and several underlying state models, sometimes referred to as process models and parameter models. The state models may be split into different processes, where one may be a purely spatial process, another a purely temporal process and one may be a spatio-temporal process. Furthermore, inference is done in a Bayesian setting, relying on results from Bayesian statistics. In the

following, a brief introduction to these main characteristics of the models presented in this book will be given and reference is made to [8] for more in-depth discussions.

1.2.2.1 Hierarchical Models

The basis of hierarchical models can be expressed in the following relationship between joint and conditional densities, where x, y and z denotes some random quantities and $f(\cdot)$ are distribution functions:

$$f(x, y, z) = f(x|y, z)f(y|z)f(z)$$

Complex systems can be described as a collection of random variables, and modeling such systems involves establishing the joint distribution of these random variables. Using the relationship above, a complicated joint distribution that may be extremely difficult to determine can be decomposed into a series of conditional models that are much simpler to specify. The product of a series of conditional models can be quite complex, even with simple conditional models and in this way, a complex modeling problem can be reduced to several sub-problems that are much easier to handle. Such conditional models may incorporate uncertainties from different sources, e.g., uncertainty in the data (for example due to measurement inaccuracy), uncertainty in the models that tries to explain the data and uncertainty in the parameters in the models. If uncertainties of the model parameters are included in the model, i.e., including prior distributions for the model parameters (or parameter models), the resulting hierarchical model is often referred to as a Bayesian hierarchical model [8].

A hierarchical model may contain different levels, and the first level will typically be the observation model or data model. At this level, the observations are often modelled as some hidden or latent process, often construed as the true process, and some uncertainty. In other words, a conditional distribution for the observations are specified conditioned on the latent process and the process model parameters. At the next level of abstraction, the state model or process model may be specified as a distribution conditional on a set of model parameters, i.e., a distribution is specified for the latent process given a set of model parameters. At the final level, uncertainty may be assigned to the model parameters by assigning distributions to them; the prior distributions. These three levels constitute the main levels of a Bayesian hierarchical model, but each of the levels may be further divided into different components and may comprise various sub-levels. For example, in the models for significant wave height presented in this book, the state process is split into a purely spatial process, a purely temporal process, and a process with space-time interactions at short timescales.

A simple hierarchical model may be built up in the following way, letting Z denote the data, H denote the latent process and θ denote the model parameters, and defining the (1) Observation model: $f(Z|H, \theta)$; (2) State model: $f(H|\theta)$; (3) Prior distribution on model parameter $f(\theta)$:

$$f(Z, H, \theta) = f(Z|H, \theta) f(H|\theta) f(\theta)$$

The conditional distribution of the latent process and the parameters given the data can now easily be found from Bayes' theorem,

$$f(H, \theta|Z) = \frac{f(Z|H, \theta) f(H|\theta) f(\theta)}{f(Z)}$$

and this is normally referred to as the posterior distribution. By construction, this can be obtained by specifying sensible state models and prior distributions for the parameters that appears on the right-hand side of this equation. Within the framework of Bayesian statistics, all inference, and consequently all predictions, on the process H and the model parameters θ will depend on this posterior, and the main task becomes estimating the posterior distribution. Often, environmental models in space and time are quite complex and of high dimensionality and the computation of the posterior distribution analytically may be far from straightforward. However, Markov chain Monte Carlo methods have been demonstrated to be a useful computational tool in many cases that allows simulating from such posterior distributions.

1.2.2.2 Spatial Random Processes

The stochastic models for significant wave height have been specified within the framework of Bayesian hierarchical models outlined in the previous subsection, where the state model included a contribution from a separate spatial process. The spatial field was modelled as a Markov random field (MRF), an example of models defined by conditional distributions, but an alternative approach to model spatial variability could be to assume a geostatistical process and estimating the associated variogram (see e.g., [8]).

The main idea behind Markov random fields is to specify the spatial process, $\boldsymbol{Z} = (Z_1, \ldots, Z_n)$ through the conditional distributions $p(Z_i|Z_j, j \neq i)$. The Markovian property is an important basis for Markov random fields and it specifies conditional independence, which may significantly simplify the conditional distributions and reduce the number of model parameters. For example, assuming observations on a two-dimensional lattice, the Markov assumption implies that the conditional distribution at a certain location only depends on the values of some nearby locations; locations belonging to its *neighbourhood*. The size of the neighbourhood can be specified and for a first order Markov random field, the neighbourhood is simply all nearest neighbours. Hence, in a first order Markov spatial field, the conditional distributions are only dependent on the values of the nearest neighbours. Letting N_i denote the neighbourhood of location i, this means that, for all locations i, $p(Z_i|Z_j, j \neq i) = p(Z_i|Z_j, j \in N_i)$, and the spatial process can be defined at each location conditioned on the process values of all nearest neighbours.

There are some restrictions on possible conditional distributions that gives a well-defined model, but it can be shown that by assuming for example conditional distri-

butions on the form [25]

$$p(Z_i|Z_j, j \neq i) = \mu_i + \sum_{j \in N_i} \beta_{ij}(Z_j - \mu_j) + \varepsilon_i, \qquad \varepsilon_i \sim N(0, \sigma^2)$$

one gets the auto-normal model with the multivariate normal joint distribution $p(Z_1, \ldots, Z_n) = MVN(\mu, \sigma^2 B^{-1})$, if the following restrictions are met:

1. $j \in N_i \Leftrightarrow i \in N_j$
2. $\beta_{ij} = \beta_{ji}$
3. $B = \{b_{ij}\}$ is positive definite, with
4. $b_{ij} = \begin{cases} 1 & \text{if } i = j \\ -\beta_{ij} & \text{if } i \in N_j \\ 0 & \text{otherwise} \end{cases}$

In the model for significant wave height, such a spatial model was assumed with the neighbourhood defined as the nearest neighbour in all cardinal directions and with different dependence parameters in longitudinal and lateral directions.

1.2.2.3 Temporal Random Processes

The models for significant wave height also contain some purely temporal components independent in space. Those purely temporal components were modelled as simple Gaussian processes but there are many other ways one could have modelled temporal processes. Basic time-series can for example be modelled as white noise processes, random-walk processes or so-called moving-average processes. In the model for significant wave height, purely temporal processes for long-term trends and seasonal variability were modelled as simple regression models with time as covariate and Gaussian white noise. In [30], various time-series models were applied to spatially averaged significant wave height data in order to investigate possible trends.

One type of temporal processes or time-series models is the autoregressive process (AR), and this type of models is used when observations of the process depend on one or more observations immediately preceding it. For example, an autoregressive model of order p is defined as follows

$$X_t = \mu + \sum_{i=1}^{p} \varphi_i(X_{t-i} - \mu) + \varepsilon_t, \quad \varepsilon_t \sim N(0, \sigma^2)$$

In the first order autoregressive process, AR(1), for example, the process is only dependent on the previous observation and may be expressed as $X_t = \mu + \varphi(X_{t-1} - \mu) + \varepsilon_t$.

1.2.2.4 Spatio-Temporal Models

Spatio-temporal processes consider dependencies in both spatial location and time as well as interdependencies between space and time. Two possible approaches for modeling such processes could be by way of multivariate time series, where each spatial location is represented by a temporal process, or by temporal evolution of a spatial process. In the model for significant wave height presented in this book, a process describing short-term dynamic behaviour is included in the state model as a multivariate time-series; a vector autoregressive process.

A vector autoregressive process or model (VAR) can be used to model linear interdependencies among multiple time series and is a generalization of the autoregressive models introduced above. The evolution of each variable in a vector autoregressive model is explained by linear functions of its own past evolution and on the past evolution of the other variables in the model. In the model for significant wave height, short-term dynamic behaviour was modelled as a multivariate time-series at each spatial location with a first-order, nearest neighbour vector autoregressive model. Interdependent time-series at each location were modelled as linear combinations of all neighbouring time-series, including itself, at the previous time-point.

A full Bayesian hierarchical spatio-temporal process can be constructed from a combination of spatial processes, temporal processes and spatio-temporal processes in order to model dependencies in both space and time at various scales. In the model for significant wave height presented in this book, the state or process model or the latent process is modelled as a combination of a spatial process, temporal processes for long-term trends, and seasonality and a short-term dynamic spatio-temporal process.

1.2.3 Waves as Stochastic Processes

Although the dynamics of the sea and the mechanisms underlying the generation of waves on the sea surface inevitably follow the laws of physics and therefore, in principle, the sea state could be described deterministically, in reality this is not possible due to the complexity of the system. Hence, the description of waves and the sea must be done probabilistically. The state of the oceans and the characteristics of the waves are influenced by innumerable external factors, and the most influential boundary conditions are related to the atmosphere and the global and local climate in general. Atmospheric pressure, wind, temperature, precipitation, solar radiation and heat, tidal movements, the rotation of the earth, and movements of the seabed (e.g., from earthquakes or volcanic activities) are examples of external factors that jointly influence the generation of waves on the sea surface.

Hence, the oceans are dynamic systems that are influenced by innumerable factors and an infinite number of interrelated parameters would be needed in order to provide an exact description of the sea in any given point in time. It is simply not possible to know all and every one of these parameters. The unknown parameters introduce

uncertainties to any description of the system and an exact description of the sea is therefore not feasible. Thus, the problem of describing the sea turns into a statistical problem, and probabilistic models are needed in order to represent waves on the sea surface and to provide a better understanding of the maritime environment in which ships operate. In this regard stochastic models would seem to be the most appropriate approach to describe extreme waves. Also, the fact that the sea state is normally described through different average and extreme properties, as discussed briefly above, indicates that statistical tools are appropriate to model waves and sea states. A comprehensive overview of statistical techniques, methodologies, theories and tools used in climatic analyses is presented in [27].

Stochastic modeling of ocean waves can be performed on two very different time scales. In the short-term models, the parameters of most concern may be those for individual waves such as individual wave height, wave length, and period, etc. The times involved in such models are normally in the order from a few seconds to a couple of hours. The long-term models mainly refer to the description of spectral parameters, and the times that are involved normally span over many years. It is the latter time scales that are of main interest in the present work, considering modeling of possible long-term trends due to climate change. However, there are tools, to be discussed later, for combining the long-term statistics of significant wave height with short-term statistics of individual wave heights in order to estimate for example extreme crest heights.

1.3 Data

As with any statistical modeling, the availability of environmental data is crucial for statistical modeling of environmental processes. For the purpose of modeling the ocean wave climate in space and time, space-time data of wave climate parameters such as the significant wave height are needed. Furthermore, when covariates are to be included in the model, data for such explanatory variables are needed. Basically, two sets of data have been needed in the modeling of ocean wave climate presented in this monograph: ocean wave data with sufficient resolution in both space and time, and data on levels of atmospheric greenhouse gases.

Ocean wave data have been collected for a long time, and sources of data include visual observations from ships, in-situ measurements such as wave-rider buoy data, satellite data, and numerical model data. However, most of these data fail to meet the requirements for spatio-temporal modeling. Buoy data for example, may contain long records of data but are restricted to a single location, whereas satellite data which typically have good spatial coverage, are associated with poor sampling characteristics and do not yet cover long time-histories needed for identifying long-term trends. Visual observations suffer from other shortcomings; even though they typically contain a long time-history and data at various spatial locations throughout the globe, the fact that ships tend to avoid the worst weather indicate that extreme events may be seriously under-represented in such data. Another alternative is numerical

data from hindcast studies, which are model-generated data and therefore not actual observations, but that may contain the best combination of spatial and temporal resolution. This alternative was chosen for the modeling presented in this book and reanalysis data from the ERA-40 reanalysis project have been exploited. These data contain data with global coverage at $1.5^\circ \times 1.5^\circ$ spatial resolution and more than 44-year coverage of 6-hourly temporal resolution. A more lengthy discussion of the various sources of wave data is provided in subsequent chapters and provides some more details of the ERA-40 data that have been used. Recently, an interesting mixed statistical model for including both reanalysis data and observational records of wave heights was proposed in [20].

The chosen data-set is global, and there is a need to select a restricted area to investigate. On the one hand, the selected area should be large enough for the spatial features of the model to contribute, but it should also be small enough for the temporal features related to long-term trends and seasonal variation to be considered homogeneous. Another issue is that the computational time increases with the amount of data, so both the spatial and the temporal coverage needed to be limited. Hence, it was decided that an area corresponding to a grid of $17 \times 9 = 153$ locations would be a reasonable compromise. Furthermore, North Atlantic conditions are normally used as a basis for ship design and therefore, an area in the North Atlantic Ocean was selected. However, in Chap. 8 , the model is also applied to data from other ocean areas.

With regards to the explanatory variables, data on atmospheric levels of greenhouse gas are needed, and it was decided that data on the atmospheric concentrations of CO_2 would serve as a reasonable proxy. Furthermore, it is acknowledged that CO_2 mixes well in the atmosphere, so that these data do not need to include spatial variability. Such data are available from the Mauna Loa observatory and have been obtained in this study. In order to make future projections of the ocean wave climate, projections of CO_2 proposed by the IPCC based on various emission scenarios are assumed.

Hence, having formulated a clear problem statement, established the structure of the stochastic model and obtained relevant data to feed the model, the model would be ready for implementation. In order to implement this rather complicated model, however, and make inference and predictions, the powerful computational tool of MCMC is utilized. In appendix A, a brief introduction to MCMC methods will be given, with an emphasis on the algorithms that have been used in the actual implementation of the model.

1.4 Some Identified Areas for Further Research

Having spent 4 years of research on the future wave climate, a relevant question to ask is whether we now can be more certain about the future climate of the oceans. Unfortunately, the answer would have to be no. As the famous saying goes, “It is

difficult to make predictions, especially about the future," [5] predictions of the future wave climate remain difficult and there are still considerable uncertainties to what the actual wave climate will be and indeed uncertainties to how large the uncertainties are. However, the aim of this book was never to give a definitive answer to such a question. It is hoped, however, that the work presented in this book can contribute to highlight an important research area and that it can motivate further research on this important topic, with serious implications for maritime, offshore and coastal societies. In particular, it promotes statistics and stochastic modeling as an important tool in oceanography and climatic sciences and it is hoped that it may motivate oceanographers to employ statistical methods as well as inspire an interest for the ocean wave climate among statisticians.

Hence, this book marks by no means the end of the road of statistical modeling of the ocean climate, and there are several unresolved research areas. In the following, some thoughts on unresolved issues that are open for further research are given. These are issues that have been identified in our research, but the issues mentioned are in no way meant to be exclusive nor exhaustive; they are merely some possible areas, out of many, which may be of interest for further research.

The models presented in this thesis have been restricted to the univariate case, modeling significant wave height in space and time. In practical engineering applications, however, the joint distribution of several environmental parameters are often needed, and it would be interesting to extend the models to include bivariate or multivariate descriptions of the wave climate. Relevant parameters that could be included in such models are wave period, wave direction, storm surge, tide and wind speed. Furthermore, in extreme value analyses it is still an open question how to define multivariate return periods, and this could be an interesting area for further research, see e.g., [7].

It is also acknowledged that the statistical models presented in this book could have been extended with other explanatory variables. It is well known that waves are basically driven by winds which are results of pressure gradients. Hence, it would be interesting to investigate how wind fields and pressure fields could have been included as covariates. One complicating issue in this regards is that if such covariates are non-stationary, it could be difficult to isolate the long term trends from the local and short term effects. It would also be of interest to include some more physical or geophysical components into a stochastic model, making better use of the huge knowledge base available in the meteorologic and oceanographic research communities.

A wave field typically has two main types of contributions, i.e., from locally generated wind waves and from swell. It would be interesting to develop models that distinguish between these effects and that are able to model the multimodality in the wave climate. Possibly, trends in the wind speed could be investigated separately and compared to the trends in the wave climate in order to gain insight. Correlated trends in wind speed and wave height over an area could indicate that the increasing waves are due to locally generated winds whereas increases in wave heights that are not

[5] Often attributed to the physicist Niels Boer, but the actual origin of this quote is unknown.

accompanied by increased wind would possibly be due to increasing swells, most likely due to changes in wind tracks and increasing winds in other areas.

This book has explored various alternative models, but it proved difficult to select the best one. Hence, robust and reliable model selection in complex hierarchical models has been identified as an interesting area for further research. Moreover, the sensitivity of the different assumptions adopted in the proposed models could be investigated further and various different model choices and alternative parametrizations of the models could be explored.

In summary, even though the research presented in this thesis does not provide any definitive conclusions about the future wave climate, and there are still a number of unresolved issues, it is believed that it constitutes a small but timely contribution to the current debate of climate change and its impacts on the ocean wave climate.

References

1. Arrhenius, S.: On the influence of carbonic acid in the air upon the temperature of the ground. Philos. Mag. J. Sci. **41**, 237–276 (1896)
2. Bernardo, J.M., Smith, A.F.: Bayesian theory. Wiley, Chichester (1994)
3. Bitner-Gregersen, E.M., Eide, L.I., Toffoli, A., Eide, M.: White paper on effect of climate change on marine structure design. Technical Report No UCTNO911 2008–1014, Det Norske, Veritas (2009)
4. Bitner-Gregersen, E.M., Hørte, T., Skjong, R.: Potential impact of climate change on tanker design. In: Proceedings of the 30th International Conference on Ocean, Offshore and Arctic Engineering (OMAE 2011). American Society of Mechanical Engineers (ASME) (2011)
5. Callendar, G.S.: The artificial production of carbon dioxide and its influence on temperature. Q. J. R. Meteorol. Soc. **64**, 223–240 (1938)
6. Collins, M., Chandler, R.E., Cox, P.M., Huthnance, J.M., Rougier, J.: Quantifying future climate change. Nat. clim. change **2**, 403–409 (2012)
7. Corbella, S., Stretch, D.D.: Multivariate return periods of sea storms for coastal erosion risk assessment. Nat. Hazards Earth Syst. Sci. **12**, 2699–2708 (2012)
8. Cressie, N., Wikle, C.K.: Statistics for spatio-temporal data. Wiley, Hoboken (2011)
9. Dessler, A.E.: Introduction to modern climate change. Cambridge University Press, Cambridge (2012)
10. Grabemann, I., Weisse, R.: Climate change impact on extreme wave conditions in the North Sea: an ensemble study. Ocean Dyn. **58**, 199–212 (2008)
11. Group, T.W., Cavaleri, L., Alves, J.H., Ardhuin, F., Babanin, A., Banner, M., Belibassakis, K., Benoit, M., Donelan, M., Groeneweg, J., Herbers, T., Hwang, P., Janssen, P., Janssen, T., Lavrenov, I., Magne, R., Monbaliu, J., Onorato, M., Polnikov, V., Resio, D., Rogers, W., Sheremet, A., McKee Smith, J., Tolman, H., van Vledder, G., Wolf, J., Young, I.: Wave modelling—the state of the art. Prog. Oceanogr. **75**, 603–674 (2007)
12. Haver, S., Winterstein, S.: Environmental contour lines: a method for estimating long term extremes by a short term anaysis. Trans. Soc. Naval Archit. Marine Eng. **116**, 116–127 (2009)
13. IPCC: Climate Change: The IPCC scientific assessment. Cambridge University Press, Cambridge (1990)
14. IPCC: Climate Change 1995: The science of climate change. Cambridge University Press, Cambridge (1996)
15. IPCC: Climate Change 2001: The scientific basis. Cambridge University Press, Cambridge (2001)

16. IPCC: Climate Change 2007: The physical sciences basis. Contribution of Working Group I to the Fourth Assessment Report of the Intergovernmental Panel on Climate Change. Cambridge University Press, Cambridge (2007)
17. IPCC: Managing the risks of extreme events and disasters to advance climate change adaptation. Cambridge University Press, Cambridge (2011)
18. Longuet-Higgins, M.S.: On the statistical distribution of the height of sea waves. J. Mar. Res. **11**, 245–266 (1952)
19. Meinshause, M., Smith, S.J., Calvin, K., Daniel, J.S., Kainuma, M.L.T., Lamarque, J.F., Matsumoto, K., Montzka, S.A., Raper, S.C.B., Riahi, K., Thomson, A., Velders, G.J.M., van Vuuren, D.P.P.: The RCP greenhouse gas concentrations and their extensions from 1765 to 2300. Clim. Change **109**, 213–241 (2011)
20. Mínguez, R., Tomás, A., Méndez, F.J., Medina, R.: Mixed extreme wave climate model for reanalysis databases. Stoch. Env. Res. Risk Assess. **27**, 757–768 (2013)
21. Moss, R.H., Edmonds, J.A., Hibbard, K.A., Manning, M.R., Rose, S.K., van Vuuren, D.P., Carter, T.R., Emori, S., Kainuma, M., Kram, T., Meehl, G.A., Mitchell, J.F.B., Nakicenovic, N., Riahi, K., Smith, S.J., Stouffer, R.J., Thomson, A.M., Weyant, J.P., Wilbanks, T.J.: The next generation of scenarios for climate change research and assessment. Nature **463**, 747–756 (2010)
22. Nakićenović, N., Alcamo, J., Davis, G., de Vries, B., Fenhann, J., Gaffin, S., Gregory, K., Grügler, A., Jung, T.Y., Kram, T., La Rovere, E.L., Michaelis, L., Mori, S., Morita, T., Pepper, W., Pitcher, H., Price, L., Riahi, K., Roehrl, A., Rogner, H.H., Sankovski, A., Schlesinger, M., Shukla, P., Smith, S., Swart, R., van Rooijen, S., Victor, N., Dadi, Z.: Emissions scenarios. Cambridge University Press, Cambridge (2000)
23. Natvig, B., Tvete, I.F.: Bayesian hierarchical space-time modeling of earthquake data. Methodol. Comput. Appl. Probab. **9**, 89–114 (2007)
24. Prigogine, I.: The end of certainty. Free Press, New York (1997)
25. Smith, R.L.: Environmental statistics. University of North Carolina (2001). http://www.stat.unc.edu/postscript/rs/envnotes.pdf. Accessed 21 Oct 2010
26. Stephenson, D.B., Collins, M., Rougier, J.C., Chandler, R.E.: Statistical problems in the probabilistic prediction of climate change. Environmetrics **23**, 364–372 (2012)
27. von Storch, H., Zwiers, F.W.: Statistical analysis in climate research. Cambridge University Press, Cambridge (1999)
28. Talley, L.D., Pickard, G.L., Emery, W.J., Swift, J.H.: Descriptive physical oceanography an introduction, 6th edn. Elsevier, Boston (2011)
29. Tebaldi, C., Knutti, R.: The use of the multi-model ensemble in probabilistic climate projections. Philos. Trans. R. Soc. A **365**, 2053–2075 (2007)
30. Vanem, E., Walker, S.E.: Identifying trends in the ocean wave climate by time series analyses of significant wave height data. Ocean Eng. **61**, 148–160 (2012)
31. van Vuuren, D.P., Edmonds, J., Kainuma, M., Riahi, K., Thomson, A., Hibbard, K., Hurtt, G.C., Kram, T., Krey, V., Lamarque, J.F., Masui, T., Meinshausen, M., Nakicenovic, N., Smith, S.J., Rose, S.K.: The representative concentration pathways: an overview. Clim. Change **109**, 5–31 (2011)
32. West, M., Harrison, J.: Bayesian forecasting and dynamic models, 2nd edn. Springer, Heidelberg (1997)
33. Wikle, C.K.: Hierarchical Bayesian models for predicting the spread of ecological processes. Ecology **84**, 1382–1392 (2003)
34. Wikle, C.K.: Hierarchical models in environmental science. Int. Stat. Rev. **71**, 181–199 (2003)
35. Wikle, C.K., Berliner, L.M., Cressie, N.: Hierarchical Bayesian space-time models. Environ. Ecol. Stat. **5**, 117–154 (1998)
36. Wikle, C.K., Milliff, R.F., Nychka, D., Berliner, L.M.: Spatiotemporal hierarchical Bayesian modeling: tropical ocean surface winds. J. Am. Stat. Assoc. **96**, 382–397 (2001)

Chapter 2
Literature Survey on Stochastic Wave Models

This chapter aims at providing a comprehensive, up-to-date review of statistical models proposed for modeling long-term variability in extreme waves and sea states as well as a review of alternative approaches from other areas of application. A review of wave climate projections is also included. Efforts have been made to include all relevant and important work to make this literature survey as complete as possible, which has resulted in a rather voluminous list of references at the end of the chapter. Notwithstanding, due to the enormous amount of literature in this field some important works might inevitably have been omitted. This is unintended and it should be noted that important contributions to the discussion herein might exist of which I have not been aware. Nevertheless, it is believed that this literature study contains a fair review of relevant literature and as such that it gives a good indication of state-of-the art within the field and may serve as a basis for further research on stochastic modeling of extreme waves and sea states. A brief review of available wave data sources is also presented in this chapter. The literature survey presented in this chapter is based on [196].

2.1 Wave Data and Data Sources

As in all statistical modeling, a crucial prerequisite for any sensible modeling and reliable analysis is the availability of statistical data. For example, if models describing the spatio-temporal variability of extreme waves are to be developed, wave data with sufficient spatio-temporal resolution is needed. Furthermore, the lack of adequate coverage in the data will restrict the scope of the statistical models that can be used.

Wave data can be obtained from buoys, laser measurements, satellite images, shipborne wave recorders, or be generated by numerical wave models. Of these, buoy measurements are most reliable, but the spatial coverage is limited. For regions where buoy data are not available, satellite data may be an alternative for estimation of wave heights [117, 152], and there are different satellites that collect such data.

E. Vanem, *Bayesian Hierarchical Space-Time Models with Application to Significant Wave Height*, Ocean Engineering & Oceanography 2,
DOI: 10.1007/978-3-642-30253-4_2, © Springer-Verlag Berlin Heidelberg 2013

Examples of satellite missions are the European Remote Sensing Satellites (ERS-1 and ERS-2), the Topex/Poseidon mission and Jason-1 and -2 missions. Some of the data from these satellite missions are available from various online sources on the Internet.

Wave parameters derived from satellite altimeter data were demonstrated to be in reasonable agreement with buoy measurements by the end of last century [102]. More recently, further validation of wave heights measured from altimeters have been performed, and the agreement with buoy data is generally good [63, 156]. However, corrections due to biases may be required, and both negative and positive biases for the significant wave height have been reported, indicating that corrections are region-dependent [136]. Sea state parameters such as significant wave height derived from synthetic aperture radar images taken from satellites were addressed in [123].

Ship observations are another source of wave data which covers areas where buoy wave measurements are not available. The Voluntary Observing Ship (VOS) scheme has been in operation for almost 150 years and has a large set of voluntary collected data. However, due to the fact that ships tend to avoid extreme weather whenever possible, extreme wave events are likely to be under-represented in ship observations and hence such data are not ideally suited to model extreme wave events [57, 150].

Recently, a novel wave acquisition stereo system (WASS) based on a variational image sensor and video observational technology in order to reconstruct the 4D dynamics of ocean waves was developed [68]. The spatial and temporal data provided by this system would be rich in statistical content compared to buoy data, but the availability of such data are presumably still limited. Data quality and validation may also be an open issue.

In general, measurements of wave parameters are more scarce than meteorological data such as wind and pressure fields which are collected more systematically and covering a wider area. An alternative is therefore to use output from wave models that uses meteorological data as input rather than to use wave data that are measured directly.

Wave models are normally used for forecast or hindcast of sea states [90]. Forecasts typically predict sea states up to 3–5 days ahead. Hindcast modeling can be used to calibrate the models after precise meteorological measurements have been collected. It can also be used as a basis for design but it is stressed that quality control is necessary and possible errors and biases should be identified and corrected [24]. In general, it is acknowledged that wave buoys are regarded as highly accurate instruments, and it is stated in, e.g., [22] that both the systematic and random error of significant wave height measurements by buoys are negligible. However, when calibrating hindcast data against observations, the data will still be subject to epistemic uncertainty due to the way the calibration is carried out and high values of significant wave height will normally be more affected by uncertainties, as discussed in [24].

Currently, data are available from various reanalysis projects [38]. For example, 40 year of meteorological data are available from the NCEP/NCAR reanalysis project [111] that could be used to run wave models [52, 187]. A more recent reanalysis project, ERA-40 [193], was carried out by the European Center for Medium-Range Weather Forecasts (ECMWF) and covers a 45-year period from 1957 to 2002. The

data contain six-hourly fields of global wave parameters such as significant wave height, mean wave direction and mean wave period as well as mean sea level pressure and wind fields and other meteorological parameters. A large part of this reanalysis data are freely available for download from their website for research purposes.[1]

It has been reported that the ERA-40 dataset contains some inhomogeneities in time and that it underestimates high wave heights [185], but corrected datasets for the significant wave height have been produced [36]. Hence, a new 45-year global six-hourly dataset of significant wave height has been created, and the corrected data show clear improvements compared to the original data. In [39] it is stated that this dataset can be obtained freely from the authors for scientific purposes.

2.2 Review of Statistical Models for Extreme Waves

In order to model long-term trends in the intensity and frequency of occurrence of extreme wave events or extreme sea states due to climate change, appropriate models must be used. There are numerous stochastic wave models proposed in the literature, but most of these are developed for other purposes than predicting such long-term trends. Models used for wave forecasting, for example in operational simulation of safety of ships and offshore structures typically have a short-term perspective, and cannot be used to investigate long-term trends. Also, many wave models assume stationary or cyclic time series, which would not be the case if climate change is a reality.

There are different approaches to estimating the extreme wave heights at a certain location based on available wave data, and some of the most widely used are the initial distribution method, the annual maxima method, the peak-over-threshold method, and the MEan Number of Up-crossings (MENU) method. The initial distribution method uses data (measured or calculated) of all wave heights and the extreme wave height of a certain return period is estimated as the quantile h_p of the wave height distribution $F(h)$ with probability p. The annual maxima approach uses only the annual (or block) maxima and the extreme wave height will have one of the three limit distributions referred to as the family of the Generalized Extreme Value distribution. The peak-over-threshold approach uses data with wave heights greater than a certain threshold, and thus allows for increased number of samples compared to the annual maxima approach. Waves exceeding this threshold would then be modeled according to the Generalized Pareto distribution. However, the peaks-over-threshold method has demonstrated a clear dependence on the threshold and is therefore not very reliable. The MENU method determines the return period of an extreme wave of a certain wave height by requiring that the expected or mean number of up-crossings of this wave height will be one for that time interval.

Another approach useful in extreme event modeling is the use of quantile functions, an alternative way of defining a probability distribution [78]. The quantile func-

[1] Data available from url: http://data-portal.ecmwf.int/data/d/era40_daily/

tion, Q, is a function of the cumulative probability of a distribution and is simply the inverse of the cumulative density function: $Q(p) = F^{-1}(p)$ and $F(x) = Q^{-1}(x)$. This function can then be used in frequency analysis to find useful estimates of the quantiles of relevant return periods T of extreme events in the upper tail of the frequency distribution, $Q_T = Q(1 - 1/T)$.

Yet another approach for estimating the maxima of a stationary process is to model the number of extreme events, defined as the number of times the process crosses a fixed level u in the upward direction, as a Poisson process (a counting process $\{N(t), t \geq 0\}$ with $N(0) = 0$, independent increments and with number of events in a time interval of length t Poisson distributed with mean λt is said to be a Poisson process with rate λ) and apply the Rice formula to compute the intensity of the extreme events (see e.g., [164]).

In the following, a brief review of some wave models proposed in the literature will be given. This includes a brief description of some short-term and stationary wave models as well as a more comprehensive review of proposed approaches to modeling long-term trends due to global climatic changes. An introduction to stochastic analysis of ocean waves can be found in [149] and [191], albeit the latter with a particular emphasis on freak or rogue waves.

2.2.1 Short-Term Stochastic Wave Models

Waves are generated from wind actions and wave predictions are often based on knowledge of the generating wind and wind-wave relationships. Most wave models for operational wave forecasting are based on the energy balance equation; there is a general consensus that this describes the fundamental principle for wave predictions, and significant progress has been made in recent decades [106]. Currently, the third-generation wave model WAM is one of the most widely used models for wave forecasting [82, 115] computing the wave spectrum from physical first principles. Other widely used wave models are Wave Watch and SWAN, and there exist a number of other models as well [84]. However, wave generation is basically an uncertain and random process which makes it difficult to model deterministically, and in [19, 58] approaches using neural networks were proposed as an alternative to deterministic wave forecasting models.

There are a number of short-term, statistical wave models for modeling of individual waves and for predicting and forecasting sea states in the not too distant future. Most of the models for individual waves are based on Gaussian approaches, but other types of stochastic wave models have also been proposed to account for observed asymmetries (e.g., adding random correction terms to a Gaussian model [129] or based on Lagrangian models [2, 125]). Asymptotic models for the distribution of maxima for Gaussian processes for a certain period of time exist, and under certain assumptions, the maximum values are asymptotically distributed according to the Gumbel distribution. However, as noted in [165], care should be taken when using

this approximation for the modeling of maxima of wave crests. A similar concern was expressed in [48], albeit not related to waves.

A comparison between significant wave height data predicted by a numerical wave prediction model and corresponding satellite measurements was recently published in [73]. A novel approach utilizing information geometry was used to quantify bias, and one important finding was that the wave prediction model seemed to overestimate the significant wave height slightly but consistently. They also reported significant spatial variation in the distribution of the significant wave height data.

Given the short-term perspective of these types of models, they cannot be used to describe long-term trends due to climate change, nor to formulate design criteria for ships and offshore structures, even though they are important for maritime safety during operation. Improved weather and wave forecasts will of course improve safety at sea, but the main interest in the present study is on long-term trends in ocean wave climate, and the effect this will have on maritime safety and on the design of marine structures. Therefore, short-term wave models will not be considered in great detail herein.

2.2.1.1 Significant Wave Height as a Function of Wind Speed

The significant wave height for a fully developed sea, sometimes referred to as the equilibrium sea approximation, given a fixed wind speed has been modeled as a function of the wind speed in different ways, for example as $H_S \propto U^{5/2}$ or $H_S \propto U^2$ [112]. This makes it possible to make short-term predictions of the significant wave height under the assumptions of a constant wind speed and assuming unlimited fetch and duration. For developing sea conditions, with limited fetch or limited wind duration, the significant wave height as a function of wind speed, U (m/s), and respectively fetch X (km) and duration D (h) has been modeled in different ways, for example as $H_S \sim X^{1/2}U$ and $H_S \propto D^{5/7}U^{9/7}$ [151].

However, it is observed that the equilibrium wind sea approximation is seldom valid, and an alternative model for predicting the significant wave height for wind waves, H_S from the wind speed U_{10} at a reference height of 10 m was proposed in [7], using a different, yet simple parametrization. 18 years of hourly data of significant wave height and winds speed for 12 different buoys were used in order to estimate the model which can be written on the following form:

$$H_S = C(D)I(U_{10} \leq 4\,\text{m/s}) + \left[a(D)U_{10}^2 + b(D)\right] I(U_{10} > 4\,\text{m/s}) \tag{2.1}$$

D denotes the water depth and C, a and b are depth-dependent parameters. Based on comparison with measurements it was concluded that this model is reliable for wind speeds up to at least $U_{10} = 25\,\text{m/s}$.

It is out of scope of the present literature survey to review all models for predicting wave heights from wind speed or other meteorological data. Such models are an integral part of the various wave models available for wave forecasting, but cannot be

used directly to model long-term variations in wave height. However, given adequate long-term wind forecasts, such relationships between wind speed and wave height may be exploited in simulating long-term wave data for long-term predictions of wave climate.

2.2.2 Stationary Models

A thorough survey of stochastic models for wind and sea state time series is presented in [142]. Only time series at the scale of the sea state have been considered without modeling events at the scale of individual waves, and only at given geographical points. One section of [142] is discussing how to model non-stationarity such as trends in time series and seasonal components, but for the main part of the paper it is assumed that the studied processes are stationary. The models have been classified in three groups: Models based on Gaussian approximations, other non-parametric models and other parametric models. In the following, the main characteristics for these different types of wave models are highlighted.

Although ocean wave time series cannot normally be assumed to be Gaussian, it may be possible to transform these time series into time series with Gaussian marginal distributions when they have a continuous state space [142]. The transformed time series can then be simulated by using existing techniques to simulate Gaussian processes. If $\{Y_t\}$ is a stationary process in $\mathbf{R}^d$, assume that there exists a transformation $f: \mathbf{R}^d \to \mathbf{R}^d$ and a stationary Gaussian process $\{X_t\}$ so that $Y_t = f(X_t)$. Such a procedure consists of determining the transformation function f, generation of realizations of the process $\{X_t\}$ and then transforming the generated samples of $\{X_t\}$ into samples of $\{Y_t\}$ using f. A number of such models for the significant wave height have been proposed in the literature (e.g., [54, 198] for the univariate time series for significant wave height, H_s, [85, 144] for the bivariate time series for significant wave height and mean wave period, (H_s, T) and [57] for the trivariate time series for significant wave height, mean wave period and mean wave direction, (H_s, T, Θ_m)). However, it is noted that the duration statistics of transformed Gaussian processes have been demonstrated not to fit too well with data, even though the occurrence probability is correctly modeled [107].

Multimodal wave models for combined seas (e.g., with wind-sea and swell components) have also been discussed in the literature (see e.g., [66, 189, 190]), but these are generally not required to describe severe sea states where extremes occur [23].

A few non-parametric methods for simulating wave parameters have been proposed, as reported in [142]. One may for example assume that the observed time series are Markov chains and use non-parametric methods such as nearest-neighbor resampling to estimate transition kernels. In [36], a non-parametric regression method was proposed to correct outputs of meteorological models. A continuous space, discrete time Markov model for the trivariate time-series of wind speed, significant wave height and spectral peak period was presented in [143]. However, one major drawback of non-parametric methods is the lack of descriptive and predictive power.

An approach based on copulas for multivariate modeling of oceanographic variables, accounting for dependencies between the variables, was proposed in [197] and applied to the joint bivariate description of extreme wave heights and wave periods.

Parametric models for wave time series include various linear autoregressive models, nonlinear retrogressive models, finite state space Markov chain models and circular time series models. A modified Weibull model was proposed in [145] for modeling of significant and maximum wave height. For short-term modeling of wave parameters, different approaches of artificial neural networks (see e.g., [11, 58, 133, 134]) and data mining techniques [130, 131] have successfully been applied. A nonlinear threshold autoregressive model for the significant wave height was proposed in [174].

2.2.3 Non-Stationary Models

Many statistical models for extreme waves assume the stationarity of extreme values, but there are some non-stationary models proposed in the literature. In the following, some non-stationary models for extreme waves that are known and previously presented in the literature will be reviewed. A review of classical methods for asymptotic extreme value analysis used in extreme wave predictions is presented in [178].

2.2.3.1 Microscopic Models

A number of statistical models have been presented in the literature where the focus has been to use sophisticated statistical methods to estimate extreme values at certain specific geographical points (e.g., based on data measurements at that location). This approach is natural, given the limited spatial resolution of available wave data, and aims at exploiting available data measurements at certain locations to the maximum, i.e., to obtain as good predictions as possible for locations where wave data are available. In the following, some of these will be briefly reviewed, even though it is noted that the aim of this study is to extend the scope and broaden the perspective of the statistical models to also include the spatial dimension.

A method for calculating return periods of various levels from long-term non-stationary time series data of significant wave height based on a new definition of the return period is presented in [182, 183]. This definition is based on the mean number of upcrossings of a particular level and was first introduced in the context of prediction of sea-level extremes in [140]. In [179] and [89], new de-clustering methods and filtering techniques are proposed in order to apply the r-largest-order statistics for long-term predictions of significant wave height. A new de-clustering method was also suggested in [177] for applying the peaks-over-threshold method for H_s time series. An approach using stochastic differential equations for clarifying the relationship between long-term time-series data and its probability density functions in order to extrapolate long-term predictions from shorter historical data is proposed in [141]. Two approaches for estimating long-term extreme waves are

discussed in [94] (i.e., an initial distribution approach and a Peak Over Threshold (POT) approach for storm events) and issues related to sampling variability, model fitting and threshold selection (for the POT analysis) are addressed.

Duration statistics of long time series of significant wave height H_s (i.e., the duration of sea states with different intensities) where analyzed in [181] using a bottom–up segmentation algorithm. This analysis makes use of the increasing or decreasing intensity of successive sea state conditions, and subdivide long-term H_s time series into subsequent series of monotonically increasing or decreasing intensities. This would correspond to developing and decaying sea states, and the segmentation algorithm should ensure that a meaningful subdivision of the long-term time series is obtained. A sensitivity analysis of this approach, investigating the effect of the maximum allowed error on the segmentation of the H_s time series is reported in [180].

Return periods of storms with an extreme wave above a certain threshold are found based on an equivalent triangular storm model in [9]. This approach is extended to find return periods analytically for storms with two or more waves exceeding the threshold in [8, 10]. The basic idea behind the equivalent triangular storm model is that it, for a fixed location, associates a triangle to each actual storm and represents a significant wave height time series by means of a sequence of triangular storms. The triangle height is the maximum significant wave height during the actual storm and the triangle base is such that the maximum expected wave height in the actual storm equals the maximum expected wave height in the triangular storm model [25]. The equivalent power storm model was presented in [67] as a generalization of the equivalent triangular storm model to predict return periods for waves above a certain threshold. It is noted that the equivalent triangular storm is firmly based on what has become known as the Borgman Integral [27], which gives the distribution function for the largest wave, $F_m(h) = P(H_m \leq h)$ as follows, with H_m denoting the largest wave height, $a^2(t)$ time varying Rayleigh parameter and $T(t)$ typical wave period at time t:

$$F_m(h) = e^{\int \log[1-e^{-h^2/a^2(t)}]\frac{\mathrm{d}t}{T(t)}} \tag{2.2}$$

A non-stationary stochastic model for long-term time series of significant wave height is presented in [12], where the time series is modeled by decomposing de-trended time series to a periodic mean value and a residual time series multiplied with a periodic standard deviation: $X(\tau) = \overline{X}_{\text{trend}}(\tau) + \mu(\tau) + \sigma(\tau)W(\tau)$. It was then showed that $W(\tau)$ could be considered stationary. Short-term and long-term wave characteristics of ocean waves were combined in order to develop nested, stochastic models for the distribution of maximum wave heights in [155]. Different time scales were introduced, i.e., fast time and slow time, and a stochastic process was modeled in the fast time where the state variables were modeled as a stochastic process in the slow time.

The seasonal effects on return values of significant wave height were investigated in [139], where a time-dependent generalized extreme value model was used for monthly maxima of significant wave height. Non-stationarity representing annual

and semiannual cycles is introduced in the model via the location, scale, and shape parameters and the inclusion of seasonal variabilities is found to reduce the residuals of the fitted model substantially. Hence, the model provides a way of quantitatively examining the long-term seasonal distribution of significant wave height.

Various other models for the long-term distribution of significant wave height have been suggested (e.g., using the Beta and Gamma models [69], using the Annual Maxima and Peak Over Threshold methods [88] using nonlinear threshold models [174], using time-dependent Peak Over Threshold models for the intensity combined with a Poisson model for frequency [137, 138], employing different autoregressive models [86, 87], and using a transformation of the data and a Gaussian model for the transformed data [70]). Short- and long-term statistics were combined in [116] in order to establish distributions of maximum wave heights and corresponding periods. Some considerations of bias and uncertainty in methods of extreme value analysis were discussed in [77], leading to some recommended approaches for such analyses and applied on a set of wave data.

More recently, an interesting approach to long-term predictions of significant wave height, combining Bayesian inference methodology, extreme value techniques and Markov chain Monte Carlo (MCMC) procedures is presented in [175]. The benefits of using a Bayesian approach compared to a traditional likelihood-based approach is that prior knowledge about parameter values θ can be used together with observed data x to update a posterior distribution $\pi(\theta|x)$. Simulations of this posterior distribution can be obtained by constructing a Markov chain whose invariant distribution, or target distribution, is proportional to the posterior distribution by employing the Metropolis-Hastings algorithm (see [161]). This Bayesian approach was used to analyze a dataset of significant wave height collected in the northern North Sea.

Another Bayesian approach to estimating posterior distributions of return periods for extreme waves is proposed in [65]. Here, the occurrence of extreme events is modeled as a Poisson-process with extreme wave heights distributed according to a generalized Pareto distribution.

2.2.3.2 Combining Long- and Short-Term Wave Height Statistics

The Borgman Integral (Eq. 2.2) is a fundamental tool for combining the long-term distribution of significant wave height with short-term distributions for the individual wave heights [27]. This is often desired for estimating the maximum wave or crest height occurring in a long return interval. A similar method was proposed by [15]. It is noted that the particular expression of the Borgman Integral as presented in Eq. 2.2 is based on the assumption of a Rayleigh distribution for the individual wave height. A more general form would be, letting $P(h|H_s)$ denote the short-term distribution of the individual wave height conditioned on the sea state,

$$F_m(h) = e^{\int \log[P(h|H_s)] \frac{\mathrm{d}t}{T(t)}} \tag{2.3}$$

Long time series of individual wave heights are typically not available and calculations must therefore be based on time series of sea state parameters such as the significant wave height. Hence, the problem of modeling the maximum wave height in a long time interval comprises three aspects: modeling of long-term sea state parameters (e.g., significant wave height), short-term modeling of individual wave heights conditioned on the sea state and combining the two distributions. This can be done by first fitting a short-term distribution and then apply the Borgman Integral to this distribution. Integration of short-term second order models over time series of measured sea states was performed by [118]. A recent study concerned with finding the most accurate method for combining long- and short-term wave statistics was reported in [71].

2.2.3.3 Spatio-Temporal Models for Extreme Waves

The spatial and temporal variability of ocean wave fields is complex, and the fields will generally be inhomogeneous in space and non-stationary in time, with strong temporal and spatial variation [108]. Different models have been proposed in the literature for modeling these variabilities and for analysing and synthesizing spatio-temporal wave data.

There has been significantly more focus on the temporal variability compared to the spatial variability of wave fields, but the spatial behavior (i.e., the spatial interdependence and radius of influence of a set of spatially distributed stations) of significant wave height is investigated in [5]. The methodology is based on the concept of trigonometric point cumulative semivariograms, consisting of cumulative broken lines where the angle between two successive lines connecting two station records is a measure of the regional dependence, ranging from 0 (complete independence) to 1 (complete dependence). Another approach for predicting the maximum wave height over a spatial area was proposed in [68], based on 4D video data of sea states acquired through a wave acquisition stereo system (WASS) and using Euler Characteristics' theory. A regional frequency analysis of extreme wave heights, analyzing peaks-over-threshold wave data from 9 locations along the Dutch North Sea coast was reported in [195]. The different locations could be considered as a homogeneous region and it was shown that the Generalized Pareto Distribution is an optimal regional probability distribution for the extreme wave heights for the region. Notable differences were found for the regional quantile estimates compared to the at-site quantile estimates, indicating that it would be better to rely on the regional estimates in decision making.

Models for stochastic simulation of the annual [28] and synoptic [29] variability of inhomogeneous met-ocean fields were proposed as expansions of the field $\zeta(r, t)$ in terms of periodical empirical orthogonal functions in [28, 29]:

$$\zeta(\mathbf{r}, t) = m(\mathbf{r}, t) + \sum_k a_k(t)\phi_{kt}(\mathbf{r}, t) + \varepsilon(\mathbf{r}, t) \tag{2.4}$$

where $m(\mathbf{r}, t)$ are the mathematical expectations, $\phi_{kt}(\mathbf{r}, t)$ are the spatio-temporal basis functions, $\varepsilon(k, t)$ is inhomogeneous white noise and $a_k(t)$ are the coefficients. $\mathbf{r}$ denotes the geographical coordinates and t time. The results of simulating these models are a set of simulated met-ocean fields $\zeta(r, t)$ in a discrete set of grid points and at discrete times. They could then be used to investigate the field extremes and rare events in terms of both spatial and temporal extremes, and wave data from the Barents Sea region have been used to test the models with reasonable agreement. The stochastic models for annual variability can be regarded as field generalizations of periodically correlated stochastic processes. The model for synoptic variability uses a Lagrangian approach and the temporal sequence of storm centers is modeled as a finite-state Markov chain with the storm extensions and field properties as spatio-temporal impulses.

Recently, spatio-temporal statistical models for the significant wave height have been reported that describes the variability of significant wave height over large areas by stochastic fields [17, 18]. This is based on constructing a homogeneous model valid for a small region and then extending this to a non-homogeneous model valid for large areas. Global wave measurements from satellites have been used for model fitting, providing wave data of spatial variability, but limited physical knowledge about the wave phenomena have been incorporated into the models. The resulting models can then be used to estimate the probability of a maximum significant wave height to exceed a certain level or to estimate the distribution of the (spatial) length of a storm [16]. However, the temporal validity of this model is limited to the order of hours [17], and therefore it does not seem suited for studying long-term trends and the effects of climate change.

The study reported in [40] used two approaches to model the extremes of non-stationary time series, i.e., the non-homogeneous Poisson process and a non-stationary generalized extreme value model. The non-homogeneous Poisson process was used to model extreme values of the significant wave height, obtained from the 40-year ECMWF reanalysis (ERA-40) [193] and compared to estimates obtained using a non-stationary generalized extreme value model (NS-GEV). The parameter of the Poisson distribution in this model was on the form $\lambda = \int\int \lambda(t, x)\mathrm{d}t\mathrm{d}x$, where :

$$\lambda(t, x) = \frac{1}{\sigma(t)}\left[1 + \xi(t)\frac{x - \mu(t)}{\sigma(t)}\right]_{+}^{-(\frac{1}{\xi(t)})-1} \tag{2.5}$$

From projections of the sea level pressure under three different forcing scenarios ([26, 146]), projections of the parameters in the non-homogeneous Poisson process are made up to the end of the twenty-first century. Trends in these parameters are then determined, projections of return value estimates of H_S are projected and their uncertainties are assessed.

2.3 Relevant Statistical Models from Other Areas of Application

Extreme value analysis has a wide area of applications aside from ocean waves, in particular in various environmental sciences where events are also associated with spatio-temporal variations, and it is believed that some lessons can be learned by examining different statistical models for other types of extreme events.

An interesting discussion on the use of asymptotic models for the description of the variation of extremes is available in [48], within the context of extreme rainfall modeling. It is concerned with the lack of ability of such models to predict extreme, catastrophic events leading to inadequate designs and lack of preparedness for such rare events. One of the reasons for this, according to [48] is models that do not take the uncertainties in both model and predictions adequately into account. For example, it is argued that even in cases where data support the reduction of the generalized extreme value model to a Gumbel model, this should not be done without an appraisal of the uncertainty this decision introduces and as a general advice it is suggested to use the generalized extreme value model rather than Gumbel reduction. Furthermore, the preference for Bayesian analysis over the classical likelihood analysis is emphasized, even if using diffuse priors.

In this section, a review of relevant time- and space-dependent statistical models from other areas of application is presented. Further work will then focus on how these approaches can be used for statistical modeling of extreme waves and sea states.

2.3.1 Bayesian Hierarchical Space-Time Models

Modeling of wave data in space and time is an alternative to the common approach of extreme value analysis based on a point process representation, provided that adequate space-time wave data can be obtained. [209] proposes a hierarchical Bayesian space-time model as an alternative to traditional space-time statistical models and applies it on an atmospheric data set of monthly maximum temperatures. Such models generally consist of three stages often referred to as the data stage, the process stage, and the parameter stage.

Similar models have also been used for modeling tropical ocean surface winds [210], North Atlantic sea surface temperatures [124], concentrations of PM_{10} pollution[2] [46], ozone levels [167], and earthquake data [147]. A brief overview of hierarchical approaches applied to environmental processes is presented in [208]. More recently, various hierarchical Bayesian space-time models for extreme precipitation events were proposed in [168]. Bayesian hierarchical space-time models are treated in the recent book by Cressie and Wikle [53].

[2] PM_{10} is the fraction of aerosol particles with aerodynamic diameter less than 10 μm

The modeling of earthquake data for earthquake prediction, using a Bayesian hierarchical space-time approach in [147] considered a spatial resolution of $0.5 \times 0.5°$ (about 50×50 km) and a temporal resolution of 4 months. The observations are, for each time period, the magnitude of the largest earthquakes (by the Richter scale) observed within each grid. The model is implemented within a Markov chain Monte Carlo framework using Gibbs sampling and additional Metropolis-Hastings steps. Four different model alternatives were suggested in a hierarchical structure, one main model and three levels of simplified models, nested within the model at the higher level. The model contains a large number of parameters, and all prior parameter distributions are considered independent. A Markov chain Monte Carlo approach using the Gibbs sampler and also an additional Metropolis-Hastings step for some of the parameters, was adopted for generating independent samples from the posterior distributions in order to arrive at posterior estimates and predictions. A brief introduction to Markov chain Monte Carlo methods, including the Gibbs sampler and the Metropolis-Hastings algorithm, are given in appendix A. For a more detailed treatment, reference is made to [161] or similar textbooks.

2.3.2 Continuous Space Models

Although wave data are generally only available at certain specific locations, extreme waves should in principle be considered as a continuous process in space and time rather than a spatially discrete process. Considering the continuous space modeling of a process' extremes, this would require the specification of a continuous space model for the marginal behavior of the extremes of the process and a continuous space specification of the dependence structure of the extremes. Hence, a generalization of the dependence structure of multivariate extremes to the infinite dimensional case is needed, and one such generalization is provided by the theory of max-stable processes [93]. By definition, a stochastic process $\{Y_t\}$ is called a max-stable process if the following property holds:

> If $\{Y_t^{(i)}\}_{t\in T}$, $i = 1, \ldots, r$, are independent copies of the process then the process $\{\max_{i\le r} Y_t^{(i)}\}_{t\in T}$ has the same distribution as $\{r\, Y_t^{(1)}\}_{t\in T}$.

In the following, a procedure for using the theory of max-stable processes for modeling data which are collected on a grid of points in space are reviewed. This approach is considered as an infinite dimensional extension of multivariate extreme value theory and has the advantage that it can be used to aggregate the process over the whole region and for interpolation to anywhere within the whole region. Models based on the resulting family of multivariate extreme value distributions are suitable for a large number of grid points.

In [50, 51] a class of max-stable process models for regional modeling of extreme storms was specified which can be estimated using all relevant extreme data and which is consistent with the multivariate extreme structure of the data. The essence of this approach is to describe the process of storms by the following components:

i. A phase space S of storm types so that the storm type is independent of their size
ii. An index space T for the region, conveniently referred to as the region itself
iii. A measure $\nu(ds)$ on S describing the relative frequency of storm types
iv. A function $f(s,t)$ interpreted as the proportion of a storm of type s observed at t.

With x_j interpreted as the size of the jth storm, s_j the type of the jth storm, if $\{(x_i, s_i); i = 1, \ldots\}$ are taken to be the points of a Poisson process on $(0,\infty) \times S$ with intensity $\mu(\mathrm{d}x, \mathrm{d}s) = x^{-2}\mathrm{d}x\nu(\mathrm{d}s)$ and letting $f(x,s)$ be a positive function on $S \times T$, then the process

$$Z_t = \max_i \{X_i f(Si, t)\} \tag{2.6}$$

is a max-stable process for $t \in T$.

For statistical modeling of extreme storms as such a max-stable process, it was assumed that the spatial variability of storms could be described adequately by variability within a subset of data sites T_1 [50]. Then, a multivariate extreme value model is fitted to the data for this subset and the model is extended smoothly as a max-stable process through suitable functions $f(\cdot,\cdot)$ on the basis of information from the remaining data sites. Such a model was fitted for rainfall data collected from 11 sites, and in spite of some interesting qualitatively observations, the quality of fit of the model was rather poor.

In [33] a somewhat different approach of using max-stable processes for the modeling of spatial extreme rainfall is proposed based on random fields. Whereas [50, 51] indicate how to analytically calculate quantiles of areal rainfall, in [33], the 100-year quantile of the total rainfall over an area in Holland is found by simulating synthetic daily rainfall fields using their estimated model. An extended Gaussian max-stable model for spatial extreme rainfall was also presented in [176], where Bayesian techniques are used in order to incorporate information other than data into the model, i.e., by using informative priors for the marginal site parameters and non-informative priors for parameters relating to the dependence structure of the process. The extended model is estimated using a pairwise likelihood within the Bayesian analysis and Markov chain Monte Carlo techniques were used to simulate from the posterior distributions, using a Gibbs sampler with a Metropolis step. Max-stable processes have also been applied to, e.g., modeling of extreme wind speeds [49].

2.3.3 Process Convolution Models

Several models for spatio-temporal processes based on process convolution have been proposed in the literature (e.g., [41, 42, 99, 169]). The main idea is to convolve independent processes to construct a dependent process by some convolution kernel. This kernel may evolve over space and time thus specifying models with non-stationary dependence structures.

The model proposed in [99] is motivated by estimation of the mean temperature field in the North Atlantic Ocean based on 80 year of temperature data for a region.

First, the temperature field $y(s,t)$ is modeled as a process over space s and time t as the sum of two processes

$$y(s,t) = z(s,t) + \varepsilon(s,t) \tag{2.7}$$

where $z(s,t)$ is a smooth Gaussian process and $\varepsilon(s,t)$ is an independent error process. The smooth process $z(s,t)$ is constructed to model the data by taking the convolution of a three-dimensional lattice process. Given a grid process $x = (x_1, \ldots, x_m)$ with space-time coordinates $(\omega_1, \tau_1), \ldots, (\omega_m, \tau_m)$, the smooth field is expressed as

$$z(s,t) = \sum_{j=1}^{m} K_s(s - \omega_j, t - \tau_j) \cdot x_j \tag{2.8}$$

where the properties of the convolution kernel determine the smoothness of z. A separable kernel were used (i.e., a product of a kernel that smooths over space and one that smooths over time): $K_s(\Delta s, \Delta t) = C_s(\Delta s) \cdot R(\Delta t)$. Inference on the resulting model was made using a Bayesian approach and simulating the posterior distribution of the mean temperature field over space and time using Markov chain Monte Carlo methods.

Following a similar approach, but using non-separable, discrete convolution kernels, regional temperature measurements were modeled in space and time in [169]. Two alternative sets of models were suggested. The first was to convolute spatial Gaussian processes with a kernel providing temporal dependencies and the second was to convolute autoregressive models with a kernel providing spatial interactions. In other words, the data could either be considered as a number of time series at each location (temporal convolution model) or as a number of realizations of spatial processes observed at some locations (spatial convolution model).

A dynamic process convolution model extends the discrete process convolution approach by defining the underlying process x to be a time-dependent process that is spatially smoothed by a smoothing kernel at each time-step [41, 42]. Such models have been used in air quality assessment (e.g., in bivariate modeling of levels of particulate matter $PM_{2.5}$ and PM_{10} in [42] and for multivariate modeling of the concentration of five pollutants in [41]). A continuous version in space and time is considered in [31], where a model is formulated in discrete time and continuous space and a limit argument is applied to obtain continuous time as well. A general approach using cross-convolution of covariance functions for modeling of multivariate geostatistical data were proposed in [132]. All of the convolution models discussed above used Bayesian approaches and Markov chain Monte Carlo methods for model specification.

Finally, it is noted that some limitations to the convolution model approach are reported in [99] and [42]. One is the impact of prior assumptions on the posterior distributions. Furthermore, it is stated that it would be preferable to allow the data to determine the kernels, which could depend on space and time, rather than specifying

it apriori. In addition, the model for particulate matter is not able to handle extreme observations very well and permits non-sensible predictions.

2.3.4 Non-Stationary Covariance Models

Many spatio-temporal models assume separability in space and time so that that the space-time covariance function can be represented as the product of two models: one as a function of space and the other as a function of time. However, the rationale for using a separable model is often convenience rather than the ability of such models to describe the data well, and the assumption is often unrealistic. Other simplifying assumptions often employed are stationarity (e.g., second order stationarity which means that the mean function is assumed constant and the space-time covariance function is assumed to depend only on the directional distance between measurement sites) and isotropy (i.e., that the covariance function is dependent only on the length of the separation and not on its direction). An example of a spatio-temporal covariance model where the assumptions of stationarity and separability is relaxed is presented in [32], applied to tropospheric ozone data.

Due to the increased availability of satellite measurements of many geophysical processes, global data are increasingly available. Such data often show strong non-stationarity in the covariance structure. For example, processes may be approximately stationary with respect to longitude but with highly dependent covariance structures with respect to latitude. In order to capture the non-stationarity in such global data, with a spherical spatial domain, a class of parametric covariance models is proposed in [110]. These assume that processes are axially symmetric, i.e., that they are invariant to rotations about the earth's axis and hence stationary with respect to longitude.

Assuming a homogeneous, zero-mean process Z_0, a zero-mean non-stationary process Z may be defined by applying differential operators with respect to latitude and longitude, letting L and l denote latitude and longitude, respectively [109],

$$Z(L,l) = \left\{ A(L)\frac{\partial}{\partial L} + B(L)\frac{\partial}{\partial l} \right\} Z_0(L,l) + C Z_0(L,l) \tag{2.9}$$

Now, A and B denote non-random functions depending on latitude (and may also in principle depend on longitude, but this would break the axial symmetry). A non-negative constant C corresponds to including homogeneous models for the case $A(L) = B(L) = 0$. In order to apply this model to real applications, the A and B functions need to be estimated, and it is suggested to use linear combinations of Legendre polynomials [110].

The covariance model is applied to global column ozone level data and it is shown that the strong non-stationarity with respect to latitudes as well as the local variation of the process can be well captured with only a modest number of parameters. Thus, it may be a promising candidate for modeling spatially dependent data on a

sphere. Furthermore, an extension to spatio-temporal processes would be obtained by introducing a similar differential operator with respect to time in addition to the ones with respect to latitude and longitude. Then, such models should be able to capture spatial-temporal non-stationary behavior and to create flexible space-time interactions such as space-time asymmetry. Reviews of various methods and recent developments for the construction of spatio-temporal covariance models are presented in [113] and [127].

2.3.5 Coregionalization Models

A multivariate spatial process is a natural modeling choice for multivariate, spatially collected data. When the interest is in modeling and predicting such joint processes it will be important to account for the spatial correlation as well as the correlation among the different variables. If this is modeled using a Gaussian process, the main challenge is the specification of an adequate cross-covariance function [173], which can be developed through linear models of coregionalization (LMC). The linear model of coregionalization is reviewed in [76] where the notion of spatially varying LMC is proposed in order to enhance the usefulness by providing a class of multivariate non-stationary processes.

Traditionally, linear models of coregionalization have been used to reduce dimensions, approximating a multivariate process through a lower dimensional representation. However, it may also be used in multivariate process construction, i.e., obtaining dependent multivariate processes by linear transformation of independent processes. A general multivariate spatial model could be on the form

$$\mathbf{Y}(s) = \boldsymbol{\mu}(s) + \mathbf{v}(s) + \boldsymbol{\varepsilon}(s) \tag{2.10}$$

where $\boldsymbol{\varepsilon}(s)$ is a white noise vector (i.e., $\boldsymbol{\varepsilon}(s) \sim N(0, \mathbf{D})$ where $\mathbf{D}$ is a diagonal matrix with $(D_{jj}) = \tau_j^2$), $\mathbf{v}(s)$ arises from a linear model of coregionalization from independent spatial processes $\mathbf{w}(s) = (w_1(s), \ldots w_p(s))$: $\mathbf{v}(s) = \mathbf{A}\,\mathbf{w}(s)$ and where $\boldsymbol{\mu}(s)$ may be assumed to arise linearly in the covariates, i.e., $\boldsymbol{\mu}_j(s) = \mathbf{X}_j^T(s)\beta_j$ where each component may have its own set of covariates $\mathbf{X}_j$ and its own coefficient vector β_j. If ignoring the term $\boldsymbol{\mu}(s)$ and the $w_j(s)$ processes are assumed to have mean 0, variance 1 and a stationary correlation function $\rho_j(h)$, then $E(\mathbf{Y}(s)) = 0$ and the cross-covariance matrix associated with $\mathbf{Y}(s)$ becomes

$$\Sigma_{\mathbf{Y}(s),\mathbf{Y}(s')} \equiv C(s - s') = \sum_{j=1}^{p} \rho_j(s - s')\mathbf{T}_j, \qquad \mathbf{T}_j = \mathbf{a}_j\mathbf{a}_j^T \tag{2.11}$$

with $\mathbf{a}_j$ the jth column of $\mathbf{A}$. Priors on the model parameters $\boldsymbol{\theta}$ consisting of $\{\beta_j\}$, $\left\{\tau_j^2\right\}$, $\mathbf{T}$ and ρ_j, $j = 1, \ldots, p$ would then complete the model specification in a Bayesian setting, obtaining the posterior distribution of the model parameters

$$\pi(\boldsymbol{\theta}|\mathbf{Y}) \propto f(\mathbf{Y}|\left\{\beta_j\right\}, \mathbf{D}, \left\{\rho_j\right\}, \mathbf{T})\pi(\boldsymbol{\theta}) \tag{2.12}$$

The extension to a spatially varying linear model of coregionalization is obtained by letting $\mathbf{A}$ be spatially dependent, i.e., replacing $\mathbf{A}$ with $\mathbf{A}(s)$ in $\mathbf{v}(s) = \mathbf{A}(s)\mathbf{w}(s)$ [76]. $\mathbf{v}(s)$ will then no longer be a stationary process. Further extensions to spatio-temporal versions of the model, modeling $\mathbf{v}(s,t) = \mathbf{A}(s,t)\mathbf{w}(s,t)$, where the components of $\mathbf{w}(s,t)$ are independent spatio-temporal processes may also be feasible, but this was not further investigated.

A stationary Bayesian linear coregionalization model for multivariate air pollutant data was presented in [173] and [76] presents a commercial real estate example of a spatially varying model. Rather than taking the Bayesian approach, an Expectation-Maximization (EM) algorithm for the maximum-likelihood estimation of the parameters in a linear coregionalization model is developed in [215], and applied on a spatial model of soil properties.

2.3.6 Generalized Extreme Value Models

The Generalized Extreme Value distribution is a cornerstone of extreme value modeling, and in [101] non-stationary, location-dependent processes are studied using the GEV distribution where the parameters are allowed to vary in space and time. The modeling is based on a hierarchical structure assuming an underlying spatial model. Parameter changes over time (i.e., for the location, scale, and shape parameters) are modeled by use of Dynamic Linear Models (DLM) [207] which is a very general class of time series models. Now, the trends are not constrained to have a specific parametric form and the significance of short-term changes can be assessed together with the long-term changes. It is also possible to estimate how the effects of covariates change over time. An extension of this model to include changes in space as well as in time is made using a process convolution approach in defining a Dynamic Linear Model on the parameters.

Several approaches for estimation of parameters and quantiles of the GEV distribution have been applied, such as maximum likelihood estimation, L-moments estimation, Probability Weighted Moments estimation and the method of moments. Recently, an alternative to these, employing a full Bayesian GEV estimation method which contains a semi-Bayesian framework of generalized maximum likelihood estimators and considers the shape, location, and scale parameters as random variables was developed [214]. However, these approaches do not consider non-stationarity.

A generalized Probability Weighted Moments (PWM) method was suggested in [159] to model temporal covariates and provide accurate estimation of return levels from maxima of non-stationary random sequences modeled by a GEV distribution. This is a generalization of the PWM method that has proved to be efficient in estimating the parameters of the GEV distribution for iid processes and is an alternative to Maximum Likelihood Estimation (MLE) for cases when the iid assumption is violated (e.g., in non-stationary cases). The approach is illustrated by applying it

on time series of annual maxima of CO_2 concentrations and seasonal maxima of accumulated daily precipitations.

An alternative to GEV models could be to use threshold models [20]. For example, various statistical methods for exploring the properties of extreme events in large grid point datasets were presented in [47], and a flexible generalized Pareto model that is able to account for spatial and temporal variation in the distribution of excesses was outlined. The generalized Pareto distribution parameters may incorporate the dependence of the extreme values and different explanatory variables related to spatial and temporal changes such as climate change. The methods were illustrated using mean surface temperatures of the Northern Hemisphere.

A generalized PWM method was introduced in [59] in order to estimate the parameters of the generalized Pareto distribution (GPD) from finite length time series. A Bayesian framework for analysis of extremes in a non-stationary context was proposed in [158] with a case study on peak-over-threshold data. Several probabilistic models, including stationary, step-wise changing and linear trend models, and different extreme value distributions were considered allowing modeling uncertainty to be taken into account.

An alternative to the standard approach of modeling non-stationarity in threshold models (i.e., retaining a constant threshold and letting the parameters of the GPD be functions of some covariates) is proposed in [64]. This involves preprocessing; attempting to model the non-stationarity in the entire data set and then removing this non-stationarity from the data. If this preprocessing is successful, the extremes of the preprocessed data will have most, if not all, of its non-stationarity removed and a simple extreme value analysis of the preprocessed data can be employed. It is argued that this approach provides improved description of the non-stationarity of the extremes, clearer interpretation, easier threshold selection and reduced threshold sensitivity. The approach was also found to be superior to approaches with continuous varying thresholds.

A brief introduction to traditional approaches to extreme value modeling is given in appendix B.

2.3.7 Optimality Models

One type of statistical models that has recently been applied in evolutionary sciences is optimality models. These assume the evolution of some biological trait toward an optimal state dictated by the environmental conditions. Due to a randomly changing environment, the optimal state is assumed to change over time, and the species are assumed to be adapting to this changing optimality with a certain phylogenetic inertia. One choice of process models for analysing such an adaptation-inertia problem is the Ornstein-Uhlenbeck process, as suggested in, e.g., [95, 157], represented by the stochastic differential equation

$$\mathrm{d}y = -\alpha(y - \theta)\mathrm{d}t + \sigma_y \mathrm{d}W_y \tag{2.13}$$

Here, dy is the change in some random variable y over a time step dt, α is a parameter measuring the rate of adaptation toward the optimum θ, dW_y is a random noise process and σ_y is the standard deviation of the random changes. Thus, evolution according to this model has two components: One is a deterministic pull toward the primary optimum and the other is a stochastic change without direction.

A layered process is introduced for modeling adaptation to a randomly changing optimum, assuming that the optimum at any point on the phylogeny (that is, the history of organismal lineages as they change through time) is a function of a randomly changing predictor variable x. Thus, the model is extended to the coupled stochastic differential equations below where the predictor indirectly influences the trait through its influence of the optimum.

$$dy = -\alpha(y - \theta(x))dt + \sigma_y dW_y \tag{2.14}$$

$$dx = \sigma_x dW_x \tag{2.15}$$

Additional layers of hidden processes may also be modeled in this way, where each layer is responding to changes in the layer beneath. The model may also be extended in that the predictor variable itself may be modeled as an Ornstein-Uhlenbeck process, tracing some optimum. The Ornstein-Uhlenbeck process has also been proposed for modeling of drought and flood risks [192] and survival data [1] and has been widely used in financial modeling [14, 21, 184].

It could be worthwhile to investigate whether an analogy to this approach would be appropriate for the development of extreme waves, i.e., whether the distribution of extreme sea states are trying to adapt to a changing mean state due to the changing environment. For example, will there be a certain average wave climate given the changing environmental conditions such as the level of CO_2 concentration in the atmosphere, global temperatures, greenhouse gas emissions etc? In other words, it could be investigated whether the distribution of extreme waves in a changing environment could be adequately modeled using layered Ornstein-Uhlenbeck processes in some way.

2.3.8 Bayesian Maximum Entropy Models

Bayesian maximum entropy (BME) models have been used to model spatio-temporal random fields. For example, in [45], this approach was used for developing a systematic epidemic forecasting methodology used to study the space-time risk patterns of influenza mortality in California during wintertime. Influenza mortality rates were represented as spatio-temporal random fields and the Bayesian maximum entropy method was used to map the rates in space and time and thus generate predictions. Bayesian maximum entropy models have also been used for space-time mapping of soil salinity [61], urban climate [122] and the contamination pattern from the Chernobyl fallout [172] and for modeling geographic distributions of species [154].

In short, the principle of maximum entropy states that the probability distribution best representing the current state of knowledge, which may be incomplete, is the one with the largest entropy. If some testable information about a probability distribution function is given, then, considering all trial probability distributions that encode this information, the probability distribution that maximizes the information entropy is the true probability distribution with respect to the testable information. This principle is applicable to problems of inference with a well-defined hypothesis space and incomplete data without noise and the Bayesian maximum entropy method can be used to predict the value of a spatio-temporal random field at an unsampled point in space-time based on precise (hard) and imprecise (soft) data.

The BME method applied to influenza mortality risk [45] consists of three stages with different knowledge bases at each stage: the general knowledge base (core knowledge), the specificatory knowledge base (case-specific knowledge) and the integration knowledge base (union of the general and specificatory knowledge bases). The influenza risk is represented as a spatio-temporal random field $X(\mathbf{p})$ defined at each space-time point $\mathbf{p} = (s, t)$. The influenza modeling approach then follows the three BME stages:

a. A probability density function, $f_g(\mathbf{x}_{\text{map}})$ is constructed on basis of the general knowledge base, where the vector $\mathbf{x}_{\text{map}}$ denotes a possible realization of the random field associated with the point vector $\mathbf{p}_{\text{map}}$. The $\mathbf{x}_{\text{map}}$ generally includes hard data $\mathbf{x}_{\text{hard}} = (x_1, \ldots, x_h)$ at points $\mathbf{p}_{\text{hard}} = (\mathbf{p}_1, \ldots, \mathbf{p}_{m_h})$, soft data $\mathbf{x}_{\text{soft}} = (x_{m_h+1}, \ldots, x_m)$ at points $\mathbf{p}_{\text{soft}} = (\mathbf{p}_{m_h+1}, \ldots, \mathbf{p}_m)$ and the unknown estimates x_k at points $\mathbf{p}_k$.
b. At the specificatory stage, the specificatory knowledge base considers hard data and soft data.
c. At the integration stage, the general and specificatory knowledge bases are combined in a total knowledge base to give the integration pdf $f_\kappa(x_\kappa)$ at each mapping point $\mathbf{p}_k$ using the operational Bayesian formula,

$$f_\kappa(x_\kappa) = A^{-1} \int_D f_g(x_{\text{map}}) d\,\Xi_S(x_{\text{soft}}) \tag{2.16}$$

where A is a normalizing constant and Ξ_S and D denote an integration operator and the range determined by the specificatory knowledge base respectively.

From the integration probability density function above, mortality estimates can be derived across space and time and an estimate of the mode is obtained by maximizing $f_\kappa(x_\kappa)$.

2.3.9 Stochastic Diffusion Models

A continuous time parameter stochastic process is referred to as a diffusion process if it possesses the Markov property and its sample paths $X(t)$ are continuous functions of time t. Many physical and other phenomena can be reasonably modeled by diffusion processes. Diffusion processes may be characterized by two infinitesimal parameters describing the mean and the variance of the infinitesimal displacements, defined as the following limits: Let the increment of the process accrued over a time interval h be $\Delta_h X(t) = X(t+h) - X(t)$, then the infinitesimal parameters of the process are:

$$\mu(x,t) = \lim_{h \to 0} E\left[\Delta_h X(t) | X(t) = x\right] \tag{2.17}$$

$$\sigma^2(x,t) = \lim_{h \to 0} E\left[\{\Delta_h (X(t)\}^2 | X(t) = x\right] \tag{2.18}$$

$\mu(x,t)$ is sometimes referred to as the drift parameter, infinitesimal mean or the expected infinitesimal displacement and $\sigma^2(x,t)$ is called the diffusion parameter or the infinitesimal variance and these are generally continuous functions in x and t. Alternative characterizations of diffusion processes exist, e.g., based on stochastic differential equations.

A methodology for analyzing secular trends in the time evolution of certain variables, modeling the variables by non-homogenous stochastic diffusion processes with time-continuous trend functions is proposed in [92]. The methodology was applied to the evolution of CO_2 emissions in Spain with the Spanish GDP as an exogenous factor affecting the trend component and hence introducing non-homogeneity. The trend can be analyzed by means of statistical fit of the trend functions of the stochastic diffusion model to the observed data, and the models were also found appropriate for medium-term forecasts.

Stochastic diffusion models have been applied to other temporal or spatial problems as well, such as modeling of tumor growth [4], ion channel gating [194], financial volatility [188] and scaling behavior of precipitation statistics [119].

2.3.10 Regional Frequency Analysis

A method commonly used in hydrology, referred to as Regional Frequency analysis, utilizes data from several similar sites in order to estimate event frequencies, typically extreme events, at a particular site. The main idea is that data from neighboring or other sites where the frequency of the event to be investigated is similar provide additional information and hence yield more accurate predictions than data from the particular site alone. This approach can also be used to interpolate to ungauged sites where there are no data, based on data from similar sites.

The main idea is that, given data from N similar sites so that one may assume the sites to form a homogeneous region, i.e., that the frequency distributions of the different sites are identical apart from a site-specific scaling factor, the quantile function of the frequency distribution at a site i can be modeled by this scaling factor and a regional quantile function common to every site, referred to as the regional growth curve:

$$Q_i(F) = \mu_i q(F), \qquad i = 1, \ldots, N \tag{2.19}$$

In the equation above, $Q_i(F)$ denotes the site-specific quantile function at site i, μ_i denotes the site-specific scaling factor, often referred to as the index flood, and $q(F)$ is the regional growth curve. F is the cumulative distribution function of the frequency distribution of the quantity of interest (e.g., significant wave height).

A typical regional frequency analysis will consist of the following four steps:

i Screening of the data: Eliminating gross errors and inconsistencies and checking whether the data are homogeneous over time
ii Identification of homogeneous regions: Assign the sites to regions whose frequency distributions are similar
iii Choice of regional frequency distribution
iv Estimating the frequency distribution: Estimating the distribution at each site to give a regional average.

A thorough description of the regional frequency analysis approach is given in [100], together with an outline of regional model estimators based on L-moments, a widely used approach for estimation in regional frequency analysis. Estimation based on Bayesian Markov chain Monte Carlo methods in regional frequency analysis was proposed in [75]. Regional frequency analysis is widely used in hydrology and there is abundant literature on applications to extreme rainfall [72, 148, 213] and flooding [121, 166]. Regional frequency analysis has also been applied in ocean engineering problems such as modeling of significant wave heights [128, 195] and the height of wave crests [105].

2.4 Selecting a Modeling Approach

In the preceding sections of this chapter, a number of different modeling approaches have been reviewed, which may all be appropriate for modeling long-term trends in extreme wave climate. However, the approach based on Bayesian hierarchical space-time models are believed to be superior and offer several benefits compared to the other approaches that has been reviewed. The hierarchical Bayesian approach to modeling data and processes with different scales of spatial and temporal variability consists of different stages (e.g., the data stage, the process stage, and the parameter stage) and such models are generally very flexible and intuitive to work with, as outlined in [209].

Some of the advantages of a hierarchical approach are the flexibility such models allow. One may build up the models in a modular, hierarchical manner where different aspects of the model can be treated separately. Extensions to the model may easily be incorporated, if necessary, and the different modules may be updated individually as knowledge and insight increase. Knowledge about physical aspects may be incorporated in the models, as illustrated by the earthquake model in [147] and such models are very flexible with regard to how they are built up. Furthermore, hierarchical models, incorporating knowledge about the physical phenomena they represent, perform better with regard to interpretation of results.

One crucial assumption applied in the model of earthquakes [147] is the Markovian assumption (i.e., that the spatial process or field in one location is only dependent on its nearest neighbours). Although this assumption needs to be challenged on a case by case basis, it is presumably a reasonable assumption also for ocean waves. Hence, it may be reasonable to model ocean waves as a random Markov field along the lines of [147].

There are also benefits from utilizing a Bayesian approach, related to the fact that knowledge about the physical process and its characteristics may be exploited by way of the prior distributions. This is clearly an advantage in modeling of physical phenomena where such knowledge are available, as is the case of ocean waves. Furthermore, by adopting a Bayesian approach the uncertainty in model parameters is taken into account. Hence, of all the modeling approaches reviewed herein, Bayesian hierarchical space-time models are believed to be the most promising candidate for further developments in long-term time-dependent stochastic modeling of extreme waves and it is suggested that further research and model development are focused in this direction. Indeed, in the following chapters of this book, various Bayesian hierarchical space-time models for significant wave height will be presented, and it is argued that they generally perform well also for modeling of oceanic sea states.

2.5 Wave Climate Projections

2.5.1 Climate Change

The IPCC's fourth assessment report states that "*Warming of the climate system is unequivocal, as is now evident from observations of increases in global average air and ocean temperatures, widespread melting of snow and ice and rising global average sea level*" [103]. It predicts further global warming and that many changes in the global climate are very likely to be larger during the twenty-first century than what has been observed during the twentieth century. Furthermore, the frequency and intensity of extreme events are expected to change as the global climate changes, some of which have already been observed. A more recent up-to-date overview on climate change research [160] has as one of its key messages that recent observations indicate that the climate change may be more severe and occur earlier than the fourth

assessment report predicts. Even though a more recent IPCC report is somewhat more moderate [104], there are reasons to believe that the future climate may be more severe than past and present climates.

However, in spite of climate change being a global phenomenon, regional variability is large, and it has been observed that for example the Arctic has warmed at double rate compared to the rest of the world in recent decades [3]. Regional differences are also presumed to be predominant in future changes of the climate, but overall, the globe is expected to warm and the intensity and frequency of extreme climatic events are likely to increase.

Hence, one important question for the stakeholders involved in maritime transport is to what extent the observed and projected global warming will influence the wave climate on short and long term and what impact this will have on the safety of maritime transportation. In the following, a review of some projections of wave climate within the context of this global warming will be presented as well as analyses of previous and current trends.

2.5.2 Current Trends in the Wave Climate

Evidence for a statistical significant increasing trend in mean wave height in the North Atlantic was observed more than 30 years ago [13, 44]. Since then, there are a number of studies reported in the literature which try to identify and assess previous and current trends in extreme wave climate, most with a focus on the North Atlantic, by different hindcast and reanalysis techniques combined with statistical analyses (see e.g., [12, 111, 193]). Some of these will be briefly outlined in the following.

Seasonal trends in extremes of significant wave height were assessed in [200, 201] for the North Atlantic and the North Pacific by simulating a 40-year global wave hindcast. For both oceans, no statistically significant changes were observed for the past century, but significant changes were found in some regions and for some seasons for the past four decades. Most notably an increase was found for the winter season in the North Atlantic, matched by a decrease in the subtropical North Atlantic and a significant increase in the North Pacific for the winter and spring seasons. Extensive validation of a 40 year global wave hindcast against available wave observations (from buoys, platforms, ships and satellites) has shown generally good agreement over the entire frequency distribution for such reanalyzed data [52].

A previous study, somewhat limited in scope with regards to the period and area covered compared to the assessments in [200, 201], reported a similar increasing trend in significant wave height at several north-east Atlantic locations since 1960, as well as a decrease south of 40°N [120]. Similar patterns were also suggested in [186]. An increase in frequency of extreme events in the last four decades were reported for the North Sea in [206], although no significant changes were found with regard to intensity and duration. Also, an analysis of wave hindcast for 1955–1994 reported in [83] suggests an increasing trend in both the North Sea and the Norwegian Sea, but with decreasing trends in other regions. A global wave climate trend analysis was

reported in [39] where an ERA-40 dataset, corrected for inhomogeneities, was used and significant increasing trends for mean, 90- and 99-percentiles were found for a large part of the global oceans. An intercomparison of significant wave height data derived from different reanalyses was presented in [38], and in spite of differences in the data quality and scope, it was reported that most of the long-term characteristics such as trends and variability, were equally present in all datasets.

Hence, most studies from the turn of the century generally agree that the wave climate of the North Atlantic became rougher in the past decades of the twentieth century. These general conclusions have been supported by analysis of microseismological data [81], by significant wave height data from ship observations [91] and by satellite altimetry data [43, 212]. Buoy measurements have also suggested an increase in wave height for the western Atlantic Ocean, but only for the summer hurricane season [114]. More recent studies observe the continuation of this increasing trend into the twenty-first century [34, 60], although there are still uncertainties as to whether, or to what extent, the trend can be ascribed to global warming [205, 211]. Increasing trends have also been found in other oceans than the Atlantic [39, 79, 163, 171].

However, it is noted that opposite trends have been reported for different regions, some studies reporting decreasing trends for particular regions [62, 135] and for different seasons (e.g., decreasing trends for the months February was reported in contrast to increasing trends in January for the Baltic Sea in [162]) so care should always be exercised when extrapolating conclusions arrived at from one location to another or from one season to another. Notwithstanding, there are evidence for a general overall trend of rougher wave climate in the North Atlantic as well as in various other ocean areas.

2.5.3 Projections of Future Trends in the Wave Climate

In light of the observed increasing trends in recent extreme wave climate in many areas of the world, a much relevant question is whether, or to what extent, this trend will prevail in the coming decades and how the future wave climate is expected to develop. In the following, a review of some attempts to make projections of future trends in the wave climate will be presented, with an emphasis on the trends for extreme waves.

The modeling approach outlined in [40], modeling extreme waves as non-homogeneous Poisson processes (NPP), utilizing the statistical relationship between wave height and sea level pressure, and compared to a non-stationary generalized extreme value model (NS-GEV), is already discussed briefly in previous sections. Previous works focusing on the relationship between wave height and sea level pressure include [199, 202, 203]. One interesting finding is that the regression model best describing the 20-year significant wave height time series toward 2099 is quadratic in time, in contrast to the the present climate where the trends are linear [37].

The changes of the projected extreme wave climate toward 2099 arrived at from the NPP model were found to be dependent on season and location and the spatial patterns were very similar for the different scenarios that were investigated. However, the magnitude of the estimated changes as well as the time evolution of the projections (i.e.,how fast the changes will occur) were scenario dependent. Comparing the projected times series of significant wave height return values obtained from the NPP and the NS-GEV models, it was found that they are highly correlated and hence compatible in some sense, but significant differences in means and variances were found, mainly in tropical areas. The seasonal projections of the 20-year significant wave height toward 2099, under different forcing scenarios and using a NPP model with parameters estimated from present climate data [40], predict significant changes in SWH_{20} in different regions of the world. The rate of future changes depends on the scenario, but under all scenarios considered, significant positive trends are predicted in the North Pacific. This is in agreement with the projections made in [170], which predict increases in significant wave height by up to 0.4 m over a wide area of the western North Pacific.

Projections of future wind, wave, and storm surge climate in the North Atlantic based on regional wave models are reported in [55, 56], where a future climate for the period 2030–2050 is compared to a control climate for the period 1980–2000. The initial study did not identify statistically significant changes in wave height [55], but when the study was revisited with more recent IPCC scenarios, the following statistically significant changes in extreme significant wave height were found: Significant increases west of the British Isles and in the eastern North Sea and in the Skagerrak and significant decreases west of 30°W [56].

Projections of extreme wave heights for the Northwest Pacific Ocean toward the year 2032 were presented in [163], based on various approaches, i.e., time-dependent Generalized Pareto-Poisson model with time-dependent event rate, Generalized Extreme Value-model with time-dependent trends in the location and scale parameters of the GEV distribution, and based on non-stationary r-largest extreme value analysis. The projected 100-year return level from the different modeling approaches showed a robust trend but with significant spread for the year 2032. Projections further into the future would yield still greater spread in the model projections. It is therefore cautioned against using projected extreme values in actual engineering problems and such projections should be considered as uncertain until the underlying causes of the long-term trends are better understood

In order to extend the confidence and coverage of future wave climate projections a proposal for a coordinated effort toward global wave climate projections was made in [96], suggesting a shift in focus from regional projections. Such a global study was recently published in [97], where projected changes in the global wave climate based on projections from an ensemble of previous studies, obtained by different models, were presented. The study reports an agreed projected decrease in annual mean significant wave height over 25.8 % of the global oceans and a projected increase over 7.1 %, predominantly in the Southern Ocean. However, a general caveat when using multimodel mean projections is that there might be a tendency of underestimating projected trends from individual models. Significant trends from different models

might cancel each other out and become insignificant in a multimodel average and it might also be difficult to interpret the multimodel results. It is also noted in [97] that the study methodology is the dominating source of uncertainty. Notwithstanding, it is noted that results presented in [97] indicate a projected decrease in the annual mean significant wave height for a notable part of the global oceans.

Other wave climate projections based on dynamical downscaling of projections from global atmosphere-ocean climate models are reported for different regions of the world in [6, 35, 98, 126, 153], the details of which will not be covered herein.

Various downscaling methods for estimation of statistics for significant wave height were investigated in [204], evaluated against the ERA-40 wave data. Statistical downscaling approaches, typically based on the observed statistical relationship between atmospheric variables and wave height were deemed better than dynamical methods, which typically involves using atmospheric variables to drive ocean wave models. Furthermore, different atmospheric covariates were analysed in nested regression models (i.e., sea level pressure anomalies, sea level pressure gradients and anomalies of seasonal mean squared surface wind speeds) and analysis of the various models suggests that it is sufficient to use the wind-based predictor alone since this model performs very similar to the full model. Projections made from the different approaches show similar patterns for both seasonal means and extremes. In wintertime, increases in the eastern and western subtropical North Atlantic and decreases most other places were the predominant pattern whereas autumn projections were characterized by increases in the mid-latitudes and eastern subtropical North Atlantic and decreases in some other areas.

Dynamic and statistical downscaling techniques were also investigated in [74], and a combination of dynamical and statistical approaches was proposed as a faster, less computational-intensive alternative to purely dynamical methods for downscaling of medium-scale wave data, a conclusion supported by [30]. The method demonstrated reasonable agreement with observed wave conditions for simulations of an near-shore area around Helgoland.

The uncertainty of the impact of climate change on future extreme wave conditions in the North Sea was investigated in [80] by running the WAM wave model [82] over an ensemble of four different climate change realizations for the 30-year period 2071–2100. Wind field data sets were obtained by simulation outputs from two global circulation models for two emission scenarios, and compared to two control scenarios. The study revealed that there are large uncertainties in the magnitude and the spatial patterns of the climate change signals, and results indicate that the uncertainties due to different climate models are larger, by a factor exceeding five in some regions, than the uncertainties related to the different scenarios. Notwithstanding these uncertainties, it was general agreement between the simulations in that extreme wave heights will increase in large parts of the North Sea and that the future frequency of severe sea states will increase due to global warming.

2.6 Summary and Conclusions

This chapter has presented a comprehensive review of the literature concerning probabilistic modeling of ocean waves and sea states. It has addressed the importance of available wave data in order to develop sensible probabilistic models, and although buoy measurements are generally regarded as most reliable, the spatial coverage of such data may be inadequate for spatial models. Alternatives exist in satellite data and in reanalysis data obtained from wave models forced by various meteorological parameters. In particular, data from the ERA-40 reanalysis project that are freely available for scientific purposes have been identified.

Numerous statistical models for extreme waves have been reported in the literature, and some of these have been presented herein. Many of these either have short-term scope or are microscopic in the sense that they focus on a particular location where wave data have been available. That is, the spatial variability is not covered by many of these models. The long-term trends and time-dependencies due to observed and projected climate change are also poorly incorporated in some of these models. There have been some attempts to develop spatio-temporal models for extreme waves, and these have been discussed herein. However, due to the modest number of attempts to establish spatio-temporal models for extreme waves, a glance at models proposed in other areas of application has also been reported. Hence, a review of some models used in earthquake modeling, storm modeling, temperature modeling, and air pollution modeling has been presented. It is suggested that similar approaches might be appropriate for spatio-temporal modeling of extreme waves and further work should focus on developing such models.

In particular, the framework of Bayesian hierarchical space-time models has been identified as a promising candidate for further development of long-term stochastic models of extreme wave climate. It is believed that such a framework offers significant improvements in the statistical understanding and modeling of extreme waves and may be used in modeling and projecting long-term trends due to climate change.

Following the review of different stochastic models, a review of projections of future wave climate has been presented. Most of these predict changes in the global wave climate toward the end of the century, but the changes are very region-dependent and also highly dependent on the methodologies and models that have been applied. However, the overall message is that, at least for some parts of the Northern Atlantic, the wave climate will tend to become rougher during the present century. This means that historic wave data may no longer be adequate as basis for design of ships and offshore structures or for use in risk assessment and that new knowledge about the time-dependence and long-term trends of extreme wave climate is of crucial importance. However, different studies of wave climate projections disagree and this just serves to illustrate the complexity and the high degree of uncertainty that persist related to future projections of regional and global wave climates. On the other hand, this should motivate further research into the statistical relationships and development of improved spatio-temporal models for extreme waves.

References

1. Aalen, O.O., Gjessing, H.K.: Survival models based on the Ornstein-Uhlenbeck process. Lifetime Data Anal. **10**, 407–423 (2004)
2. Aberg, S., Lindgren, G.: Height distribution of stochastic Lagrange ocean waves. Probab. Eng. Mech. **23**, 359–363 (2008)
3. ACIA: Arctic Climate Impact Assessment. Cambridge University Press, Cambridge (2005)
4. Albano, G., Giorno, V.: A stochastic model in tumor growth. J. Theor. Biol. **242**, 329–336 (2006)
5. Altunkaynak, A.: Significant wave height prediction by using a spatial model. Ocean Eng. **32**, 924–936 (2005)
6. Andrade, C., Pires, H., Taborda, R., Freitas, M.: Projecting future changes in wave climate and coastal response in Portugal by the end of the 21st century. J. Coast. Res. SI **50**, 253–257 (2007)
7. Andreas, E.L., Wang, S.: Predicting significant wave height off the northeast coast of the United States. Ocean Eng. **34**, 1328–1335 (2007)
8. Arena, F., Barbaro, G., Romolo, A.: Return periods of a sea storm with at least two waves higher than a fixed threshold. In: Proceedings of the 28th International Conference on Offshore Mechanics and Arctic Engineering (OMAE 2009). American Society of Mechanical Engineers (ASME) (2009)
9. Arena, F., Pavone, D.: Return period of nonlinear high wave crests. J. Geophys. Res. **111**, C08, 004 (2006)
10. Arena, F., Pavone, D.: A generalized approach for long-term modelling of extreme crest-to-trough wave heights. Ocean Model. **26**, 217–225 (2009)
11. Arena, F., Puca, S.: The reconstruction of significant wave height time series by using a neural network approach. J. Offshore Mech. Arct. Eng. **126**, 213–219 (2004)
12. Athanassoulis, G., Stefanakos, C.N.: A nonstationary stochastic model for long-term time series of significant wave height. J. Geophys. Res. **100**(C8), 16, 149–16, 162 (1995)
13. Bacon, S., Carter, D.: Wave climate changes in the North Atlantic and North Sea. Int. J. Climatol. **11**, 545–558 (1991)
14. Barndorff-Nielsen, O.E., Shephard, N.: Non-gaussian Ornstein-Uhlenbeck-based models and some of their uses in financial economics. J. R. Stat. Soc. B **63**, 167–241 (2001)
15. Battjes, J.A.: Long-term wave height distribution at seven stations around the british isles. Ocean Dyn. **25**, 179–189 (1972)
16. Baxevani, A., Borgel, C., Rychlik, I.: Spatial models for the variability of the significant wave height on the world oceans. In: Proceedings of the 17th International Offshore and Polar Engineering Conference (ISOPE 2007). The International Society of Offshore and Polar Engineering (ISOPE) (2007)
17. Baxevani, A., Caires, S., Rychlik, I.: Spatio-temporal statistical modelling of significant wave height. Environmetrics **20**, 14–31 (2009)
18. Baxevani, A., Rychlik, I., Wilson, R.J.: A new method for modelling the space variability of significant wave height. Extremes **8**, 267–294 (2005)
19. Bazargan, H., Bahai, H., Aryana, F.: Simulation of the mean zero-up-crossing wave period using artificial neural networks trained with a simulated annealing algorithm. J. Mar. Sci. Technol. **12**(1), 22–33 (2007)
20. Behrens, C.N., Lopes, H.F., Gamerman, D.: Bayesian analysis of extreme events with threshold estimation. Stat. Modelling **4**, 227–244 (2004)
21. Benth, F.E., Kallsen, J., Meyer-Brandis, T.: A non-gaussian Ornstein-Uhlenbeck process for electricity spot price modeling and derivatives pricing. Appl. Math. Finance **14**, 153–169 (2007)
22. Bitner-Gregersen, E.M., Hagen, Ø.: Uncertainties in data for the offshore environment. Struct. Saf. **7**, 11–34 (1990)

23. Bitner-Gregersen, E.M., Toffoli, A.: Uncertainties of wind sea and swell prediction from the Torsethaugen spectrum. In: Proceedings of the 28th International Conference on Offshore Mechanics and Arctic Engineering (OMAE 2009). American Society of Mechanical Engineers (ASME) (2009)
24. Bitner-Gregersen, E.M., de Valk, C.: Quality control issues in estimating wave climate from hindcast and satellite data. In: Proceedings of the 27th International Conference on Offshore Mechanics and Arctic Engineering (OMAE 2008). American Society of Mechanical Engineers (ASME) (2008)
25. Bocotti, P.: Wave mechanics for ocean engineering. Elsevier Oceanography Series. Elsevier Science B.V., New York (2000)
26. Boer, G.J., Flato, G., Reader, M.C., Ramsden, D.: A transient climate change simulation with greenhouse gas and aerosol forcing: experimental design and comparison with the instrumental record for the twentieth century. Clim. Dyn. **16**, 405–425 (2000)
27. Borgman, L.E.: Probabilities for highest wave in hurricane. J. Waterw. Harb. Coast. Eng. Div. ASCE **99**, 185–207 (1973)
28. Boukhanovsky, A.V., Krogstad, H.E., Lopatoukhin, L.J., Rozhkov, V.A.: Stochastic simulation of inhomogeneous metocean fields. parti: Annual variability. In: P. Sloot, D. Abramson, A. Bogdanov, J. Dongarra, A. Zomaya, Y. Gorbachev (eds.) Computational science—ICCS 2003, Lecture notes in computer science, vol. 2658, pp. 213–222. Springer, Heidelberg (2003)
29. Boukhanovsky, A.V., Krogstad, H.E., Lopatoukhin, L.J., Rozhkov, V.A., Athanassoulis, G.A., Stephanakos, C.N.: Stochastic simulation of inhomogeneous metocean fields. partii: Synoptic variability and rare events. In: P. Sloot, D. Abramson, A. Bogdanov, J. Dongarra, A. Zomaya, Y. Gorbachev (eds.) Computational science—ICCS 2003, Lecture notes in computer science, vol. 2658, pp. 223–233. Springer, Heidelberg (2003)
30. Breivik, Ø., Gusdal, Y., Furevik, B.R., Aarnes, O.J., Reistad, M.: Nearshore wave forecasting and hindcasting by dynamical and statistical downscaling. J. Mar. Syst. **78**, 235–243 (2009)
31. Brown, P.E., Karesen, K.F., Roberts, G.O., Tonellato, S.: Blur-generated non-separable space-time models. J. R. Stat. Soc. Ser. B **62**, 847–860 (2000)
32. Bruno, F., Guttorp, P., Sampson, P.D., Cocchi, D.: A simple non-seperable, non-stationary spatiotemporal model for ozone. Environ. Ecol. Stat. **16**, 515–529 (2009)
33. Buishand, T., de Haan, L., Zhou, C.: On spatial extremes: with application to a rainfall problem. Ann. Appl. Stat. **2**, 624–642 (2008)
34. Caires, S., Groeneweg, J., Sterl, A.: Changes in the North Sea extreme waves. In: Preprints of 9th International Workshop on Wave Hindcasting and Forecasting (2006)
35. Caires, S., Groeneweg, J., Sterl, A.: Past and future changes in the North Sea extreme waves. In: Proceedings of the 31st International Conference on Coastal Engineering (ICCE 2008) (2008)
36. Caires, S., Sterl, A.: A new nonparametric method to correct model data: application to significant wave height from ERA-40 re-analysis. J. Atmospheric Ocean. Technol. **22**, 443–459 (2005)
37. Caires, S., Sterl, A., Bidlot, J.R., Graham, N., Swail, V.: Climatological assessment of reanalysis ocean data. In: Preprints of 7th International Workshop on Wave Hindcasting and Forecasting (2002)
38. Caires, S., Sterl, A., Bidlot, J.R., Graham, N., Swail, V.: Intercomparison of different wind-wave reanalyses. J. Clim. **17**, 1893–1913 (2004)
39. Caires, S., Swail, V.: Global wave climate trend and variability analysis. In: Preprints of 8th International Workshop on Wave Hindcasting and Forecasting (2004)
40. Caires, S., Swail, V.R., Wang, X.L.: Projection and analysis of extreme wave climate. J. Clim. **19**, 5581–5605 (2006)
41. Calder, C.A.: Dynamic factor process convolution models for multivariate space-time data with application to air quality assessment. Environ. Ecol. Stat. **14**, 229–247 (2007)
42. Calder, C.A.: A dynamic process convolution approach to modeling ambient particulate matter concentrations. Environmetrics **19**, 39–48 (2008)

43. Carter, D.: Variability and trends in the wave climate of the North Atlantic: a review. In: Proceedings of the 9th International Offshore and Polar Engineering conference (ISOPE 1999). The International Society of Offshore and Polar Engineering (ISOPE) (1999)
44. Carter, D., Draper, L.: Has the north-east Atlantic become rougher? Nature **332**, 494 (1988)
45. Choi, K.M., Yu, H.L., Wilson, M.L.: Spatiotemporal statistical analysis of influenza mortality risk in the State of California during the period 1997–2001. Stoch. Env. Res. Risk Assess. **22**, S15–S25 (2009)
46. Cocchi, D., Greco, F., Trivisano, C.: Hierarchical space-time modelling of PM_{10} pollution. Atmos. Environ. **41**, 532–542 (2007)
47. Coelho, C., Ferro, C., Stephenson, D., Steinskog, D.: Methods for exploring spatial and temporal variability of extreme events in climate data. J. Clim. **21**, 2072–2092 (2008)
48. Coles, S., Pericchi, L.R., Sisson, S.: A fully probabilistic approach to extreme rainfall modeling. J. Hydrol. **273**, 35–50 (2003)
49. Coles, S., Walshaw, D.: Directional modelling of extreme wind speeds. J. R. Stat. Soc. **43**, 139–157 (1994)
50. Coles, S.G.: Regional modelling of extreme storms via max-stable processes. J. R. Stat. Soc. B **55**, 797–816 (1993)
51. Coles, S.G., Tawn, J.A.: Modelling extremes of the areal rainfall process. J. R. Stat. Soc. B **58**, 329–347 (1996)
52. Cox, A.T., Swail, V.R.: A global wave hindcast over the period 1958–1997: validation and climate assessment. J. Geophys. Res. **106**, 2313–2329 (2001)
53. Cressie, N.: Wikle, C.K.: Statistics for spatio-temporal Data. Wiley, Hoboken (2011)
54. Cunha, C., Guedes Soares, C.: On the choice of data transformation for modelling time series of significant wave height. Ocean Eng. **26**, 489–506 (1999)
55. Debernard, J., Sætra, Ø., Røed, L.P.: Future wind, wave and storm surge climate in the northern North Atlantic. Clim. Res. **23**, 39–49 (2002)
56. Debernard, J.B., Røed, L.P.: Future wind, wave and storm surge climate in the Northern Seas: a revisit. Tellus **60A**, 427–438 (2008)
57. DelBalzo, D.R., Schultz, J.R., Earle, M.D.: Stochastic time-series simulation of wave parameters using ship observations. Ocean Eng. **30**, 1417–1432 (2003)
58. Deo, M., Jha, A., Chaphekar, A., Ravikant, K.: Neural networks for wave forecasting. Ocean Eng. **28**, 889–898 (2001)
59. Diebolt, J., Guillou, A., Rached, I.: Approximation of the distribution of excesses through a generalized probability-weighted moments method. J. Stat. Plan. Inference **137**, 841–857 (2007)
60. Dodet, G., Bertin, X., Tabora, R.: Wave climate variability in the North-East Atlantic Ocean over the last six decades. Ocean Model. **31**, 120–131 (2010)
61. Douanik, A., van Meirvenne, M., Tóth, T., Serre, M.: Space-time mapping of soil salinity using probabilistic bayesian maximum entropy. Stoch. Env. Res. Risk Assess. **18**, 219–227 (2004)
62. Dupuis, H., Michel, D., Sottolichio, A.: Wave climate evolution in the Bay of Biscay over two decades. J. Mar. Syst. **63**, 105–114 (2006)
63. Durrant, T.H., Greenslade, D.J., Simmonds, I.: Validation of Jason-1 and Envisat remotely sensed wave heights. J. Atmospheric Ocean. Technol. **26**, 123–134 (2009)
64. Eastoe, E.F., Tawn, J.A.: Modelling non-stationary extremes with application to surface level ozone. J. R. Stat. Soc. Ser. C (Appl. Stat.) **58**, 25–45 (2009)
65. Egozcue, J., Pawlowsky-Glahn, V., Ortego, M.: Wave-height hazard analysis in eastern coast of Spain - Bayesian approach using generalized Pareto distribution. Adv. Geosci. **2**, 25–30 (2005)
66. Ewans, K., Bitner-Gregersen, E., Guedes Soares, C.: Estimation of wind-sea and swell components in a bimodal sea state. J. Offshore Mech. Arct. Eng. **128**(4), 265–270 (2006)
67. Fedele, F., Arena, F.: The equivalent power storm model for long-term predictions of extreme wave events. In: Proceedings of the 28th International Conference on Offshore Mechanics and Arctic Engineering (OMAE 2009). American Society of Mechanical Engineers (ASME) (2009)

68. Fedele, F., Sampath, P., Benetazzo, A., Forristall, G., Gallego, G., Yezzi, A., Tayfun, M., Cavaleri, L., Sclavo, M., Bastianini, M.: Beyond waves & spectra: Euler characteristics of ocean sea states. In: Proceedings of the 28th International Conference on Offshore Mechanics and Arctic Engineering (OMAE 2009). American Society of Mechanical Engineers (ASME) (2009)
69. Ferreira, J., Guedes Soares, C.: Modelling the long-term distribution of significant wave height with the Beta and Gamma models. Ocean Eng. **26**, 713–725 (1999)
70. Ferreira, J., Guedes Soares, C.: Modelling distributions of significant wave height. Coast. Eng. **40**, 361–374 (2000)
71. Forristall, G.Z.: How should we combine long and short term wave height distributions? In: Proceedings of the 27th International Conference on Offshore Mechanics and Arctic Engineering (OMAE 2008). American Society of Mechanical Engineers (ASME) (2008)
72. Fowler, H., Kilsby, C.: A regional frequency analysis of United Kingdom extreme rainfall from 1960 to 2000. Int. J. Clim. **23**, 1313–1334 (2003)
73. Galanis, G., Chu, P.C., Kallos, G., Kuo, Y.H., Dodson, C.T.J.: Wave height characteristics in the north Atlantic ocean: a new approach based on statistical and geometrical techniques. Stoch. Env. Res. Risk Assess. **26**, 83–103 (2012)
74. Gaslikova, L., Weisse, R.: Estimating near-shore wave statistics from regional hindcasts using downscaling techniques. Ocean Dyn. **56**, 26–35 (2006)
75. Gaume, E., Gaál, L., Viglione, A., Szolgay, J., Kohnová, S., Blöschl, G.: Bayesian MCMC approach to regional flood frequency analysis involving extraordinary flood events an ungauged sites. J. Hydrol. **394**, 101–117 (2010)
76. Gelfand, A.E., Schmidt, A.M., Benerjee, S., Sirmans, C.: Nonstationary multivariate process modeling through spatially varying coregionalization. Test **13**, 263–312 (2004)
77. Gibson, R., Forristall, G.Z., Owrid, P., Grant, C., Smyth, R., Hagen, O., Leggett, I.: Bias and uncertainty in the estimation of extreme wave heights and crests. In: Proceedings of the 28th International Conference on Offshore Mechanics and Arctic Engineering (OMAE 2009). American Society of Mechanical Engineers (ASME) (2009)
78. Gilchrist, W.G.: Statistical modelling with quantile functions. Chapman & Hall/CRC, Boca Raton (2000)
79. Gower, J.: Temperature, wind and wave climatologies, and trends from marine meteorological buoys in the northeast Pacific. J. Clim. **15**, 3709–3718 (2002)
80. Grabemann, I., Weisse, R.: Climate change impact on extreme wave conditions in the North Sea: an ensemble study. Ocean Dyn. **58**, 199–212 (2008)
81. Grevemeyer, I., Herber, R., Essen, H.H.: Microseismological evidence for a changing wave climate in the northeast Atlantic Ocean. Nature **408**, 349–352 (2000)
82. Group, T.W.: The WAM model—a third generation ocean wave prediction model. J. Phys. Oceanogr. **18**, 1775–1810 (1988)
83. Group, T.W.: Changing waves and storms in the Northeast Atlantic. Bull. Am. Meteorol. Soc. **79**, 741–760 (1998)
84. Group, T.W., Cavaleri, L., Alves, J.H., Ardhuin, F., Babanin, A., Banner, M., Belibassakis, K., Benoit, M., Donelan, M., Groeneweg, J., Herbers, T., Hwang, P., Janssen, P., Janssen, T., Lavrenov, I., Magne, R., Monbaliu, J., Onorato, M., Polnikov, V., Resio, D., Rogers, W., Sheremet, A., McKee Smith, J., Tolman, H., van Vledder, G., Wolf, J., Young, I.: Wave modelling—the state of the art. Prog. Oceanogr. **75**, 603–674 (2007)
85. Guedes Soares, C., Cunha, C.: Bivariate autoregressive models for the time series of significant wave height and mean period. Coast. Eng. **40**, 297–311 (2000)
86. Guedes Soares, C., Ferreira, A.: Representatin of non-stationary time series of significant wave height with autoregressive models. Probab. Eng. Mech. **11**, 139–148 (1996)
87. Guedes Soares, C., Ferreira, A., Cunha, C.: Linear models of the time series of significant wave height on the Southwest Coast of Portugal. Coast. Eng. **29**, 149–167 (1996)
88. Guedes Soares, C., Scotto, M.: Modelling uncertainty in long-term predictions of significant wave height. Ocean Eng. **28**, 329–342 (2001)

89. Guedes Soares, C., Scotto, M.: Application of the r largest-order statistics for long-term predictions of significant wave height. Coast. Eng. **51**, 387–394 (2004)
90. Guedes Soares, C., Weisse, R., Carretero, J.C., Alvarez, E.: A 40 years hindcast of wind, sea level and waves in European waters. In: Proceedings of the 21st International Conference on Offshore Mechanics and Arctic Engineering (OMAE 2002). American Society of Mechanical Engineers (ASME) (2002)
91. Gulev, S.K., Hasse, L.: Changes of wind waves in the North Atlantic over the last 30 years. Int. J. Climatol. **19**, 1091–1117 (1999)
92. Gutiérrez, R., Gutiérrez-Sánchez, R., Nafidi, A.: Trend analysis using nonhomogeneous stochastic diffusion processes. Emission of CO2; Kyoto protocol in Spain. Stoch. Env. Res. Risk Assess. **22**, 57–66 (2008)
93. de Haan, L.: A spectral representation for max-stable processes. Ann. Probab. **12**, 1194–1204 (1984)
94. Hagen, Ø.: Estimation of long term extreme waves from storm statistics and initial distribution approach. In: Proceedings of the 28th International Conference on Offshore Mechanics and Arctic Engineering (OMAE 2009). American Society of Mechanical Engineers (ASME) (2009)
95. Hansen, T.F., Pienaar, J., Orzack, S.H.: A comparative method for studying adaptation to a randomly evolving environment. Evolution **62**, 1965–1977 (2008)
96. Hemer, M., Church, J., Swail, V., Wang, X.: Coordinated global wave climate projections. In: Preprints of 11th International Workshop on Wave Hindcasting and Forecasting and Coastal Hazards, Symposium (2009)
97. Hemer, M.A., Fan, Y., Mori, N., Semedo, A., Wang, X.L.: Projected changes in wave climate from a multi-model ensemble. Nat. Clim. Change Adv. (online publication), 1–6 (2013)
98. Hemer, M.A., McInnes, K., Ranasinghe, R.: Future projections of the East Australian wave climate. In: Preprints of 11th International Workshop on Wave Hindcasting and Forecasting and Coastal Hazards, Symposium (2009)
99. Higdon, D.: A process-convolution approach to modelling temperatures in the North Atlantic Ocean. Environ. Ecol. Stat. **5**, 173–190 (1998)
100. Hoskins, J.R.M., Wallis, J.R.: Regional frequency analysis. Cambridge University Press, Cambridge (1997)
101. Huerta, G., Sansó, B.: Time-varying models for extreme values. Environ. Ecol. Stat. **14**, 285–299 (2007)
102. Hwang, P.A., Teague, W.J., Jacobs, G.A.: A statistical comparison of wind speed, wave height, and wave period derived from satellite altimeters and ocean buoys in the Gulf of Mexico region. J. Geophys. Res. **103**, 10, 451–10, 468 (1998)
103. IPCC: Climate change 2007: Synthesis report. Technical report. Intergovernmental Panel on Climate Change (2007)
104. IPCC: Managing the risks of extreme events and disasters to advance climate change adaptation. Cambridge University Press, Cambridge (2011)
105. Izadparast, A.H., Niedzwecki, J.M.: Estimating wave crest distributions using the method of L-moments. Appl. Ocean Res. **31**, 37–43 (2009)
106. Janssen, P.A.: Progress in ocean wave forecasting. J. Comput. Phys. **227**, 3572–3594 (2008)
107. Jenkins, A.D.: Wave duration/persistence statistics, recording interval and fractal dimension. Int. J. Offshore Polar Eng. **12**, 109–113 (2002)
108. Jönsson, A., Broman, B., Rahm, L.: Variations in the Baltic Sea wave fields. Ocean Eng. **30**, 107–126 (2002)
109. Jun, M., Stein, M.L.: An approach to producing space-time covariance functions on spheres. Technometrics **49**, 468–479 (2007)
110. Jun, M., Stein, M.L.: Nonstationary covariance models for global data. Ann. Appl. Stat. **2**, 1271–1289 (2008)
111. Kalnay, E., Kanamitsu, M., Kistler, R., Collins, W., Deaven, D., Gandin, L., Iredell, M., Saha, S., White, G., Woollen, J., Zhu, Y., Chelliah, M., Ebisuzaki, W., Higgins, W., Janowiak, J., Mo, K., Ropelewski, C., Wang, J., Leetmaa, A., Reynolds, R., Jenne, R., Joseph, D.: The NCEP/NCAR 40-year reanalysis project. Bull. Am. Meteorol. Soc. **77**, 437–471 (1996)

112. Kinsman, B.: Wind Waves: their generation and propagation on the ocean surface. Prentice-Hall, Englewood Cliffs (1965)
113. Kolovos, A., Christakos, G., Hristopulos, D., Serre, M.: Methods for generating non-separable spatiotemporal covariance models with potential environmental applications. Adv. Water Resour. **27**, 815–830 (2004)
114. Komar, P.D., Allan, J.C.: Increasing hurricane-generated wave heights along the U.S. east coast and their climate controls. J. Coastal Res. **24**, 479–488 (2008)
115. Komen, G., Cavaleri, L., Donelan, M., Hasselmann, K., Hasselmann, S., Janssen, P.: Dynamics and modelling of ocean waves. Cambridge University Press, Cambridge (1994)
116. Krogstad, H.E.: Height and period distributions of extreme waves. Appl. Ocean Res. **7**, 158–165 (1985)
117. Krogstad, H.E., Barstow, S.F.: Satellite wave measurements for coastal engineering applications. Coast. Eng. **37**, 283–307 (1999)
118. Krogstad, H.E., Barstow, S.F.: Analysis and applications of second-order models for maximum crest height. J. Offshore Mech. Arct. Eng. **126**, 66–71 (2004)
119. Kundu, P.K., Bell, T.L.: Space-time scaling behaviour of rain statistics in a stochastic fractional diffusion model. J. Hydrol. **322**, 49–58 (2006)
120. Kushnir, Y., Cardone, V., Greenwood, J., Cane, M.: The recent increase in north atlantic wave heights. J. Clim. **10**, 2107–2113 (1997)
121. Leclerc, M., Ourada, T.B.: Non-stationary regional flood frequency analysis at ungauged sites. J. Hydrol. **343**, 254–265 (2007)
122. Lee, S.J., Balling, R., Gober, P.: Bayesian maximum entropy mapping and the soft data problem in urban climate research. Ann. Assoc. Am. Geogr. **98**, 309–322 (2008)
123. Lehner, S., Koenig, T., Schulz-Stellenfleth, J.: Global statistics of extreme windspeed and sea state from SAR. In: Proceedings of the Envisat Symposium 2007. European Space Agency (2007)
124. Lemos, R.T., Sansó, B.: A spatio-temporal model for mean, anomaly and trend fields of north atlantic sea surface temperature. J. Am. Stat. Assoc. **104**, 5–18 (2009)
125. Lindgren, G.: Slepian models for the stochastic shape of individual Lagrange sea waves. Adv. Appl. Probab. **38**, 430–450 (2006)
126. Lionello, P., Cogo, S., Galati, M., Sanna, A.: The Mediterranean surface wave climate inferred from future scenario simulations. Global Planet. Change **63**, 152–162 (2008)
127. Ma, C.: Recent developments on the construction of spatio-temporal covariance models. Stoch. Env. Res. Risk Assess. **22**, S39–S47 (2008)
128. MA, Q.S., Li, Y.B., Li, J.: Regional frequency analysis of significant wave heights based on L-moments. China Ocean Eng. **20**, 85–98 (2006)
129. Machado, U., Rychlik, I.: Wave statistics in non-linear random sea. Extremes **6**, 125–146 (2003)
130. Mahjoobi, J., Etemad-Shahidi, A.: An alternative approach for the prediction of significant wave heights based on classification and regression trees. Appl. Ocean Res. **30**, 172–177 (2008)
131. Mahjoobi, J., Mosabbeb, E.A.: Prediction of significant wave height using regressive support vector machines. Ocean Eng. **36**, 339–347 (2009)
132. Majumdar, A., Gelfand, A.E.: Multivariate spatial modeling for geostatistical data using convolved covariance functions. Math. Geol. **39**, 225–245 (2007)
133. Makarynskyy, O., Pires-Silva, A., Makarynska, D., Ventura-Soares, C.: Artificial neural networks in wave predictions at the west coast of Portugal. Comput. Geosci. **31**, 415–424 (2005)
134. Mandal, S., Prabaharan, N.: Ocean wave forecasting using recurrent neural networks. Ocean Eng. **33**, 1401–1410 (2006)
135. Martucci, G., Carniel, S., Chiggiato, J., Sclavo, M., Lionello, P., Galati, M.: Statistical trend analysis and extreme distribution of significant wave height from 1958 to 1999—an appliaction to the Italian seas. Ocean Sci. Discuss. **6**, 2005–2036 (2009)
136. Meath, S.E., Aye, L., Haritos, N.: Accuracy of satellite-measured wave heights in the Australian region for wave power applications. Bull. Sci. Technol. Soc. **28**, 244–255 (2008)

137. Méndez, F.J., Menéndez, M., Luceño, A., Losada, I.J.: Estimation of the long-term variability of extreme significant wave height using time-dependent Peak Over Threshold (POT) model. J. Geophys. Res. **111**, C07, 024 (2006)
138. Méndez, F.J., Menéndez, M., Luceño, A., Medina, R., Graham, N.E.: Seasonality and duration in extreme value distributions of significant wave height. Ocean Eng. **35**, 131–138 (2008)
139. Menéndez, M., Méndez, F.J., Izaguirre, C., Luceño, A., Losada, I.J.: The influence of seasonality on estimating return values of significant wave height. Coast. Eng. **56**, 211–219 (2009)
140. Middleton, J.F., Thompson, K.R.: Return periods of extreme sea levels from short records. J. Geophys. Res. **91**, 11, 707–11,716 (1986)
141. Minoura, M., Naito, S.: Stochastic sea climate simulation based on hindcast data. In: Proceedings of the 16th International Offshore and Polar Engineering conference (ISOPE 2006). The International Society of Offshore and Polar Engineering (ISOPE) (2006)
142. Monbet, V., Ailliot, P., Prevesto, M.: Survey of stochastic models for wind and sea state time series. Probab. Eng. Mech. **22**, 113–126 (2007)
143. Monbet, V., Marteau, P.F.: Continuous space discrete time markov models for multivariate sea state parameter processes. In: Proceedings of the 11th International Offshore and Polar Engineering conference (ISOPE 2001). The International Society of Offshore and Polar Engineering (ISOPE) (2001)
144. Monbet, V., Prevosto, M.: Bivariate simulation of non stationary and non Gaussian observed processes—application to sea state parameters. Appl. Ocean Res. **23**, 139–145 (2001)
145. Muraleedharan, G., Rao, A., Kurup, P., Unnikrishnan Nair, N., Sinha, M.: Modified Weibull distribution for maximum and significant wave height simulation and prediction. Coast. Eng. **54**, 630–638 (2007)
146. Nakićenović, N., Alcamo, J., Davis, G., de Vries, B., Fenhann, J., Gaffin, S., Gregory, K., Grügler, A., Jung, T.Y., Kram, T., La Rovere, E.L., Michaelis, L., Mori, S., Morita, T., Pepper, W., Pitcher, H., Price, L., Riahi, K., Roehrl, A., Rogner, H.H., Sankovski, A., Schlesinger, M., Shukla, P., Smith, S., Swart, R., van Rooijen, S., Victor, N., Dadi, Z.: Emissions scenarios. Cambridge University Press, Cambridge (2000)
147. Natvig, B., Tvete, I.F.: Bayesian hierarchical space-time modeling of earthquake data. Methodol. Comput. Appl. Probab. **9**, 89–114 (2007)
148. Nguyen, V., Nguyen, T., Ashkar, F.: Regional frequency analysis of extreme rainfalls. Water Sci. Technol. **45**, 75–81 (2002)
149. Ochi, M.K.: Ocean waves: the stochastic approach. Cambridge Ocean Technology series no. 6. Cambridge University Press, Cambridge (1998)
150. Olsen, A., Schrøter, C., Jensen, J.: Wave height distribution observed by ships in the North Atlantic. Ships Offshore Struct. **1**, 1–12 (2006)
151. Özger, M., Şen, Z.: Triple diagram method for the prediction of wave height and period. Ocean Eng. **34**, 1060–1068 (2007)
152. Panchang, V., Zhao, L., Demirbilek, Z.: Eestimation of extreme wave heights using GEOSAT measurements. Ocean Eng. **26**, 205–225 (1999)
153. Perrie, W., Jiang, J., Long, Z., Toulany, B., Zhang, W.: NW Atlantic wave estimates and climate change. In: Preprints of 8th International Workshop on Wave Hindcasting and Forecasting (2004)
154. Phillips, S.J., Anderson, R.P., Schapire, R.E.: Maximum entropy modeling of species geographic distributions. Ecol. Model. **190**, 231–259 (2006)
155. Prevesto, M., Krogstad, H.E., Robin, A.: Probability distributions for maximum wave and crest heights. Coast. Eng. **40**, 329–360 (2000)
156. Queffeulou, P.: Long-term validation of wave height measurements from altimeters. Mar. Geodesy **27**, 495–510 (2004)
157. Reitan, T., Schweder, T., Henderiks, J.: Phenotypic evolution studied by layered stochastic differential equations. Ann. Appl. Stat. **6**, 1531–1551 (2012)
158. Renard, B., Lang, M., Bois, P.: Statistical analysis of extreme events in a non-stationary context via a Bayesian framework: case study with peak-over-threshold data. Stoch. Env. Res. Risk Assess. **21**, 97–112 (2006)

159. Ribereau, P., Guillou, A., Naveau, P.: Estimating return levels from maxima of non-stationary random sequences using the Generalized PWM method. Nonlinear Process. Geophys. **15**, 1033–1039 (2008)
160. Richardson, K., Steffen, W., Schellnhuber, H.J., Alcamo, J., Barker, T., Kammen, D.M., Leemans, R., Liverman, D., Munasinghe, M., Osman-Elasha, B., Stern, N., Wæver, O.: International scientific congress climate change: global risks, challenges & decisions—synthesis report. Technical report, International Alliance of Research Universities (2009)
161. Robert, C.P., Casella, G.: Monte Carlo statistical methods, 2nd edn. Springer, Heidelberg (2004)
162. Różyński, G.: Long-term evolution of Baltic Sea wave climate near a coastal segment in Poland; its drivers and impacts. Ocean Eng. **37**, 186–199 (2010)
163. Ruggiero, P., Komar, P.D., Allan, J.C.: Increasing wave heights and extreme value projections: the wave climate of the U.S. Pacific Northwest. Coast. Eng. **57**, 539–552 (2010)
164. Rychlik, I.: On some reliability applications of Rice's formula for the intensity of level crossings. Extremes **3**, 331–348 (2000)
165. Rydén, J.: A note on asymptotic approximations of distributions for maxima of wave crests. Stoch. Env. Res. Risk Assess. **20**, 238–242 (2006)
166. Saf, B.: Assessment of the effects of discordant sites on regional flood frequency analysis. J. Hydrol. **380**, 362–375 (2010)
167. Sahu, S.K., Gelfand, A.E., Holland, D.M.: High resolution space-time ozone modeling for assessing trends. J. Am. Stat. Assoc. **102**, 1212–1220 (2007)
168. Sang, H., Gelfand, A.E.: Hierarchical modeling for extreme values observed over space and time. Environ. Ecol. Stat. **16**, 407–426 (2009)
169. Sansó, B., Schmidt, A.M., Nobre, A.A.: Bayesian spatio-temporal models based on discrete convolutions. Can. J. Stat. **36**, 239–258 (2008)
170. Sasaki, W., Hibiya, T., Kayahara, T.: Interannual variability and future projections of summertime ocean wave heights in the western North Pacific. Ocean Sci. Discuss. **3**, 1637–1651 (2006)
171. Sasaki, W., Iwasaki, S., Matsuura, T., Iizuka, S.: Recent increase in summertime extreme wave heights in the western North Pacific. Geophys. Res. Lett. **32**, L15, 607 (2005)
172. Savelieva, E., Demyanov, V., Kanevski, M., Serre, M., Christakos, G.: BME-based uncertainty assessment of the Chernobyl fallout. Geoderma **128**, 312–324 (2005)
173. Schmidt, A.M., Gelfand, A.E.: A Bayesian coregionalization approach for multivariate pollutant data. J. Geophys. Res. **108**, STS 10 (2003)
174. Scotto, M., Guedes Soares, C.: Modelling the long-term time series of significant wave height with non-linear threshold models. Coast. Eng. **40**, 313–327 (2000)
175. Scotto, M., Guedes Soares, C.: Bayesian inference for long-term prediction of significant wave height. Coast. Eng. **54**, 393–400 (2007)
176. Smith, E.L., Stephenson, A.G.: An extended gaussian max-stable process model for spatial extremes. J. Stat. Plan. Inference **139**, 1266–1275 (2009)
177. Soukissian, T.H., Kalantzi, G., Karagali, I.: De-clustering of Hs-time series for applying the peaks-over-threshold method. In: Proceedings of the 16th International Offshore and Polar Engineering conference (ISOPE 2006). The International Society of Offshore and Polar Engineering (ISOPE) (2006)
178. Soukissian, T.H., Kalantzi, G.D.: Extreme value analysis methods used for extreme wave prediction. In: Proceedings of the 16th International Offshore and Polar Engineering conference (ISOPE 2006). The International Society of Offshore and Polar Engineering (ISOPE) (2006)
179. Soukissian, T.H., Kalantzi, G.D.: A new method for applying the r-largest maxima model for design sea-state prediction. In: Proceedings of the 17th International Offshore and Polar Engineering Conference (ISOPE 2007). The International Society of Offshore and Polar Engineering (ISOPE) (2007)
180. Soukissian, T.H., Photiadou, C.S.: A sensitivity analysis of the bottom-up algorithm for the segmentation of H_s-time series. In: Proceedings of the 16th International Offshore and Polar Engineering conference (ISOPE 2006). The International Society of Offshore and Polar Engineering (ISOPE) (2006)

181. Soukissian, T.H., Samalekos, P.E.: Analysis of the duration and intensity os sea states using segmentation of significant wave height time series. In: Proceedings of the 16th International Offshore and Polar Engineering conference (ISOPE 2006). The International Society of Offshore and Polar Engineering (ISOPE) (2006)
182. Stefanakos, C.N., Athanassoulis, G.A.: Extreme value predictions based on nonstationary time series of wave data. Environmetrics **17**, 25–46 (2006)
183. Stefanakos, C.N., Monbet, V.: Estimation of wave height return periods using a nonstationary time series modelling. In: Proceedings of the 25th International Conference on Offshore Mechanics and Arctic Engineering (OMAE 2006). American Society of Mechanical Engineers (ASME) (2006)
184. Stein, E.M., Stein, J.C.: Stock price distributions with stochastic volatility: an analytic approach. Rev. Financial Stud. **4**, 727–752 (1991)
185. Sterl, A., Caires, S.: Climatology, variability and extrema of ocean waves: the web-based KNMI/ERA-40 wave atlas. Int. J. Climatol. **25**, 963–977 (2005)
186. Sterl, A., Komen, G., Cotton, P.: Fifteen years of global wave hindcasts using winds from the European Centre for Medium-Range Weather Forecast reanalysis: validating the reanalyzed winds and assessing the wave climate. J. Geophys. Res. **103**, 5477–5492 (1998)
187. Swail, V.R., Cox, A.T.: On the use of NCEP-NCAR reanalysis surface marine wind fields for a long-term North Atlantic wave hindcast. J. Atmospheric Ocean. Technol. **17**, 532–545 (2000)
188. Todorov, V.: Estimation of continuous-time stochastic volatility models with jumps using high-frequency data. J. Econom. **148**, 131–148 (2009)
189. Torsethaugen, K.: A two-peak wave spectral model. In: Proceedings of the 12th International Conference on Offshore Mechanics and Arctic Engineering (OMAE 1993). American Society of Mechanical Engineers (ASME) (1993)
190. Torsethaugen, K., Haver, S.: Simplified double peak spectral model for ocean waves. In: Proceedings of the 14th International Offshore and Polar Engineering conference (ISOPE 2004). The International Society of Offshore and Polar Engineering (ISOPE) (2004)
191. Trulsen, K.: Weakly nonlinear and stochastic properties of ocean wave fields. application to an extreme wave event. In: J. Grue, K. Trulsen (eds.) Waves in geophysical fluids—Tsunamis, rogue waves, internal waves and internal tides, CISM Courses and lectures No. 489, pp. 49–106. Springer, Heidelberg (2006)
192. Unami, K., Abagale, F.K., Yangyuoru, M., Alam, A.H.M.B., Kranjac-Berisavljevic, G.: A stochastic differential equation model for assessing drought and flood risks. Stoch. Env. Res. Risk Assess. **24**, 725–733 (2010)
193. Uppala, S.M., Kållberg, P.W., Simmons, A.J., Andrae, U., Da, Costa Bechtold, V., Fiorino, M., Gibson, J.K., Haseler, J., Hernandez, A., Kelly, G.A., Li, X., Onogi, K., Saarinen, S., Sokka, N., Allan, R.P., Andersson, E., Arpe, K., Balmaseda, M.A., Beljaars, A.C.M., Van de Berg, L., Bidlot, J., Bormann, N., Caires, S., Chevallier, F., Dethof, A., Dragosavac, M., Fisher, M., Fuentes, M., Hagemann, S., Hólm E. Hoskins, B.J., Isaksen, L., Janssen, P.A.E.M., Jenne, R., McNally, A.P., Mahfouf, J.F., Morcrette, J.J., Rayner, N.A., Saunders, R.W., Simon, P., Sterl, A., Trenberth, K.E., Untch, A., Vasiljevic, D., Vitebro, P., Woolen, J.: The ERA-40 re-analysis. Q. J. R. Meteorol. Soc. **131**, 2961–3012 (2005)
194. Vaccaro, S.: Position-dependent stochastic diffusion model of ion channel gating. Phys. Rev. E **78**, 061, 915 (2008)
195. Van Gelder, P., De Ronde, J., Neykov, N.M., Neytchev, P.: Regional frequency analysis of extreme wave heights: trading space for time. In: B.L. Edge (ed.) Coastal engineering (2000), Proceedings of the 27th International Conference on Coastal Engineering Held in Sydney, Australia, July 16–21, 2000, pp. 1099–1112. American Society of Civil Engineers (2001)
196. Vanem, E.: Long-term time-dependent stochastic modelling of extreme waves. Stoch. Env. Res. Risk Assess. **25**, 185–209 (2011)
197. de Waal, D., van Gelder, P.: Modelling of extreme wave heights and periods through copulas. Extremes **8**, 345–356 (2005)

198. Walton, T.L., Borgman, L.E.: Simulation of nonstationary, non-Gaussian water levels on Great Lakes. J. Waterw. Port Coast. Ocean Eng. **116**, 664–685 (1990)
199. Wang, X.J., Zwiers, F.W., Swail, V.R.: North Atlantic ocean wave climate change scenarios for the twenty-first century. J. Clim. **17**, 2368–2383 (2004)
200. Wang, X.L., Swail, V.R.: Changes of extreme wave heights in northern hemisphere oceans and related atmospheric circulation regimes. J. Clim. **14**, 2204–2221 (2001)
201. Wang, X.L., Swail, V.R.: Trends of Atlantic wave extremes as simulated in a 40-yr wave hindcast using kinematically reanalyzed wind fields. J. Clim. **15**, 1020–1035 (2002)
202. Wang, X.L., Swail, V.R.: Climate change signal and uncertainty in projections of ocean wave heights. Clim. Dyn. **26**, 109–126 (2006)
203. Wang, X.L., Swail, V.R.: Historical and possible future changes of wave heights in northern hemisphere oceanc. In: W. Perrie (ed.) Atmosphere-ocean interactions, Advances in fluid mechanics, vols. 2, 39, pp. 185–218. WIT Press, Southampton (2006)
204. Wang, X.L., Swail, V.R., Cox, A.: Dynamical versus statistical downscaling methods for ocean wave heights. Int. J. Climatol. **30**, 317–332 (2010)
205. Wang, X.L., Swail, V.R., Zwiers, F.W., Zhang, X., Feng, Y.: Detection of external influences on trends of atmospheric storminess and northern oceans wave heights. Clim. Dyn. **32**, 189–203 (2009)
206. Weisse, R., Stawarz, M.: Long-term changes and potential for future developments of the North Sea wave climate. In: Preprints of 8th International Workshop on Wave Hindcasting and Forecasting (2004)
207. West, M., Harrison, J.: Bayesian forecasting and dynamic models, 2nd edn. Springer, Heidelberg (1997)
208. Wikle, C.K.: Hierarchical models in environmental science. Int. Stat. Rev. **71**, 181–199 (2003)
209. Wikle, C.K., Berliner, L.M., Cressie, N.: Hierarchical Bayesian space-time models. Environ. Ecol. Stat. **5**, 117–154 (1998)
210. Wikle, C.K., Milliff, R.F., Nychka, D., Berliner, L.M.: Spatiotemporal hierarchical Bayesian modeling: tropical ocean surface winds. J. Am. Stat. Assoc. **96**, 382–397 (2001)
211. Wolf, J., Woolf, D.K.: Waves and climate change in the north-east Atlantic. Geophys. Res. Lett. **33**, L06, 604 (2006)
212. Woolf, D., Challenor, P., Cotton, P.: Variability and predictability of the North Atlantic wave climate. J. Geophys. Res. **107**, 9(1–14) (2002)
213. Yang, T., Shao, Q., Hao, Z.C., Chen, X., Zhang, Z., Xu, C.Y., Sun, L.: Regional frequency analysis and spatio-temporal pattern characterization of rainfall extremes in the Pearl River Basin, China. J. Hydrol. **380**, 386–405 (2010)
214. Yoon, S., Cho, W., Heo, J.H.: A full Bayesian approach to generalized maximum likelihood estimation of generalized extreme value distribution. Stoch. Env. Res. Risk Assess. **24**, 761–770 (2010)
215. Zhang, H.: Maximum-likelihood estimation for multivariate spatial linear coregionalization models. Environmetrics **18**, 125–139 (2007)

Chapter 3
A Bayesian Hierarchical Space-Time Model for Significant Wave Height

In the previous chapter, a literature survey on statistical models for ocean waves was reported, and based on this review, the Bayesian hierarchical space-time modeling approach was selected for modeling of significant wave height. In this chapter, such a model will be outlined and the results obtained from fitting the model to significant wave height data for an area in the North Atlantic Ocean will be discussed. Parts of this chapter have been previously presented in [30, 31].

3.1 Data and Area to be Considered

3.1.1 Data Description

There are various sources of data for significant wave height, as discussed in [28] and in the previous chapter. For the purpose of building a space-time model, data with both spatial and temporal coverage are needed, and data sources are less numerous. In this study, the modeling has been based on the ERA-40 data of significant wave height.

The reanalysis project ERA-40 [27] was carried out by the European Centre for Medium-Range Weather Forecasts (ECMWF) and covers the 45-year period from September 1957 to August 2002. Data obtained from this reanalysis include i.a. six-hourly fields of global wave parameters such as significant wave height, mean wave direction and mean wave period, as well as meteorological parameters such as mean sea level pressure and wind fields. A large part of this dataset is freely available for research purposes and may be downloaded from their website.[1] Global, continuous data are available on a $1.5° \times 1.5°$ grid, making this perhaps the most complete wave dataset available to date.

[1] Data available from URL: http://data-portal.ecmwf.int/data/d/era40_daily/

E. Vanem, *Bayesian Hierarchical Space-Time Models with Application to Significant Wave Height*, Ocean Engineering & Oceanography 2,
DOI: 10.1007/978-3-642-30253-4_3, © Springer-Verlag Berlin Heidelberg 2013

It has been reported that the ERA-40 dataset contains some inhomogeneities in time and that it underestimates high wave heights [24]. Both these limitations indicate problems in using these data for modeling long-term trends in extreme waves, but corrected datasets for the significant wave height have been produced in order to cope with these deficiencies in the original data [6]. Hence, a new 45-year global six-hourly dataset of significant wave height has been created, and when compared to buoy measurement and global altimeter data, this corrected dataset, referred to as the C-ERA-40 data, shows clear improvements compared to the original data [7]. Hence, this corrected dataset, which was kindly provided by the Royal Netherlands Meteorological Institute (KNMI)[2] has been used in this study. It includes fields of significant wave height sampled every 6th hour with a spatial resolution of $1.5° \times 1.5°$ covering the period from January 1958 to February 2002 (i.e., a total of 44 years and 2 months which corresponds to a sequence of 64 520 points in time).

For the purpose of this study, it is emphasized that all modeling and all results are conditional on the input data. Hence, data validation and assessment of data uncertainty are considered out of scope of this study. It is also noted that physical phenomena such as wave breaking and the physical limits to steepness of ocean waves need not be modeled explicitly in this case [3, 25]. The significant wave height data inarguably incorporate any such effects and hence it is argued that, by way of the data, these and related effects are already implicitly accounted for. However, it may affect future projections if there are strong increasing trends so that future wave climate will contain larger waves than what is recorded in the data, possibly influencing the physical processes involved.

3.1.2 Area Description

For the purpose of this study, an area in the North Atlantic Ocean between 51°–63° north and 12°–36° west (324°–348° east) will be considered. For this area, the dataset is complete and there are no missing data. Even though this particular study is restricted to this area in the North Atlantic, it is assumed that the structure of the model will be general enough to be fitted and used in other ocean areas as well (see also the results in Chap. 8 where the model has been applied to 11 other ocean areas around the globe).

The spatial resolution of the data is $1.5° \times 1.5°$, hence a grid of $9 \times 17 = 153$ data points covers the area. It is noted that due to the curvature of the surface of the earth, the distance between grid points will not be constant throughout the area. In particular, the distance between data points will vary with latitude; the distance in the north–south direction is fairly constant but the distance in the longitudinal direction (east–west) differs significantly for different latitudes [29]. Notwithstanding, in the following analysis of spatial variability the fact that the area is curved will be ignored. The area under consideration is illustrated on a map in Fig. 3.1.

[2] Private communication with Dr. Andreas Sterl, KNMI.

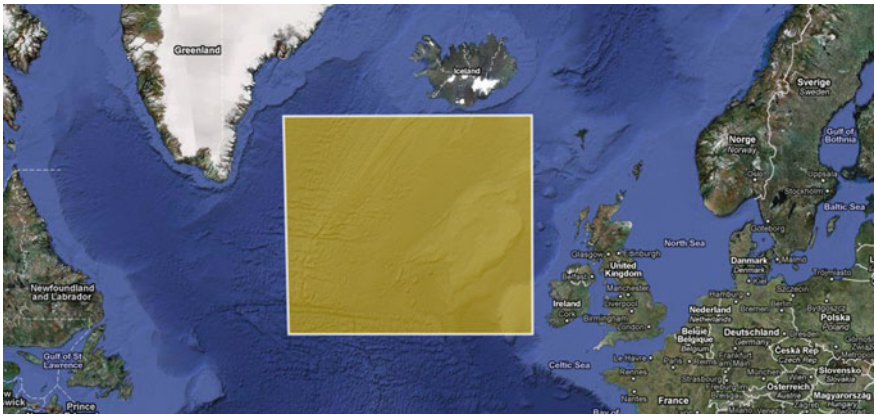

Fig. 3.1 The area of the North Atlantic Ocean under consideration

3.1.3 Initial Data Analysis

Before developing the spatio-temporal models for the significant wave height data, an initial data analysis and data inspection will be performed to get a feel of the data at hand, and also to ensure that the data look reasonable. Identification of missing data is also a part of the initial data analysis, but the area described above is selected so that it does not contain missing data.

The original data were tested for normality, and such tests failed, as illustrated by the normal probability plot of all the data in Fig. 3.2. Similar tests were also performed for all data at the same locations and for all data at the same times, but neither subsets of the data were Gaussian. A few parametric distributions were also tried fitted directly to the data, i.e., the log-normal, Weibull, gamma, skew-normal, and GEV distributions, but neither seemed to fit very well and all were rejected. The empirical mean and standard deviation in the data are 3.48 and 1.80 m respectively.

The densities of the monthly data together with the monthly maximum data are shown in Fig. 3.3. For the monthly maximum data, two distinct modes can be identified, one around 5 m and another at about 8 m. It is believed that these correspond to different characteristics during calm and rough seasons. For the whole dataset, the mean monthly maximum is 7.5 m, but the average monthly maxima for each month varies from 4.42 (July) to 9.87 (January) (see Table 3.1). The density plots for individual months (Fig. 3.4) reveal that the months January–March and October–December have peaks around 8 m and the months May–August around 5 m. The remaining months seem to be rather flat with most probability mass between 5 and 8 m. Hence, the two modes in the density may be explained by typical monthly maximum at 5 or 8 m for calm and rough seasons respectively.

The data were also investigated for trends, both with respect to the temporal and spatial mean and the maxima of individual months over the period. Indications of positive trends could be seen for some months, but not for others. These observations

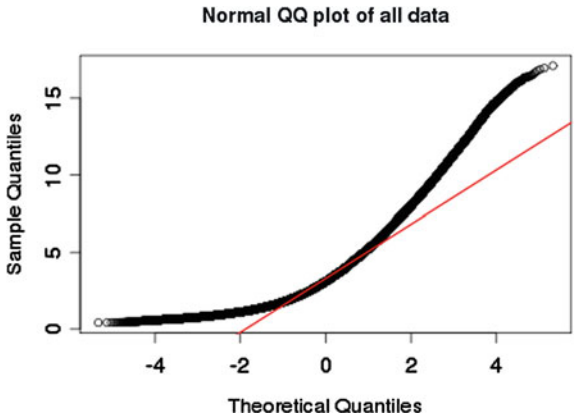

Fig. 3.2 Normal Probability plot of the data

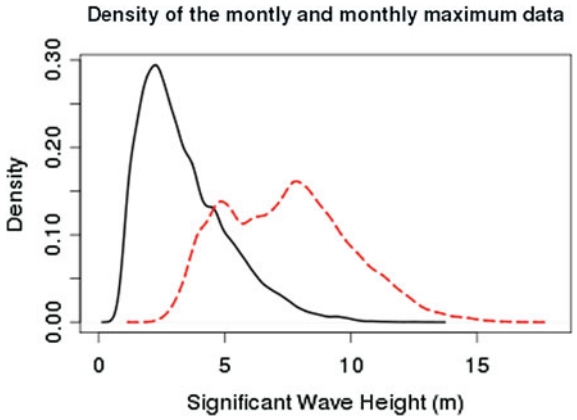

Fig. 3.3 The density of the monthly data and the monthly maximum data

Table 3.1 Average monthly maxima for each month

January	February	March	April	May	June	July	August	September	October	November	December
9.87	9.63	8.91	7.18	5.89	5.03	4.42	5.04	6.96	8.21	8.69	9.79

are supported by various time series trend analyses presented in [33]. Since the available data are space-time data, it may be sensible to do an initial data analysis independently in space and time, and highlights from temporal and spatial analyses are presented below (also reported in [29]).

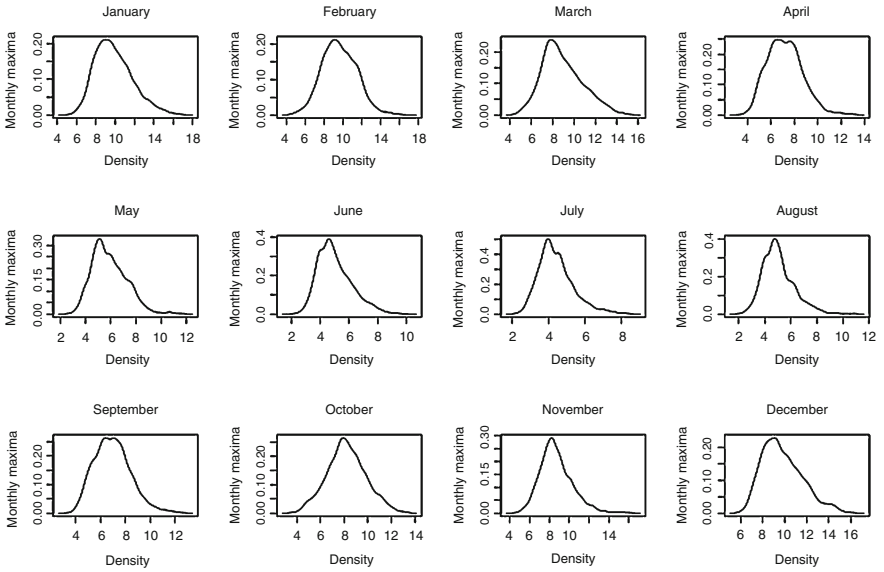

Fig. 3.4 The density of the monthly maximum data for each month

3.1.3.1 Temporal Analysis

In order to carry out an initial temporal analysis of the data, a particular location within the area was selected, i.e., the time series of significant wave height at 57°N 36°W has been subject to an initial temporal analysis. This choice of location is arbitrary, but similar analyses for other locations have also been made and the same features were displayed at all locations, yielding similar results. Hence, the analysis below is presumed to be representative for the whole area.

The first test was to inspect the time-series for normality or lognormality. Such tests were rejected by formal statistical tests, and it is also straightforward to reject normality and log-normality based on simple visual checks; it is clearly seen that the data neither follow a normal nor a lognormal probability law. It was then tried to fit various other parametric models to the data: the Weibull, gamma, skew-normal and GEV distributions. These performed quite similarly, although the skew-normal seemed to yield the best fit (it also has the highest log-likelihood).

It is noted that the significant wave height is always positive, and it was also discovered that the distribution of significant wave height is quite skewed. Therefore, the seasonal mean was removed and the variation around this mean value was investigated. Then a few different parametric models were fitted to the data where the seasonal mean had been removed and it was observed that, among them, the skew-normal distribution was still the best fit, albeit not a very good fit.

In order to check if there are any visible detectable trends in the data after the seasonal mean has been removed, the time-series for the mean and maximum of each

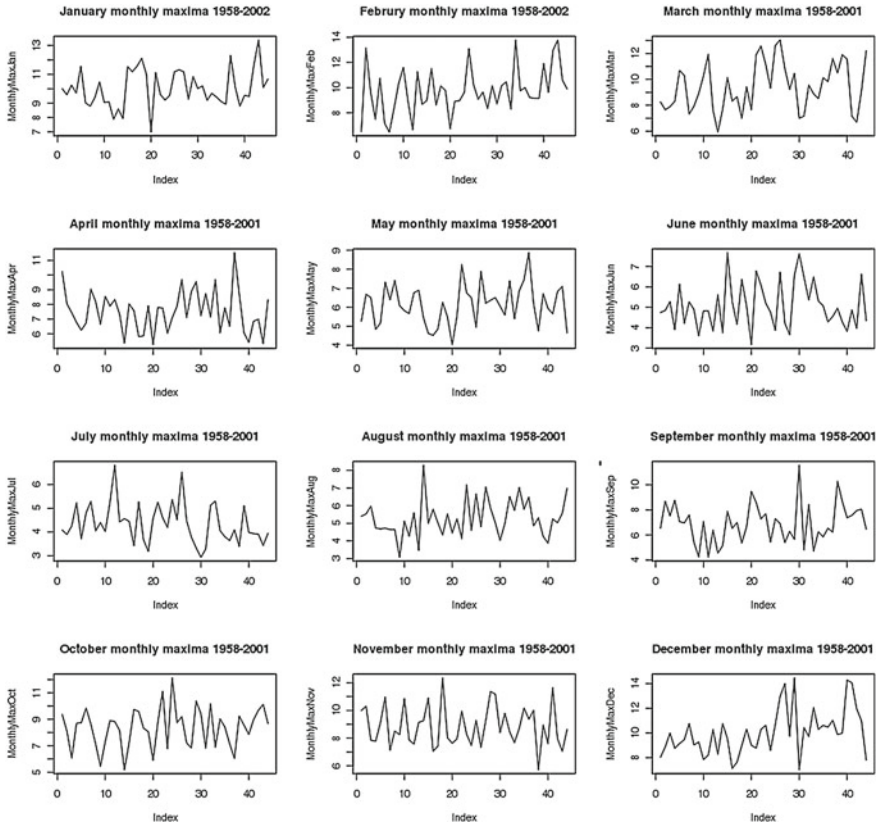

Fig. 3.5 Time series for monthly maxima at one location

month were investigated (time series for maximum significant wave height for each month is plotted in Fig. 3.5). From these investigations, it is observed that upward trends can be detected for some months, but not for others.

In order to have a look at the temporal dependence, plots of the autocorrelation function were produced for the original data, without removing the seasonal mean. It appears from these plots that there is strong cyclic temporal correlation which does not decline notably for increasing lags. It is observed that the period of this cyclic dependence is about 1 year and clearly there is a strong seasonal effect. Trying to fit an autoregressive time-series model to these data results in a model of order 48, indicating a quite complex temporal dependence structure.

The autocorrelation function for the data with the seasonal mean removed would give a better idea of the temporal dependence in the data and plots of this autocorrelation function are shown in Fig. 3.6. The upper plot includes all data (4 per day) and the lower plot shows the autocorrelation function for daily data. Now the temporal dependence quickly decays and is low for temporal distances of more than 5–6 days. Fitting an autoregressive model on the form of Eq. 3.1 to these data, with zero-mean

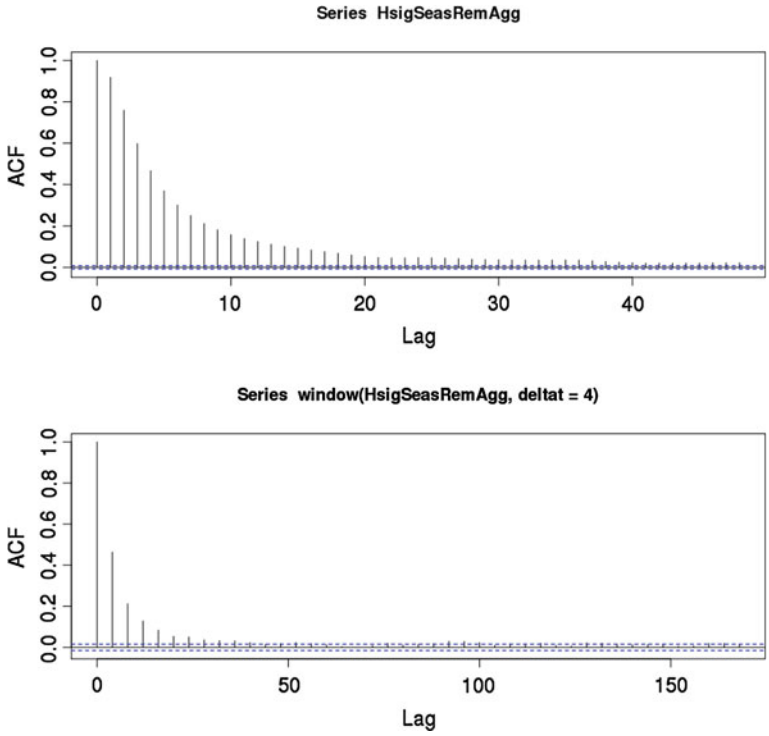

Fig. 3.6 Autocorrelation function with seasonal mean subtracted; all data (*top*) and daily data (*bottom*)

Table 3.2 Autoregressive model parameters

Parameters	All data (order 3)	Daily data (order 1)
a_1	1.4939	0.4641
a_2	−0.7657	–
a_3	0.1671	–
σ^2	0.2258	1.616

normal error terms, $\varepsilon_t \sim N(0, \sigma^2)$, it is found that when considering all data, an autoregressive model of order 3 would be appropriate ($m = 3$), whereas for daily data a first-order model would suffice ($m = 1$). The model parameters obtained for the two alternative models (six-hourly or daily data) are shown in Table 3.2.

$$H_s(t) = a_1 H_s(t-1) + a_2 H_s(t-2) + \cdots + a_m H_s(t-m) + \varepsilon_t \tag{3.1}$$

These results seem to indicate a somewhat shorter memory of the significant wave height time series compared to the autoregressive models presented in [11], but it should be kept in mind that the latter used three-hourly data and considered another location so direct comparison is not possible. The difficulty of using linear

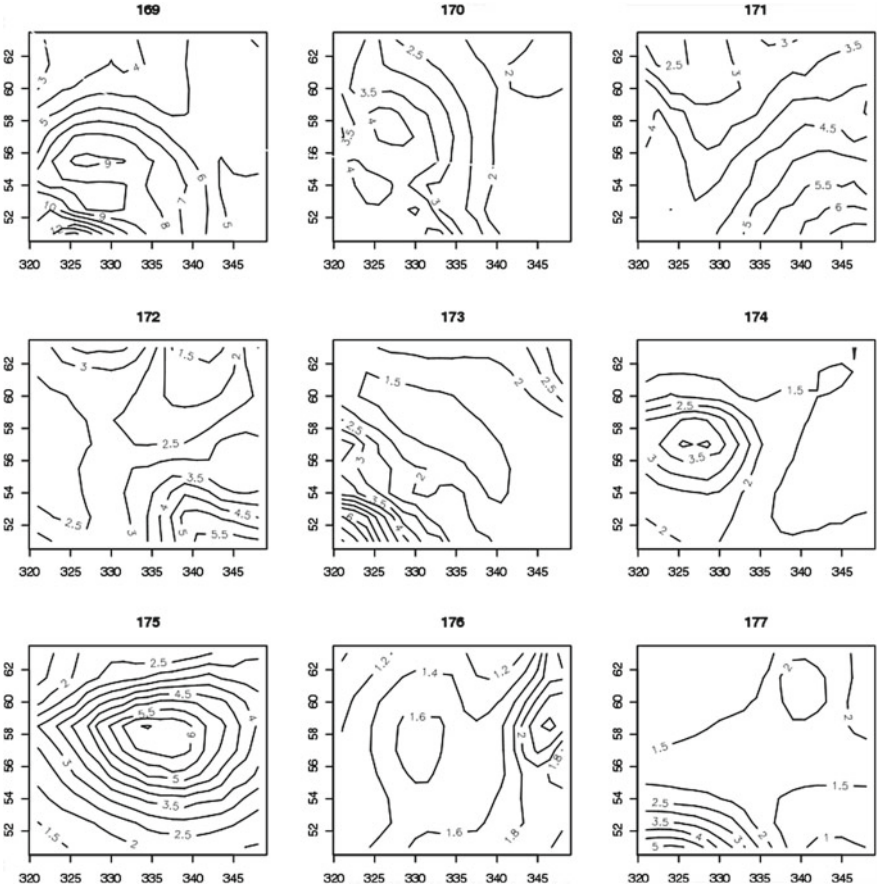

Fig. 3.7 Contour plots of the spatial fields at arbitrary selected times

autoregressive models for time series of significant wave height is also discussed in [21].

3.1.3.2 Spatial Analysis

Having performed a crude temporal analysis at some locations, an initial spatial analysis is performed as well. Fields of significant wave height covering the whole area were considered at arbitrary selected time points and contour-plots of the spatial fields at these times were produced. An example of nine contour plots of such spatial fields is shown in Fig. 3.7, showing the fields at the seventh day of January through September of 1972. In order to check whether the spatial data are Gaussian or lognormally distributed, histograms and QQ-plots were produced, and visual tests

clearly demonstrate that the spatial data follow neither a normal nor a log-normal probability law (not shown herein).

In order to see whether a simple linear regression model with the N- and E-coordinates as covariates could describe the spatial variation in the data, a linear regression model on the form of Eq. 3.2 was fitted to the data for spatial fields at selected time points.

$$H_s = \beta_0 + \beta_1 N + \beta_2 E + \varepsilon \tag{3.2}$$

Here, N denotes the lateral coordinate (north) while E denotes the longitudinal coordinate (east). The βs are model parameters and ε denotes error terms, assumed iid normal. Inspecting various residual plots resulting from such a model shows that the error terms will not be normal, and the model is rejected. One may also try including an interaction term between the N- and E-coordinates in the model, Eq. 3.3, but this did not improve the model much.

$$H_s = \beta_0 + \beta_1 N + \beta_2 E + \beta_3 (N \cdot E) + \varepsilon \tag{3.3}$$

It is realized that comparing data from different months may not be wise, considering the strong seasonal component in the data, so one may want to consider only data from 1 month at a time. However, upon inspection of the data, it is realized that the data are still not normally or log-normally distributed. Furthermore, linear regression models, with or without interaction terms, are again easily rejected based on graphical plots of the residuals. Finally, a linear regression model including interaction terms was also fitted for the logarithm of the data but also this model was rejected based on visual checks of the residuals. Hence, such linear regression models cannot explain the spatial variation of the H_s-values in the data and such simple models for the spatial variation are rejected. It is concluded from this crude initial data inspection that a more complex dependence structure is present in the data, and a more sophisticated spatio-temporal stochastic model will be developed to capture these.

3.1.3.3 Initial Spatio-Temporal Analysis

In order to see if there are any detectable temporal trends in the spatial fields, the time series of the spatial mean of each field is plotted. One may also check for trends in the spatial maxima in the same way. However, the time series are quite noisy, and it is difficult to detect long-term trends. This may be partly due to the fact that different months are plotted together, and plots of the spatial maxima for each individual month are plotted in Fig. 3.8. Analysing these time-series, some upward trends can be detected for both the mean and the maxima for some months, albeit not all. Various time-series trend analyses on spatially reduced time series are also presented in [33].

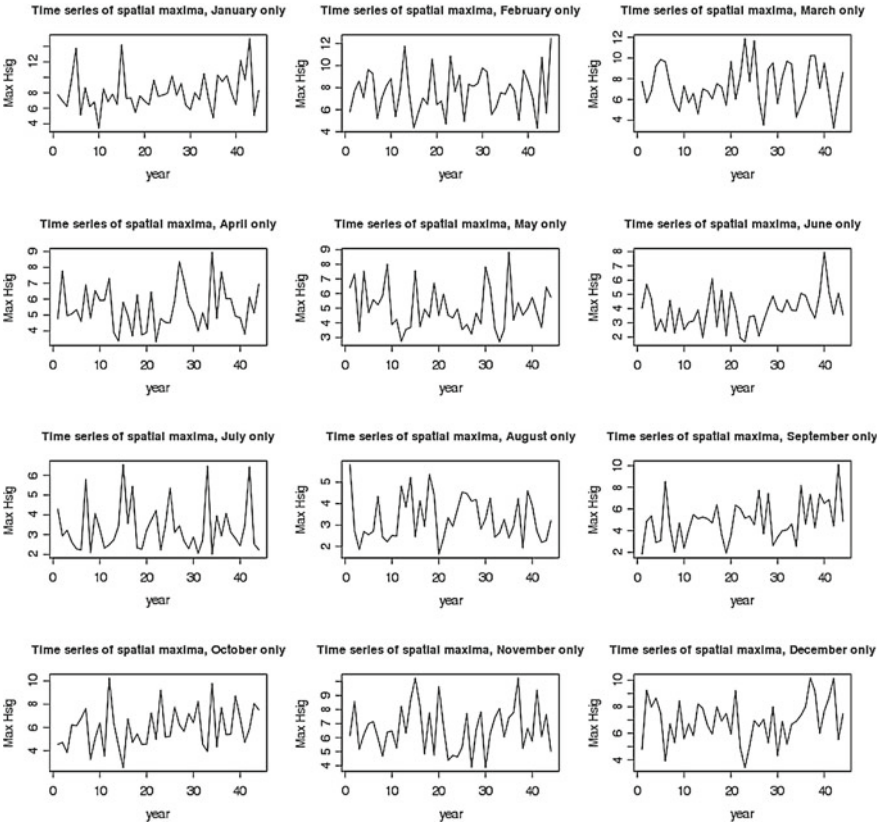

Fig. 3.8 Time series of spatial maxima for individual months

3.2 Model Description

From the initial data-inspection, it is clear that the data cannot be well described by a simple Gaussian model or as a linear regression model with the spatial coordinates as covariates; a somewhat more sophisticated model must be constructed. Hierarchical models are known to model spatio-temporal processes with complex dependence structures at different scales [37]. Therefore, a Bayesian hierarchical space-time model, along the lines drawn out by e.g. [38] will be attempted to model the significant wave height data in space and time, modeling the spatial and temporal variation by conditional probabilities.

The spatio-temporal data will be indexed by two indices; an index x to denote spatial location with $x = 1, 2, \ldots, X = 153$ and an index t to denote a point in time with $t = 1, 2, \ldots, T = 64{,}520$. Hence, each data-point in the rather huge set of data (nearly 10 million data points) is unambiguously identified by these two indices.

The spatial dependencies will be modeled as a Markov random field (MRF) with dependence on nearest neighbours in all cardinal directions (some basic theory pertaining to Markov random fields are given in Appendix C; further details may be found in for example [22]). The temporal dependence is modeled by three terms. Two, assumed independent in space, are included to model the strong seasonal dependence in the data and possible long term temporal trends. The last one, a short-term temporal contribution with a spatial description, is modeled as a vector autoregressive model of order one, conditionally dependent on the nearest neighbors. The model resembles the model for earthquake data presented in [17], but differs in some aspects due to fundamentally different characteristics of the underlying dynamics of earthquakes and ocean waves. Most notable, the model presented herein contains a seasonal component, which has been seen to dominate the temporal variation in the data, whereas there are no strain term similar to the strain term in the earthquake model. Furthermore, the significant wave height data is not zero-inflated; in fact, zero significant wave height is not meaningful so the significant wave height will always be strictly positive. In a sense, this simplifies the modeling, but care should be taken so that negative significant wave heights are not predicted by the model. Finally, a long-term temporal trend component is included, which is a novel feature for such models.

The structure of the model will be outlined below; first the basic or main model will be outlined, and then various model alternatives are suggested for comparison. Then possible extensions to this model are discussed, where for example different meteorological data can be used as covariates for regression, as explored further in Chap. 5.

3.2.1 Main Model

At the first level, the observations, Z at location x and time t, are modeled in the observation model as the latent (or hidden) variable, H, corresponding to the underlying significant wave height process, and some random noise, ε_z, which may be construed to include statistical measurement error:

$$Z(x,t) = H(x,t) + \varepsilon_z(x,t) \qquad \forall\, x \geq 1, t \geq 1 \tag{3.4}$$

All the noise terms, in this and in subsequent components, are assumed independent in space and time, having a zero-mean Gaussian distribution with some random, but identical variance; with generic notation, $\varepsilon_N(x,t) \overset{i.i.d}{\sim} N(0, \sigma_N^2)$. It is noted that all noise terms to be included in the model are assumed to be independent of all other noise terms in the model.

The underlying process for the significant wave height at location x and time t is modeled by the following state model (or system model), which is assumed split into a time-independent component, $\mu(x)$, a temporally and spatially dependent

component $\theta(x,t)$ and a spatially independent seasonal component, $M(t)$, as shown in Eq. 3.5. A separate term is included to model long-term temporal trends, $\mathrm{T}(t)$, which is assumed to be spatially invariant and which is, in fact, the component of most interest in this particular study. In line with the model presented in [17], no additional noise terms are introduced in the model at this level.

$$H(x,t) = \mu(x) + \theta(x,t) + M(t) + \mathrm{T}(t) \qquad \forall\, x,t \tag{3.5}$$

The time-independent part is modeled as a first-order Markov random field, conditional on its nearest neighbors in all cardinal directions, and with different dependence parameters in lateral and longitudinal direction, as shown in Eq. 3.6. For the remainder of this book, the following notation is used for neighboring locations of x in space: x^D = the location of the nearest grid point in direction D from x, where $D \in \{N, S, W, E\}$ and N = North, S = South, W = West and E = East. If x is at the border of the area, the value at the corresponding neighboring grid point outside the data area is taken to be zero. Hence, no particular adjustments are made to account for edge effects.

$$\begin{aligned}\mu(x) = {} & \mu_0(x) + a_\phi \left\{\mu(x^N) - \mu_0(x^N) + \mu(x^S) - \mu_0(x^S)\right\} \\ & + a_\lambda \left\{\mu(x^E) - \mu_0(x^E) + \mu(x^W) - \mu_0(x^W)\right\} + \varepsilon_\mu(x) \qquad \forall\, x\end{aligned} \tag{3.6}$$

In the equation above, $\mu_0(x)$ is the Markov random field mean at grid point x and a_ϕ and a_λ are spatial dependence parameters in lateral (i.e., north–south) and longitudinal (i.e., east–west) direction, respectively. σ_μ^2 is the homogeneous Markov random field noise variance. The spatially specific mean, $\mu_0(x)$, is modeled as having a quadratic form with an interaction term in latitude and longitude. Letting $m(x)$ and $n(x)$ denote the longitude and latitude of location x respectively, it is assumed that

$$\mu_0(x) = \mu_{0,1} + \mu_{0,2} m(x) + \mu_{0,3} n(x) + \mu_{0,4} m(x)^2 + \mu_{0,5} n(x)^2 + \mu_{0,6} m(x) n(x) \quad \forall\, x \tag{3.7}$$

The spatio-temporal dynamic term $\theta(x,t)$, with interactions in space and time, is modeled as a vector autoregressive model of order one, conditionally specified on its nearest neighbors in all cardinal directions, as shown in Eq. 3.8.

$$\begin{aligned}\theta(x,t) = {} & b_0 \theta(x, t-1) + b_N \theta(x^N, t-1) + b_E \theta(x^E, t-1) \\ & + b_S \theta(x^S, t-1) + b_W \theta(x^W, t-1) + \varepsilon_\theta(x,t) \qquad \forall\, x,t\end{aligned} \tag{3.8}$$

There were no obvious rationale for allowing the grid-point specific autoregressive parameter b_0 to vary spatially, as in [17]. Hence, b_0 as well as the parameters corresponding to the nearest neighbors, b_N, b_E, b_S, b_W are assumed invariant in space. These parameters are assumed to have interpretations connected with the underlying ocean dynamics and how sea states behaves and changes over an area; the component

may be construed to model, inter alia, the propagation of storms over the investigated area. Since the various components are specified conditionally, the different noise contributions $\varepsilon_z(x,t)$, $\varepsilon_\mu(x)$ and $\varepsilon_\theta(x,t)$ can be identified, as pointed out by [17].

The seasonal component is modeled as an annual cyclic contribution (as opposed to the model in [26] which used a combination of an annual and a semi-annual seasonal contribution) where the seasonal contribution is assumed independent of space, see Eq. 3.9. It is believed that there are no pressing reasons to allow these parameters to vary in space, and the seasonal effects are assumed invariant over the area under consideration, but a noise term is included in this part of the model, as opposed to the model in [38]. Another difference from the model in [38] is that this model used monthly data only, whereas the significant wave height data have a temporal resolution of 6 h, and the model will be tried out for different temporal resolutions of the data. The period of the seasonal cycle is 1 year, so $\omega = \frac{2\pi}{12}$ for monthly data, $\omega = \frac{2\pi}{365.25}$ for daily data and $\omega = \frac{2\pi}{1461}$ for six-hourly data, taking the average number of observations over normal and leap-years. Apriori, it is known that the worst weather normally occurs around the beginning of the year (January), so d, which represents a temporal shift from a pure cosine cyclic component, is presumably small.

$$M(t) = c\cos(\omega t) + d\sin(\omega t) + \varepsilon_m(t) \qquad \forall\, t \geq 1 \tag{3.9}$$

The long-term trend is modeled as a simple Gaussian process with a quadratic trend, as shown in Eq. 3.10. Noise terms, assumed independent and identically distributed with zero mean and variance σ_t^2, are included in this component as well even though it is acknowledged that, in reality, these cannot be separated from the other temporal noise terms, $\varepsilon_m(t)$. Presumably, the parameters γ and η will be very small since they correspond to the increase over 1 month/1 day/6 h due to the long-term trend. However, the trend may not be negligible as it accumulates over time, even for very small γ and η.

$$\mathrm{T}(t) = \gamma t + \eta t^2 + \varepsilon_{\mathrm{T}}(t) \qquad \forall\, t \geq 1 \tag{3.10}$$

3.2.2 Model Alternatives

Different model alternatives were tried out and simulations were run for five different model alternatives. Alternatives with a quadratic trend, linear trend and no temporal trend respectively were explored, as summarized below.

In addition, model alternatives with one or two temporal noise terms were investigated in order to check if this has any significant influence on the results. As noted above, it would, strictly speaking, be more correct to include only one temporal noise term due to identifiability issues, but on the other hand, it is convenient to single out the long-term trend component in a separate component if this is found to

have no major effect on the overall results. In any case, the temporal noise terms by themselves should be interpreted with caution. For the models with only one temporal noise term, the long-term trend and the seasonal components are combined in a temporal part $M(t)$. All other model components remain unchanged.

1: $M(t) = c\cos(\omega t) + d\sin(\omega t) + \varepsilon_m(t)$
$\mathrm{T}(t) = \gamma t + \eta t^2 + \varepsilon_{\mathrm{T}}(t)$
2: $M(t) = c\cos(\omega t) + d\sin(\omega t) + \varepsilon_m(t)$
$\mathrm{T}(t) = \gamma t + \varepsilon_{\mathrm{T}}(t)$
3: $M(t) = c\cos(\omega t) + d\sin(\omega t) + \varepsilon_m(t)$
$\mathrm{T}(t) = 0$
4: $M(t) = c\cos(\omega t) + d\sin(\omega t) + \gamma t + \eta t^2 + \varepsilon_m(t)$
$\mathrm{T}(t) = 0$
5: $M(t) = c\cos(\omega t) + d\sin(\omega t) + \gamma t + \varepsilon_m(t)$
$\mathrm{T}(t) = 0$

3.2.3 Prior Distributions on the Model Parameters

The model outlined in the preceding section will be specified in a Bayesian setting, and the model is completed by specifying prior distributions on the various model parameters. In line with the assumptions made in [17], all prior distributions are assumed independent, and the following model parameters requires specification of a prior distribution: The noise variances σ_Z^2, σ_μ^2, σ_θ^2, σ_m^2 and σ_{T}^2, the MRF parameters a_ϕ and a_λ, the spatial mean parameters $\mu_{0,i}$ for $i = 1, \ldots, 6$, the vector autoregressive parameters b_0, b_N, b_E, b_S and b_W, the variables of the autoregressive process $\theta(x, 0)$ for $x = 1, \ldots, X = 153$, the seasonal parameters c and d and the temporal trend parameters γ and η. Specification of prior distributions for these 175 parameters together with initial values for $\theta(x, 0)$ would thus complete the specification of the model, and for sensible prior distributions the full posterior conditional distributions can be derived. This will be ensured by specifying conditionally conjugate priors for all these parameters.

Analogue to the priors suggested in [17], all parameters except the priors for the variance of the noise terms are assigned Gaussian priors, i.e., $\kappa \sim N(\xi_\kappa, \sigma_\kappa^2)$ for $\kappa = a_\phi, a_\lambda, \mu_{0,i \text{ for } i=1,\ldots 6}, b_0, b_N, b_E, b_S, b_W, \theta(x, 0), c, d, \gamma$ and η. The variance of the noise terms are all assigned inverse gamma[3] conjugate priors, i.e., $\sigma_\iota^2 \sim IG(\alpha_\iota, \beta_\iota)$ for $\iota = Z, \mu, \theta, m$ and T. It is acknowledged that [9] recommended uniform rather than inverse gamma priors for the variances to avoid constraints on the posteriors, but inverse gamma priors were still regarded as reasonable in this study. This has

[3] The following parametrization of the inverse gamma distribution will be used:

$$X \sim IG(\alpha, \beta) \Rightarrow f(x) = \frac{\beta^\alpha}{\Gamma(\alpha)} \left(\frac{1}{x}\right)^{\alpha+1} e^{-\beta/x} \quad \text{for} \quad x > 0$$

been substantiated by running some control simulations were noninformative priors were adopted for the noise variances, i.e., using $\pi(\sigma_\cdot^2) \propto \frac{1}{\sigma_\cdot^2}$.

To determine the 350 hyperparameters, some physical insight is employed for the parameters where relevant information is available. However, it is noted that the amount of data is large, so the posteriors are not believed to be overly sensitive to the exact values of the hyperparameters. Notwithstanding, some efforts have been made to suggest sensible prior distributions.

It is assumed that the MRF parameters and the vector autoregressive parameters will be small but positive since there will presumably be a positive correlation between significant wave heights at neighbouring points and/or previous time-points. Hence, priors for all these will take hyperparameters $(\xi_\kappa, \sigma_\kappa^2) = (0.2, 0.25)$, as was also used in [17]. For the spatial mean parameters, $\mu_{0,i}$, it is assumed that the last five will be close to zero, and zero-mean priors with variance = 2 will be adopted for $i = 2, \ldots, 6$ (still, in agreement with [17]). For $\mu_{0,1}$ it is acknowledged that previous knowledge are available that suggests that mean significant wave height in the area should lie around 2–4 m (this is also in agreement with the initial data analysis) and prior distribution with mean = 3.5 and variance = 2 will be employed (see for example, [14], or some other previous works referred to in [28]). It is noted that a negative spatial mean would be unphysical, and one may consider imposing restrictions on this parameter. However, zero lies at the 0.67-percentile of the prior distribution so no restrictions are deemed necessary.

With respect to the seasonal parameters, prior knowledge suggests that the amplitude should be around 2 (see e.g., [13]. This also agrees well with the initial data analysis). Furthermore, it is known that the worst weather normally occurs in January (the beginning of the year), so a pure cosine-term would probably be close to the real seasonal component, and d is presumably small. Therefore, a prior distribution for the parameter c with mean = 2 and variance = 0.5 and a prior distribution for the shift parameter d with mean = 0 and variance = 0.2 will be adopted. The temporal trend parameters are assumed small, but positive, and prior distributions with zero mean and variance = 0.1 will be assumed.

There is also a need to specify prior distributions for the starting values of $\theta(x, 0)$ at all spatial locations. Assuming these are independent and Gaussian corresponds to a total of 306 hyperparameters that needs to be specified. In [17], informative priors based on data prior to some specified data were used to establish similar hyperparameters, but it was noted that the final results were insensitive to the values of these hyperparameters. It is assumed that this is also the case for the significant wave height model, especially since the amount of data is much larger. Therefore, less informative priors that are rather flat will be specified for these 153 parameters. Furthermore, the same prior distributions will be assumed for all locations, with zero mean and variance = 15.

Hyperparameters for all five noise terms are assumed equal, with values $\alpha_\iota = 3$ and $\beta_\iota = 2$, corresponding to mean = 1 and variance = 1 for the variance parameters. All hyperparameters for the prior distributions are summarized in Table 3.3 and the model is then fully specified. It is noted that the same priors were used for monthly,

Table 3.3 Specification of prior distributions

Parameters	Prior distribution
$\sigma_Z^2, \sigma_\mu^2, \sigma_\theta^2, \sigma_m^2$ and σ_T^2	$IG(3, 2)$
$a_\phi, a_\lambda, b_0, b_N, b_E, b_S$ and b_W	$N(0.2, 0.25)$
$\mu_{0,i}$ for $i = 2, \ldots, 6$	$N(0, 2)$
$\mu_{0,1}$	$N(3.5, 2)$
$\theta(x, 0)$ for all x	$N(0, 15)$
c	$N(2, 0.5)$
d	$N(0, 0.2)$
γ and η	$N(0, 0.1)$

daily and monthly maximum data and it can be questioned whether this is appropriate. However, a few simulations were run with different priors for some of the parameters, and the results were not very sensitive to this. This might not be unexpected, however, as it is generally known that the priors become asymptotically irrelevant and the amount of data is big in this case.

3.3 Model Comparison and Selection

Model comparison in such a complex model is challenging. Statistical models are often compared by way of the AIC or BIC criteria [2, 20], but neither are straightforward to use for complex hierarchical models. Alternative criteria for complex hierarchical models are the deviance information criterion (DIC) [23] and the posterior predictive checks as described in [4]. Neither of these methods have been employed in the current study, which rather employs two loss functions based on predictive power. However, these are based on short-term predictive power and may not be ideal for a model aiming at identifying long-term trends. Furthermore, only the observational level is used for model comparison and the outcomes are conditional on the underlying system levels. Hence, robust model selection remains an open issue.

3.3.1 Sum of Squares of the Residuals

Different model alternatives can be briefly compared by comparing the resulting posterior estimates of the model parameters. In order to assess the different model alternatives and get a measure of the model fit to the data, the sum of squares of the residuals, SS_{res}, can be considered, calculated according to Eq. 3.11, where n is the number of samples ($n = 1,000$ in this case) and m is the number of observations ($m = X \times (T - 1)$). These are relative measures and cannot be used to determine how good a model is, but merely to compare different model alternatives applied to

the same dataset.

$$SS_{\text{res}} = \sum_{i=1}^{m} \left(Z_i - \frac{1}{n} \sum_{j=1}^{n} \hat{H}_{i,j} \right)^2 \tag{3.11}$$

3.3.2 Loss Functions Based on Predictive Power

Two loss functions based on predictive power were constructed as alternative ways of comparing model alternatives. Only one-step predictions were considered. Hence, the models were fitted with all data except the last time-point and predictions of the spatial field at this time-point for the various models were then compared to the data. Analogue to the standard loss function used in [17], the standard loss function in Eq. 3.12 is defined where $Z(x)$ denotes the data at location x and $Z(x)_j^*$ denotes the predicted value of Z at location x in iteration j, both at time T. It is noted that the time dependence in Eq. 3.12 is suppressed since only the time $t = T$ is considered.

$$L_s = \left[\frac{1}{Xn} \sum_{x=1}^{X} \sum_{j=1}^{n} \left(Z(x) - Z(x)_j^* \right)^2 \right]^{\frac{1}{2}} \tag{3.12}$$

More specially designed loss functions may also be used, for example where a greater penalty is introduced for failing to predict an extreme sea state compared to prediction errors for less severe sea states or where the spatial predicted fields are smoothed by averaging over neighboring grid points (as in [17]). In this study, one alternative loss function has been designed, where the squared prediction errors have been weighted according to the actual observed significant wave height. More precisely, a weight of $Z(x)$ is included in order to give greater emphasis on prediction errors at locations where large significant wave heights have been observed. Hence, an alternative loss function as given in Eq. 3.13 is calculated.

$$L_w = \left[\frac{1}{n \sum_x Z(x)} \sum_{x=1}^{X} \sum_{j=1}^{n} Z(x) \left(Z(x) - Z(x)_j^* \right)^2 \right]^{\frac{1}{2}} \tag{3.13}$$

The predictions $Z(x)_j^*$ are taken as the estimated value of $Z(x)$ given the samples for all model parameters and variables in iteration j. The model specification gives

$$\begin{aligned} \boldsymbol{Z}(x)_j^* &= \mu(x)_j + \theta(x,T)_j + M(T)_j + \mathrm{T}(T)_j + \varepsilon_Z(x,T) \\ &= \mu(x)_j + \boldsymbol{B}_j \boldsymbol{\theta}(T-1)_j + c_j \cos(\omega T) + d_j \sin(\omega T) + \gamma_j T + \eta_j T^2 + \varepsilon_\zeta(x)_j \end{aligned} \tag{3.14}$$

where the subscript $_j$ denotes the sampled parameters in iteration j and the noise terms $\varepsilon_\zeta(x)$ are sampled independently from a zero-mean normal distribution with variance

$$\sigma^2_{\zeta,j} = \sigma^2_{Z,j} + \sigma^2_{\theta,j} + \sigma^2_{m,j} + \sigma^2_{\mathrm{T},j} \tag{3.15}$$

Note that since $\mu(x)$ is independent of time, the sampled values of $\mu(x)_j$ can be used and these have already incorporated the noise term ε_μ. Hence, this noise term is not a part of $\varepsilon_\zeta(x)$ when making the predictions. $\boldsymbol{B}$ is an $X \times X$ matrix as outlined in Appendix D.

3.4 Implementation and Simulations

In order to simulate posterior samples from the model, Markov chain Monte Carlo techniques (Gibbs sampling with Metropolis-Hastings steps, see e.g., [18]) have been employed. This requires the full conditional distributions for all the parameters involved, as presented in Appendix D. Gaussian distributions and conjugate priors have been used, so the derivation of the full conditional distributions has been rather straightforward in most cases, although the full conditional distribution for a_ϕ and a_λ was difficult to sample from directly. In order to overcome this difficulty, Metropolis-Hastings steps were incorporated in the Gibbs sampler for these parameters, where the joint pseudo conditional distribution was used as proposal. A mixing rate of about 25 % was achieved, and the Metropolis-Hastings steps were repeated four times in each iteration to achieve an overall acceptance rate of about 65–68 % for the various simulations. An implementation has been made in Java. 45,000 iterations were run for the monthly and monthly maximum data, with an initial burn-in period of 20,000 and then keeping every 25th sample (batch size = 25). For the daily and six-hourly data, when simulations became increasingly time consuming, the batch size was reduced to 5, retaining the burn-in period of 20,000. Thus, a total of 1,000 samples of the multi-dimensional parameter vector were obtained from each simulation.

In order to determine the batch size, initial simulations keeping all samples were carried out and the autocorrelation functions were investigated. A set of simulations were also run for the monthly data with a batch size of 5, and this produced nearly identical results, but with slightly wider credibility bands. This can be explained by the greater Monte Carlo variance for samples that are more correlated, and is as expected. In addition, goodness-of-fit and short-term predictions are minimally affected. Notwithstanding, for daily and six-hourly simulations, which are much more time consuming, a batch size of 5 was used.

No formal tests on convergence have been carried out, but visual inspection indicates that convergence occurs relatively quickly. A few simulations have been performed with different starting values for the parameter set and the results indicate that the Gibbs sampler has indeed converged. In addition, two control simulations with considerably longer burn-in periods were run for the monthly data, and these showed nearly identical results, indicating that convergence did indeed occur within

the burn-in period. However, it cannot be taken for granted that convergence occur equally fast for daily and six-hourly data.

It is noted that applying the Kalman filter [1, 12, 16] could have been an alternative to running MCMC simulations. The state model is basically a linear combination of Gaussian components and hence the model can be regarded as a type of Gaussian dynamic linear models as outlined in [36], for which the Kalman filter should work. Even though this could possibly have a computational advantage in terms of reduced computational time, the technique has not been employed in this study, and it is therefore not known how such an approach would have performed. The integrated nested Laplace approximations (INLA) approach could also be a possible alternative [19], but this was neither tried out in this study.

3.5 Results and Predictions

3.5.1 Results for Monthly Data

The following results were obtained when running the model with monthly data, i.e., the first observation from each month. It is agreed that the selection of a particular observation within each month may be regarded as arbitrary, but it is believed that no notable biases are introduced by this over the time history of 44+ years. Furthermore, this arbitrariness disappears when focusing on monthly maximum data in subsequent analyses.

In order to check the Gaussian model assumption in Eq. 3.4, a visual check of the residuals was carried out, and this indicates that the model assumptions are reasonable, as shown in the normal probability plot in Fig. 3.9 (top) (this plot is for the quadratic model but plots pertaining to the other model alternatives are nearly identical). It is observed that some deviation from a straight line occurs, and by closer inspection, there seems to be some dependence in the residuals, which may indicate that some of the model assumptions are violated. More specifically, there seems to be a spatial dependence in the residuals. This could be due to edge-effects and it is observed that the residuals are consistently lower at the border, i.e., where there are no neighbour in one direction. This pattern is present for all model alternatives, and it is seen that the effect is not affected by different temporal parts. Since this is a spatial feature, this is reasonable. For comparison, a normal probability plot of the monthly data is shown at the bottom in Fig. 3.9, and it is clearly seen that the data itself are not normal.

Most of the marginal posterior distributions appear symmetric, and the mean and standard deviation of the posterior distributions for different parameters of the different model alternatives are given in Tables 3.4 and 3.5. It is observed that apart from the temporal trend part, most of the model parameters do not vary significantly between model alternatives. The posterior distributions for a_ϕ and a_λ are not symmetric, however, and the posterior distributions for these are presented in Table 3.4 in terms of the triplets (mean; median; standard deviation).

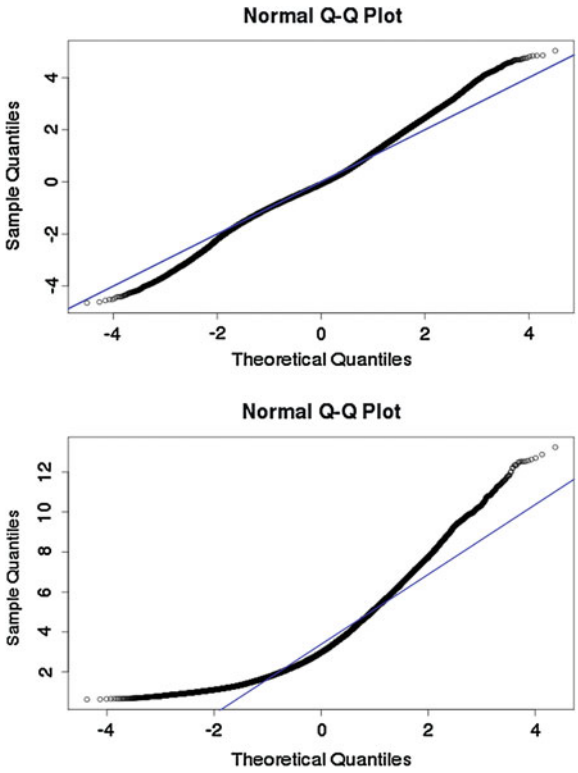

Fig. 3.9 Normal probability plot of the residuals (*top*) and the monthly data (*bottom*)

Two control runs, for model 1 and 2 respectively, with considerably longer burn-in period (500, 000) and batch size (200) were performed and the resulting posteriors were almost identical. This indicates two important findings: (a) The initial burn-in periods were sufficient to arrive at the stationary distributions and (b) the initial batch size of 25 is sufficient to arrive at approximately uncorrelated samples (otherwise, one would expect higher variance due to correlated samples). Hence, the control runs suggest that convergence of the Markov chain is not an issue, at least for the monthly data.

The six parameters $\mu_{0,\cdot}$ determine the spatially varying mean $\mu_0(x)$ over the area, which is displayed in Fig. 3.10. As for the time-independent part $\mu(x)$, both the mean of $\mu(x)$ (top) and the mean deviation from the mean $\mu(x) - \mu_0(x)$ (bottom) are illustrated in Fig. 3.11. The contribution from the time-independent part $\mu(x)$ is in the order of 2.7–3.3 m, which seems reasonable. The mean deviation from the spatially varying mean is small, with range of deviations from -0.22 to 0.11 m. The figures below are all from simulations over the main model (model 1), but the alternative models give very similar results.

It is somewhat more difficult to visualize the space-time dynamic part, $\theta(x, t)$. Figure 3.12 shows the mean and variance of the $\theta(x)$ field for an arbitrary time. For

Table 3.4 Posterior marginal distributions, mean and standard deviation (mean; sd); monthly data

	Model 1	Model 2	Model 3	Model 4	Model 5
σ_Z^2	0.79; 0.0048	0.79; 0.0049	0.79; 0.0047	0.79; 0.0048	0.79; 0.0049
σ_μ^2	0.030; 0.0035	0.031; 0.0036	0.031; 0.0037	0.031; 0.0035	0.031; 0.0036
σ_θ^2	0.074; 0.0026	0.074; 0.0027	0.074; 0.0025	0.074; 0.0027	0.074; 0.0026
σ_m^2	0.69; 0.12	0.67; 0.12	1.1; 0.072	1.1; 0.070	1.1; 0.070
b_0	0.22; 0.0088	0.22; 0.0088	0.22; 0.0087	0.22; 0.0088	0.22; 0.0087
b_N	0.21; 0.012	0.21; 0.013	0.21; 0.013	0.21; 0.012	0.21; 0.012
b_E	0.24; 0.011	0.24; 0.011	0.24; 0.011	0.24; 0.011	0.24; 0.010
b_S	0.13; 0.012	0.13; 0.012	0.13; 0.012	0.13; 0.012	0.13; 0.012
b_W	0.18; 0.010	0.18; 0.010	0.18; 0.0097	0.18; 0.010	0.18; 0.0099
c	1.13; 0.064	1.14; 0.069	1.13; 0.064	1.13; 0.064	1.13; 0.067
d	0.80; 0.065	0.79; 0.065	0.79; 0.067	0.80; 0.068	0.79; 0.065
$\mu_{0,1}$	3.4; 1.4	3.4; 1.4	3.5; 1.4	3.4; 1.4	3.4; 1.5
$\mu_{0,2}$	−0.22; 0.047	−0.21; 0.044	−0.21; 0.049	−0.22; 0.046	−0.22; 0.048
$\mu_{0,3}$	1.3; 0.27	1.3; 0.26	1.3; 0.28	1.3; 0.26	1.3; 0.28
$\mu_{0,4}$	0.00041; 0.00012	0.00041; 0.00011	0.00041; 0.00012	0.00042; 0.00012	0.00043; 0.00012
$\mu_{0,5}$	−0.0075; 0.0015	−0.0073; 0.0015	−0.0075; 0.0015	−0.0074; 0.0015	−0.0075; 0.0016
$\mu_{0,6}$	−0.0011; 0.00068	−0.0012; 0.00064	−0.0012; 0.00068	−0.0012; 0.00067	−0.0012; 0.00068
a_ϕ	0.12; 0.11; 0.062	0.12; 0.11; 0.066	0.11; 0.11; 0.064	0.11; 0.11; 0.063	0.11; 0.11; 0.064
a_λ	0.13; 0.13; 0.067	0.13; 0.13; 0.067	0.13; 0.13; 0.066	0.13; 0.13; 0.068	0.13; 0.13; 0.067

Table 3.5 Posteriors for the trend components, mean and standard deviation; monthly data

	Model 1	Model 2	Model 3	Model 4	Model 5
σ_T^2	0.45; 0.12	0.48; 0.11	–	–	–
γ	0.00098; 0.0011	0.00054; 0.00026	–	0.0012; 0.0012	0.00070; 0.00029
η	-6.1×10^{-7}; 2.0×10^{-6}	–	–	-9.9×10^{-7}; 2.2×10^{-6}	–

all times (except t = 0) and locations, the mean ranges from ± 1.5 m with variances ranging from 0.06 to 0.48 m^2. Hence, a notable part of the modeled significant wave height can be ascribed to this space-time dynamic part. One interesting observation is that, of the b-parameters except b_0, b_E is the largest. This should mean that the model captures that more storms arrive from east than from the other directions. However, it is noted that such interpretation of this component is not very meaningful when using monthly data, and a better interpretation will presumably be obtained when running the model on daily and six-hourly data. In that case, it is expected that the model should correctly capture the direction most storm tracks follow in the area.

One may also want to investigate the seasonal and trend components as obtained from the model. The sampled seasonal term for the first 10 years is shown in Fig. 3.13, and a clear cyclic behavior is observed. The mean seasonal contribution without the error term, $c\cos(\omega t) + d\sin(\omega t)$ calculated with the posterior mean values of c and d, is also shown in the figure and agrees well with the sampled seasonal contribution. The estimated amplitude of the seasonal component is $\sqrt{\hat{c}^2 + \hat{d}^2} \approx 1.4$ m.

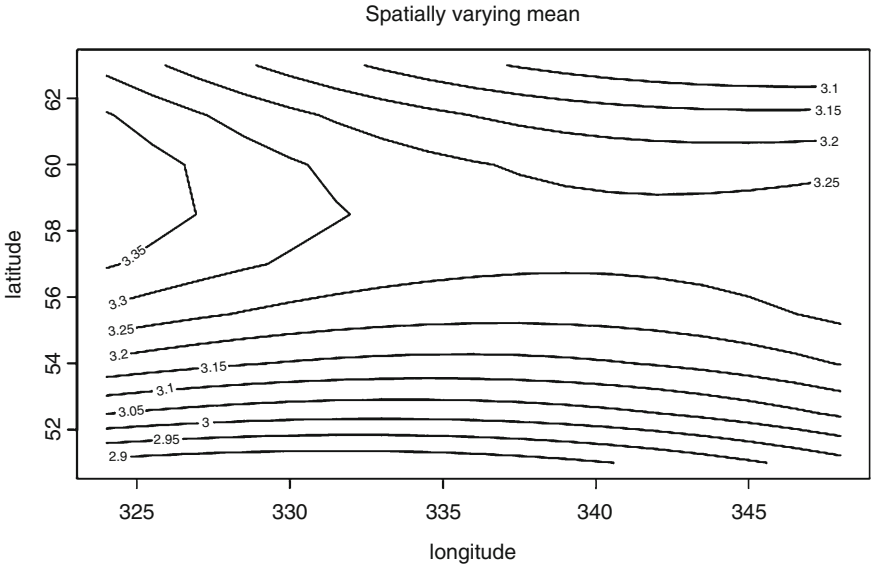

Fig. 3.10 The spatially varying mean, $\mu_0(x)$, monthly data, ranging between 2.7 and 3.3 m

The temporal trend part of the quadratic model is illustrated in Fig. 3.14. The figure shows the sampled mean annual trend together with the mean, 5- and 95-percentiles of the trend contribution obtained by calculating $\gamma t + \eta t^2$ from the joint posterior distribution of (γ, η). As can be seen from this plot, a mean yearly trend corresponding to a noticeable increase in significant wave height, about 35 cm over the period, can be extracted from the data with a 90 % credible interval ranging from 6.7 to 62 cm. It is observed that the expected increase over the period due to this trend is comparable to the mean trend estimated with slightly different priors for the variance terms [29].[4]

One may also investigate the temporal trend part of the model with a linear trend (obtained by setting $\eta = 0$ in the main model) and this is also shown in Fig. 3.14. The sampled mean annual trend is plotted together with the mean, 5- and 95-percentiles of the trend contribution obtained from γt, and also now a significant increasing trend can be detected. Indeed, the whole 90 % credible interval for the long-term temporal trend is positive. The mean estimate of the long-term trend from the linear model corresponds to an increase in significant wave height of about 28 cm over the whole period. Alternatively, one may observe that this model gives, with 95 % credibility, an increase in significant wave height of at least 5 cm between 1958 and 2002. The expected trend contribution is slightly less than for the alternative priors used in [29], but the difference is not very significant.

For the models with one temporal noise term, the seasonal and trend components were not sampled individually, but the mean and 90 % credible interval for the trend

[4] Note that the credible bands in [29] were wrongly calculated, but not the mean.

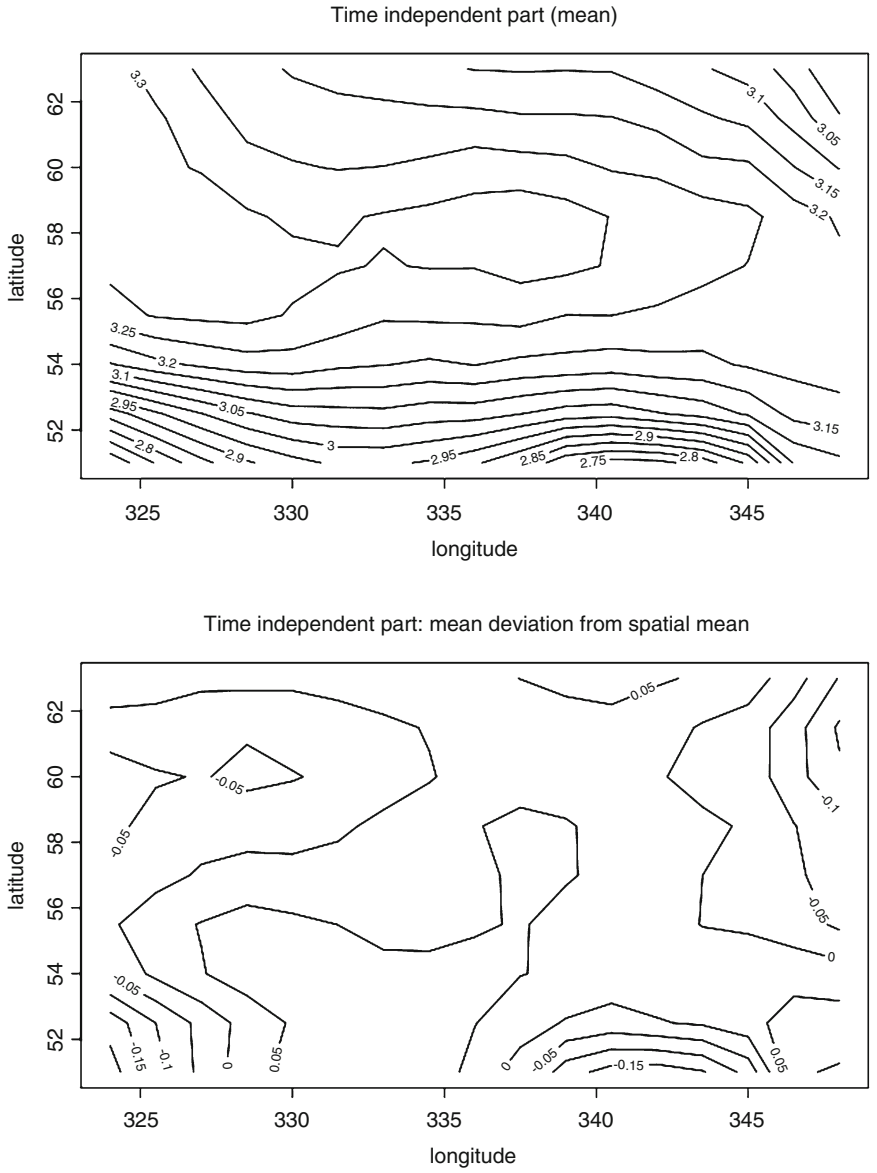

Fig. 3.11 Mean time-independent part (*top*) and deviation from the spatial mean (*bottom*), monthly data

estimated from the posterior γ and η estimates are illustrated in Fig. 3.15. The long-term trends estimated from these models are very similar to the ones estimated with two noise terms. The quadratic trend model (Model 4) estimates a mean increase over the period of 38 cm, with the 90 % credible interval ranging from 12 to 65 cm.

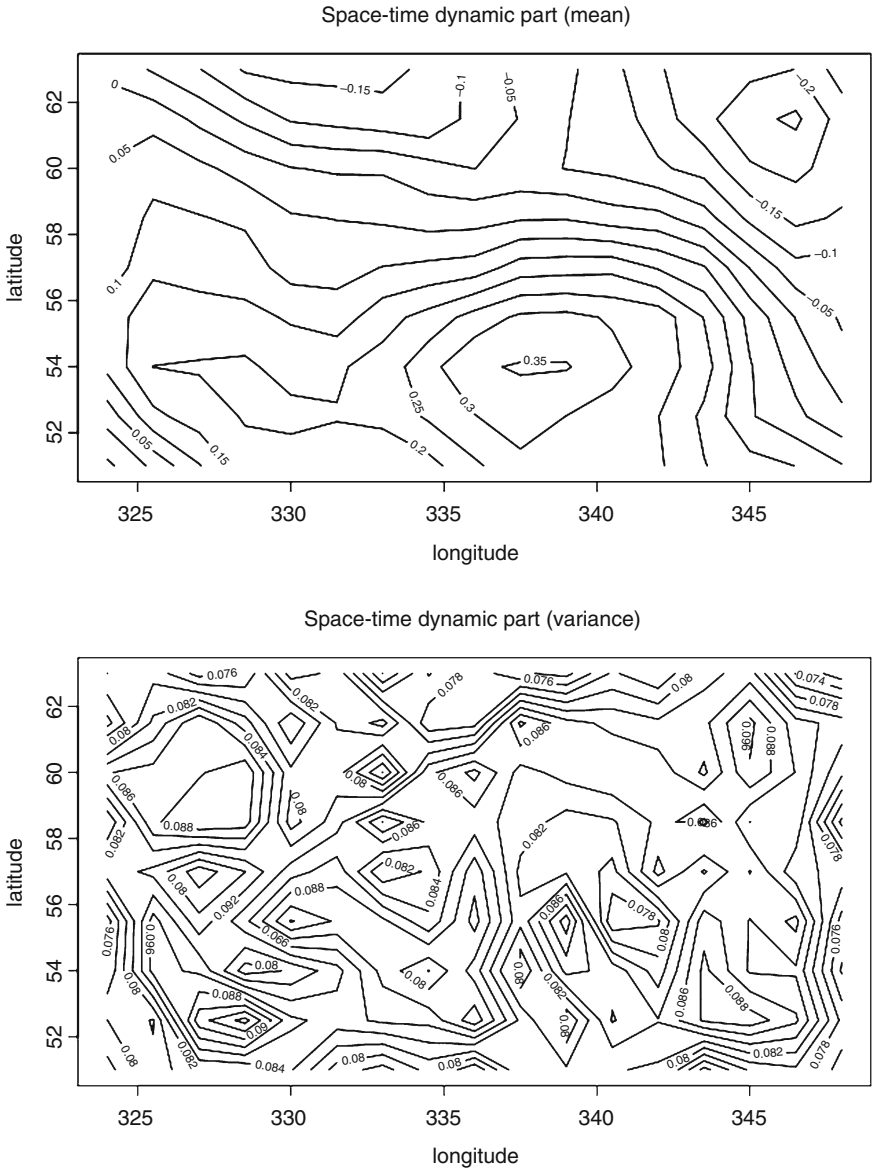

Fig. 3.12 Mean and variance of the dynamic part, monthly data

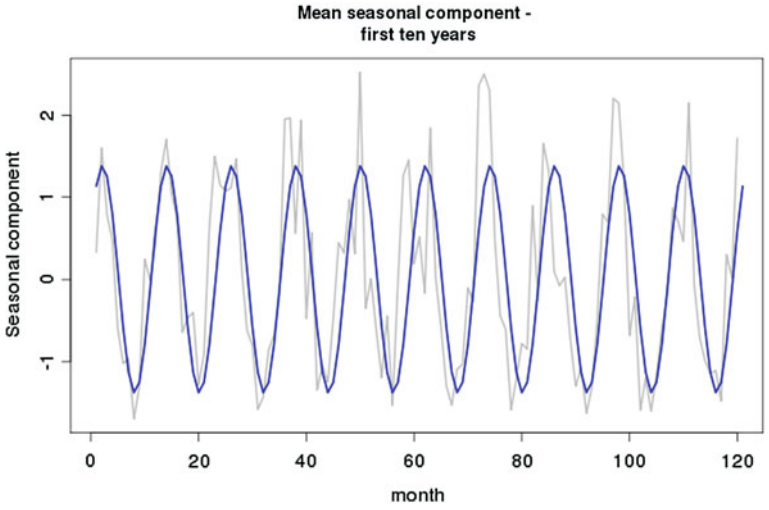

Fig. 3.13 The seasonal component for 10 years, monthly data; $M(t)$ (*grey lines*) and $c\cos(\omega t) + d\sin(\omega t)$ (*blue lines*)

The linear trend model (Model 5) estimates a mean increase of 37 cm during the period, with a 90 % credible interval ranging from 13 to 61 cm.

3.5.2 Results for Daily Data

The same models were run for daily data. Running these simulations was much more computational intensive than for monthly data, but less so than for the full dataset; one set of simulations completed in about 200 h. The results from these simulations are summarized below. A visual check of the residuals was carried out, suggesting that model assumptions are reasonable, as shown in Fig. 3.16 (for the full model). Some deviation from a straight line is observed again, which may be be due to edge-effects of the Markov Random Field.

Again, most of the marginal posterior distributions are symmetric and resemble Gaussian distributions, and the mean and standard deviation of the marginal posterior distributions for the different model alternatives are given in Tables 3.6 and 3.7. Apart from the temporal trend part, again most of the model parameters do not vary significantly between model alternatives.

The figures illustrating these results are very similar to the ones obtained for the monthly data and are not presented herein, but the main results are summarized briefly in the following. The contribution from the time-independent part is now within the range of 2.9–3.6 m with deviations from the spatially varying mean ranging from −0.24 to 0.10 m. This is slightly higher, but comparable to the results obtained for

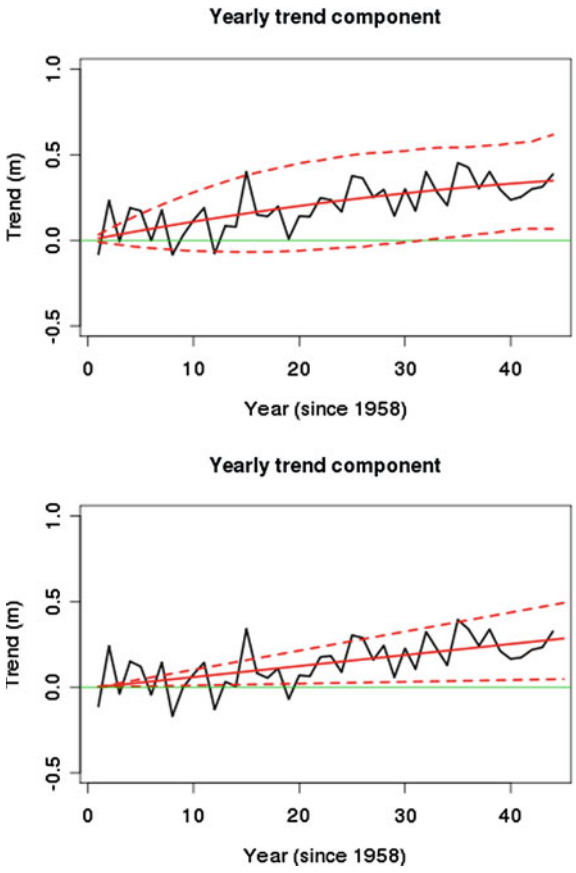

Fig. 3.14 Annual trend over the period, model 1 (*top*) and model 2 (*bottom*), monthly data; mean T(t) (*black lines*) and mean and 90 % credible interval of $\gamma t + \eta t^2$ (*red lines*). *Green lines* correspond to no trend

monthly data. The mean contribution from the dynamic part ranges from -2.79 to 3.44 m, with variances ranging from 0.11 to 0.43 m^2. Now, of the b-parameters except b_0, b_W is the largest, which indicates that the model captures that more storms arrive from west than from the other directions. This is different from the results obtained for monthly data, but it is believed that the interpretation of this component now becomes more meaningful, and that the dynamic part now seems to capture the development and transition of storms in the area, which are believed to follow a predominantly eastward direction, i.e., coming from the west. The seasonal contribution for the first 5 years is shown in Fig. 3.17.

The temporal trend part of the quadratic model is illustrated in Fig. 3.18, as for the monthly data. Again, an increasing trend can be extracted from the data with the mean yearly trend corresponding to a noticeable increase in significant wave height, about 23 cm over the period. The 90 % credible interval ranges from 19 to 28 cm. This is somewhat less than the trend estimated from the monthly data, with a narrower credible band.

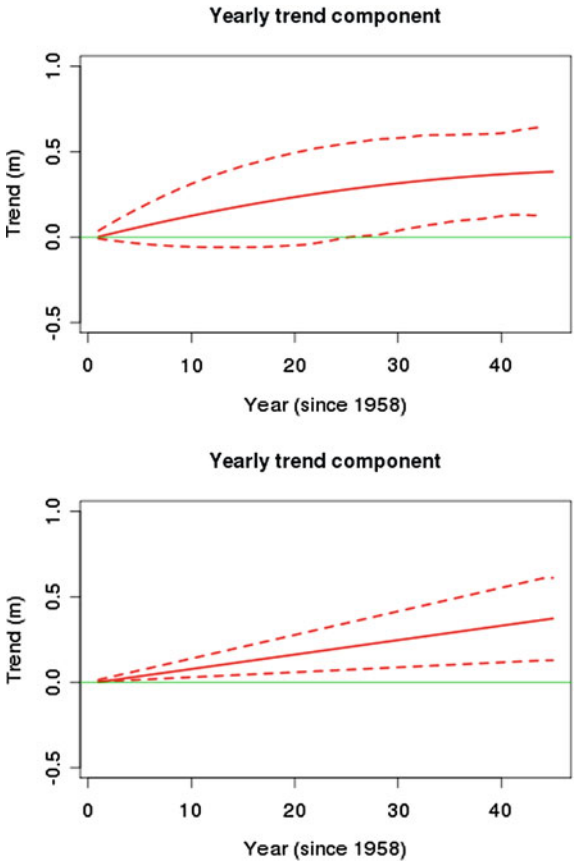

Fig. 3.15 Mean and 90-% credible interval for the estimated trend contribution for models 4 (*top*) and model 5 (*bottom*), monthly data (*red lines*). *Green lines* correspond to no trend

The trend component of the linear model (model 2) is also shown in Fig. 3.18 and again a significant increasing trend can be detected. Indeed, all sampled trend contributions for this model are positive, corresponding to a near-100 % credible interval for the long-term temporal trend to be positive. The mean estimate of the long-term trend from the linear model corresponds to an increase in significant wave height of about 22 cm over the whole period of 44 years and 2 months. Alternatively, this model gives a 90 % credible interval ranging from 17 to 31 cm. Again, the credible interval is notable narrower for daily data compared to monthly data.

The estimated trend components for models 4 and 5 including the 90 % credible bands are illustrated in Fig. 3.19. The long-term trends estimated from these models are very similar to the ones estimated with two temporal noise terms. The quadratic trend model (Model 4) estimates a mean increase over the period of 23 cm, with the 90 % credible interval ranging from 19 to 27 cm. The linear trend model (Model 5) also estimates a mean increase of 23 cm during the period, with a 90 % credible interval ranging from 20 to 27 cm. Compared to the results using monthly data, the estimated trends are somewhat less with much narrower credible intervals.

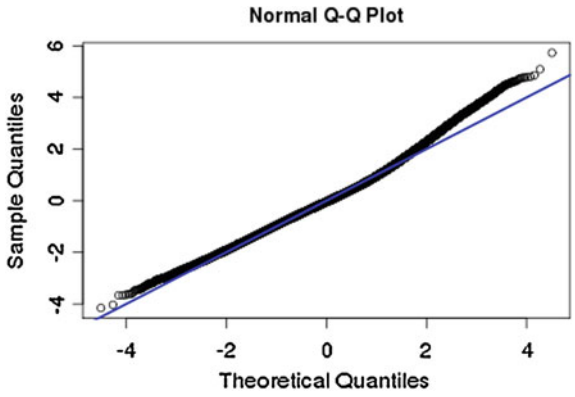

Fig. 3.16 Normal probability plot of the residuals, daily data

Table 3.6 Posterior marginal distributions, mean; standard deviation for daily data

	Model 1	Model 2	Model 3	Model 4	Model 5
σ_Z^2	0.56; 0.00075	0.56; 0.00074	0.56; 0.00080	0.56; 0.00075	0.56; 0.00076
σ_μ^2	0.029; 0.0033	0.029; 0.0035	0.030; 0.0034	0.030; 0.0035	0.030; 0.0034
σ_θ^2	0.17; 0.00058	0.17; 0.00052	0.17; 0.00059	0.17; 0.00056	0.17; 0.00057
σ_m^2	0.85; 0.012	0.93; 0.015	1.1; 0.012	1.05; 0.012	1.05; 0.012
b_0	0.24; 0.0012	0.24; 0.0012	0.24; 0.0012	0.24; 0.0011	0.24; 0.0012
b_N	0.12; 0.0012	0.12; 0.0011	0.12; 0.0011	0.12; 0.0011	0.12; 0.0011
b_E	0.15; 0.0012	0.15; 0.0012	0.15; 0.0012	0.15; 0.0011	0.15; 0.0012
b_S	0.18; 0.0012	0.18; 0.0012	0.18; 0.0013	0.18; 0.0012	0.18; 0.0012
b_W	0.28; 0.0012	0.28; 0.0012	0.28; 0.0012	0.28; 0.0012	0.28; 0.0012
c	1.4; 0.012	1.4; 0.012	1.4; 0.012	1.4; 0.012	1.4; 0.012
d	0.31; 0.012	0.31; 0.012	0.31; 0.012	0.31; 0.012	0.31; 0.012
$\mu_{0,1}$	3.4; 1.5	3.3; 1.4	3.4; 1.4	3.4; 1.4	3.4; 1.4
$\mu_{0,2}$	−0.22; 0.044	−0.22; 0.044	−0.22; 0.044	−0.22; 0.044	−0.22; 0.044
$\mu_{0,3}$	1.3; 0.26	1.3; 0.26	1.3; 0.26	1.3; 0.26	1.3; 0.26
$\mu_{0,4}$	0.00042; 0.00011	0.00042; 0.00011	0.00042; 0.00011	0.00042; 0.00011	0.00043; 0.00011
$\mu_{0,5}$	−0.0078; 0.0014	−0.0078; 0.0014	−0.0078; 0.0014	−0.0077; 0.0014	−0.0078; 0.0014
$\mu_{0,6}$	−0.0012; 0.00064	−0.0012; 0.00064	−0.0012; 0.00062	−0.0012; 0.00064	−0.0012; 0.00061
a_ϕ	0.13; 0.13; 0.067	0.13; 0.13; 0.065	0.13; 0.13; 0.066	0.13; 0.12; 0.065	0.13; 0.13; 0.066
a_λ	0.15; 0.15; 0.066	0.15; 0.15; 0.066	0.14; 0.14; 0.066	0.15; 0.15; 0.072	0.15; 0.15; 0.067

Table 3.7 Posteriors related to the trend component, daily data

	Model 1	Model 2	Model 3	Model 4	Model 5
σ_T^2	0.20; 0.0058	0.12; 0.0096	–	–	–
γ	-1.1×10^{-5}; 4.5×10^{-6}	1.4×10^{-5}; 2.4×10^{-6}	–	-1.0×10^{-5}; 5.2×10^{-6}	1.4×10^{-5}; 1.3×10^{-6}
η	1.6×10^{-9}; 2.7×10^{-10}	–	–	1.5×10^{-9}; 3.5×10^{-10}	–

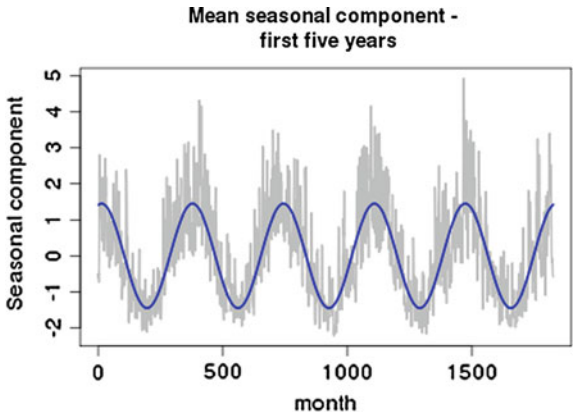

Fig. 3.17 The seasonal component for 5 years, daily data; $M(t)$ (*grey lines*) and $c\cos(\omega t) + d\sin(\omega t)$ (*blue lines*)

3.5.3 Results for Monthly Maximum Data

Finally, the models were run on monthly maximum data, i.e., the maximum significant wave height at each spatial location for each month. The results from these simulations are presented in the following. A visual check of the residuals indicates that the Gaussian model assumptions in Eq. 3.4 might be reasonable, although model fit seems to be somewhat poorer than for nonmaximum data.

Most of the marginal posterior distributions are symmetric and resemble Gaussian distributions, and the mean and standard deviation of the posterior distributions for some of the parameters of the different model alternatives are given in Table 3.8. Apart from the temporal trend part, most of the model parameters do not vary significantly between model alternatives. It is observed that b_N is smaller than the other $b_\cdot$ parameters, but no particular explanations for this have been sought.

The posterior time-independent part $\mu(x)$ looks reasonable with values in the order of 6.1–7.3 m. The posteriors of the space-time dynamic part take values between -1.1 and 1.8 m and a notable part of the variation in the data is explained by this component. The seasonal contribution corresponds to an annual cyclic variation of about ± 2.5 m.

The long-term trend part is illustrated in Fig. 3.20. For the quadratic model (model 1) the mean yearly trend corresponds to nearly 70 cm over the period. The 90 % credible interval embraces overall trends between 44 and 93 cm. The corresponding trend from the linear model (Model 2) corresponds to an increase of about 69 cm over the period with a 90 % credible interval ranging from 45 to 94 cm. For the models with one temporal noise term, the seasonal and trend components were not sampled individually, but the joint temporal components are shown along with the mean seasonal part and the mean, 5- and 95-percentiles of the trend contribution. The quadratic trend model (Model 4) estimates a mean increase over the period of 68 cm, with the 90 % credible interval ranging from 39 to 96 cm. The linear trend model (Model 5) estimates a mean increase of 69 cm during the period, with a 90 % credible interval ranging from 40 to 96 cm.

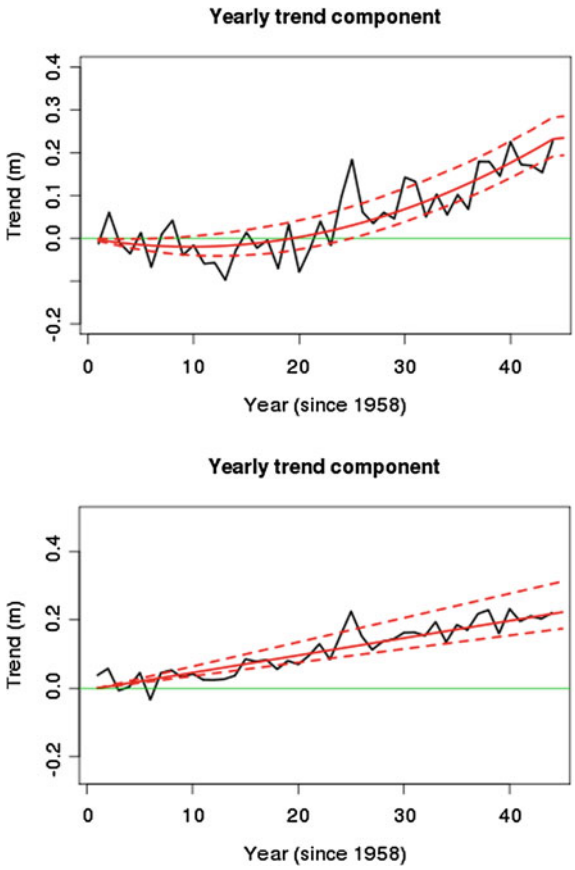

Fig. 3.18 Annual trend over the period, model 1 (*top*) and model 2 (*bottom*), daily data; mean T(t) (*black lines*) and mean and 90 % credible interval of $\gamma t + \eta t^2$ (*red lines*). *Green lines* correspond to no trend

3.5.4 Model Comparison and Selection

The different model alternatives can be briefly compared by comparing the resulting posterior estimates of the model parameters, as presented in for example Table 3.4. From these tables, it is observed that the parameters related to the spatial features of the model seem to be little affected by the model reductions. Keeping in mind that the model reductions were only related to the temporal trend, it is reassuring to observe that all model alternatives give similar estimates for the spatial parts of the model. Also, the seasonal part of the model seems to behave rather similarly for the various model alternatives. Hence, the main differences are, as would be expected, related to the long-term temporal trend.

The losses corresponding to the two loss functions were estimated for the various datasets and model alternatives and are given in Table 3.9. No reward is given here for parsimony, and only predictive power is included in the loss functions. Note

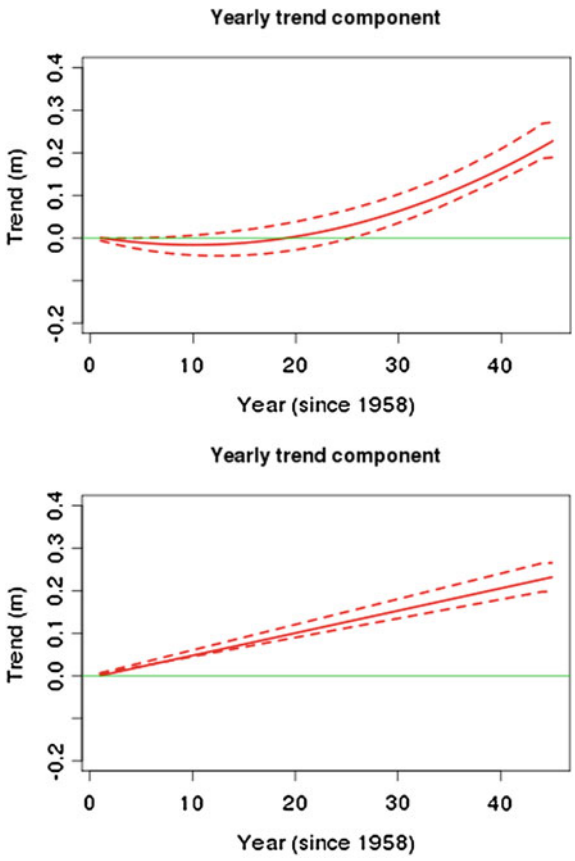

Fig. 3.19 Mean and 90-% credible interval of the estimated trend components for models 4 (*top*) and 5 (*bottom*), daily data (*red lines*). *Green lines* correspond to no trend

however, that comparison between results pertaining to different datasets might not be applicable.

According to these criteria, preference is given to the linear trend models for the monthly and monthly maximum data, but the models with quadratic trends seem to be favoured for the daily data. Hence, at least for short-term prediction, these model alternatives seem to perform best for the various subsets of data. This inconsistency might be bothersome, but it is observed that the differences in the values in Table 3.9 are relatively small and it is difficult to distinguish between the model performances based on these. Hence, it cannot be determined which model performs best with any strong confidence, and they all seem to describe the data equally well. Furthermore, it is difficult to assess the models in terms of long-term prediction and it is still an open question which model alternative that should be regarded as superior in this respect.

Table 3.8 Posterior marginal distributions, mean; standard deviation for monthly maximum data

	Model 1	Model 2	Model 3	Model 4	Model 5
σ_Z^2	1.2; 0.0085	1.2; 0.0081	1.2; 0.0080	1.2; 0.0079	1.2; 0.0081
σ_μ^2	0.035; 0.0042	0.035; 0.0042	0.035; 0.0040	0.035; 0.0042	0.035; 0.0044
σ_θ^2	0.074; 0.0059	0.074; 0.0056	0.076; 0.0054	0.074; 0.0052	0.074; 0.0051
σ_m^2	0.63; 0.16	0.56; 0.13	1.1; 0.073	1.1; 0.068	1.1; 0.069
b_0	0.23; 0.0094	0.23; 0.0095	0.23; 0.0094	0.23; 0.0095	0.23; 0.0096
b_N	0.0068; 0.011	0.0064; 0.012	0.0090; 0.011	0.0055; 0.011	0.0059; 0.011
b_E	0.22; 0.010	0.22; 0.0097	0.22; 0.0098	0.22; 0.0098	0.22; 0.0098
b_S	0.35; 0.026	0.35; 0.023	0.34; 0.023	0.35; 0.023	0.35; 0.022
b_W	0.23; 0.011	0.23; 0.010	0.23; 0.0099	0.23; 0.010	0.23; 0.010
c	2.4; 0.062	2.4; 0.065	2.4; 0.067	2.4; 0.064	2.4; 0.067
d	1.0; 0.067	1.0; 0.063	1.0; 0.067	1.0; 0.066	1.0; 0.065
$\mu_{0,1}$	3.4; 1.5	3.4; 1.3	3.4; 1.4	3.4; 1.4	3.3; 1.3
$\mu_{0,2}$	−0.28; 0.068	−0.28; 0.068	−0.28; 0.067	−0.29; 0.066	−0.29; 0.064
$\mu_{0,3}$	1.9; 0.39	1.8; 0.40	1.9; 0.39	1.9; 0.39	1.9; 0.38
$\mu_{0,4}$	0.00049; 0.00017	0.00048; 0.00017	0.00049; 0.00017	0.00050; 0.00017	0.00050; 0.00016
$\mu_{0,5}$	−0.013; 0.0024	−0.13; 0.0023	−0.013; 0.0022	−0.013; 0.0023	−0.013; 0.0023
$\mu_{0,6}$	−0.0010; 0.00095	−0.0010; 0.00097	−0.0011; 0.00098	−0.0011; 0.00097	−0.0011; 0.00096
σ_t^2	0.50; 0.16	0.56; 0.13	–	–	–
γ	0.0022; 0.0011	0.0013; 0.00028	–	0.0018; 0.0014	0.0013; 0.00033
η	-1.7×10^{-6}; 2.1×10^{-6}	–	–	-9.1×10^{-7}; 2.5×10^{-6}	–

Table 3.9 Model selection: estimated losses

Model alternative	Monthly data		Daily data		Monthly max	
	L_s	L_w	L_s	L_w	L_s	L_w
Model 1	2.861	3.150	2.223	2.319	2.630	2.748
Model 2	2.857	3.144	2.266	2.372	2.576	2.691
Model 3	2.917	3.233	2.312	2.430	2.775	2.902
Model 4	2.868	3.160	2.223	2.321	2.609	2.726
Model 5	2.851	3.136	2.263	2.369	2.580	2.695

3.5.5 Future Projections

Even though extrapolation beyond the time interval for which the models are fitted might not be valid, it is tempting to extend the estimated trends into the future. It is acknowledged that this might be somewhat speculative. Notwithstanding, assuming that such trends as the ones predicted from the linear models will continue into the future, the corresponding expected increases over 100 years are summarized below.

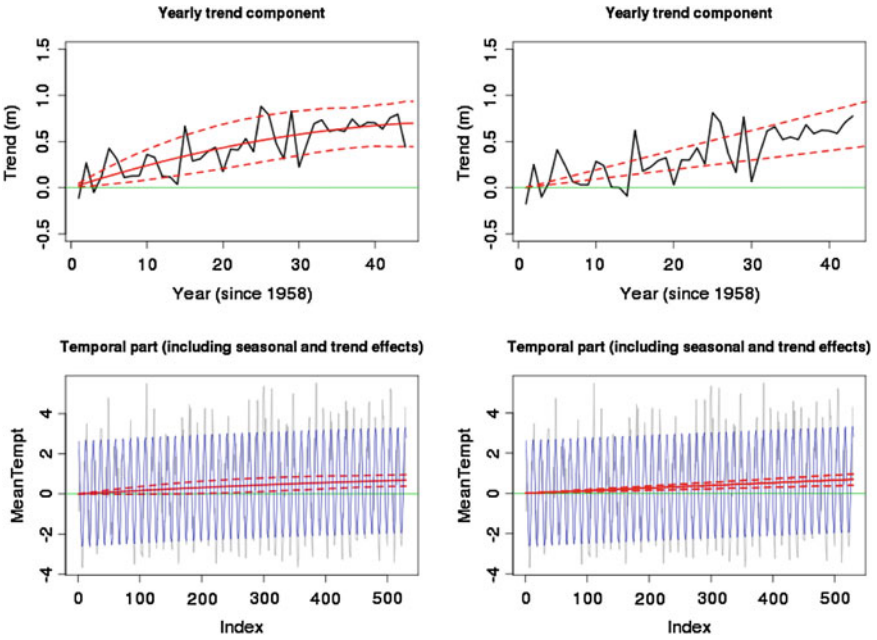

Fig. 3.20 Estimated temporal trends of the 45-year period; Model 1 (*top left*), Model 2 (*top right*), Model 4 (*bottom left*) and Model 5 (*bottom right*)

Extrapolations of the quadratic trend functions are deemed even more speculative, as the quadratic term in t would dominate completely, and will not be performed herein.

3.5.5.1 Monthly Data

Assuming that a trend such as the one predicted from the linear trend models with monthly data will continue into the future, it is interesting to note that this would correspond to an expected increase in significant wave height of 64 cm with a 95 % credibility of an increase of at least 11 cm over 100 years (for the model with two temporal noise terms) or 84 cm with a 95 % credibility of an increase of at least 29 cm over 100 years (for the model with one temporal noise term).

3.5.5.2 Daily Data

Assuming that a trend such as the one predicted from the linear trend model with daily data will continue into the future, it is interesting to note that this would correspond to an expected increase in significant wave height of 51 cm with a 95 % credibility

of an increase of at least 40 cm over 100 years. A very similar trend was obtained for the linear model with one temporal noise term.

3.5.5.3 Monthly Maxima Data

Assuming that estimated linear trends from the monthly maxima data will continue, the results correspond to an expected increase in monthly maximum significant wave height of 1.6 m over 100 years, with a 95 % credibility of an increase of at least around 1.0 m. The two linear trend estimates, with credibility bands, are nearly identical. It is noted that this trend is significantly stronger than for the monthly and daily data, but this might not be surprising. Indeed, it is reported elsewhere that trends might be stronger for extremes compared to average conditions [39], so this is believed to be a genuine feature that is reflected in the data and picked up by the models.

3.5.6 General Comments

Different model alternatives have been tried, e.g., with respect to number of noise terms included. Initially, two temporal noise terms were included in the model as this would presumably yield the most flexible model. However, it is realized that including two temporal noise terms in the model might lead to identifiability problems. This is illustrated in Fig. 3.21, where it is seen that for different iterations (index), different parts of the temporal noise are ascribed to the seasonal noise term and the trend noise term respectively even though the sum of the two is fairly stationary. Since there is no way for the models to be able to distinguish between temporal noise from the seasonal contribution and the long-term trend contribution, this is as expected. It was attempted to improve the models by removing one of the temporal noise terms. However, simulations do not indicate that the models with only one temporal noise term perform consistently different. It is also argued that identifiability problems between the two temporal noise terms are not crucial, as long as the other components and the overall results are not heavily influenced by this, and that the models with two terms can be kept as alternatives. The difference in performance does not seem to be substantial and it is not assumed to influence the results much. Furthermore, trace-plots of the other model parameters show no sign of being affected by the instability of the individual temporal noise terms, and it is assumed that since the total temporal noise seem to have converged to stationary conditions, this does not create any serious problems for the other model parameters and the overall model as such. Furthermore, informal tests indicate that the models do converge within the burn-in period in spite of this issue.

It is observed that the iid-assumptions of the residuals are mildly violated. Upon closer examination, there seems to be a spatial dependence of the residuals and this is construed as an effect of the borders of the area with unobserved neighbours. In Fig. 3.22 residuals for a fixed time and iteration are plotted for all locations; a

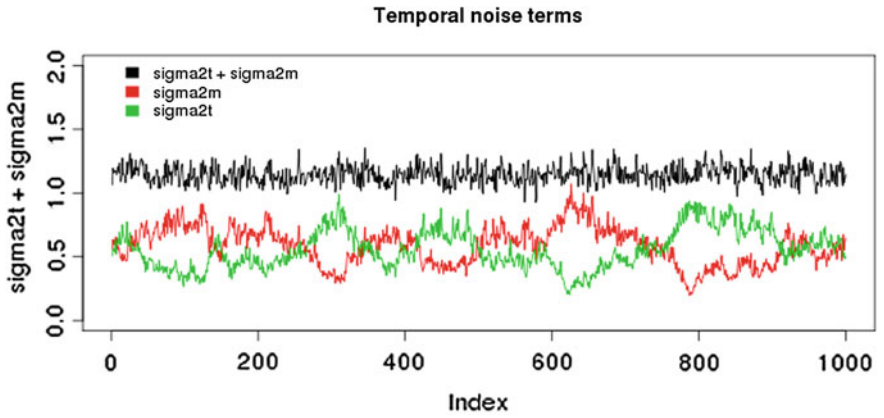

Fig. 3.21 Example of sampled temporal noise terms: Even though $\sigma_{\mathrm{T}}^2 + \sigma_m^2$ seem to be fairly stationary, there seem to be identifiability problems regarding the distribution of the temporal noise

dependence structure caused by the borders of the area is clearly seen. Recalling that the area consists of a grid of 17×9 locations, 17 subsequent residuals in the plot corresponds to locations at a fixed latitude and it is clearly seen that there are nine peaks corresponding to the nine points in lateral direction. Hence, at each border-point to the east or west, the iid-assumption seems to break down. However, it is argued that this does not disqualify the model, but rather that care should be taken in applying it to locations close to the borders of the area. The spatial part of the model might not perform well at the borders but in the more central parts of the area the model assumptions seem to hold. This is a rather well-known characteristic of spatial models without adjustments for edge effects and is not particular to this model (see e.g., [15]). One physical explanation for the observed border effects could be that swell wave information coming from neighbouring areas are lost at the borders, especially since the area under consideration is known to be in a swell dominated region. Apart from this, the spatial part of the model seems to be robust to changes in temporal resolution of the data and to changes in the temporal parts of the model, and the purely spatial part of the model overall is believed to perform well.

It was noted previously that there are arguments against using inverse gamma priors on the noise variances, and noninformative priors could have been used instead. Two examples of vague priors are uniform priors, $\sigma_\cdot^2 \sim U[\cdot]$ and inverse priors, $\pi(\sigma_\cdot^2) \propto \frac{1}{\sigma_\cdot^2}$. The rationale for using inverse gamma priors on the noise variances is, obviously, to restrain the error terms from becoming too large. However, in order to investigate how sensitive the results are to this choice of priors on the noise variances, simulations were also run with the inverse noninformative priors. As could be expected, using noninformative priors leads to the temporal noise being unevenly distributed between ε_t and ε_m. In fact, ε_m becomes quite large and ε_t becomes almost zero, but this is easily explained by the fact that ε_m is sampled first. Since the prior

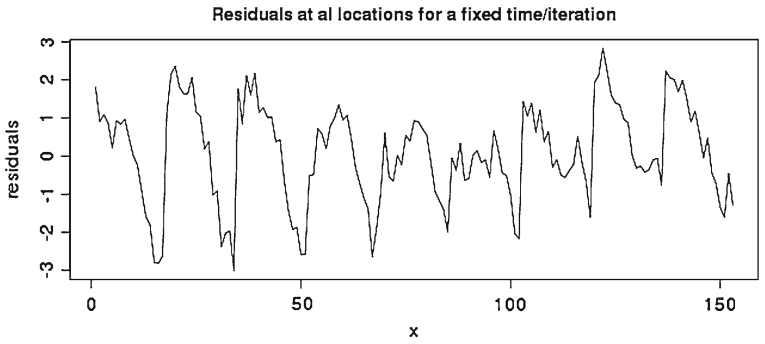

Fig. 3.22 Residuals for all spatial locations at a fixed time/iteration

does not impose any restrictions on how large this should be, all of the temporal noise will be ascribed to this term, and there will be little noise left for ε_t. Other effects are that the acceptance rate of the Metropolis-Hastings steps seemed to decrease. The results pertaining to the posterior spatial, short-term space-time and seasonal parts are more or less the same regardless of the noise variance priors. For the long-term trends, there might be a tendency towards somewhat smaller trends when using noninformative priors on the noise variances. According to the loss functions, the models generally seem to perform worse with noninformative priors, and it is concluded that replacing the inverse gamma priors with noninformative priors does not represent an improvement. Thus, the inverse gamma priors will be kept. Details of results from some simulations with noninformative priors are reported in [32].

3.5.6.1 Simulations of Six-Hourly Data

The models were also run for all the data, trying to exploit the full temporal resolution of 6 h. Running these simulations was very computational intensive with each set of simulations requiring about 6,000 CPU-hours. The burn-in-period was still 20,000 and with a batch size of 5. The initial check of model assumptions seems satisfactory, but there are indications of nonconvergence of the Gibbs-sampler. Hence, the quantitative estimates from these simulations are regarded as unreliable. Nevertheless, it is believed that the results provide some useful insight and a qualitative description of these simulations will be given below.

The contribution from the time-independent part is almost identical to the results obtained using monthly and daily data, which is reassuring. However, the contribution from the short-term space-time dynamic part, $\theta(x, t)$, is significantly larger than what was obtained from the daily (and monthly) data. It is expected that a higher temporal resolution would make this dynamic part more meaningful, so this might not be problematic. Again, b_W is the largest of the b-parameters except b_0 and it is observed that b_E and b_S have negative posterior expectations. This further substantiates that

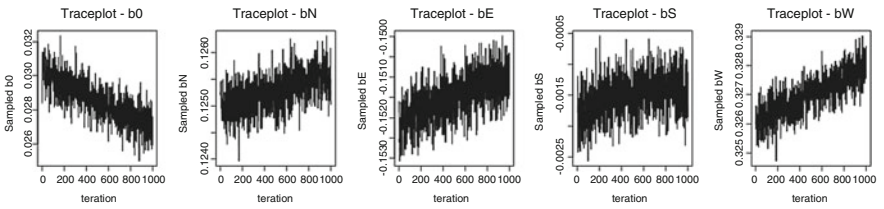

Fig. 3.23 Traceplots for the b-parameters (six-hourly data) indicate lack of convergence

sea states travels predominantly from the west or from the north in this particular area. However, trace plots indicate that the parameters determining the contribution from this component may not have converged, so reservations should be made in the interpretation of this component. Trace plots for the five b-parameters are given in Fig. 3.23 and it can be seen that all the b_D's, $D = N, E, S, W$, are increasing at the expense of b_0.

The temporal trend contributions of the models with two temporal noise terms are very small, but increasing. However, trace plots suggest that the trend did not yet converge; e.g., an overall positive drift can be seen for the sampled trends at $t = T$. Even though the drift is small, it is not possible to know at what level stationarity would occur if the drift continues. The trend contributions for the models with one temporal noise term (models 4 and 5) are considerably larger than the ones estimated with two noise terms, and it is observed that there are no longer any visible drift in the trend-parameters. Possibly, the removal of one temporal noise term speeds up convergence so that the results for these model alternatives might be from, or closer to, the stationary distributions. The quadratic trend model (Model 4) estimates a mean increase over the period which is smaller but still comparable to the trend obtained using monthly and daily data.

It is uncertain whether the model, when applied to six-hourly data, converges within the burn-in period, and less confidence is put on the results from these simulations. These simulations were extremely time consuming, requiring more than 30,000 CPU-hours for the simulations reported herein, so it is impractical to perform new simulations with increased burn-in. Hence, lack of convergence might be the reason for the lower trends estimated from the six-hourly data. Another possible explanation may be that the space-time dynamic part, $\theta(x, t)$, incorporates, partly, a long-term trend. The long-term effect of this component should ideally be zero, but no constraints are imposed to ensure this. Therefore, it might be that this component absorbs and camouflages trends in the data. This is supported by the fact that $\theta(x, t)$ becomes increasingly important for increasing temporal resolution. A possible solution could be to introduce restrictions on the autoregressive parameters to make them stationary over long-time periods and prevent them from absorbing long-term trend, but this has not been pursued in this study. Nevertheless, the long term effect of this component is found to be negligible upon inspection of the results also for the six-hourly data. Possibly, nonlinear dynamic effects start to dominate for higher temporal resolutions, which are not properly accounted for by the model.

3.6 Discussion

Regarding the different long-term trend components, it is acknowledged that the simple selection criteria employed are not really able to confidently distinguish between them; they all seem to describe the data similarly well. However, if the estimated trends should be used for future projections, it is assumed that the quadratic trend cannot be extrapolated into the future, and estimates of future trends could only be based on the linear trend. Even this might not be valid, but assuming that one might make such projections, the models project an expected increase of significant wave height around 50–80 cm, with a 95 % credible increase of at least between 11 and 40 cm over 100 years. For monthly maximum significant wave height, the increasing trends are bigger, with an expected increase of 1.6 m over the next 100 years. This seem to be in reasonable agreement to other projections made for significant wave height in the North Atlantic [8, 10, 34, 35]. The estimated trends are also found to agree reasonably well with trends identified in the data by more conventional time series trend analyses on spatially reduced data, as reported in [33].

However, it is noted that even though the models seem to detect trends in the data, it does not necessarily mean that there is a trend related to climate change. The trend might be a result of decadal natural variability, as discussed in for example [5]. Great care should therefore be taken when interpreting the meaning and the origin of this trend. Notwithstanding, if the model should be used for projections and long-term predictions, it is believed that the model could be extended with appropriate covariates, as briefly discussed above and explored in Chap. 5.

It is observed that the goodness-of-fit seems to decrease for the model when applied to monthly maximum data, as seen by the relatively larger observational variance compared to the other stochastic terms. Furthermore, when going from monthly or daily to monthly maximum data, it is observed that, e.g., the b_N-parameter becomes notably smaller than for the other $b_.$-parameters. There could be different explanations for this, but these have not been further pursued.

Different attempts at model comparison and selection have been considered, but neither are optimal for such a complex model. In particular, if the aim is to estimate long-term temporal trends and to extrapolate those into the future, neither goodness-of-fit nor short-term predictive power seem to be suitable as selection criteria. In fact, according to the model selection approaches employed, simulations on monthly and monthly maximum data seem to favour linear trends, daily data quadratic trends and six-hourly data no trends. This inconsistency is troublesome, but it might just be that this indicates that estimation of such a comparably small trend, distinguishing a genuine trend, which is relatively insignificant compared to the other contributions, from the noise, is difficult. It may also illustrate the sensitivity of such models on the temporal resolution of the data. At any rate, it is merely noted that model selection for the model presented herein remains an open issue.

3.7 Summary and Conclusions

This chapter has outlined a Bayesian hierarchical space-time model for significant wave height data, and applied it on a set of data extracted from ERA-40 for an area in the North Atlantic Ocean, covering the period from 1958 to February 2002. Different temporal resolutions have been tried, illustrating the sensitivity of the model results to such changes. Five model alternatives have been considered, where the differences have been in how a long-term temporal trend is modeled and in the number of temporal noise terms (one or two). All model alternatives give similar results with respect to the spatial features of the model but the different models and different data resolutions yield slightly different estimates for the temporal features. The space-time dynamic term is seen to become increasingly important for increasing temporal resolution, and different trend components obviously affect the estimated long-term trends. However, model selection remains inconclusive.

The trends estimated from the various simulations are fairly consistent, disregarding the simulations for six-hourly data, with expected trends of 22–23 cm for the daily data and 28–38 cm for the monthly data over the period from 1958 to 2002. For monthly maxima, the mean estimated trends were about 70 cm, indicating that there is a stronger trend in extreme conditions than in average conditions. Extrapolating the linear trends over 100 years corresponds to expected increases within the range of 50–80 cm for normal conditions and about 1.6 m for monthly maxima, which overall are in reasonable agreement with previous studies.

References

1. Aggoun, L.: Kalman filtering of a space-time markov random field. Math. Comput. Model. **36**, 1193–1209 (2002)
2. Akaike, H.: A new look at the statistical model identification. IEEE Trans. Autom. Control **19**, 716–723 (1974)
3. Babanin, A.V., Chalikov, D., Young, I., Savelyev, I.: Numerical and laboratory investigation of breaking of steep two-dimensional waves in deep water. J. Fluid Mech. **644**, 433–463 (2010)
4. Banerjee, S., Carlin, B.P., Gelfand, A.E.: Hierarchical modeling and analysis for spatial data. Chapman & Hall/CRC, Boca Raton (2004)
5. Caires, S., Sterl, A.: 100-year return value estimates for ocean wind speed and significant wave height from the ERA-40 data. J. Clim. **18**, 1032–1048 (2005)
6. Caires, S., Sterl, A.: A new nonparametric method to correct model data: application to significant wave height from ERA-40 re-analysis. J. Atmospheric Ocean. Technol. **22**, 443–459 (2005)
7. Caires, S., Swail, V.: Global wave climate trend and variability analysis. In: Preprints of 8th International Workshop on Wave Hindcasting and Forecasting (2004)
8. Caires, S., Swail, V.R., Wang, X.L.: Projection and analysis of extreme wave climate. J. Clim. **19**, 5581–5605 (2006)
9. Gelman, A.: Prior distributions for variance parameters in hierarchical models. Bayesian Anal. **1**, 515–533 (2006)
10. Grabemann, I., Weisse, R.: Climate change impact on extreme wave conditions in the North Sea: an ensemble study. Ocean Dyn. **58**, 199–212 (2008)

11. Guedes Soares, C., Ferreira, A., Cunha, C.: Linear models of the time series of significant wave height on the Southwest Coast of Portugal. Coast. Eng. **29**, 149–167 (1996)
12. Kalman, R.: A new approach to linear filtering and prediction problems. J. Basic Eng. **82**, 35–45 (1960)
13. Konig, T., Lehner, S., Schulz-Stellenfleth, J.: Global analysis of a 2 year ERS-2 wavemode dataset over the oceans. In: Proceedings of the Geoscience and Remote Sensing Symposium (IGARSS 2007). IEEE International (2007)
14. Kushnir, Y., Cardone, V., Greenwood, J., Cane, M.: The recent increase in north atlantic wave heights. J. Clim. **10**, 2107–2113 (1997)
15. Lim, J., Wang, X., Sherman, M.: An adjustment for edge effects using an augmented neighborhood model in the spatial auto-logistic model. Comput. Stat. Data Anal. **51**, 3679–3688 (2007)
16. Meinhold, R.J., Singpurwalla, N.D.: Understanding the kalman filter. Am. Statist. **37**, 123–127 (1983)
17. Natvig, B., Tvete, I.F.: Bayesian hierarchical space-time modeling of earthquake data. Methodol. Comput. Appl. Probab. **9**, 89–114 (2007)
18. Robert, C.P., Casella, G.: Monte Carlo statistical methods, 2nd edn. Springer, Heidelberg (2004)
19. Rue, H., Martino, S., Chopin, N.: Approximate Bayesian inference for latent Gaussian models by using integrated nested Laplace approximations. J. R. Stat. Soc. B **71**, 319–392 (2009)
20. Schwarz, G.: Estimating the dimension of a model. Annal. Stat. **6**, 461–464 (1978)
21. Scotto, M., Guedes Soares, C.: Modelling the long-term time series of significant wave height with non-linear threshold models. Coast. Eng. **40**, 313–327 (2000)
22. Smith, R.L.: Environmental statistics. University of North Carolina (2001). http://www.stat.unc.edu/postscript/rs/envnotes.pdf. Accessed 21 Oct 2010
23. Spiegelhalter, D.J., Best, N.G., Carlin, B.P., van der Linde, A.: Bayesian measures of model complexity and fit. J. R. Stat. Soc. Ser. B **64**, 583–639 (2002)
24. Sterl, A., Caires, S.: Climatology, variability and extrema of ocean waves: the web-based KNMI/ERA-40 wave atlas. Int. J. Climatol. **25**, 963–977 (2005)
25. Toffoli, A., Babanin, A., Onorato, M., Waseda, T.: Maximum steepness of oceanic waves: field and laboratory experiments. Geophys. Res. Lett. **37**, L05, 603 (2010)
26. Tvete, I.F., Natvig, B.: A comparison of an analytical approach and a standard simulation approach in Bayesian forecasting applied to monthly data from insurance of companies. Methodol. Comput. Appl. Probab. **4**, 95–113 (2002)
27. Uppala, S.M., Kållberg, P.W., Simmons, A.J., Andrae, U., Da Costa Bechtold, V., Fiorino, M., Gibson, J.K., Haseler, J., Hernandez, A., Kelly, G.A., Li, X., Onogi, K., Saarinen, S., Sokka, N., Allan, R.P., Andersson, E., Arpe, K., Balmaseda, M.A., Beljaars, A.C.M., Van de Berg, L., Bidlot, J., Bormann, N., Caires, S., Chevallier, F., Dethof, A., Dragosavac, M., Fisher, M., Fuentes, M., Hagemann, S., Hólm E. Hoskins, B.J., Isaksen, L., Janssen, P.A.E.M., Jenne, R., McNally, A.P., Mahfouf, J.F., Morcrette, J.J., Rayner, N.A., Saunders, R.W., Simon, P., Sterl, A., Trenberth, K.E., Untch, A., Vasiljevic, D., Vitebro, P., Woolen, J.: The ERA-40 re-analysis. Q. J. R. Meteorol. Soc. **131**, 2961–3012 (2005)
28. Vanem, E.: Long-term time-dependent stochastic modelling of extreme waves. Stoch. Env. Res. Risk Assess. **25**, 185–209 (2011)
29. Vanem, E., Huseby, A.B., Natvig, B.: A Bayesian-hierarchical space-time model for significant wave height data. In: Proceedings of the 30th International Conference on Ocean, Offshore Mechanics and Arctic Engineering (OMAE 2011). American Society of Mechanical Engineers (ASME) (2011)
30. Vanem, E., Huseby, A.B., Natvig, B.: A Bayesian hierarchical spatio-temporal model for significant wave height in the North Atlantic. Stoch. Env. Res. Risk Assess. **26**, 609–632 (2012)
31. Vanem, E., Huseby, A.B., Natvig, B.: A stochastic model in space and time for monthly maximum significant wave height. In: P. Abrahamsen, R. Haugen, O. Kolbjørnsen (eds.) Geostatistics Oslo 2012, pp. 505–517. Springer, Heidelberg (2012)
32. Vanem, E., Huseby, A.B., Natvig, B.: Bayesian hierarchical spatio-temporal modelling of trends and future projections in the ocean wave climate with a CO_2 regression component. Environ. Ecol. Stat. (in press) (2013)

33. Vanem, E., Walker, S.E.: Identifying trends in the ocean wave climate by time series analyses of significant wave height data. Ocean Eng. **61**, 148–160 (2012)
34. Wang, X.J., Zwiers, F.W., Swail, V.R.: North Atlantic ocean wave climate change scenarios for the twenty-first century. J. Clim. **17**, 2368–2383 (2004)
35. Wang, X.L., Swail, V.R.: Climate change signal and uncertainty in projections of ocean wave heights. Clim. Dyn. **26**, 109–126 (2006)
36. West, M., Harrison, J.: Bayesian forecasting and dynamic models, 2nd edn. Springer, Heidelberg (1997)
37. Wikle, C.K.: Hierarchical models in environmental science. Int. Stat. Rev. **71**, 181–199 (2003)
38. Wikle, C.K., Berliner, L.M., Cressie, N.: Hierarchical Bayesian space-time models. Environ. Ecol. Stat. **5**, 117–154 (1998)
39. Young, I., Zieger, S., Babanin, A.: Global trends in wind speed and wave height. Science **332**, 451–455 (2011)

Chapter 4
Including a Log-Transform of the Data

In this chapter, the Bayesian hierarchical space-time model developed in Chap. 3 has been fitted to log-transformed data of significant wave height. There are two main motivations for this; performing a log-transform of the data yields a model with greater estimated trends for rougher sea states compared to more moderate conditions and the log-transform could account for observed heteroscedasticity in the data. This chapter is based on material previously presented in [13, 14].

4.1 Introduction and Motivation

There are several reasons for wanting to perform a log-transform of the data. It can account for different contributions from the various model components for different parts of the significant wave height distribution. In particular, the model with a log-transform is able to account for a stronger trend in extremes than in non-extremes. Hence, including the log-transform yields a fundamentally different interpretation of the various components and the results, perhaps most importantly those pertaining to the long-term temporal trend part, and this makes it particularly interesting to explore.

There were observed some heteroscedastic features in the original time-series with variances varying seasonally. Higher significant wave heights seem to be associated with greater variance, and it is questionable whether the model without a log-transform is able to capture this satisfactorily. However, after the log-transform, the data appear to be homoscedastic and hence it is believed that the model will perform better on the log-transformed data. This is illustrated by comparing the time series in Fig. 4.1 with the time series in Fig. 4.2. The latter shows a time series of the log-transformed data with and without the seasonal mean removed. Figure 4.1 (middle) also shows the seasonal mean that was subtracted from the original data; an annual cyclic component.

E. Vanem, *Bayesian Hierarchical Space-Time Models with Application to Significant Wave Height*, Ocean Engineering & Oceanography 2,
DOI: 10.1007/978-3-642-30253-4_4, © Springer-Verlag Berlin Heidelberg 2013

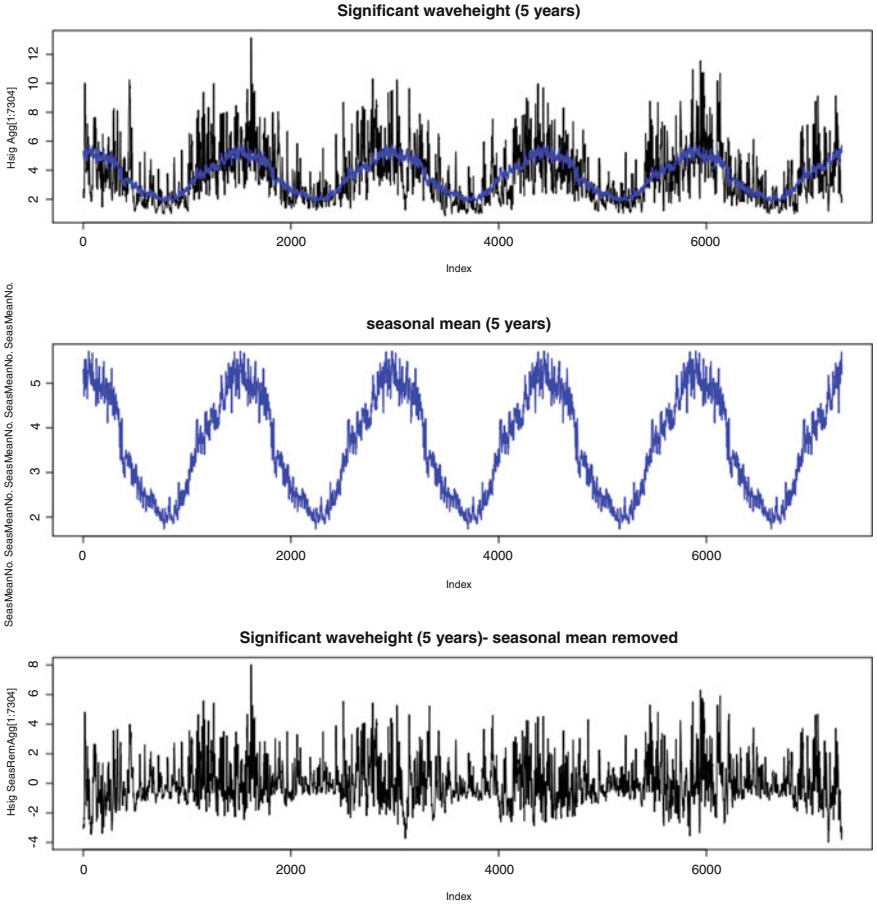

Fig. 4.1 Time series with and without seasonal mean

Another advantage of performing a log-transform is the impossibility of estimating negative significant wave heights. This would, of course, be unphysical and any sensible model for significant wave heights should be restricted from predicting negative significant wave heights. However, as it turns out, even with the original data this is not a serious problem, and the model simulates a negligible number of significant wave heights less than or equal to zero. At any rate, by taking the logarithmic transform this is no longer an issue. It is also interesting to note that good results have been reported for a log-normal transformation when modeling time series of significant wave height [3].

For inference made on log-transformed data, biases may be introduced when re-transforming back to the original scale and care should be taken to include appropriate bias correction factors when presenting and interpreting the results on the

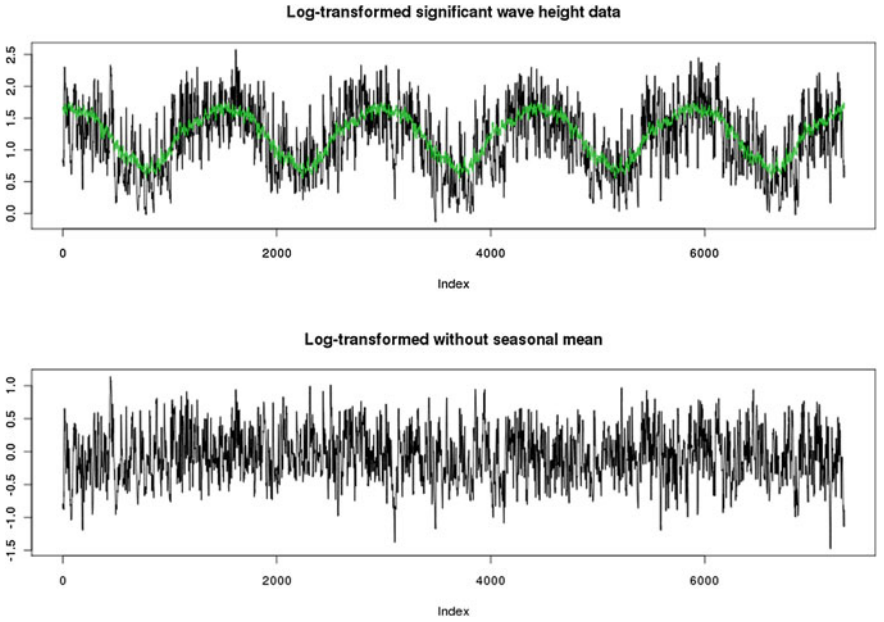

Fig. 4.2 Log-transformed time series with and without seasonal mean

non-transformed scale. Additionally, this chapter explores the effect of including a semiannual contribution in the seasonal component.

4.2 Re-Transformation Bias Correction

It has been known for quite some time that logarithmic transformation, as indeed any nonlinear transformation, of the data might lead to biased estimators on the original, i.e., re-transformed scale [2, 5, 8]. Hence, one should be aware of this fact when working with transformed data and bias corrections should be employed whenever necessary. A number of different correction factors for logarithmic transformation induced biases are reviewed in [10]. Basically, the bias is introduced when the re-transformation is performed on the mean, or other moments, of the transformed data in order to obtain estimators for the corresponding moments of the original data since, for the mean,

$$E[e^X] \neq e^{E[X]} \tag{4.1}$$

Hence, simply exponentiating the mean of X will give a biased estimator for the mean of $Y = e^X$, i.e., $\hat{Y} = e^{\bar{X}}$ will be biased. One way to account for this is to introduce

one of many alternative bias corrections that will give exact or approximate unbiased estimators of expected values.

However, the bias can also be avoided if the entire distribution, not just the moments, are exponentiated. A Bayesian approach to re-transformation back to the natural metric by exponentiating the entire posterior distribution is outlined in [11], thus resolving the bias problem in a straightforward manner. For the work presented herein, the bias is avoided in a similar but even simpler way; within the framework of Monte-Carlo simulations each individual sample is exponentiated which effectively re-transforms the entire distribution. Hence, re-transformed distributions on the original scale is obtained, and the mean and various quantiles can be estimated from those simulated distributions. In those cases, there is no reason to introduce any bias correction as long as all individual samples are re-transformed correctly. The exceptions are the estimates related to $\theta(x,t)$ where only the mean and the variance were kept during the simulations, due to data storage limitations, and a bias correction factor is needed. However, it turns out that the bias and thus also the bias correction is practically negligible for this component.

When the estimated seasonal and trend components $c\cos(\omega t) + d\sin(\omega t)$ and $\gamma t + \eta t^2$ are to be re-transformed, respective correction factors of $e^{0.5\bar{\sigma}_m^2}$ and $e^{0.5\bar{\sigma}_\mathrm{T}^2}$ are introduced, corresponding to the quasi maximum likelihood estimator (QMLE) [4]. For the model alternatives with one temporal noise term, a slight dilemma occurs related to how to incorporate the bias correction for the seasonal and trend contributions individually. However, it is observed that for the models with two temporal noise terms, the two variances are almost equal and the sum nearly identical to the variance for the single noise term in the models with one temporal noise term. Therefore, for the purpose of this study, a correction factor corresponding to half the variance will be adopted, i.e., $e^{0.25\sigma_m^2}$ for each part related to seasonal variation and long-term trend, for model alternatives 4 and 5. Due to the identifiability issues of the temporal noise contribution, the exact value to use in the bias correction factor of each temporal noise component is somewhat arbitrary. However, combined with the actual trend, this bias correction of the noise contribution corresponds to adding a constant and it would therefore not influence the estimated trends as such.

It is noted that failure to re-transform the entire posterior distributions of quantities of interest or to include appropriate correction factors would lead to biased results although the bias would presumably be small for large samples.

4.3 Revised Model Description

Denoting $Z(x,t)$ the significant wave height at location x and time t, the log-transforms are first carried out for each location and time-point,

$$Y(x,t) = \ln Z(x,t) \tag{4.2}$$

Then, at the observation level, the log-transformed data, Y, are modeled as the latent (or hidden) variables, $H(x,t)$, corresponding to some underlying significant wave height process, and some random noise, ε_Y:

$$Y(x,t) = H(x,t) + \varepsilon_Y(x,t) \qquad \forall\, x \geq 1, t \geq 1 \tag{4.3}$$

An equivalent representation of the observation model would be

$$Z(x,t) = e^{H(x,t)} e^{\varepsilon_Y(x,t)} \qquad \forall\, x,t \tag{4.4}$$

where now the noise term has become a multiplicative factor rather than an additive term and, conditioned on $H(x,t)$, the significant wave height $Z(x,t)$ will be log-normally distributed.

The underlying process for the significant wave height at location x and time t is modeled by the state model which is identical to the state model in Chap. 3. It will therefore not be repeated here, but it corresponds to the alternative representation in Eq. (4.5) on the original scale; the significant wave height can be modeled as the product of five multiplicative factors and therefore, the contribution from each of the model components will have a fundamentally different interpretation compared to the model for the original data.

$$Z(x,t) = e^{\mu(x)} e^{\theta(x,t)} e^{M(t)} e^{\mathrm{T}(t)} e^{\varepsilon_Y(x,t)} \qquad \forall\, x,t \tag{4.5}$$

The same five model alternatives outlined in Chap. 3 were also adopted for the log-transformed data.

4.3.1 Prior Distributions

The same priors as used in the model for the original data [12] are adopted for all model parameters. It can be questioned whether it is appropriate to use the same priors, in particular for some of the parameters (most notably perhaps, the different $\mu_{0,\cdot}$ parameters). However, a few simulations have been run with different priors for selected parameters, and overall, results seem not to be very sensitive to the choice of prior. For example, different priors for the $\mu_{0,\cdot}$ parameters give different posteriors as well, but the resulting $\mu_0(x)$-field, and consequently also the $\mu(x)$-field, remains largely unaffected. Hence, it is argued that the results are not overly sensitive to the exact values adopted for the hyperparameters. This may not be unexpected, as it is well known in Bayesian analysis that the priors become asymptotically irrelevant as the amount of data increases, and the amount of data is quite large in this case.

4.3.2 Loss Functions for Model Comparison

The same loss functions as in Chap. 3 are used also in the log-transformed case, but they are based on prediction errors on the original scale. Thus, the loss functions are

based on $Z(x)$ and not $Y(x)$ and should therefore, in principle, be suited for comparison with the results for the original data. Likelihood approaches and criteria based on sum of squares are not ideally suited for model selection in complex hierarchical models, but it is merely noted that the goodness-of-fit seemed to improve with the log-transformation compared to the results for the original data.

The predictions $Z(x)_j^*$ are taken as the estimated values of $Z(x)$ given the samples for all model parameters and variables in iteration j. The model specification gives

$$\begin{aligned} \boldsymbol{Z}(x)_j^* &= e^{\boldsymbol{Y}(x)_j^*} = e^{\mu(x)_j+\theta(x,t)_j+M(t)_j+\mathrm{T}(t)_j+\varepsilon_Y(x,t)_j} \\ &= e^{\mu(x)_j+\boldsymbol{B}_j\boldsymbol{\theta}(t-1)_j+c_j\cos(\omega t)+d_j\sin(\omega t)+\gamma_j t+\eta_j t^2+\varepsilon_\zeta(x)_j} \end{aligned} \tag{4.6}$$

where the subscript $_j$ denotes the sampled parameters in iteration j and the noise terms $\varepsilon_\zeta(x)$ are sampled independently from a zero-mean normal distribution with variance $\sigma^2_{\zeta,j} = \sigma^2_{Y,j} + \sigma^2_{\theta,j} + \sigma^2_{m,j} + \sigma^2_{T,j}$.

4.4 Simulations and Results

The same settings were used for the MCMC simulation on the log-transformed data as for the original data, i.e., a burn-in period of 20,000 and a batch size of 25 (with the batch size reduced to 5 for daily and six-hourly data). Visual inspection of trace plots indicates that convergence occurs relatively quickly and a few simulations have been performed with different starting values for the parameter set, indicating that the Gibbs sampler has converged. Again, some control simulations with considerably longer burn-in periods were run for the monthly data, and these showed nearly identical results, providing further evidence that convergence did indeed occur within the burn-in period. However, it cannot be taken for granted that convergence occurs equally fast for daily and six-hourly data.

4.4.1 Results for Monthly Data

In order to check the Gaussian model assumption in Eq. (4.3) for the log-transformed data, a visual check of the residuals was carried out. It is observed that the normal probability plot in Fig. 4.3 (for the quadratic model) looks much better than the corresponding plot for non-transformed data (see Chap. 3 [12]). This indicates that the log-transform may represent an improvement. There still seem to be some spatial dependences in the residuals, but this is presumably due to edge-effects, i.e., where there are no neighbour in at least one direction. This is the same features that were observed for the non-transformed data.

Most of the marginal posterior distributions are almost symmetric, and the posterior mean and standard deviation for different parameters of the different model

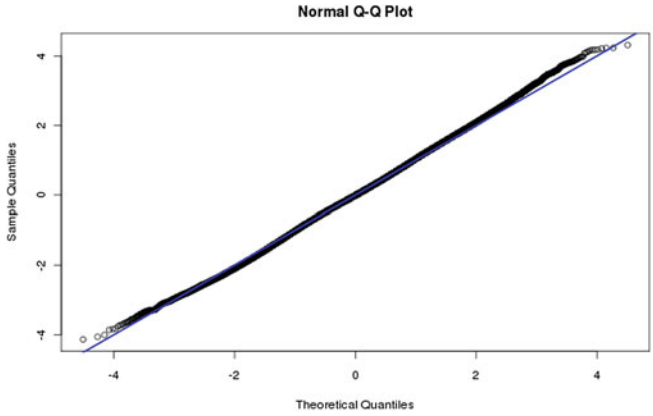

Fig. 4.3 Normal probability plot of the residuals, monthly data

alternatives are given in Table 4.1. With the exception of the temporal trend part, most of the model parameters do not vary significantly between model alternatives. It is emphasized that these parameters pertain to the log-transformed data, and the values are therefore not comparable to the values obtained for the non-transformed data. The posterior distributions for a_ϕ and a_λ are not symmetric, so the posterior distributions for these are presented in Table 4.1 in terms of the triplets (mean, median, standard deviation).

The six parameters $\mu_{0,\cdot}$ determine the spatially varying mean $\mu_0(x)$, and gives a similar picture as for the non-transformed data, but with different values. Also the time independent part $\mu(x)$ looks reasonable; Fig. 4.4 displays the mean of $\mu(x)$. The contribution from the time-independent part $\mu(x)$ is seen to be in the order of 0.83–1.1 but the interpretation is now different. $e^{\mu(x)}$ is a multiplicative factor for the significant wave height at location x varying between 2.3 and 2.9. The mean deviation from the spatially varying mean, $\mu_0(x)$, is small. In the following, all figures unless stated otherwise are from simulations over the main model (model 1), but the alternative models yield very similar results. It is emphasized that in estimating the mean contribution from this component at each location, as with all other components in the following, it is not sufficient to exponentiate the mean of $\mu(x)$ as this would bias the results (see also the discussion in Sect. 4.2). All samples of $\mu(x)$ have been exponentiated and then the mean has been estimated from the re-transformed distribution. However, it is observed that the bias that would be introduced in re-transforming the mean would have been negligible.

For the space-time dynamic part, $\theta(x,t)$, the mean ranges from -0.26 to 0.40 for all times (except $t=0$) and locations. For the log-transformed data, $\theta(x,t)$ corresponds to a multiplicative factor, $e^{\theta(x,t)}$, of the significant wave height at time-point (x,t) and the estimated mean values, $E[e^{\theta(x,t)}]$, correspond to factors between 0.77 and 1.5. The average corresponds to a factor of 1 as it should. Hence, a noticeable part of the modeled significant wave height can be ascribed to this space-time

Table 4.1 Posterior marginal distributions, mean; sd; monthly log-transformed data

	Model 1	Model 2	Model 3	Model 4	Model 5
σ_Z^2	0.057; 0.00034	0.057; 0.00036	0.057; 0.00034	0.057; 0.00036	0.057; 0.00036
σ_μ^2	0.027; 0.0030	0.027; 0.0030	0.027; 0.0030	0.027; 0.0032	0.027; 0.0030
σ_θ^2	0.0079; 0.00021	0.0079; 0.00021	0.0079; 0.00022	0.0079; 0.00020	0.0079; 0.00020
σ_m^2	0.063; 0.0065	0.061; 0.0068	0.10; 0.0061	0.10; 0.0062	0.10; 0.0061
b_0	0.21; 0.0079	0.21; 0.0078	0.21; 0.0076	0.21; 0.0079	0.21; 0.0081
b_N	0.17; 0.0091	0.17; 0.0094	0.17; 0.0094	0.17; 0.0090	0.17; 0.0093
b_E	0.21; 0.0087	0.21; 0.0087	0.21; 0.0084	0.21; 0.0086	0.21; 0.0086
b_S	0.16; 0.0092	0.16; 0.0090	0.16; 0.0094	0.16; 0.0094	0.16; 0.0099
b_W	0.19; 0.0081	0.19; 0.0079	0.19; 0.0078	0.19; 0.0084	0.19; 0.0079
c	0.35; 0.022	0.35; 0.021	0.35; 0.019	0.35; 0.020	0.35; 0.019
d	0.26; 0.021	0.26; 0.021	0.26; 0.019	0.26; 0.020	0.26; 0.019
$\mu_{0,1}$	3.5; 1.4	3.4; 1.4	3.5; 1.4	3.4; 1.5	3.5; 1.4
$\mu_{0,2}$	−0.089; 0.038	−0.087; 0.037	−0.089; 0.038	−0.089; 0.039	−0.087; 0.037
$\mu_{0,3}$	0.43; 0.22	0.43; 0.22	0.44; 0.22	0.44; 0.22	0.42; 0.22
$\mu_{0,4}$	0.00016; 9.5×10^{-5}	0.00016; 9.5×10^{-5}	0.00016; 9.4×10^{-5}	0.00016; 9.6×10^{-5}	0.00016; 9.5×10^{-5}
$\mu_{0,5}$	−0.0027; 0.0012	−0.0026; 0.0011	−0.0026; 0.0012	−0.0027; 0.0012	−0.0026; 0.0012
$\mu_{0,6}$	−0.00037; 0.00054	−0.00035; 0.00054	−0.00038; 0.00052	−0.00037; 0.00052	−0.00036; 0.00054
a_ϕ	0.083; 0.074; 0.058	0.083; 0.074; 0.056	0.086; 0.077; 0.058	0.086; 0.080; 0.056	0.086; 0.075; 0.059
a_λ	0087; 0.079; 0.058	0.085; 0.076; 0.057	0.086; 0.080; 0.056	0.088; 0.080; 0.058	0.085; 0.079; 0.055
σ_T^2	0.059; 0.0064	0.062; 0.0070)	–	–	–
γ	0.00039; 0.00039	0.00019; 9.8×10^{-5}	–	5.9×10^{-5}; 0.00042	0.00016; 8.0×10^{-5}
η	-4.0×10^{-7}; 7.3×10^{-7}	–	–	1.1×10^{-7}; 7.4×10^{-7}	–

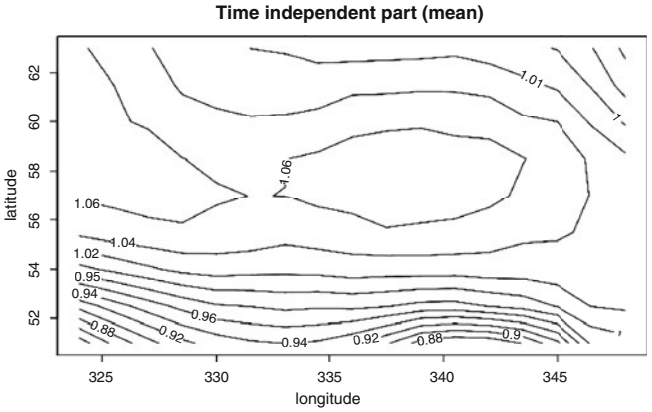

Fig. 4.4 Mean time-independent part varying between 2.3 and 2.9, monthly data

dynamic part. It is noted that for this particular component, a bias correction factor was needed, since only the mean and the variance were kept for each time-point of $\theta(x,t)$. Therefore the entire distribution could not be re-transformed and a bias correction is needed. The QMLE-estimator was used, i.e., multiplying $e^{\bar{\theta}(x,t)}$ with a factor $e^{0.5s^2}$, where s^2 corresponds to the estimated variance of $\theta(x,t)$ at each time-point [4]. However, the bias corrections are negligible, ranging from 1.003084 to 1.027433 for the various time-points, and the range of values for $E[e^{\theta(x,t)}]$ was not changed by this bias correction.

The mean seasonal term, $E[e^{M(t)}]$, for the first ten years is shown in Fig. 4.5, and a clear cyclic behavior is observed. The expected seasonal contribution without the error term, $E[e^{c\cos(\omega t)+d\sin(\omega t)}]$, multiplied with a bias correction factor corresponding to $e^{0.5\bar{\sigma}_m^2}$, is also shown in the figure and agrees well with the sampled seasonal contribution. The bias correction factor is needed for re-transforming to the mean relative to the stochastic term $\varepsilon_m(t)$ whereas no correction factor is needed for the uncertainty in $c\cos(\omega t) + d\sin(\omega t)$ since all samples of this distribution are effectively re-transformed. A horizontal line through 1.0 is also shown. Again, for the log-transformed data, this component corresponds to a multiplicative constant. The expected seasonal component varies cyclically between ± 0.43, and the corresponding expected seasonal factor varies between 0.67 for quiet seasons and 1.6 in rough seasons. For example, for a mean of 3 m, this corresponds to variations between 2.0 and 4.8 m due to seasonal effects. This seems reasonable and is comparable to the seasonal component derived for the non-transformed data. One interesting observation from Fig. 4.5 is the asymmetry between the positive and negative peaks which is different from the seasonal component obtained with non-transformed data.

The temporal trend parts of model alternatives 1 and 2 are illustrated in Fig. 4.6. The figure shows the re-transformed sampled mean annual trend together with the mean, 5- and 95-percentiles of the expected trend. In estimating the mean on the re-transformed scale, a bias correction factor of $e^{0.5\bar{\sigma}_T^2}$ was used (effectively only shifting

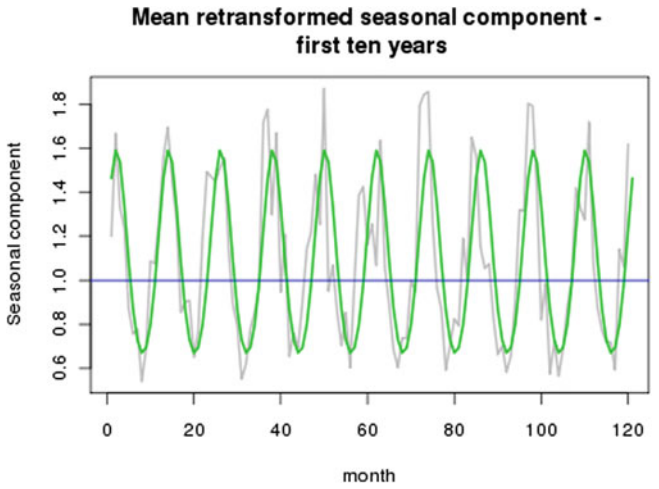

Fig. 4.5 The re-transformed seasonal component for 10 years, monthly data; $E[e^{M(t)}]$ (*gray line*) and $E[e^{c\cos(\omega t)+d\sin(\omega t)}]e^{0.5\bar{\sigma}_m^2}$ (*green line*)

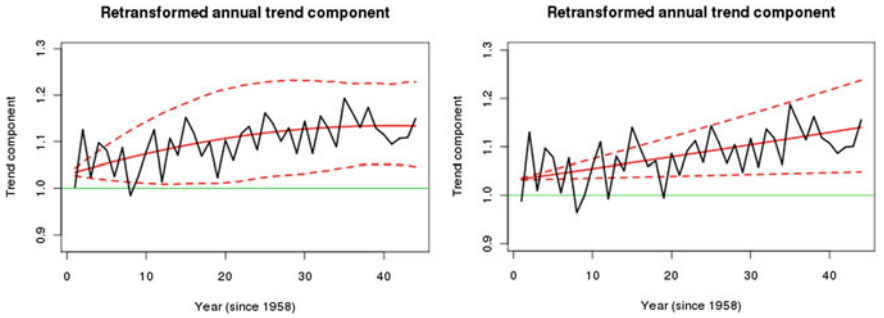

Fig. 4.6 Re-transformed annual trend over the period, model 1 (*left*) and model 2 (*right*), monthly data; $E[e^{\mathrm{T}(t)}]$ (*black lines*) and the mean and 90 % credible interval of $e^{\gamma t+\eta t^2}$ with bias correction (*red lines*)

the whole trend by a constant and not influencing the relative trend contribution). It is stressed that the credible intervals obtained in this way reflect the uncertainty in the estimation of (γ, η) but does not incorporate the uncertainty in $\mathrm{T}(t)$ due to the stochastic term $\varepsilon_{\mathrm{T}}(t)$. A horizontal line corresponding to no trend is also included in the figures. The mean yearly trend according to the quadratic model (model 1) corresponds to a noticeable increase in significant wave height, about 13 % over the period. The 90 % credible interval ranges from a factor of 1.0 to 1.2. It is observed that for a mean significant wave height of 3 m, this expected increase corresponds to an increase of 40 cm. However, for extremes, say above 10 m, such a multiplicative trend would correspond to an increase of over 1.3 m over the period.

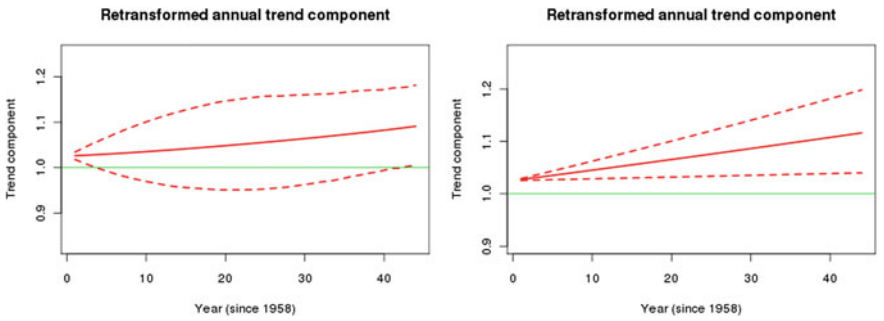

Fig. 4.7 Estimated re-transformed trend contribution from model 4 (*left*) and model 5 (*right*), monthly data; mean and 90 % credible interval of $e^{\gamma t+\eta t^2}$ with bias correction

The linear model (model alternative 2) estimates a mean long-term trend corresponding to an expected increase in significant wave height of about 14 % over the whole period. The 90 % credible interval corresponds to an increasing trend between 4.9 and 24 %. For an average sea state with significant wave height 3 m, such an increase corresponds to an expected increase of about 42 cm. For extremes, say above 10 m, this increase would correspond to an expected increase of just over 1.4 m. For the mean sea states, these estimates correspond reasonably well with the estimates of the trend obtained from the non-transformed data. However, with a multiplicative trend rather than an additive one, the increase in the extremes will be greater than the increase in average and less extreme sea states.

The estimated trend components for models 4 and 5 are illustrated in Fig. 4.7. The long-term trends estimated from these models are comparable to the ones estimated with two noise terms. The quadratic trend model (Model 4) estimates a mean increase over the period of about 9.1 %, but with the 90 % credible interval ranging from 0.5 to 18 % increase. For sea states of 3 and 10 m significant wave height, such increases correspond to expected increases of 27 and 91 cm respectively, somewhat less than what was estimated by the model with two temporal noise terms. 90 % credible intervals would range from 1 to 54 cm and 5 to 180 cm respectively. The linear trend model (Model 5) estimates a mean increase of 12 % during the period, with a 90 % credible interval ranging from 4 to 20 %. Corresponding expected increase for moderate ($H_s = 3$ m) and rough ($H_s = 10$ m) sea states are 35 and 120 cm respectively, with 90 % credible intervals ranging from 12 to 60 cm and 40 to 200 cm respectively.

4.4.2 Results for Daily Data

The normal probability plots of the residuals look better than the corresponding plot for non-transformed data, suggesting that the model assumptions are reasonable and

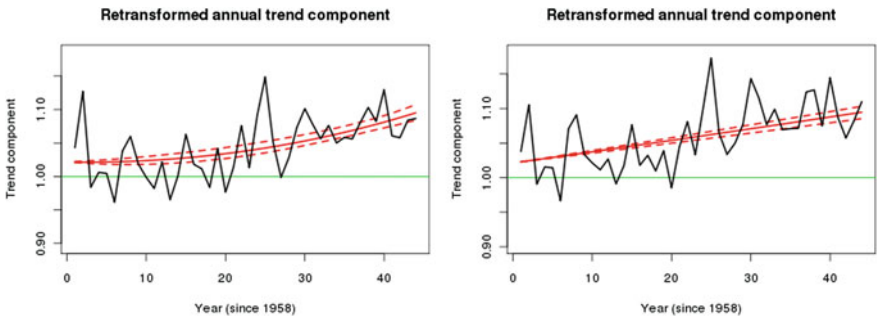

Fig. 4.8 Re-transformed annual trend over the period, model 1 (*left*) and model 2 (*right*), daily data; $E[e^{\mathrm{T}(t)}]$ (*black lines*) and the mean and 90 % credible interval of $e^{\gamma t+\eta t^2}$ with bias correction (*red lines*)

that the log-transform might represent an improvement. Again, most of the marginal posterior distributions are symmetric, and the mean and standard deviation of the posterior distributions are given in Table 4.2 (mean, median, and standard deviation for a_ϕ and a_λ). Apart from the temporal trend part, most of the model parameters do not vary significantly between model alternatives.

The contribution from the time-independent component, $\mu(x)$, is a factor between 0.89 and 1.2, corresponding to a multiplicative factor varying between 2.5 and 3.2 for different locations, x. This is slightly higher than the factors obtained with monthly data, but within the same order of magnitude. The deviations from the spatially varying means are again small.

The contribution from the space-time dynamic component, $\theta(x, t)$, has become more important with the mean ranging from -0.91 to 0.75, with corresponding multiplicative factors between 0.40 and 2.1 on the original scale. This corresponds to a ratio of 5.25 between significant wave heights during storms and quiet periods. The corresponding ratio obtained with monthly data was less than 2. Now, b_W is the largest of the b-parameters, except b_0, and this is reassuring. It indicates that the model is able to capture the main storm tracks, which are known to be predominantly from west to east in this particular area. It is not surprising, however, that this was not well captured when using monthly data, since no storms endure for that long. At any rate, it is reassuring to observe that this component behaves as it should for temporal resolutions comparable to duration of storms, and this component now has a more meaningful interpretation. The QMLE-estimator was used for bias correction but correction factors were negligible, varying between 1.004481 and 1.019004 for the different time-points.

The expected seasonal component varies cyclically between ± 0.46, corresponding to a seasonal factor of 0.64 for quiet seasons and 1.6 in rough seasons. For example, for a mean of 3 m, this corresponds to variations between 1.9 and 4.8 m due to seasonal effects.

The temporal trend part of the quadratic and linear models (models 1 and 2) are illustrated in Fig. 4.8. The quadratic model (model 1) estimates a mean factor of

Table 4.2 Posterior marginal distributions, mean; sd; daily log-transformed data

	Model 1	Model 2	Model 3	Model 4	Model 5
σ_Z^2	0.035; 5.5×10^{-5}	0.035; 5.3×10^{-5}	0.035; 5.8×10^{-5}	0.035; 5.5×10^{-5}	0.035; 5.6×10^{-5}
σ_μ^2	0.027; 0.0031	0.027; 0.0030	0.027, 0.0030	0.027; 0.0032	0.027; 0.0030
σ_θ^2	0.016; 4.8×10^{-5}	0.016; 4.6×10^{-5}	0.016; 4.9×10^{-5}	0.016; 4.7×10^{-5}	0.016; 4.7×10^{-5}
σ_m^2	0.040; 0.00090	0.040; 0.0013	0.082; 0.00095	0.081; 0.00092	0.082; 0.00093
b_0	0.24; 0.0011	0.24; 0.0012	0.24; 0.0011	0.24; 0.0012	0.24; 0.0011
b_N	0.12; 0.0011	0.12; 0.0010	0.12; 0.0011	0.12; 0.0011	0.12; 0.0010
b_E	0.13; 0.0011	0.13; 0.0011	0.13; 0.0011	0.13; 0.0012	0.13; 0.0011
b_S	0.16; 0.0011	0.16; 0.0011	0.16; 0.0011	0.16; 0.0011	0.16; 0.0011
b_W	0.28; 0.0012	0.28; 0.0011	0.28; 0.0012	0.28; 0.0012	0.28; 0.0011
c	0.45; 0.0034	0.45; 0.0035	0.45; 0.0032	0.45; 0.0032	0.45; 0.0033
d	0.097; 0.0035	0.096; 0.0034	0.096; 0.0033	0.097; 0.0032	0.097; 0.0033
$\mu_{0,1}$	3.4; 1.4	3.5; 1.4	3.5; 1.4	3.4; 1.4	3.4; 1.4
$\mu_{0,2}$	−0.091; 0.037	−0.086; 0.038	−0.088; 0.036	−0.089; 0.038	−0.089; 0.038
$\mu_{0,3}$	0.45; 0.21	0.42; 0.22	0.44; 0.20	0.44; 0.22	0.44; 0.22
$\mu_{0,4}$	0.00017; 9.1×10^{-5}	0.00016; 9.6×10^{-5}	0.00017; 9.1×10^{-5}	0.00017; 9.6×10^{-5}	0.00017; 9.6×10^{-5}
$\mu_{0,5}$	−0.0026; 0.0012	−0.0024; 0.0012	−0.0025; 0.0011	−0.0025; 0.0012	−0.0025; 0.0012
$\mu_{0,6}$	−0.00045; 0.00049	−0.00042; 0.00053	−0.00043; 0.00051	−0.00043; 0.00053	−0.0044; 0.00053
a_ϕ	0.085; 0.078; 0.055	0.085; 0.076; 0.057	0.086; 0.080; 0.055	0.087; 0.079; 0.056	0.085; 0.077; 0.057
a_λ	0.086; 0.077; 0.056	0.084; 0.076; 0.056	0.089; 0.081; 0.060	0.088; 0.080; 0.057	0.086; 0.078; 0.058
σ_{T}^2	0.043; 0.0011	0.042; 0.0013	–	–	–
γ	-5.6×10^{-7}; 1.3×10^{-6}	4.3×10^{-6}; 3.1×10^{-7}	–	-7.0×10^{-6}; 1.3×10^{-6}	3.9×10^{-6}; 4.3×10^{-7}
η	3.0×10^{-10}; 8.7×10^{-11}	–	–	6.4×10^{-10}; 9.0×10^{-11}	–

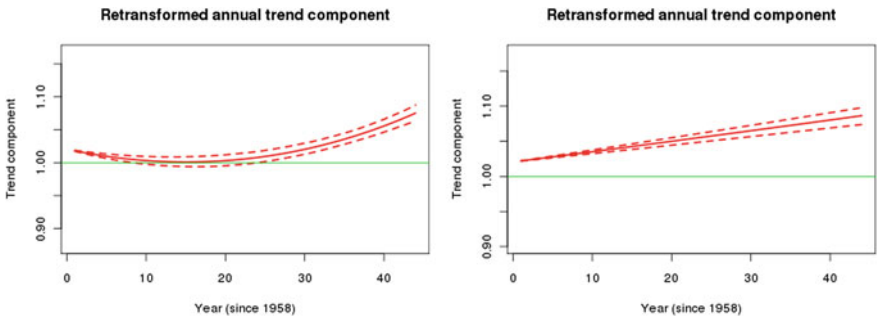

Fig. 4.9 Estimated re-transformed long-term trend contribution for model 4 (*left*) and model 5 (*right*), daily data; mean and 90 % credible interval of $e^{\gamma t+\eta t^2}$ with bias correction

about 1.095 over the period. The 90 % credible interval ranges from a factor 1.085 to a factor about 1.10. For a mean significant wave height of 3 m, this expected increase corresponds to an increase of 28 cm. However, for extremes above 10 m, such a multiplicative trend would correspond to an increase of over 95 cm over the period.

The mean estimate of the long-term trend from the linear model corresponds to an increase of about 9.5 % over the whole period. The 90 % credible interval ranges from 8.6 to 10 %. For an average sea state with significant wave height 3 m, such an increase would correspond to an expected increase of 28 cm, but with an increase of at least 26 cm with 95 % credibility. For extremes above 10 m, this corresponds to an expected increase in significant wave height of 95 cm and with 95 % credibility, at least 86 cm. These trend estimates are somewhat lower than what was extracted from the monthly data, with much narrower credibility bands.

The estimated trend components for the models with a single temporal noise term are shown in Fig. 4.9. The quadratic trend model (Model 4) estimates a mean increase over the period of about 7.6 %, but with the 90 % credible interval ranging from 6.4 to 8.9 %. This corresponds to expected increases of 23 and 76 cm for moderate and rough sea states respectively. Corresponding 90 % credible intervals range from 19 to 27 cm and 64 to 89 cm. The linear trend model (Model 5) estimates a mean increase of 8.7 % during the period, with a 90 % credible interval ranging from 7.4 to 9.8 %. Corresponding expected increases for moderate and rough sea states are 26 and 87 cm respectively, with 90 % credible intervals ranging from 22 to 29 cm and 74 to 98 cm. It is noted that these trends are slightly less than the trends estimated with two temporal noise terms, but they are within the same order of magnitude and there is general agreement among the models that there is an increasing trend in significant wave height.

4.4.3 Results for Monthly Maximum Data

Finally, the models were run on log-transformed monthly maximum data, i.e., the maximum significant wave height at each spatial location for each month. The results from these simulations are presented in the following. A visual check of the residuals indicates that the Gaussian model assumptions seem reasonable, although model fit seems to be poorer than for non-maximum data. The mean and standard deviation of some marginal posterior distributions for different parameters are given in Table 4.3.

The contribution from $\mu(x)$ is in the order of 1.76–1.95; $e^{\mu(x)}$ is a multiplicative factor varying between 5.8 and 7.0. The mean contributions from the space-time dynamic part, $\theta(x,t)$ correspond to factors between 0.70 and 1.4 for different locations and times. Hence, this space-time dynamic part contributes with a factor from -30 to $+40\,\%$. The seasonal component corresponds to a factor between 0.68 for calm seasons and 1.5 in rough seasons.

Model 1 estimates a mean yearly trend corresponding to a factor of about 1.09 over the period, with 90 % credible interval ranging from 1.03 to 1.14. For monthly maximum significant wave heights of 5 and 8 m this corresponds to a mean increase of 43 and 68 cm, respectively. The mean estimate of the long-term trend from model 2 corresponds to an increase of about 1.07 over the period. The 90 % credible interval ranges from 1.03 to 1.12. For monthly maximum significant wave heights of 5 and 8 m, this corresponds to an expected increase of about 36 and 57 cm respectively. The trends estimated from the models with one temporal noise term are very similar to the ones estimated with two noise terms. Model 4 estimates a mean increase over the period of about 1.05, but with the 90 % credible interval ranging from 1.00 to 1.10 whereas Model 5 estimates a mean increase of 1.05 during the period, with a 90 % credible interval ranging from 1.00 to 1.09. Assuming average monthly maximum significant wave heights of 5 and 8 m, these factors correspond to expected trends of about 26–27 cm and 41–43 cm respectively.

4.4.4 Simulations on 6-Hourly Data

The models were also run for the full data-set with a log-transform, but the same problems as reported for the original data were encountered (see Chap. 3 [12]). Hence, the model does not perform well on the six-hourly log-transformed data.

4.4.5 Model Comparison and Selection

The different model alternatives can generally be compared by comparing the resulting posterior estimates of the model parameters, as presented in for example Table 4.1. The parameters related to the spatial features of the model seem to be little affected

Table 4.3 Posterior marginal distributions (log-transformed monthly maximum data)

	Model 1	Model 2	Model 3	Model 4	Model 5
σ_Z^2	0.013; 0.00051	0.013; 0.00051	0.013; 0.00047	0.013; 0.00052	0.013; 0.00050
σ_μ^2	0.027; 0.0031	0.027; 0.0029	0.027; 0.0031	0.027; 0.0030	0.027; 0.0031
σ_θ^2	0.012; 0.00051	0.012; 0.00051	0.012; 0.00048	0.012; 0.00052	0.012; 0.00050
σ_m^2	0.026; 0.0021	0.025; 0.0021	0.029, 0.0017	0.029; 0.0018	0.029; 0.0018
b_0	0.012; 0.0037	0.012; 0.0037	0.013, 0.0037	0.012; 0.0038	0.012; 0.0036
b_N	0.011; 0.0041	0.011; 0.0038	0.011; 0.0040	0.011; 0.0040	0.011, 0.0040
b_E	0.0090; 0.0036	0.0092; 0.0037	0.0091; 0.0037	0.0093; 0.0037	0.0091; 0.0035
b_S	0.0043, 0.0038	0.0043; 0.0039	0.0043; 0.0039	0.0045; 0.0038	0.0041; 0.0039
b_W	0.012; 0.0035	0.012; 0.0036	0.013; 0.0036	0.013; 0.0037	0.012; 0.0039
c	0.35; 0.014	0.35, 0.014	0.35; 0.011	0.35; 0.010	0.35; 0.011
d	0.15; 0.014	0.15, 0.013	0.15; 0.010	0.15; 0.010	0.15; 0.010
$\mu_{0,1}$	3.5; 1.4	3.4; 1.4	3.5; 1.4	3.4; 1.5	3.5; 1.4
$\mu_{0,2}$	−0.056; 0.038	−0.055, 0.038	−0.054, 0.037	−0.056; 0.037	−0.058; 0.037
$\mu_{0,3}$	0.28; 0.22	0.28, 0.21	0.27; 0.21	0.29, 0.21	0.30, 0.22
$\mu_{0,4}$	9.0×10^{-5}; 9.7×10^{-5}	8.8×10^{-5}; 9.4×10^{-5}	8.7×10^{-5}; 9.3×10^{-5}	9.1×10^{-5}; 9.3×10^{-5}	9.7×10^{-5}; 9.4×10^{-5}
$\mu_{0,5}$	−0.0021; 0.0012	−0.0021; 0.0012	−0.0020; 0.0012	−0.0022; 0.0011	−0.0022; 0.0012
$\mu_{0,6}$	−0.00012; 0.00054	−0.00010; 0.00051	−0.00011; 0.00052	−0.00012; 0.00052	−0.00014; 0.00052
σ_t^2	0.026; 0.0023	0.025; 0.0021	–	–	–
γ	0.00036; 0.00024	0.00011; 5.2×10^{-5}	–	-6.4×10^{-5}; 0.00023	7.1×10^{-5}; 5.1×10^{-5}
η	-4.4×10^{-7}; 4.7×10^{-7}	–	–	2.6×10^{-7}; 4.1×10^{-7}	–

Table 4.4 Model selection: estimated losses

Model alternative	Monthly data		Daily data		Monthly max	
	L_s	L_w	L_s	L_w	L_s	L_w
Model 1	3.412	3.560	2.562	2.665	3.383	3.456
Model 2	3.425	3.546	2.573	2.684	3.346	3.412
Model 3	3.267	3.468	2.600	2.728	3.035	3.127
Model 4	3.317	3.468	2.557	2.655	2.970	3.045
Model 5	3.298	3.455	2.569	2.682	2.987	3.070

by the model reductions, which is reassuring. Also, the seasonal part of the model seems to behave rather similarly for the different model alternatives. Hence, the main differences are, as would be expected, related to the long-term temporal trend parameters γ and η.

The losses corresponding to the two loss functions were estimated for the various data sets and model alternatives and are given in Table 4.4.

For the monthly data, the standard loss function prefers the model with no trend and the weighted loss function prefers the model with linear trend and one temporal noise term. For the daily data, both loss functions favour the quadratic models, whereas for the monthly maximum data, both loss functions favour the linear model with one temporal noise term, although preferring the linear model over the quadratic model if two noise terms are included. It is also interesting to note that, in spite the fact that the models yield better goodness-of-fit for log-transformed data compared to the original data, the models for the original data seem to perform consistently better with regard to short-term prediction according to the estimated losses. Notwithstanding, it is difficult to assess the models in terms of long-term prediction and it is still an open question in which model alternative would be better in this regard.

4.4.6 Future Projections

Although extrapolation beyond the time interval for which the models are fitted might not be valid, it is tempting to extend the estimated trends into the future. In the following, future projections based on extrapolation of the estimated trends from the linear models over 100 years will be presented.

4.4.6.1 Projections Based on Monthly Data

Assuming that a trend such as the one predicted from the linear model with two temporal noise terms for monthly data will continue, this corresponds to an expected increase in significant wave height of nearly 30 % over 100 years, with a 95 % credibility of an increasing trend larger than 7.0 %. The corresponding expected increase

of 25 % with 95 % credibility of an increase of at least 5.9 % is obtained from the linear trend model with one temporal noise term for monthly data. Assuming such trends to be valid for all sea states, the expected increase of a sea state of 3 m would then be about 0.90 m (model 2) or 0.74 m (model 5) and for an extreme sea state of 10 m the expected increase would be 3.0 m (model 2) or 2.5 m (model 5) over 100 years. The trends for moderate sea states are comparable to the ones obtained from the original data (Chap. 3 [12]), but a much larger trend is estimated for extremes.

4.4.6.2 Projections Based on Daily Data

If trends predicted from the linear trend models with daily data continue, this corresponds to an expected increase in significant wave height of 20 %, with a 95 % credibility of an increase of at least 17 % over 100 years for the model with two temporal noise terms (model 2) and 18 % with 95 % credibility of an increase of at least 15 % for the model with one temporal noise term (model 5). Assuming such trends to be valid for any sea states, the expected increase of a sea state of 3 m would be about 0.59 or 0.53 m for the two model alternatives and for extreme sea states of 10 m the expected increase would be 2.0 and 1.8 m over 100 years respectively. Again, the expected trends for moderate sea states coincide with the ones estimated with the original data reported in Chap. 3 [12], whereas extremes are assigned a much larger trend.

4.4.6.3 Projections Based on Monthly Maximum Data

The estimates from the log-transformed monthly maxima correspond to an expected increasing factor of 15 % over 100 years, with a 95 % credibility of a trend-factor larger than 4.3 %. (An expected increase of 10 % with 94 % credibility of a positive trend is obtained from the linear model with one temporal noise term). Assuming such trends valid for average monthly maximum sea states of 5 and 8 m in calm and rough seasons, respectively, the expected increases would be about 75 cm and 1.2 m respectively (51 and 82 cm for one noias term) over 100 years.

4.5 Discussion

The results presented in this chapter are from the Bayesian hierarchical space-time model fitted to log-transformed significant wave height data. Even though results cannot easily be compared between the original and the log-transformed data, the loss functions have used the same scale and these suggest that the models for the original data perform best with regard to short-term prediction. However, goodness-of-fit seems to improve with the log-transform. Another observation is that the models with the log-transformed data seem to be able to estimate the extremes better. Both

models seem to underestimate the frequency of extreme sea states, but much less with the log-transformed data.

One interesting observation is that the trend-factor obtained when using the log-transformed monthly maxima is only about 50 % of the trend-factor obtained using monthly data. This is opposite to the results from the original data, where the maxima displayed a stronger trend than overall. One possible explanation for this can be that even though a transformation of the data seems to improve the results, the logarithmic transform might not be the optimal one. The results pertaining to the original data do indeed demonstrate that more severe sea states are expected to have a larger long-term trend, whereas the results from the log-transformed data suggest that a log-transform overcompensates for this effect. Possibly, other data transformations would perform better, but this has so far not been investigated.

Regarding the different long-term trend estimates, the models project an expected increase of significant wave height around 53–90 cm for moderate sea states and 1.8–3.0 m for extreme sea states over a period of 100 years. The trends for moderate sea states are comparable to the estimated trends obtained without the logarithmic transform of the data, but the estimated trends in the extremes are now much larger than the trends in the mean condition. This feature was also reported by e.g., [16].

4.5.1 Semi-Annual Seasonal Component

Climate data often display semiannual characteristics (see e.g., [9]). It is therefore natural to investigate how adding such a component in the seasonal part, $M(t)$, would influence the results. In the following, the effect of introducing such a contribution into three of the model alternatives presented in this study, namely models 1–3, will be reported for monthly data. The long-term temporal parts, $\mathrm{T}(t)$, of those model alternatives, henceforth denoted models 6, 7, and 8, are identical to models 1, 2, and 3, respectively, but the seasonal part is now extended with the second harmonic to account for possible semiannual features, as shown in Eq. (4.7).

$$M(t) = c\cos(\omega t) + d\sin(\omega t) + f\cos(2\omega t) + g\sin(2\omega t) + \varepsilon_m(t) \tag{4.7}$$

Two new parameters, f and g, are introduced. These are presumed small and as priors for both parameters, $N(0, 0.5)$ will be used. Simulations on the three additional model alternatives were run for monthly data, with similar settings as the previous simulations with respect to burn-in period, batch size, priors for the other parameters, starting point of the Gibbs sampler, etc. Trace plots suggest that the Gibbs sampler has converged. The results are briefly summarized below.

The residuals display similar features as for the previous model alternatives and also the spatial and short-term dynamic features seem minimally affected by the inclusion of a semiannual component. The mean and standard deviation of the posterior marginal distributions related to the temporal parts of the model are presented in Table 4.5 for model alternatives 6, 7, and 8.

Table 4.5 Posterior marginal distributions, mean, and standard deviation, for extended seasonal models; monthly data

	Model 6	Model 7	Model 8
σ_m^2	(0.061, 0.0068)	(0.061, 0.0064)	(0.0099, 0.0061)
σ_T^2	(0.060, 0.0070)	(0.059, 0.0066)	-
c	(0.35, 0.022)	(0.35, 0.021)	(0.35, 0.019)
d	(0.26, 0.020)	(0.26, 0.021)	(0.26, 0.019)
f	$(-0.010, 0.021)$	$(-0.011, 0.022)$	$(-0.0091, 0.020)$
g	$(-0.064, 0.021)$	$(-0.061, 0.020)$	$(-0.063, 0.020)$
γ	$(3.6\times10^{-5}, 0.00032)$	$(0.00012, 9.0\times10^{-5})$	-
η	$(1.6\times10^{-7}, 6.5\times10^{-7})$	-	-

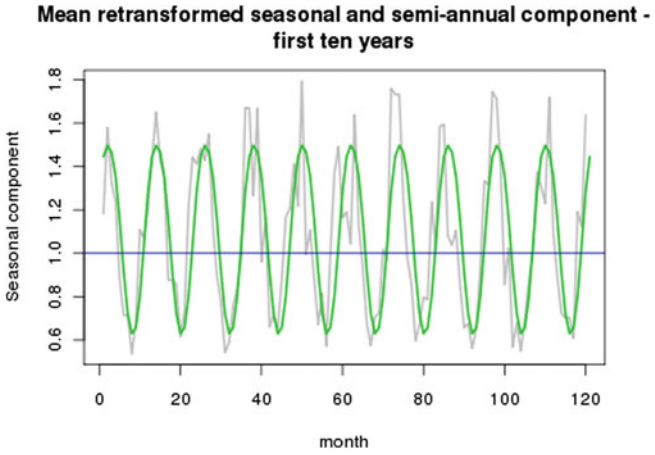

Fig. 4.10 The re-transformed seasonal component for 10 years, with annual and annual components; monthly data

The seasonal component, $M(t)$, is surprisingly unaffected by the inclusion of the semi-annual component. The parameters c and d are essentially unchanged and the new parameters f and g are very small and negative. The extended seasonal component as a whole, as illustrated in Fig. 4.10 (for model 6), shows that the seasonal contribution is somewhat diminished. The re-transformed seasonal component now varies between a factor 0.63 for quiet seasons and 1.5 for rough seasons. Notwithstanding, the effect is small and the inclusion of a semi-annual component into the models does not influence the seasonal component to a very large degree.

It is also interesting to see how the semi-annual component influences the long-term trend estimates, and these are illustrated in Fig. 4.11 for models 6 and 7 (to be compared with Fig. 4.6 without the semi-annual component). The mean long-term trend component over the period for model 6 is estimated to correspond to a factor of 1.1 and this compares well with the estimated trend without the semi-annual component (model 1). Also the extended linear model, model 7, estimates an

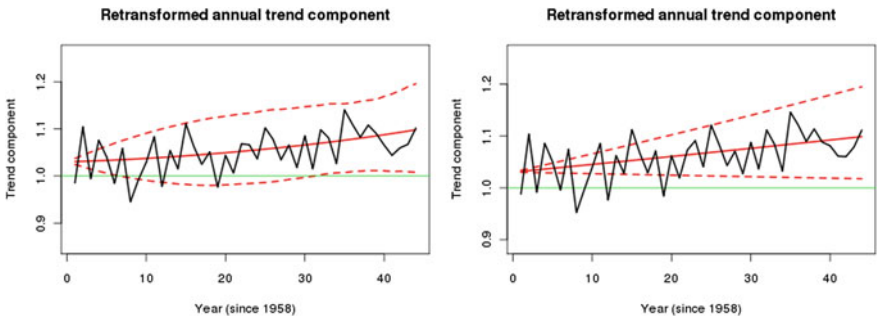

Fig. 4.11 Re-transformed annual trend over the period when a semi-annual contribution has been accounted for, model 6 (*left*) and model 7 (*right*), monthly data

Table 4.6 Values of the loss functions, monthly data with a semi-annual component

Model alternative	L_s	L_w
Model 6	3.379	3.565
Model 7	3.371	3.560
Model 8	3.263	3.518

expected trend corresponding to a factor of 1.1 and this is in reasonable agreement with what was estimated by model 2. Hence, it can be argued that the inclusion of a semi-annual component into the model does not influence the estimated long-term trends much.

Finally, the values of the loss functions for the model alternatives with a semi-annual component is presented in Table 4.6. These should be compared to the loss functions for the models without semi-annual components in Table 4.4 in order to check whether the inclusion of a semi-annual component yields improved (short-term) predictions. It is observed that the values of the standard loss functions tend to be decreased and the values for the weighted loss functions tend to be somewhat increased by the inclusion of the semi-annual component. However, the differences are small and all values are within the same range. Therefore, it is concluded that the inclusion of the semi-annual component does not improve predictions much.

Hence, it turns out that the results for neither the seasonal nor the long-term trend parts of the model are much affected by the extension of the model to include a semi-annual component. Furthermore, the loss functions reflecting short-term predictions are only minimally affected. Thus, including a semi-annual component does not influence the results much when analyzing the data for this particular area in the North Atlantic Ocean. Possibly, semi-annual oscillations are not dominating the climate in this particular area, and for example the North Atlantic Oscillation (NAO), with no particular periodicity [6] or other higher frequency components [1] may be more important. According to [7], the semi-annual effects are dominating on the Southern Hemisphere whereas the overwhelming effect on the Northern Hemisphere

is annual. It is reported that there are appreciable semi-annual components locally on the Northern Hemisphere, for example in the North Pacific Ocean. At any rate, the results presented herein suggests that the semi-annual contributions are negligible compared to the annual component which seems to capture the main seasonal effects over the area that has been analyzed. That being said, it is noted that the additional computational cost of including a semi-annual component is negligible.

4.6 Summary and Conclusions

This chapter has presented results obtained from applying the Bayesian hierarchical space-time model to log-transformed significant wave height data, and the models seem to perform quite well overall. The trends estimated from the various simulations are fairly consistent, with estimated expected trends of 27–42 cm for moderate conditions and 91–140 cm for extreme conditions for the monthly data and 23–28 cm for moderate conditions and 76–95 cm for extreme conditions for the daily data over the period from 1958 to 2002. The linear trends were also extrapolated over 100 years, to yield expected future increases within the range of 53–90 cm for moderate conditions and 1.8–3.0 m for extreme conditions. This is found to be in reasonable agreement with previous studies and also compares well with trends extracted by more standard time series techniques [15]. The estimated trends for moderate sea states compare well with trends estimated from the untransformed data. However, a fundamental difference is that the log-transform yields a different interpretation and for example the long-term trends become larger for extremes than for moderate sea states. This is a crucial difference, with practical implications in relation to design and operation of ships and other marine structures. However, whether the log-transform actually represents an improvement remains inconclusive, and it is suggested that other data transformations might be better.

References

1. Barbosa, S.M., Silva, M.E., Fernandes, M.: Multi-scale variability patterns in NCEP/NCAR reanalysis sea-level pressure. Theoret. Appl. Climatol. **96**, 319–326 (2009)
2. Beauchamp, J.J., Olson, J.S.: Corrections for bias in regression estimates after logarithmic transformation. Ecol. **54**, 1403–1407 (1973)
3. Cunha, C., Guedes Soares, C.: On the choice of data transformation for modelling time series of significant wave height. Ocean Eng. **26**, 489–506 (1999)
4. Ferguson, R.: River loads underestimated by rating curves. Water Resour. Res. **22**, 74–76 (1986)
5. Finney, D.J.: On the distribution of a variate whose logarithm is normally distributed. Suppl. J. Roy. Stat. Soc. **7**, 155–161 (1941)
6. Hurrell, J.W., Deser, C.: North Atlantic climate variability: the role of the North Atlantic oscillation. J. Mar. Syst. **78**, 28–41 (2009)
7. van Loon, H.: A review of the surface climate of the southern hemisphere and comparison with the northern hemisphere. J. Mar. Syst. **2**, 171–194 (1991)

8. Newman, M.C.: Regression analysis of log-transformed data: statistical bias and its correction. Environ. Toxicol. Chem. **12**, 1129–1133 (1993)
9. Schwerdtfeger, W., Prohaska, F.: The semi-annual pressure oscillation, its cause and effects. J. Meteorol. **13**, 217–218 (1956)
10. Smith, R.J.: Logarithmic transformation bias in allometry. Am. J. Phys. Anthropol. **90**, 215–228 (1993)
11. Stow, C.A., Reckhow, K.H., Qian, S.S.: A Bayesian approach to retransformation bias in transformed regression. Ecol. **87**, 1472–1477 (2006)
12. Vanem, E., Huseby, A.B., Natvig, B.: A Bayesian hierarchical spatio-temporal model for significant wave height in the NorthAtlantic. Stoch. Env. Res. Risk Assess. **26**, 609–632 (2012)
13. Vanem, E., Huseby, A.B., Natvig, B.: Modeling ocean wave climate with a Bayesian hierarchical space-time model and a log-transform of the data. Ocean Dyn. **62**, 355–375 (2012)
14. Vanem, E., Huseby, A.B., Natvig, B.: A stochastic model in space and time for monthly maximum significant wave height. In: Abrahamsen, P., Haugen, R., Kolbjørnsen, O. (eds.) Geostatistics Oslo 2012, pp. 505–517. Springer, Heidelberg (2012).
15. Vanem, E., Walker, S.E.: Identifying trends in the ocean wave climate by time series analyses of significant wave height data. Ocean Eng. **61**, 148–160 (2012)
16. Young, I., Zieger, S., Babanin, A.: Global trends in wind speed and wave height. Sci. **332**, 451–455 (2011)

Chapter 5
CO_2 Regression Component for Future Projections

In this chapter, the stochastic model developed in previous chapters will be extended with a regression term, where long-term trends of significant wave height are regressed on the atmospheric level of CO_2. Hence, future projections of the ocean wave climate are made based on projected levels of CO_2 in the atmosphere. Those projections are again based on various emission scenarios suggested by the IPCC, and projections based on two reference scenarios, referred to as A2 and B1, will be used. The model has been fitted by monthly maximum significant wave height data for the same area in the North Atlantic Ocean, and the results obtained from the extended model will be presented and discussed. The material in this chapter is based on [18], part of which is also presented in [14].

5.1 Introduction and Background

Even though the previous models described in Chaps. 3 and 4 were able to detect long-term trends in the significant wave height data, it might not be valid to extrapolate those trends into the future, and projections made in this way remain somewhat speculative. In this chapter, the model outlined in Chap. 3 [15] has been extended with a CO_2 regression component, and fitted to monthly maximum data [18]. In this way, the stochastic relationship between significant wave height and atmospheric levels of CO_2 is exploited in order to improve predictions and future projections of the ocean wave climate.

It is noted that only the stochastic relationship between atmospheric levels of CO_2 and the wave climate has been exploited, and the physics governing the climatic processes has not been modelled explicitly. The physical interactions are obviously highly complex, but it is argued that the overall mechanisms make it reasonable to believe that there is a strong correlation between the levels of greenhouse gases in the atmosphere and the severity of the wave climate. It is well-known that increased levels of greenhouse gases, of which CO_2 is the most important one, in the atmosphere

E. Vanem, *Bayesian Hierarchical Space-Time Models with Application to Significant Wave Height*, Ocean Engineering & Oceanography 2,
DOI: 10.1007/978-3-642-30253-4_5, © Springer-Verlag Berlin Heidelberg 2013

lead to increased radiative forcing of the globe due to the greenhouse effect. Consequently, more energy is inserted into the climate system. This may result in higher temperatures in the atmosphere and also more energetic weather systems, which may eventually result in more energy being transferred to kinetic energy in the ocean in the form of waves. Hence, a high level description indicates that increased level of CO_2 in the atmosphere will increase the energy input to the Earth overall, and parts of this excess energy may materialise as a rougher wave climate of the world's oceans.

Future projections of the ocean wave climate are made based on two future emission scenarios, referred to as A2 and B1. These are suggested as reference scenarios by IPCC and it is believed that they represent the best available knowledge of future concentrations of CO_2 in the atmosphere. The scenarios were also chosen so that one, the A2 scenario, represents an extreme scenario whereas the other, B1, is more conservative. The extended model for monthly maximum significant wave height will be outlined in this chapter, and the resulting estimated long-term trends and future projections will be reported.

5.2 Data Description

Data for significant wave height have been used to fit the stochastic model, and data on levels of CO_2 concentrations in the atmosphere have been used as covariates. The data for significant wave height have been discussed in previous chapters of this book, and in the following, a brief description of the CO_2 data will be given.

Concentrations of atmospheric CO_2 have been used as covariates for explaining possible long-term trends in the significant wave height, and basically two sets of data have been exploited; historic data for model fitting and projections of future concentration levels for future predictions of the wave climate.

5.2.1 Historic Data

There are several sources of historic data for CO_2 levels in the atmosphere that are freely available for scientific purposes. Observations are available up until present, and since the model is fitted to significant wave height data for the period 1958–2002, CO_2 data for this period are needed.

For the purpose of this study, where the aim of introducing a regression component with CO_2 levels as covariates into the model is to identify long-term trends, it is deemed sufficient to use monthly data. Hence, monthly average CO_2 data from the Mauna Loa Observatory, Hawaii, which has the longest continuous record of direct atmospheric CO_2 measurements, have been used [13]. This dataset is available from the ESRL website.[1] The data are on the format of the number of molecules of carbon

[1] URL: http://www.esrl.noaa.gov/gmd/ccgg/trends/

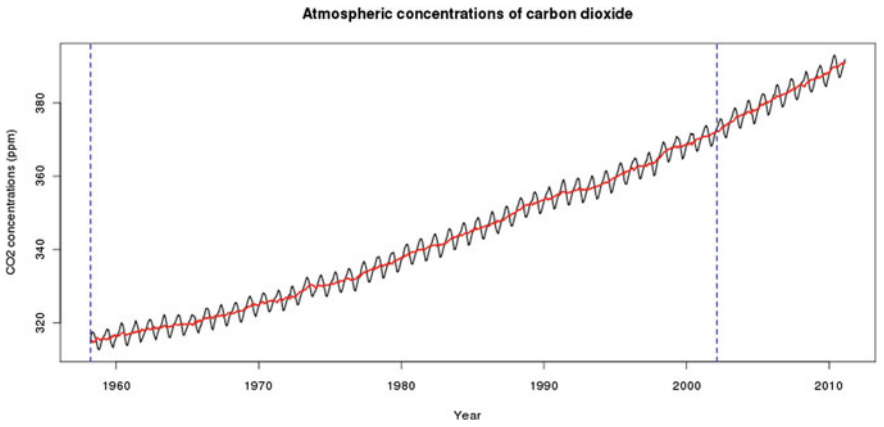

Fig. 5.1 CO_2 data from the Mauna Loa Observatory, monthly interpolated data (black line) and trend data with seasonal effects removed (red lines)

dioxide divided by the number of molecules of dry air multiplied by one million (parts per million = ppm), and data are available from March 1958 to present. The dataset contains the monthly averages determined from daily averages, as well as interpolated monthly averages where missing data have been replaced by interpolated values. Finally, monthly trend values are given where the seasonal cycle has been removed and where linear interpolation has been used for missing months. For the purpose of this study, the monthly trend time series will be used as covariates for the long-term trend. The seasonal cycle in the monthly maximum significant wave height is accounted for in a separate seasonal component in the model, and seasonal effects should therefore not be included in the long-term trend regression component.

The monthly interpolated and trend data are illustrated in the graphs in Fig. 5.1 and the vertical lines represent the part of the time series that overlap the C-ERA-40 data for significant wave height. It is noted that the CO_2 data start at March 1958, whereas the significant wave height data start at January 1958. Therefore, the model will be run with data starting at January 1959.

It is acknowledged that CO_2 is just one greenhouse gas (GHG) and that it does not alone determine the radiative forcing of the globe; other important GHGs are for example methane (CH_4) and nitrous oxide (N_2O). There is also great variability in the radiation coming from the sun. Nevertheless, it is well-known that CO_2 is the most important GHG and for the purpose of this study, it can be seen as a proxy of the concentration of GHG in the atmosphere and hence a proxy of the radiative forcing of the globe. More sophisticated models could include other GHGs and aerosols as covariates as well. It is also noted that the data stem from observations outside of the area in the North Atlantic which is the focus of this study. However, it is assumed that CO_2 is well mixed in the atmosphere, and that this does not introduce any notable bias in the results.

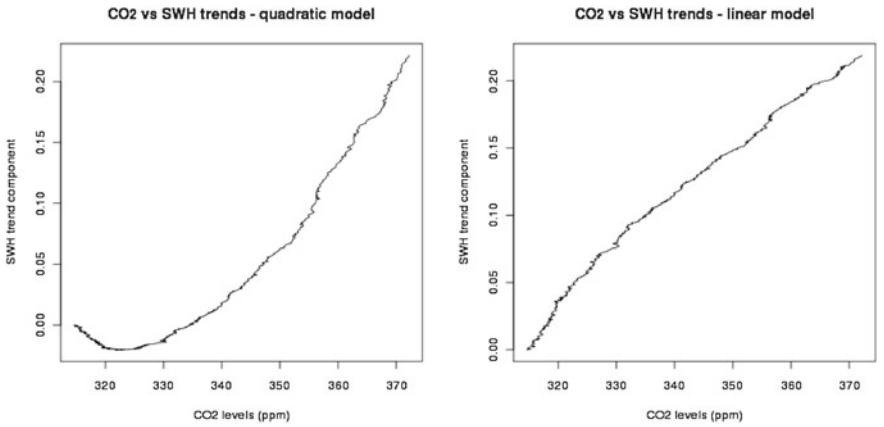

Fig. 5.2 Estimated trend in SWH vs. CO_2 concentrations

In order to get a feel of the relationship between the CO_2 concentrations in the atmosphere and the estimated trends in the significant wave height data (from [15]), the estimated trends versus the CO_2 level for the quadratic and linear model respectively have been plotted in Fig. 5.2. Obviously, the dependence is different according to what model alternative is assumed for the trend, and various alternative regression terms will also be tried out.

5.2.2 Future Projections

In order to make projections of future wave climate, future projections of the covariates are needed and projections of the atmospheric concentration of CO_2 will be exploited. Future predictions are of course uncertain, and different projections of CO_2 levels have been made based on different emission scenarios [12]. Four scenarios are commonly referred to as marker scenarios, supplemented with several illustrative scenarios. For the purpose of this study, projected emissions and concentrations presented by IPCC for the four marker scenarios (A1B, A2, B1 and B2) have been considered.[2] For each scenario, two carbon cycle models (BERN and ISAM) have been used to project CO_2 levels [8] and Fig. 5.3 shows the reference projections for the two models for the four marker scenarios. The differences between the two carbon cycle models are not significant, and for the purpose of this study it is deemed sufficient to use the results for one of them; the ISAM model has been chosen [9, 10]. Furthermore, it is observed that the scenarios A2 and B1 correspond to the highest and lowest projected CO_2 levels respectively, and it is therefore assumed sufficient to employ these two in the modelling, as the other scenarios will fall between these.

[2] The IPCC Data Distribution Centre, URL: http://www.ipcc-data.org/ddc_co2.html

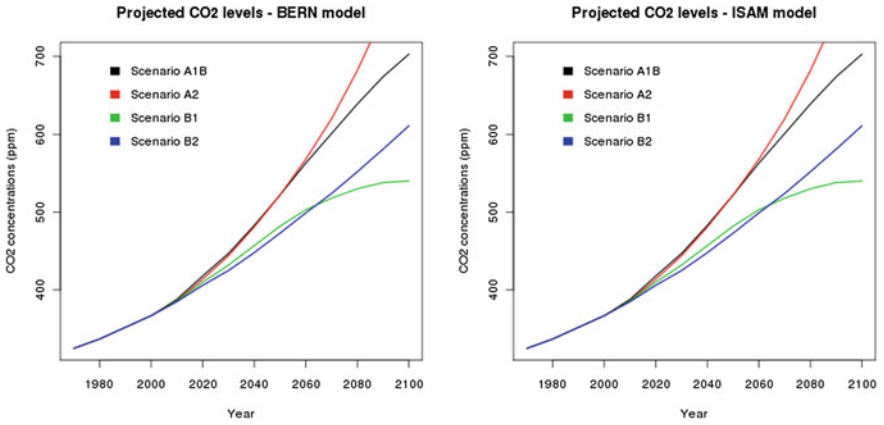

Fig. 5.3 CO_2 projections for the four marker scenarios from the carbon cycle models BERN (*left*) and ISAM (*right*)

Scenario A2 might be an extreme scenario, but from a precautionary perspective it is important to include this in the analysis as this could be construed as a worst case scenario. The CO_2 projections data can also be found in appendix II of [8].

The projected levels of atmospheric CO_2 concentrations are given for every 10 years towards 2100. For the purpose of this study, monthly averages are needed, and simple linear interpolation within each decade has been used in order to estimate monthly projections. The decadal projections are then assumed as the value for January of that year. In this way, monthly projections of CO_2 levels in the atmosphere from year 2010 until 2100 are obtained for use as covariates in the regression component of the stochastic model for significant wave height. For the years 2002 to 2010, where actual observations are available, recorded monthly averages from the Mauna Loa Observatory will be used. The interpolated monthly projections are plotted together with the original decadal projections in Fig. 5.4 (the vertical bars in the plots correspond to the decadal reference projections from the ISAM model).

It is stressed that the uncertainty of the data is not accounted for in the model, and any results are also conditional on the data used for the covariates. Uncertainties are of course large for future projections, but it is assumed that the projections suggested by the IPCC correspond to the best current knowledge available. The uncertainties of future projections of CO_2 concentrations were discussed in e.g., [11] and it was suggested to assign probabilities for the various scenarios. However, such probabilities has not been assigned in this study. It is also noted that the radiative forcings described by the representative concentration pathways [19] constitute an alternative set of covariates to the CO_2 levels derived from the emission scenarios. The historic data and the projections corresponding to the four marker scenarios are illustrated together in Fig. 5.5.

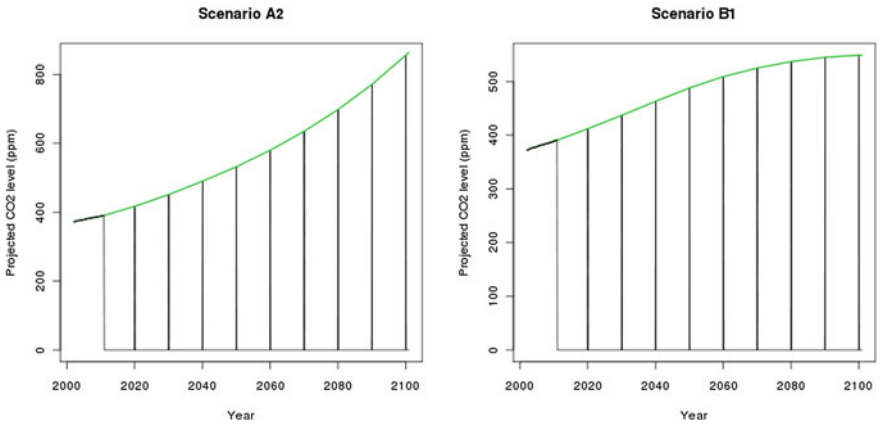

Fig. 5.4 Interpolated monthly CO_2 level projections for scenarios A2 and B1

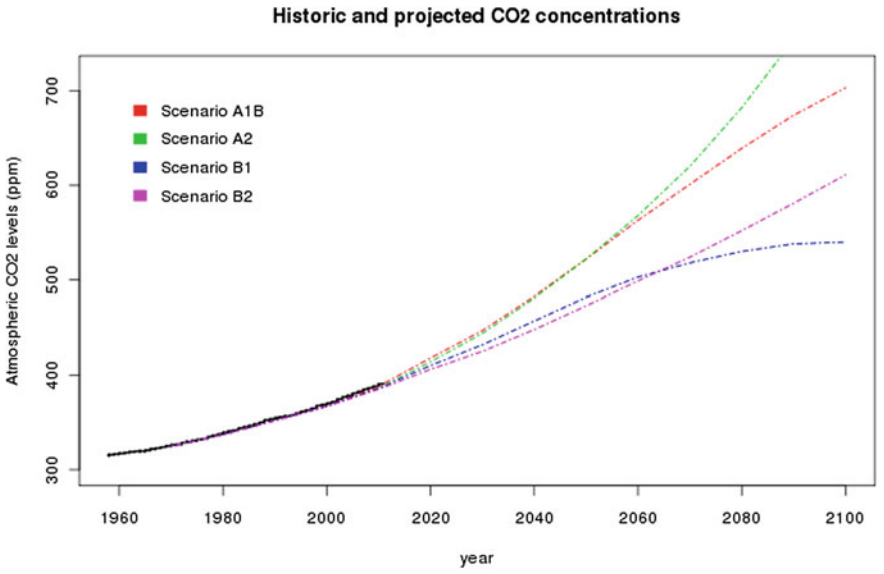

Fig. 5.5 Atmospheric CO_2 levels: Historic data and future projections

5.3 Model Extension

The extended model is similar to the previous models presented in previous chapters [15, 16], except for the modelling of the long-term trend, $T(t)$. This part will now be a regression component, where the long-term trend in the significant wave height is regressed on the atmospheric levels of CO_2, as outlined below. Seasonal components with and without the second harmonic were tried, i.e. with and without a semi-annual

contribution. However, it was observed that the inclusion of a semi-annual component did not influence the results much [18].

In order to include possible effects of climate change in the model, the following component with CO_2 concentrations in the atmosphere has been included, assuming first a combination of a linear and logarithmic trend with respect to the level of CO_2. With $G(t)$ denoting the average level of CO_2 in the atmosphere at time t, the regression component takes the form

$$\mathrm{T}(t) = \gamma G(t) + \eta \ln G(t) + \varepsilon_t(t) \tag{5.1}$$

Initially, model alternatives with a quadratic term were also considered, i.e., with the extra term $\delta G(t)^2$, but it was discovered that the quadratic term causes problems [18]. Hence, only the linear and logarithmic terms will be considered further. Even though it might not be surprising that a quadratic term for the trends performs poorly, there was no apriori evidence suggesting to leave it out but it was effectively ruled out by the data.

For identifying and predicting long-term trends, it is deemed sufficient to use monthly means of the covariates. Hence, the temporal resolution will be in the order of months. It is noted that CO_2 is known to mix well in the atmosphere, so there is no spatial part of this regression term.

5.3.1 Model Alternatives

Again, the main interest is in the long-term trend component, now modelled as a regression term with CO_2 concentrations as covariates, and the following model alternatives are considered:

Model 1: $\mathrm{T}(t) = \gamma G(t) + \eta \ln G(t) + \varepsilon_t(t)$
Model 2: $\mathrm{T}(t) = \gamma G(t) + \varepsilon_t(t)$
Model 3: $\mathrm{T}(t) = \eta \ln G(t) + \varepsilon_t(t)$
Model 4: $\mathrm{T}(t) = 0$

5.3.2 Critical Model Assumptions

The model uses a regression component towards CO_2 to describe long-term variation in the ocean wave climate. Hence, a very critical model assumption is the stochastic dependence between levels of CO_2 in the atmosphere and the ocean wave climate. It is assumed that there is such a stochastic dependence and this might be a realistic assumption, since increased levels of CO_2 in the atmosphere will lead to more energy in the weather system which may partly be transferred to kinetic wave energy in the oceans. However, it is further assumed that this stochastic dependence structure will

remain essentially unchanged over time, from the past into the future. This is of course a critical assumption inherent in the model and any results are conditional on this assumption being realistic.

Furthermore, it is assumed that the CO_2 projections are reliable and results are conditional on the CO_2 data that have been utilized. In particular, no particular attention has been drawn towards possible climate tipping points or other effects that may skew the correlation between CO_2 levels in the atmosphere and the statistics of ocean waves. This introduces considerable uncertainty that has not been accounted for. Notwithstanding, the models presented herein are still believed to be interesting to explore and they model and predict future ocean wave climate based on the best available knowledge of the future levels of CO_2 as a result of various emission scenarios.

Finally, only CO_2 levels in the atmosphere have been considered, as a proxy of the level of greenhouse gases. It is normally considered that this is the dominant greenhouse gas, but omitting all other contributions is obviously a simplification. Furthermore, aerosols and other mitigating factors have not been considered as well as the variability in solar radiation and external forcing.

5.3.3 Prior Distributions

Most of the priors for these simulations were the same as outlined in previous chapters, except for the prior for $\mu_{0,1}$ which was modified with an increased location parameter, i.e. to $N(7.5, 2)$ (to reflect that monthly maximum data are used). Furthermore, as an alternative to the inverse gamma priors for the noise terms, simulations with non-informative priors on the noise terms were also tried out, i.e. $\pi(\sigma_i^2) \propto \frac{1}{\sigma_i^2}$, as suggested by [6], but it was discovered that this was not an obvious improvement and the inverse gamma priors were kept [18].

The parameters associated with the second harmonic coefficients f and g are still assigned priors with zero mean and variance = 0.5. The correlation between significant wave height and atmospheric CO_2 is believed to be positive, but apart from that, no specific prior knowledge is assumed. Therefore, a flat, non-informative prior for γ, η and δ will be employed i.e., a uniform prior. Note that due to proportionality, there is no need to specify a proper distribution and the uniform distribution endpoints a and b need not be specified.

5.4 Results and Predictions

The model, as outlined above, has been run on the significant wave height monthly maxima at each location for the same area in the North Atlantic previously studied. In the following, the main results from each set of simulations will be highlighted.

5.4.1 MCMC Simulations

The model was simulated using the Gibbs sampler with Metropolis-Hastings steps, similarly as for the model without regression terms [15]. However, the burn in period was extended to 50,000 samples and the batch size was five. I.e. a total of 1,000 samples of the posterior parameter vector were obtained. In order to enhance the acceptance rate, six Metropolis-Hastings steps were performed at each iteration, giving an overall acceptance rate of about 35 %.

Trace plots of the posterior marginal distributions suggest that convergence occurs satisfactorily. Furthermore, some control runs with considerable longer burn-in periods were performed; one control run for each of the main model alternatives with a burn-in period of 225,000 iterations and one control run for the linear-log model with a semi-annual component with 10 times longer burn-in period and batch size, i.e. a burn-in of 500,000 and a batch size of 50. This produced very similar posterior estimates, except perhaps for the log model. Hence, it is argued that the Markov chain was run sufficiently long to ensure convergence.

Normal probability plots of the residuals again suggest that the Gaussian model assumption is not unreasonable. Plots of residuals for both the inverse gamma priors and the non-informative priors on the noise variances show that the difference between the plots are small.

5.4.2 Simulation Results

The first sets of simulations were run without the semi-annual component, i.e. setting $f = g = 0$. Inverse gamma priors were used for the noise variances as before.

Most of the marginal posterior distributions are symmetric and resemble Gaussian densities, and the mean and standard deviation of the posterior distributions for different parameters of the different model alternatives are given in Table 5.1. The posterior distributions for a_ϕ and a_λ were not symmetrical, and the mean, median, and standard deviation of the estimated posterior distribution for these parameters are given in Table 5.1. These estimates pertain to the models run with inverse gamma priors for the noise variances. For the model alternative without any trend, the results should be expected to be identical to the models without trend for previous models without CO_2 regression components, and reference is made to [17] where such results are presented.

The six parameters $\mu_{0,\cdot}$ determine the spatially varying mean $\mu_0(x)$ over the area, which together with a_ϕ and a_λ determine the time independent part, $\mu(x)$. This is illustrated in Fig. 5.6 for the linear-log model alternative. The expected contribution from the time-independent part $\mu(x)$ is seen to be between 5.2 and 6.4 m with a mean of 6.1 m over the area for the linear-log model, which seems reasonable. These results may be compared to the results presented in [17], which were obtained for the same data but using a quadratic trend function rather than a CO_2 regression term.

Table 5.1 Posterior marginal distributions, (mean, standard deviation); inverse gamma priors for the noise variances

	linear-log model (Model 1)	**linear model** (Model 2)	**log model** (Model 3)
σ_Z^2	(1.2, 0.0086)	(1.2, 0.0075)	(1.2, 0.0079)
σ_μ^2	(0.035, 0.0042)	(0.035, 0.0043)	(0.035, 0.0044)
σ_θ^2	(0.067, 0.0059)	(0.066, 0.0044)	(0.066, 0.0047)
σ_m^2	(0.44, 0.077)	(0.67, 0.082)	(0.65, 0.12))
σ_t^2	(0.68, 0.093)	(0.47, 0.068)	(0.51, 0.12))
b_0	(0.22, 0.0098)	(0.23, 0.010)	(0.23, 0.010)
b_N	(-0.0061, 0.010)	(-0.0088, 0.0086)	(-0.0081, 0.0090)
b_E	(0.22, 0.010)	(0.22, 0.0099)	(0.22, 0.010)
b_S	(0.38, 0.025)	(0.38, 0.021)	(0.38, 0.019)
b_W	(0.22, 0.010)	(0.22, 0.011)	(0.22, 0.0096)
c	(2.4, 0.062)	(2.4, 0.064)	(2.4, 0.070)
d	(1.0, 0.062)	(1.0, 0.067)	(1.0, 0.068)
$\mu_{0,1}$	(7.4, 1.4)	(7.5, 1.4)	(7.4, 1.5)
$\mu_{0,2}$	(-0.31, 0.069)	(-0.32, 0.066)	(-0.30, 0.069)
$\mu_{0,3}$	(1.8, 0.41)	(1.8, 0.39)	(1.8, 0.41)
$\mu_{0,4}$	(0.00053, 0.00018)	(0.00054, 0.00017)	(0.00051, 0.00017)
$\mu_{0,5}$	(-0.013, 0.0024)	(-0.013, 0.0024)	(-0.013, 0.0023)
$\mu_{0,6}$	(-0.0011, 0.0010)	(-0.00093, 0.00095)	(-0.0010, 0.00098)
γ	(0.012, 0.0034)	(0.0088, 0.00062)	-
η	(-0.45, 0.20)	-	(-0.085, 0.027)
a_ϕ	(0.18, 0.18, 0.053)	(0.18, 0.18, 0.052)	(0.18, 0.18, 0.053)
a_λ	(0.28, 0.28, 0.051)	(0.28, 0.28, 0.053)	(0.28, 0.28, 0.056)

Upon comparison, it is found that the CO_2 regression model estimates a smaller, by about 1 m, contribution from the time-independent part $\mu(x)$, but this is compensated for by a long-term trend starting away from zero. For the linear model, the expected time-independent part varies between 3.6 and 4.8 m, with a mean of 4.5 m, and for the log model between 7.1 and 8.3 m with a mean of 7.9 m. Even though the range of values is quite different for the different model alternatives, the patterns described by plots similar to Fig. 5.6 are very similar and seem to agree well.

For all times (except t=0) and locations, the estimated mean of the $\theta(x)$ field ranges from -1.1 to 1.9 m for the linear-log model, from -1.1 to 1.8 m for the linear model and -1.2 to 1.9 for the log model, respectively. The average is about zero and variances range from 0.059 to 0.83 m^2 for the linear-log model (0.057 to 0.91 for the linear model and 0.057 to 0.83 for the log model). This agrees well and also well with the estimated dynamic part for the models with a linear or a quadratic trend function for the long-term trends. Hence, all model alternatives estimate similar contributions from the space-time dynamic component, and a notable part of the modelled significant wave height can be ascribed to this part. It is noted that this part is expected to contribute more for data with higher temporal resolution, e.g.

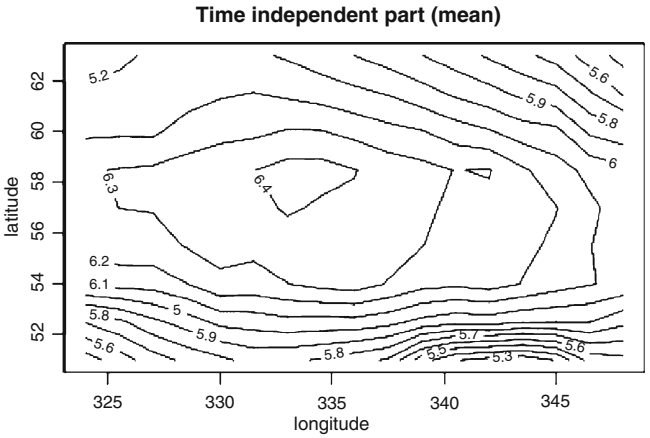

Fig. 5.6 Mean time-independent part, $\mu(x)$; linear-log model

daily maxima rather than monthly maxima, as seen in e.g. [15, 16]. One interesting observation from these results is that, of the b-parameters, b_S is the largest. However, it is noted that this component cannot be interpreted as related to individual storms and the dynamics of predominant stormtracks when run on monthly data.

The contribution from the seasonal component, $M(t)$, is shown in Fig. 5.7, and a clear cyclic behaviour is observed. The estimated values for $M(t)$ vary between -3.3 and 3.6 m for the linear-log model, between -3.6 and 4.1 m for the linear model and -3.4 to 4.0 m for the log-model. The seasonal contribution without the error term, $c\cos(\omega t) + d\sin(\omega t)$, calculated with the mean values of c and d, is also shown in the figure, corresponding to oscillations between $\pm$ 2.66 m for the linear-log model, $\pm$ 2.65 m for the linear model and $\pm$ 2.64 m for the log model. This agrees fairly well with the sampled seasonal contribution, although missing some of the extremes. It is observed that also with respect to the seasonal contributions, the different model alternatives agree well.

The contribution from the long-term trend component is illustrated in Fig. 5.8 which shows the sampled trend contribution together with the estimated mean and 90 % credible interval of the mean derived from the distribution of (γ, η). It is observed that this trend does not start at zero; the trend has a value of 1.1 m already at the beginning of the period for the linear-log model. For the linear model, the trend starts at 2.8 m and for the log model at -0.49 m. Recalling that the time-independent part was about 1 m lower for the linear-log model compared to the simulations for the models with a quadratic function (in time) for the trend, i.e. where the trend is 0 m for t=0, this makes sense, and the difference in the $\mu(x)$-fields for the different models can be explained by this. For example, the $\mu(x)$-field was about 1.7 m higher for the linear-log model compared to the linear model, and this corresponds well with the difference in starting points of the different trends. In fact, for all model alternatives, $E[\mu(x)] + E[\mathrm{T}(t = 0)]$ is in the same order of magnitude, between 7.2 and 7.4 m

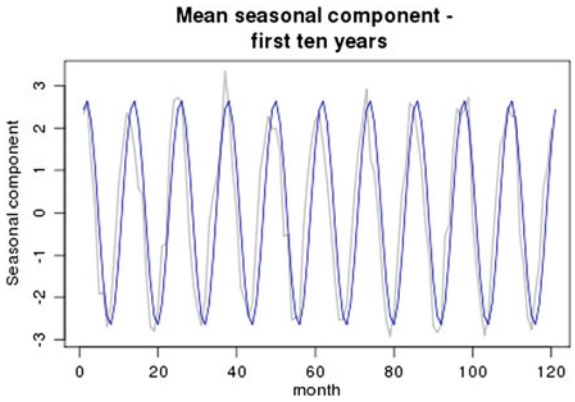

Fig. 5.7 The seasonal contribution for 10 years; linear-log model

and this is reasonable. The estimated expected trend now increases from 1.1 to 1.7 m over the period, corresponding to an increase of 59 cm for the linear-log model and from 2.8 to 3.3 m corresponding to an increase of 49 cm for the linear model. This is comparable, although slightly lower, to previously estimated trends in the monthly maxima reported in [17]. However, the log model picks up an almost vanishing but negative long-term trend that is very different from the other model alternatives; an expected decrease from -49 to -50 cm corresponding to a negative trend of 1.4 cm over the period.

One of the main motivations for including the CO_2 regression component into the model was to facilitate future projections, and projections of future significant wave heights are made from two future scenarios for CO_2 levels, referred to as the A2 and B1 scenario, respectively. The corresponding projected trends of significant wave height are illustrated in Fig. 5.9, and it can be seen that scenario A2 gives future projections corresponding to an increase of 5.4 m and the B1 scenario corresponds to an increase of 1.9 m towards the year 2100 compared to the year 2001 when using the linear-log model. The large difference between the two projections are due to the different CO_2 levels projected by the two scenarios. However, both the projected trends are considerably larger than the one obtained from extrapolating an estimated linear trend towards 2100 (1.6 m over 100 years, as reported in [17]). For the linear model, the estimated increases between 2001 and 2100 were 4.3 m for the A2 scenario and 1.6 m for the B1 scenario. For the log model, negligible decreasing trends of 7.2 and 3.3 cm, were estimated between 2001 and 2100 for the scenarios A2 and B1, respectively. However, it is deemed very unlikely with a negative correlation between levels of CO_2 and significant wave height, so the results from this model are not to be trusted.

The expected future projections including 90 % credible intervals are presented in Figs. 5.10 and 5.11. The credible intervals are calculated from the credible intervals of the distribution of (γ, η) and do not include the uncertainty due to ε_t. For scenario A2, the 90 % credible interval at year 2100 corresponds to increases in monthly maximum significant wave height over the twenty-first century ranging from 2.7 to

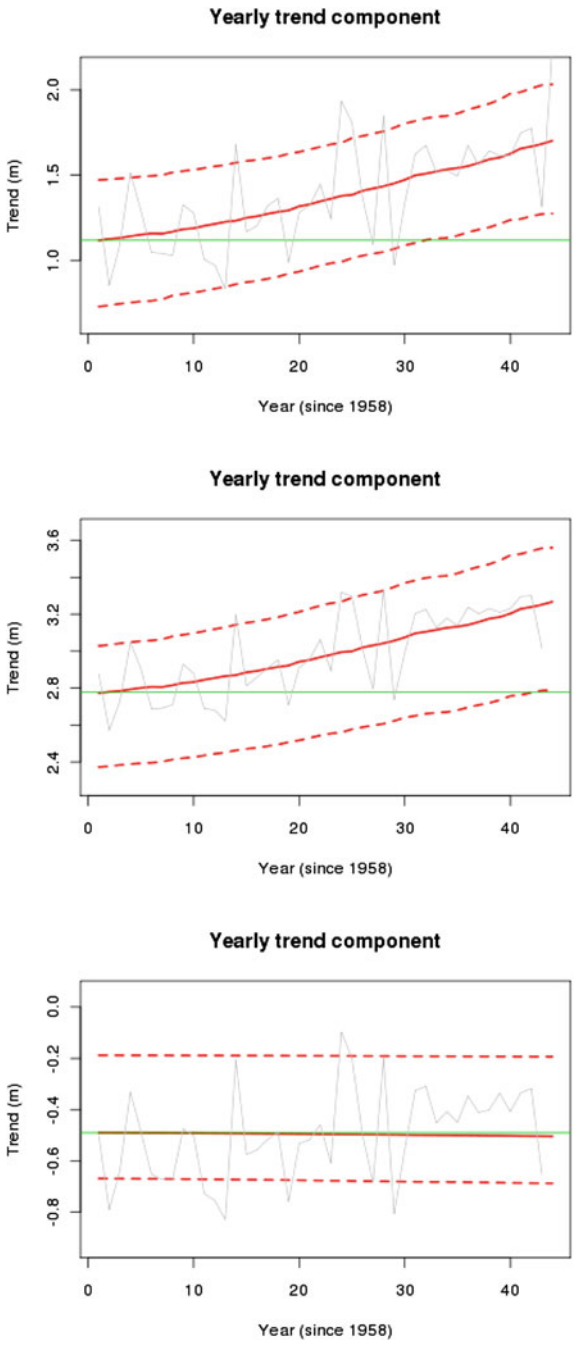

Fig. 5.8 The estimated trend over the period; linear-log model (top), linear model (middle) and log model (bottom)

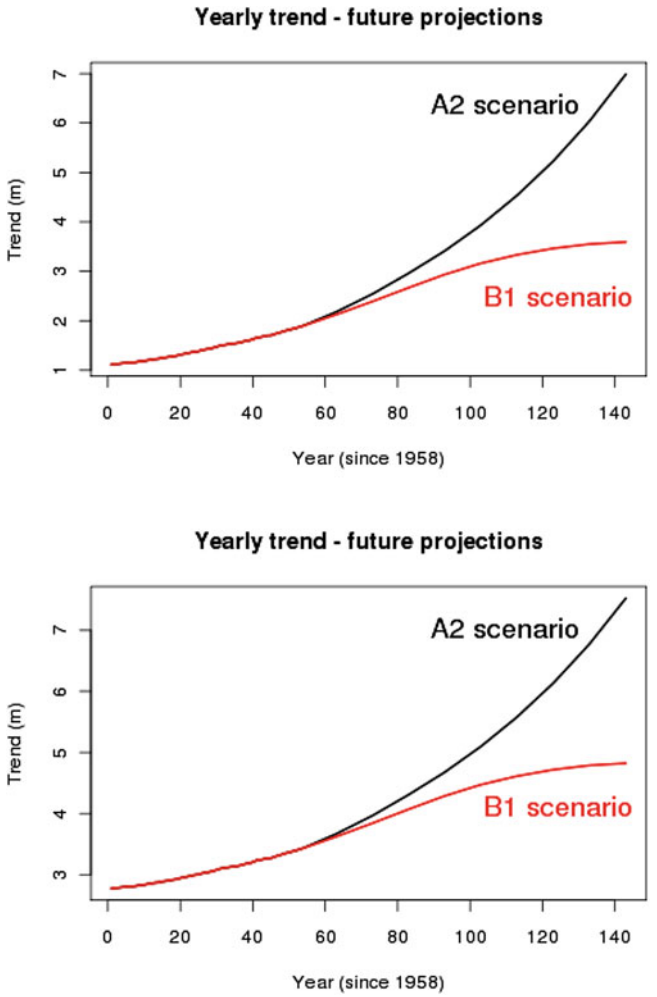

Fig. 5.9 The estimated and projected trends towards 2100; linear-log model (*top*), linear model (*bottom*)

8.1 m. For scenario B1, the corresponding credible interval covers a range between 1.2 and 2.6 m increase from 2001 to 2100 (linear-log model). For the linear model, the credible bands are asymmetric and somewhat narrower, ranging from 3.2 to 5.0 m for scenario A2 and 1.3 to 1.7 m for scenario B1.

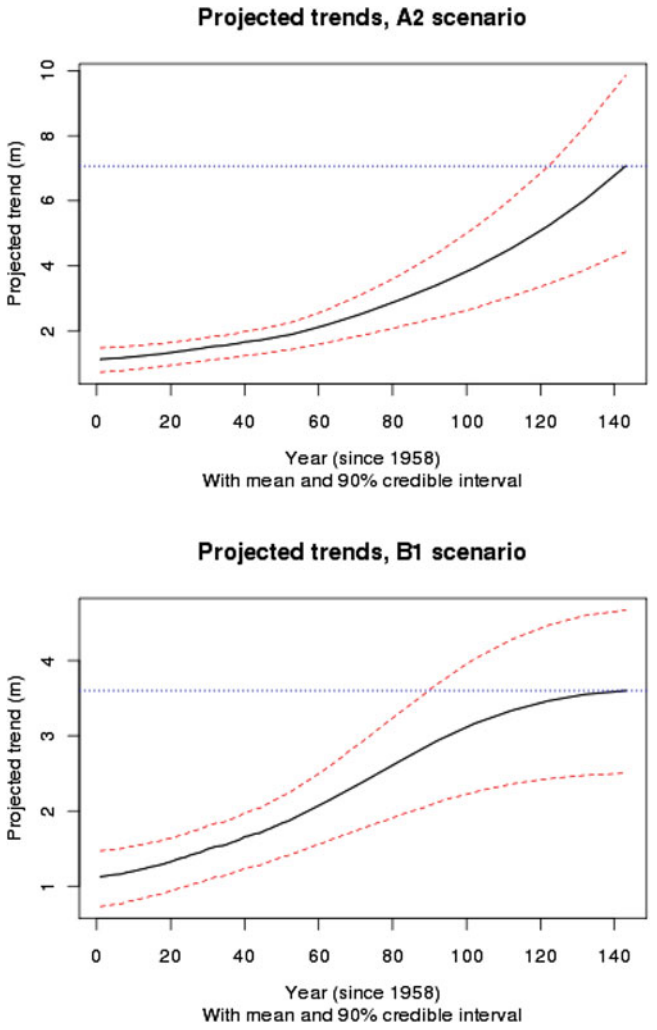

Fig. 5.10 The projected trend towards 2100 with credible bands, scenarios A2 (*top*) and B1 (*bottom*); linear-log model

5.4.3 Results with a Semi-Annual Component

In order to investigate the effect of including a semi-annual component in the seasonal model, simulations were run where the second harmonic was included, i.e., by removing the constraint $f = g = 0$. It is observed that the inclusion of a semi-annual component does not influence the overall results much. The space-time dynamic part, $\theta(x, t)$ is not notably affected, and also the seasonal part is similar, even though it is no longer symmetric around zero; the absolute value of the minima is greater

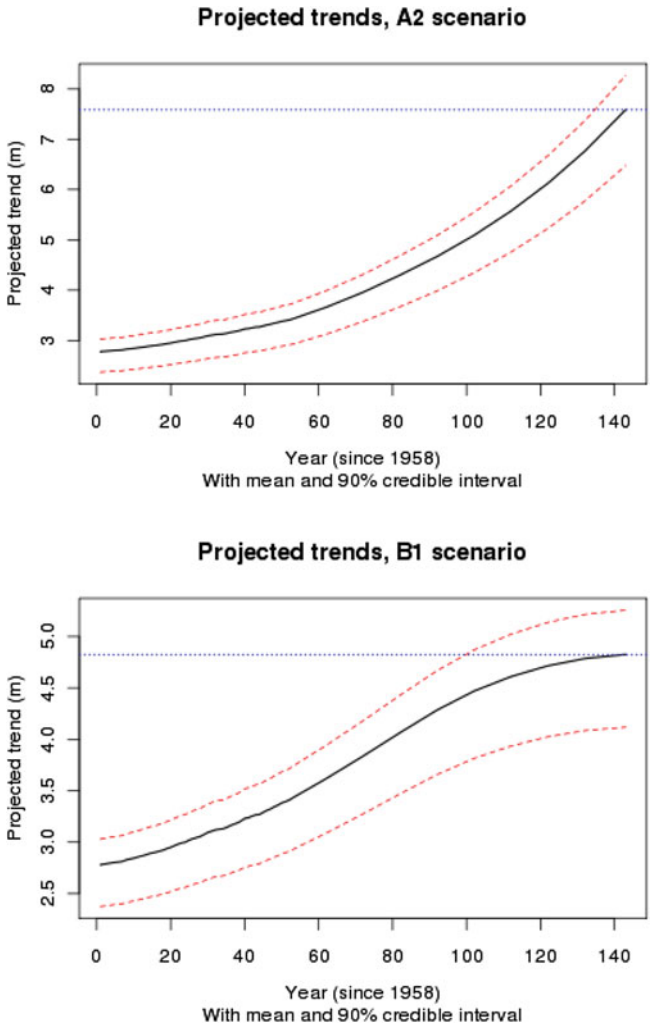

Fig. 5.11 The projected trend towards 2100 with credible bands, scenarios A2 (*top*) and B1 (*bottom*); linear model

than for the maxima, with seasonal contribution oscillating between -2.9 and 2.4 m. The time-independent field $\mu(x)$ displays the same pattern as for the models without a semi-annual part, but it lies at different levels. However, when considered together with the starting point of the trend, these results also agree with the results obtained without the semi-annual component. For the log model, the η-parameter is still negative (although small) which corresponds to a negative but almost non-existing estimated trend similar to the trend for the log model with only annual

seasonal component. Hence, also in this case little confidence is put on this model alternative.

The estimated expected trend now increases from -2.5 to -2.0 m over the period (linear-log model), corresponding to an expected increase of 53 cm, which agrees well with the estimated trends for the same model without the semi-annual component. For the linear model, the expected increase is between 1.8 and 2.1 m corresponding to an expected increase of about 32 cm over the period.

The projected trends of significant wave height for scenario A2 is an expected increase of 5.3 m and for scenario B1 an expected increase of 1.8 m between 2001 and 2100 for the linear-log model. For the linear model, scenario A2 gives a projected expected increase of 2.7 m and scenario B1 an expected increase of almost 1 m for the same period. For the linear-log model, this is in good agreement with the projections made without the semi-annual component, even though the credible intervals have become slightly narrower. For the linear model, the inclusion of the semi-annual trend yields somewhat smaller trends. Notwithstanding, it is argued that the inclusion of the semi-annual component has only minor influence on the results overall.

5.4.4 Results for Control Runs

In order to check if the Markov chains truly converge, some control runs with increased burn-in periods and a control run with increased burn-in period and batch size were performed. First, a set of simulations with 225,000 iterations as burn-in, keeping the batch size of 5, were performed for the three main model alternatives, i.e. the linear log, linear and log models without any semi-annual components. One further control run on the linear-log model with a semi-annual component was carried out, with 500,000 burn-in iterations and a batch size of 50.

For the linear log and linear models, the posterior estimates are mostly unchanged, and the posterior distributions of the few parameters that are somewhat different are largely overlapping. Hence, the results are essentially unchanged by the extended burn-in, suggesting that the initial burn-in period was sufficient. Even though the spatial field, $\mu(x)$, was estimated at a different level, this was again compensated by the starting values of the trend component, T(0), and the overall results are in good agreement for the combined spatial field and the trend, for the short-time dynamic part and for the seasonal part. For the linear-log model also the estimated trends and the future projections are comparable to the simulations with the initial burn-in period and it is argued that these results suggest that convergence of the Gibbs sampler is obtained. For the linear model, the estimated trends and future projections became smaller with the extended burn-in, so these results are perhaps less reliable.

For the log-model, which was not able to detect any notable trends with the initial burn-in, it is seen that the posterior estimate of the η-parameter is larger and strictly positive with the longer burn-in. For the other parts of the model, the performance is not much affected by the extended burn-in period, but the long-term trend is indeed affected. The estimated expected trend is now an increase of 12 cm over the period.

This is still small, but different from the previously estimated negative trend. The corresponding future projections from 2001 towards 2100 for scenarios A2 and B1 now becomes 62 cm and 29 cm, respectively. This is again very different from the previously estimated negative trend, but much smaller than the trends estimated by the linear log and the linear models. Notwithstanding, it is concluded that the log-model possibly did not converge within the initial burn-in period of 50,000 iterations and those results should therefore not be trusted. Furthermore, it is observed (see Table 5.2 below) that the loss functions indicate that the log-model performs better with the longer burn-in period.

For the linear-log model with a semi-annual component, the distribution for most parameters are essentially the same. For the parameters with some deviation, the difference is small and the densities are largely overlapping. Hence, it is argued that convergence is indeed achieved with the original burn-in period of 50,000 iterations. Also, the variances were of the same order of magnitude, so a batch size of five seems sufficient.

5.5 Model Comparison and Selection

A crude comparison of the different model alternatives can be carried out by comparing the resulting posterior estimates of the model parameters. It is observed that the spatial features of the model seem to be unaffected by the model alterations. Since the model reductions were only related to the temporal trend, this is reassuring. The seasonal part of the model also seems to behave similarly over the model alternatives. Hence, the main differences are, as would be expected, related to the long-term temporal trend and the future projections.

Somewhat more formally, the models may be compared by way of the loss functions for short-term prediction and the values for the two loss functions for each of the model alternatives are presented in Table 5.2.

It is seen that the linear-log model performs better than the linear model, which again performs better than the log-model, and that this is quite consistent over the various simulations. The log model seems to perform slightly worse than the model without any trend, and it is also observed that for this particular model alternative, the control run has slightly increased performance. Hence, this particular model alternative might not have converged properly and does not seem to perform well; the estimates from this model are not to be trusted.

Furthermore, the inclusion of the semi-annual component in the seasonal part of the model does not represent an obvious improvement, except perhaps for the log model, and this agrees with the results for the log-transformed data [16]. The control runs with considerably longer burn-in periods do not seem to improve the predictions either, and it is concluded that the initial burn-in period was sufficient, again with the exception of the log model.

Comparing the loss functions with the loss functions for the models with quadratic and linear trend functions reported in [17], it is seen that the replacement of this trend

Table 5.2 Model selection: Standard and weighted loss functions

Model alternative	L_s	L_w
linear-log model	2.5616360	2.6743827
Linear model	2.5958652	2.7115865
log model	2.7835824	2.9113850
no trend model	2.7810660	2.9085743
linear log with semi-annual trend	2.5658667	2.6801950
linear with semi-annual trend	2.6265630	2.7461653
log with semi-annual trend	2.7414825	2.8671277
control run (linear-log model)	2.5716014	2.6860570
control run (linear model)	2.6447196	2.7643920
control run (log model)	2.7183518	2.8420370
control run (linear-log model with semi-annual trend)	2.5391257	2.6515834

function with a CO_2 regression component yields a slight improvement; the values of the loss functions in Table 5.2 are consistently slightly lower than the values reported in [17].

5.6 Discussion

A Bayesian hierarchical space-time model for significant wave height with a CO_2 regression component has been developed and different model alternatives have been simulated for an area in the North Atlantic Ocean. The various model alternatives that have been explored differ in how the regression block with CO_2 data has been modelled and whether the seasonal component includes a semi-annual as well as an annual part. However, the inclusion of a semi-annual component did not seem to influence the results much and a purely annual component is deemed sufficient for the seasonal model.

Four different alternatives were investigated with respect to the regression block, $T(t)$, i.e. models with a linear and logarithmic regression term, only linear and only logarithmic regression terms as well as a model without any long-term trend. The various model alternatives obtained different estimates of the long-term trends and future projections of significant wave height, but it was found that the linear-log model seemed to be superior. Indeed, the model with a purely logarithmic regression term performed poorly and should be rejected. However, the linear-log model performed reasonably well, and it was also found that the results were robust against changes in burn-in period of the Markov chain. Hence, this model is selected as the most reliable one.

In order to compare model alternatives, two loss functions have been utilized. These are based on short-term predictive power, and might therefore not be ideally suited for comparing models aiming at long-term predictions. Notwithstanding, it is

reassuring to observe that the model selection criteria seem to be quite consistent in identifying the linear-log model as the preferred one.

Future projections were based on two future emission scenarios, denoted as the A2 and the B1 scenarios respectively. There are obviously large uncertainties with respect to future levels of atmospheric CO_2, and corresponding projected trends in the ocean wave climate are reported for both scenarios. However, both scenarios yield larger projected trends compared to the models where a linear trend was extrapolated over 100 years [15–17]. It is also noted that an implicit assumption in the models is that the correlation between atmospheric levels of CO_2 and the wave climate is unchanged, and this is obviously a critical and uncertain assumption.

The future projections estimated from the models seem to be somewhat larger than other projections made for significant wave height in the North Atlantic, reported by e.g. [2–4, 7, 20–22], but the uncertainties are large and there are some overlaps. The estimated 90% credible intervals correspond to about $\pm$ 50 % of the expected projections. It should also be kept in mind that the trends predicted herein pertain to the monthly maxima and the maxima might experience a greater change than moderate sea states, as also suggested in e.g. [23]. Furthermore, the A2 scenario is believed to correspond to an extreme emission scenario and the corresponding projections of wave climate would therefore also expectedly be on the extreme side of projections. This can be construed as a worst case scenario and is important to consider from a precautionary perspective. In contrast, the B1 scenario is much more conservative and also yields much smaller projected future trends in the wave climate.

It should be stressed that even though the models detect trends in the data, it does not necessarily mean that the trend is a direct consequence of anthropogenic climate change. It might be a result of decadal natural variability, as discussed in e.g. [1], and wave climate variability has been reported to be considerable on different temporal scales [5]. Great care should therefore be taken when interpreting the meaning and the origin of this trend, even though the correlation between anthropogenic CO_2 emissions and the wave climate is found to be strong in this study.

5.7 Summary and Conclusion

This chapter has outlined a Bayesian hierarchical space-time model that has been extended with a regression block with atmospheric CO_2 levels as covariates. This has been used to estimate trends and make future projections of the ocean wave climate over an area in the North Atlantic Ocean, i.e. trends and projections of the monthly maximum significant wave height. The models have different components in space and time and are found to generally perform well. Different model alternatives have been tried and the model with both a linear and a logarithmic relationship between the wave climate and the level of CO_2 in the atmosphere is generally found to be superior.

According to the linear-log model, a trend has been detected in the data corresponding to an expected increase in monthly maximum significant wave height of

59 cm between 1958 and 2001. Future projections have been based on two emission scenarios towards 2100, i.e. the A2 and the B1 scenarios corresponding to the most pessimistic and most optimistic of several IPCC scenarios. Assuming the A2 emission scenario, an expected future trend in monthly maximum significant wave height of 5.4 m was estimated between 2001 and 2100. For the B1 scenario, the estimated expected increase was 1.9 m towards 2100. The uncertainties in both cases are considerable, with 90 % credible intervals ranging from increases of 2.7 to 8.1 m for scenario A2 and 1.2 to 2.6 m for scenario B1. Recalling that the mean monthly maximum significant wave height was 7.5 m, the estimated expected increases correspond to centurial increases of 72 % and 25 % respectively. It is believed that especially the projections corresponding to the A2 scenario are quite high, but it should be kept in mind that the A2 emission scenario is an extreme or worst case scenario and consequently the projected increase in ocean wave climate becomes extreme.

It is acknowledged that making regression directly on the atmospheric CO_2 level is a simplification and further extensions of the model could include different layers of dependencies, i.e. including regression towards sea level pressure fields or wind fields in the area. However, this is left for further work, and it is still interesting to see that the model with a CO_2 regression block overall seems to perform reasonably well.

References

1. Caires, S., Sterl, A.: 100-year return value estimates for ocean wind speed and significant wave height from the ERA-40 data. J. Clim. **18**, 1032–1048 (2005)
2. Caires, S., Swail, V.R., Wang, X.L.: Projection and analysis of extreme wave climate. J. Clim. **19**, 5581–5605 (2006)
3. Debernard, J., Sætra, Ø., Røed, L.P.: Future wind, wave and storm surge climate in the northern North Atlantic. Clim. Res. **23**, 39–49 (2002)
4. Debernard, J.B., Røed, L.P.: Future wind, wave and storm surge climate in the Northern Seas: a revisit. Tellus **60A**, 427–438 (2008)
5. Dodet, G., Bertin, X., Tabora, R.: Wave climate variability in the North-East Atlantic Ocean over the last six decades. Ocean Model. **31**, 120–131 (2010)
6. Gelman, A.: Prior distributions for variance parameters in hierarchical models. Bayesian Anal. **1**, 515–533 (2006)
7. Grabemann, I., Weisse, R.: Climate change impact on extreme wave conditions in the North Sea: an ensemble study. Ocean Dyn. **58**, 199–212 (2008)
8. IPCC: Climate Change 2001: The Scientific Basis. Cambridge University Press, Cambridge (2001)
9. Jain, A.K., Kheshgi, H.S., Hoffert, M.I., Wuebbles, D.J.: Distribution of radiocarbon as a test of global carbon cycle models. Global Biogeochem. Cycles **9**, 153–166 (1995)
10. Jain, A.K., Kheshgi, H.S., Wuebbles, D.J.: Integrated science model for assessment of climate change. Technical Report UCRL-JC-116526, Lawrence Livermore National Laboratory (1994)
11. Kheshgi, H.S., Jain, A.K.: Projecting future climate change: implications of carbon cycle model intercomparisons. Global Biogeochem. Cycles **17**, 1047 (2003)
12. Nakićenović, N., Alcamo, J., Davis, G., de Vries, B., Fenhann, J., Gaffin, S., Gregory, K., Grügler, A., Jung, T.Y., Kram, T., La Rovere, E.L., Michaelis, L., Mori, S., Morita, T., Pepper, W., Pitcher, H., Price, L., Riahi, K., Roehrl, A., Rogner, H.H., Sankovski, A., Schlesinger, M.,

Shukla, P., Smith, S., Swart, R., van Rooijen, S., Victor, N., Dadi, Z.: Emissions scenarios. Cambridge University Press (2000)
13. Thoning, K.W., Tans, P.P., Komhyr, W.D.: Atmospheric carbon dioxide at Mauna Loa observatory 2. analysis of the NOAA GMCC data, 1974–1985. J. Geophys. Res. **94**, 8549–8565 (1989)
14. Vanem, E.: A stochastic model for long-term trends in significant wave height with a CO_2 regression component. In: Proceedings of the 31st International Conference on Ocean, Offshore Mechanics and Arctic Engineering (OMAE 2012). American Society of Mechanical Engineers (ASME) (2012)
15. Vanem, E., Huseby, A.B., Natvig, B.: A Bayesian hierarchical spatio-temporal model for significant wave height in the North Atlantic. Stoch. Env. Res. Risk Assess. **26**, 609–632 (2012)
16. Vanem, E., Huseby, A.B., Natvig, B.: Modeling ocean wave climate with a Bayesian hierarchical space-time model and a log-transform of the data. Ocean Dyn. **62**, 355–375 (2012)
17. Vanem, E., Huseby, A.B., Natvig, B.: A stochastic model in space and time for monthly maximum significant wave height. In: Abrahamsen P., Haugen R., Kolbjørnsen O. (eds.) Geostatistics Oslo 2012, pp. 505–517. Springer, Heidelberg (2012)
18. Vanem, E., Huseby, A.B., Natvig, B.: Bayesian hierarchical spatio-temporal modelling of trends and future projections in the ocean wave climate with a CO_2 regression component. Environmental and Ecological Statistics (in press) (2013)
19. van Vuuren, D.P., Edmonds, J., Kainuma, M., Riahi, K., Thomson, A., Hibbard, K., Hurtt, G.C., Kram, T., Krey, V., Lamarque, J.F., Masui, T., Meinshausen, M., Nakicenovic, N., SMith, S.J., Rose, S.K.: The representative concentration pathways: an overview. Clim. Change **109**, 5–31 (2011)
20. Wang, X.J., Zwiers, F.W., Swail, V.R.: North Atlantic ocean wave climate change scenarios for the twenty-first century. J. Clim. **17**, 2368–2383 (2004)
21. Wang, X.L., Swail, V.R.: Climate change signal and uncertainty in projections of ocean wave heights. Clim. Dyn. **26**, 109–126 (2006)
22. Wang, X.L., Swail, V.R.: Historical and possible future changes of wave heights in northern hemisphere oceanc. In: Perrie, W. (ed.) Atmosphere-Ocean Interactions, Advances in Fluid Mechanics, vol. 39, vol. 2, chap. 8, pp. 185–218. WIT Press (2006)
23. Young, I., Zieger, S., Babanin, A.: Global trends in wind speed and wave height. Sci. **332**, 451–455 (2011)

Chapter 6
Bayesian Hierarchical Modeling of the Ocean Windiness

It is generally accepted that the main physical mechanism for wave generation is transfer of energy from the atmosphere to the ocean due to wind friction on the sea surface (see. e.g., [9]). Waves that are generated by local wind fields are referred to as wind sea, whereas swell is used to refer to waves that remain after the wind has died out and that can travel considerable distances. Hence, the origin of swell may be very remote from where the waves are measured. In the open ocean, waves of many different directions and frequencies are present and wave spectra often display two distinctive frequency modes associated with wind sea and swell (bimodal waves).

In the significant wave height data used in the Bayesian hierarchical space-time models, it is not distinguished between the wind sea and the swell contributions and the models are not able to distinguish the origin of the waves contributing to the significant wave height. Therefore, the model cannot determine whether the estimated increase in significant wave height is due to increased wind sea or increased swell, or perhaps a combination of both. In order to investigate this, this chapter applies a similar stochastic model on the wind speed over the same area in the North Atlantic Ocean. It will then be argued that if a similar increasing trend is estimated for wind speed as for significant wave height, the increase in significant wave height can be attributed, at least in part, to an increase in wind sea. Conversely, if there are no detectable trends or even decreasing trends in the windiness over the same area, the estimated increase should be ascribed to increasing swell. Furthermore, it is believed that investigating the spatial and temporal variability of North Atlantic windiness is of interest in itself and that it will be interesting to explore how the Bayesian hierarchical modeling framework performs for wind speed. The results presented in this chapter are extracted from [12].

E. Vanem, *Bayesian Hierarchical Space-Time Models with Application to Significant Wave Height*, Ocean Engineering & Oceanography 2,
DOI: 10.1007/978-3-642-30253-4_6, © Springer-Verlag Berlin Heidelberg 2013

6.1 Data Description and Area of Investigation

6.1.1 Wind Data

This study exploits the ERA-40 reanalysis data for wind speed [11], which cover most of the entire globe and a period of 45 years at 6-hourly resolution (from September 1957 until august 2002). It is important to note that the ERA-40 wind data are from the same reanalysis study as the ERA-40 significant wave height data that was used in the previous chapters for modeling of significant wave height, selected due to their spatial and temporal resolutions. Hence, the data sets should be consistent and allow for comparison of results for waves and winds. The data are freely available for research purposes and may be downloaded from the ECMWF website.[1]

The ERA-40 data contain the two parameters U and V for the 10-m wind speed, i.e., the wind speed at height 10 m above the sea surface. U refers to the wind velocity component in the east–west direction, whereas V refers to the north–south component of the wind velocity, both in terms of meters per second (m/s). Jointly, U and V therefore describe both the magnitude of the wind speed and the wind direction. This study, however, is restricted to analysis of the wind speed, and the wind direction will not be considered. Hence, the parameter of interest in this study, for which the Bayesian hierarchical space-time model has been applied, is the absolute value of the wind speed, W:

$$W = \sqrt{U^2 + V^2}. \tag{6.1}$$

The temporal resolution of the data is 6 h. However, for the purpose of this study, the monthly maximum wind speed in each spatial location is analyzed, in line with the analyses reported in [15, 16]. This corresponds to time series of 540-monthly maxima, corresponding to the 45 years of data, at each spatial location.

The ERA-40 10-m wind speed data have been compared to satellite and buoy measurements in [17]. Comparison of monthly means indicates good agreement between the ERA-40 wind speeds and the satellite measurements, with high correlations and low-root mean square values for wind speed difference, although ERA-40 tend to underestimate the monthly mean wind speed. Comparison on shorter time scales, i.e., comparing with daily satellite winds, reveals larger differences, but it is assumed that the ERA-40 wind speed data for monthly maximum values are reasonable. Also the KNMI/ERA-40 wave atlas[2] states that the 10-m wind speeds compare quite well with observations. It is noted that the results from the modeling presented in this paper are conditional on the data and no attempt has been made to correct possible biases. Therefore, it is reassuring that the monthly mean 10-m wind speeds from ERA-40 agree well with satellite data.

Before applying the Bayesian hierarchical space-time model on the data, a crude data inspection will be carried out and some main features of the raw data pertaining to

[1] URL: http://data-portal.ecmwf.int/.

[2] URL: http://www.knmi.nl/waveatlas.

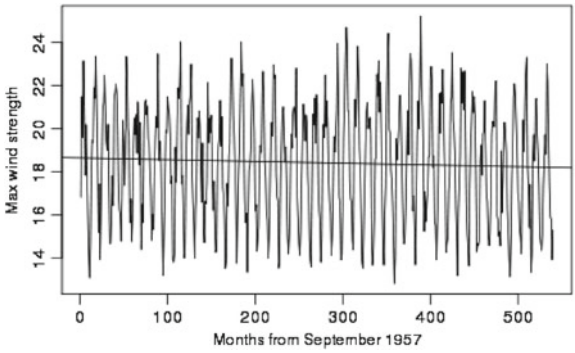

Fig. 6.1 Fitting a straight line to the raw data indicates a negative trend

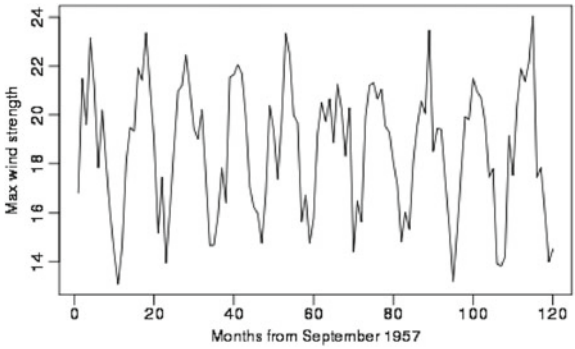

Fig. 6.2 The seasonality of the raw data

the selected area will be presented. The highest wind speed recorded in the monthly maximum data overall is just above 32 m/s and the minimum value in the dataset is about 8.6 m/s. The estimation of possible long-term trends is one of the main motivations for applying the stochastic model, and a very crude approach to see if there are any likely trends is to fit a straight line to the raw data. In Fig. 6.1 the spatially averaged data are shown with a straight line fitted to it by least squares. It is observed that this line has a negative slope of -0.0008171 m/s per month with an intercept of 18.64 m/s, corresponding to slightly decreasing monthly maximum wind speeds of about 0.44 m/s overall throughout the period. It is also interesting to observe the seasonality in the raw wind data as illustrated by Fig. 6.2 where the spatially averaged data for the first 10 years are shown.

6.1.2 Area Description

Ideally, the area selected for analysis of wind speeds should be identical to the area used in the analysis of significant wave height. However, for the significant wave height, a corrected dataset with resolution $1.5° \times 1.5°$ was used whereas the dataset

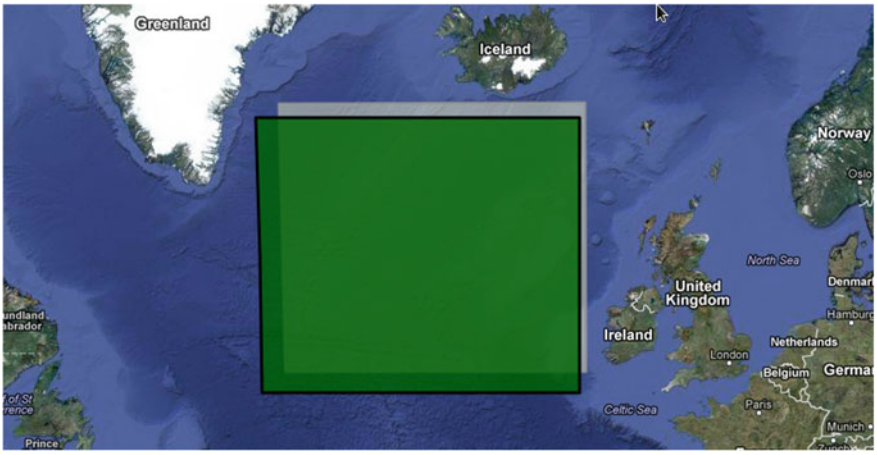

Fig. 6.3 The areas in the North Atlantic Ocean for analyzing windiness (*dark green*) and significant wave height (*light grey*)

for wind speed that is downloadable from the European Centre for Medium-Range Weather Forecasts (ECMWF) website has a spatial resolution of $2.5° \times 2.5°$ degrees. Thus, the areas are not entirely identical, but they are largely overlapping and this is assumed to be satisfactory. The area included in this study ranges from 50° to 62.5° north and 322.5° to 347.5° east corresponding to a grid of $6 \times 11 = 66$ data points. Due to the reduced spatial resolution, the distance between the grid points is larger than for the dataset used in the significant wave height modeling even though the areas are essentially overlapping. It is assumed that the different spatial resolution of the wind data compared to the wave data does not influence the overall results from the models, and particularly that any long-term trends would not be very sensitive to the difference in spatial resolution. The selected area is illustrated in Fig. 6.3 where also the area for the significant wave height analysis is indicated. Additionally, another area further to the north is investigated (not indicated in Fig. 6.3).

6.2 The Stochastic Model

The Bayesian hierarchical space-time model resembles the model for significant wave height [13] and the spatiotemporal data are indexed in a similar way by two indices; $x = 1, 2, \ldots, X = 66$ and $t = 1, 2, \ldots, T = 540$ ($t = 1$ corresponds to September 1957 and $t = T = 540$ corresponds to August 2002). The maximum windiness at location x in month t is expressed by $W(x, t)$. The structure of the main model, and the few alternative models that are also explored, is very similar to the significant wave height model and will only be briefly explained in this chapter. For a full model specification, reference is made to [12].

It is emphasized that this model is a stochastic model rather than a physics-based model and the physical mechanisms in the atmosphere responsible for generating wind are not explicitly included in the model. It is rather the complex stochastic dependence structures, in space and time at various scales, in the wind data itself that have been modeled. However, it is argued that all relevant physics are undeniably inherent in the data, so the relevant physical mechanisms are implicitly taken into account by the model, by way of the data. Hence, this probabilistic model is proposed as a complement and an alternative to more deterministic, geophysics-based models.

6.2.1 Main Model Specification

The observation or data equation (Eq. 6.2) models the maximum windiness at location x and month t as a latent (or hidden) process H, corresponding to an underlying wind speed process that may normally be construed as the true process, and some random noise, ε_W, which may be construed as measurement error or data uncertainty in much the same way as the significant wave height process was modeled.

$$W(x,t) = H(x,t) + \varepsilon_W(x,t) \qquad \forall x,t \tag{6.2}$$

The underlying process for monthly maximum windiness is modeled by the state or system model which is split into a time-independent part $\mu(x)$, a short-term temporally and spatially dependent part $\theta(x,t)$ and two spatially independent parts $M(t)$ and $T(t)$ for seasonality and long-term trends, respectively (Eq. 6.3). The various parts of the model are similar to the corresponding components of the significant wave height model, with the same parametrization, and the details are omitted in this chapter. Reference is again made to [12] for details.

$$H(x,t) = \mu(x) + \theta(x,t) + M(t) + T(t) \tag{6.3}$$

In the seasonal component, a combination of annual and semiannual contributions is included. The long-term trend of the initial model is a simple Gaussian process with a linear trend, as shown in Eq. 6.4.

$$T(t) = \gamma t + \varepsilon_{\mathrm{T}}(t) \tag{6.4}$$

6.2.2 Alternative Models

Two model alternatives have also been explored in this study, in line with the studies of significant wave height. First, a model where the trend component has been removed is applied, and this model is simply identical to the model in Eqs. 6.2 and 6.3 with $\mathrm{T}(t) = 0$ and all other components unchanged, as presented in Eq. 6.5

$$W(x,t) = H(x,t) + \varepsilon_W(x,t) = \mu(x) + \theta(x,t) + M(t) + \varepsilon_W(x,t) \tag{6.5}$$

This model would then explain the data under the assumption of no trend.

The other model alternative is obtained by taking the logarithmic transformation of the data. By taking this log-transform, the model effectively changes into the model in Eq. 6.6, where $H(x,t)$ is still modeled as in Eqs. 6.3 and 6.4, see also [14].

$$Y(x,t) = \ln W(x,t) = H(x,t) + \varepsilon_Y(x,t) \tag{6.6}$$

An equivalent representation of this model alternative on the original scale is

$$W(x,t) = e^{\mu(x)} e^{\theta(x,t)} e^{M(t)} e^{\mathrm{T}(t)} e^{\varepsilon_Y(x,t)} \tag{6.7}$$

where now the contributions from the individual components to the wind speed have become multiplicative factors rather than additive contributions. This gives a different interpretation of the model components.

Similar prior distributions as for the significant wave height model were employed and reference is made to [12] for details and exact values of the hyperparameters of the prior distributions.

6.2.3 MCMC Simulations

The MCMC simulations performed to sample from the wind speed model used a burn-in period of 100 000 samples and a batch size of 20, corresponding to a total of 120 000 simulations to obtain a collection of 1000 samples of the multi-dimensional parameter vector. The Metropolis-Hastings steps were repeated six times to obtain an overall acceptance rate of about 70 %. The burn-in period is much longer than what was used for the significant wave height model, and it ensures that the Markov chain converges. The assumption that the chain converges within the burn-in period is confirmed by trace plots and a few control runs. A simulation according to these specifications completes in about 5 h on a computer with an Intel Core i5-2500 CPU @ 3.30 GHz processor.

A normal probability plot of the residuals is investigated in order to check the main model assumption of normality at the observation level, and this indicates that the assumption is reasonable.

6.3 Results

In this section, the results for the different model alternatives and pertaining to the different model components will be reported. The estimated marginal posterior distributions (mean and standard deviation) are presented in Table 6.1. It is noted that

Table 6.1 Posterior marginal distributions (mean; standard deviation)

	Main model	No trend	Log-transform	Alternative area
γ	−0.00034; 0.084	–	$-4.9 \cdot 10^{-5}$; $4.8 \cdot 10^{-5}$	0.0014; 0.00042
$\mu_{0,1}$	20; 3.0	20; 3.0	3.1; 2.0	20; 5.2
$\mu_{0,2}$	−0.41; 0.13	−0.42; 0.13	−0.026; 0.076	−0.56; 0.37
$\mu_{0,3}$	2.6; 0.77	2.7; 0.79	0.16; 0.45	2.9; 2.3
$\mu_{0,4}$	0.00093; 0.00033	0.00094; 0.00034	$5.1 \cdot 10^{-5}$; 0.00019	0.0012; 0.0010
$\mu_{0,5}$	−0.010; 0.0047	−0.011; 0.0047	−0.00089; 0.0024	−0.012; 0.0076
$\mu_{0,6}$	−0.0043; 0.0019	−0.0044; 0.0020	−0.00018; 0.0010	−0.0038; 0.0062
a_ϕ	0.17; 0.080	0.17; 0.082	0.12; 0.079	0.14;0.093
a_λ	0.29; 0.084	0.28; 0.089	0.13; 0.081	0.19; 0.11
c	−2.7; 0.078	−2.7; 0.077	−0.15; 0.011	−3.0; 0.094
d	2.2; 0.078	2.2; 0.076	0.12; 0.012	2.1; 0.095
f	−0.0037; 0.078	−0.0078; 0.073	−0.0023; 0.011	−0.13; 0.093
g	0.48; 0.078	0.48; 0.073	0.035; 0.010	0.80; 0.093
b_0	0.30; 0.016	0.30; 0.016	0.018; 0.0048	0.20; 0.018
b_N	0.056; 0.020	0.051; 0.021	0.010; 0.0055	0.84; 0.040
b_E	0.24; 0.018	0.24; 0.017	0.012; 0.0048	0.20; 0.019
b_S	−0.14; 0.027	−0.15; 0.030	−0.0011; 0.0052	−0.041; 0.010
b_W	0.26; 0.019	0.26; 0.017	0.018; 0.0048	0.16; 0.016
σ^2_W	3.2; 0.030	3.2; 0.031	0.0057; 0.00015	2.7; 0.032
σ^2_μ	0.11; 0.022	0.11; 0.022	0.062; 0.011	0.25; 0.063
σ^2_θ	0.25; 0.018	0.26; 0.017	0.0057: 0.00015	0.055; 0.0073
σ^2_m	0.77; 0.25	1.5; 0.090	0.017; 0.0013	1.2; 0.47
σ^2_T	0.72; 0.24	–	0.017; 0.0013	1.0; 0.46

the parameter estimates for the log-transformed data are not directly comparable to the estimates pertaining to the original model.

6.3.1 Results From the Main Model

First, the results for the various components for the main model, including a linear long-term trend component will be presented. Overall, this model seems to perform well and the results appear stable; running a few control simulations provides very similar results.

The parameters $\mu_{0,\cdot}$ together with a_ϕ and a_λ determine the contribution from the time-independent spatial field $\mu(x)$. Over the area, the mean of this contribution varies between 17.0 and 19.2 m/s and this component thus explains some of the spatial variation in the wind speed data. The mean estimated posterior field $\mu(x)$ is illustrated in Fig. 6.4 and it is observed that there is variability in both north–south and in east–west directions, with generally higher wind speeds to the east and the north of the area.

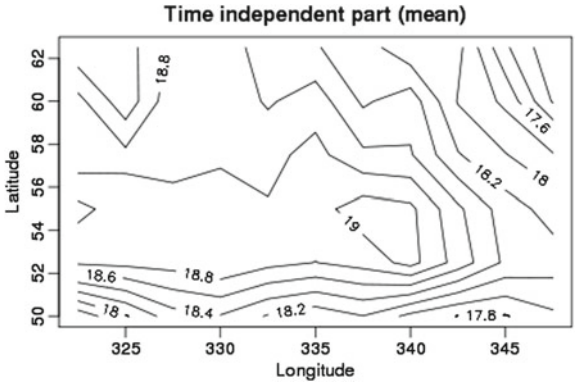

Fig. 6.4 The spatial field $\mu(x)$

The space-time dynamic component $\theta(x, t)$ is described by the $b.$ parameters, and the mean of this component is found to vary between -1.63 and 1.88 m/s over all times (except $t = 0$) and locations. Hence, a notable part of the variability of wind speeds is captured by this component. The mean contribution of this component, averaged over all times, are zero, meaning that this component is stationary over long time scales as it should, not contributing to the long-term trend part of the model.

The estimated seasonal contribution according to the model is illustrated in Fig. 6.5, and it is seen that this captures the seasonal characteristics of the raw data quite well. It is noted that the figure only shows the seasonal contribution for the first 10 years, but the contribution is valid for the complete time span of the data, and all data have been used in estimating the seasonal contribution. The seasonal component was modeled as a combination of an annual and a semiannual part and is described by the parameters c, d, f and g. The estimated parameters correspond to a first harmonic with mean amplitude $A_1 = \sqrt{c^2 + d^2} \approx 3.5\, m/s$ and a second

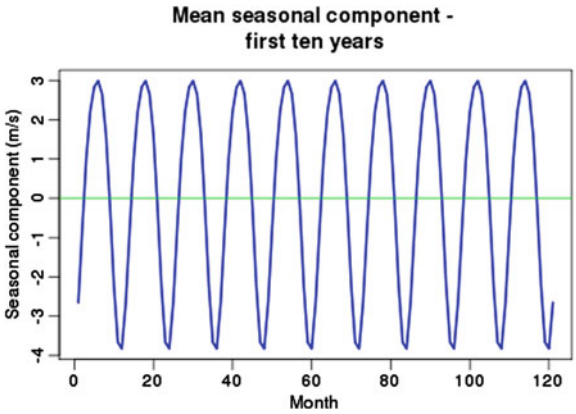

Fig. 6.5 The posterior mean seasonal contribution

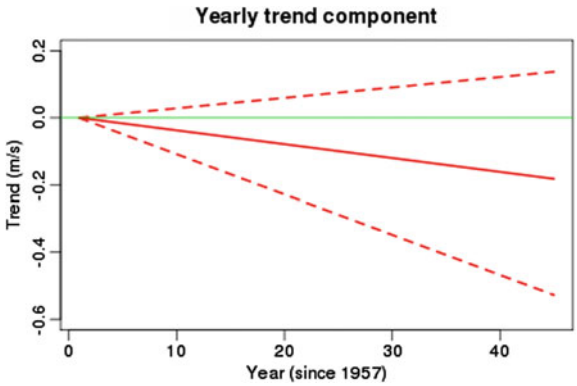

Fig. 6.6 The posterior mean long-term trend component with 90 % credible interval of γt; *green line* corresponds to no trend

harmonic with mean amplitude $A_2 = \sqrt{f^2 + g^2} \approx 0.48\ m/s$ corresponding to a seasonal contribution varying between 3.0 m/s in February and about −3.9 m/s in August. It is observed that the annual contribution is dominating, but the contribution from the semiannual component is not negligible. The mean sampled seasonal contribution $M(t)$ has an overall minimum of −4.66 and a maximum of 4.75 m/s.

The long-term trend contribution is perhaps the one of most interest, and a linear trend was assumed in the main model. The linear trend in the model is determined by the parameter γ and the mean posterior γ is estimated to −0.000345 m/s per month. This corresponds to an overall decrease of about 0.19 m/s over the whole period which is slightly less than the straight line fitted to the raw data in Fig. 6.1. The estimated mean long-term trend together with a 90 % credible interval of the mean are illustrated in Fig. 6.6. The estimated trend corresponds to a mean decrease of about 19 cm/s with a 90 % credible interval ranging from negative to positive trends in the monthly maximum wind speed over the whole period. Hence, even though the data indicate that there might be a slight decreasing trend in the wind data no statistically significant trend in the wind speed is estimated by the model.

6.3.2 Results From the Model with No Trend

The model was also tried without any long-term trends (i.e. by letting $T(t) = 0$), and apart from the absence of any trends, the results were very similar to the results from the main model. The values of the estimated spatial field are comparable, although perhaps slightly lower, without any trend, with values ranging from 17.0 to 19.0 m/s, which seems reasonable. The contributions from the short-term dynamic (mean ≈ 0.00 m/s and ranging from −1.67 to 1.92 m/s) and seasonal (ranging from −3.9 to 3.0 m/s)) components are very similar, as can also be seen from comparing the estimates in Table 6.1. The estimated mean spatial field and seasonal contribution are illustrated in Fig. 6.7. The fact that the models with a linear trend and without any

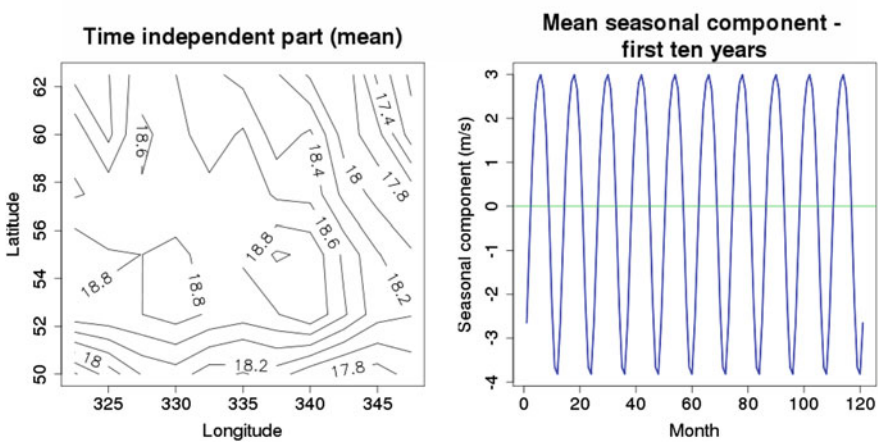

Fig. 6.7 Results from the model without trend; the mean spatial field and seasonal contribution

trend are similar is not surprising, especially since the model with a trend component failed to identify a statistically significant trend. Hence, for all practical purposes the models can be regarded as identical.

6.3.3 Results From the Log-Transformed Model

When the model was run with a logarithmic transformation of the data, the results are not directly comparable but similar main features are identified. The estimated mean spatial field now varies between 16.9 and 19.1 m/s, with the contributions from the short-term dynamic, seasonal and long-term trend parts now being multiplicative factors. The estimated spatial field and the seasonal contribution are illustrated in Fig. 6.8. The estimated seasonal contribution varies between factors of 0.80 for calm seasons and 1.2 for windy seasons. The mean factor reflecting the contribution from the short-term dynamic component, $E\left[e^{\theta(x,t)}\right]$ varies between 0.79 and 1.2 for all locations and times except $t = 0$. It is noted that the figures display the results on the re-transformed original scale, and bias corrections have been applied when necessary, see e.g. [2, 5, 8, 14] for more details.

The estimated long-term trend factor is illustrated in Fig. 6.9. The mean long-term trend is found to be decreasing but the 90 % credible interval ranges from decreasing to increasing trends. The mean estimated trend for the whole period corresponds to a factor of 0.98. The 90 % credible interval for the expected trend factor ranges from 0.94 to 1.02, hence the decreasing trend is not significant at the 90 % level. For a typical monthly maximum wind speed of about 18 m/s the estimated mean trend corresponds to a decrease of about 36 cm/s over the whole period, but for more extreme wind speeds, say 30 m/s, the trend factor corresponds to a decrease

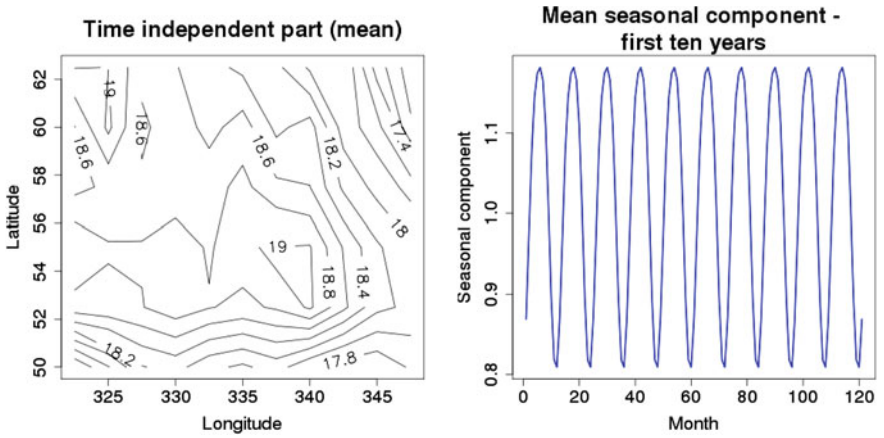

Fig. 6.8 Results from the model with log-transform of the data: spatial field and seasonal factor

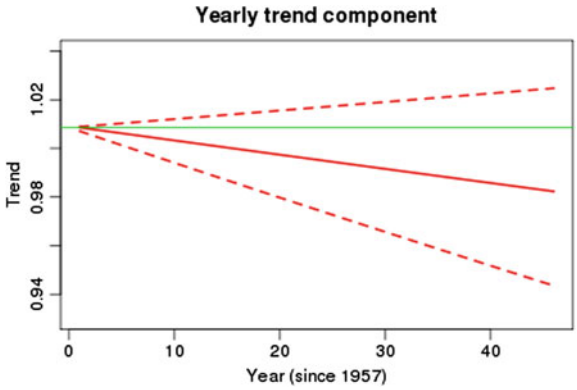

Fig. 6.9 The estimated trend factor for the log-transformed data, with 90 % credible interval

of 60 cm/s. Hence, the model on the log-transformed data yields larger trends for extremes compared to averages.

Comparing the results from the model for log-transformed data to the results pertaining to the original data, it is observed that a slightly more decreasing mean trend is estimated, but both models fail to identify any significant trends. Hence, the results generally agree. It is questionable whether the log-transform represents an improvement, and the results indicate that the original model might perform better. For example, short-term prediction losses are smaller for the original model.

6.3.4 Results Pertaining to Another Ocean Area

It seems obvious that the identified increase in significant wave height cannot be explained by the absence of any increase or even a slight *decrease* (although not

statistically significant) in wind speed over the area. Hence, the increasing significant wave height might be a result of increased swell from increased windiness in other areas. In order to investigate this, another area to the north of the initially investigated area will be analyzed. The spatial resolution and temporal span is the same as for the initial area. The coordinates of this other area are from 67.5° to 77.5° north and from 345° to 357.5° west, corresponding to a grid with $5 \times 6 = 30$ grid points north of Iceland. The lowest and highest values for monthly maximum wind speed in this area are 6.8 and 30.5 m/s, respectively, somewhat less than for the area initially studied.

The results for the new area look reasonable for the spatial field, the short-term spatiotemporal part and the seasonal component. The mean spatial field varies between 13.9 and 16.6 m/s over the area with a mean contribution of 15.7 m/s; the short-term dynamic part $\theta(x, t)$ varies between −3.69 and 3.53 m/s with a mean of about zero m/s over the area and entire period; the seasonal contribution varies between −4.47 and 2.93 m/s. The results for the spatial field and the seasonal contribution are illustrated in Fig. 6.10. It is interesting to observe that the model picks up a significantly positive long-term trend when applied to this area north of Iceland. The estimated trend is illustrated in Fig. 6.11, and the mean estimated trend corresponds to an increase in monthly maximum wind speed of about 0.75 m/s over the period. The 90 % credible interval of the expected trend ranges from 0.37 to 1.1 m/s and is hence entirely positive. Hence, even though there seems to have been an insignificant decrease in wind speeds in the area first investigated, this area further north seems to have experienced an overall increase in wind speeds. It is noted, however, that even though the increase was found to be statistically significant, an increase of 0.75 m/s is not necessarily practically significant with respect to wave generation and the effects on the significant wave height.

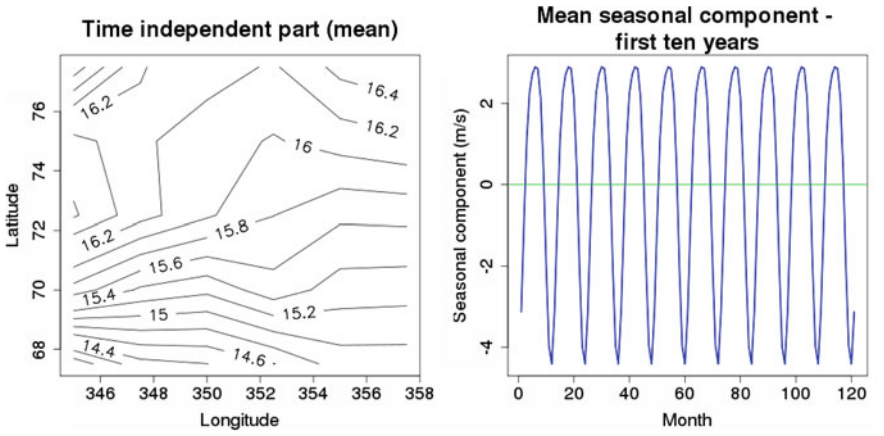

Fig. 6.10 Results from the model applied to an alternative area: spatial field and seasonal factor

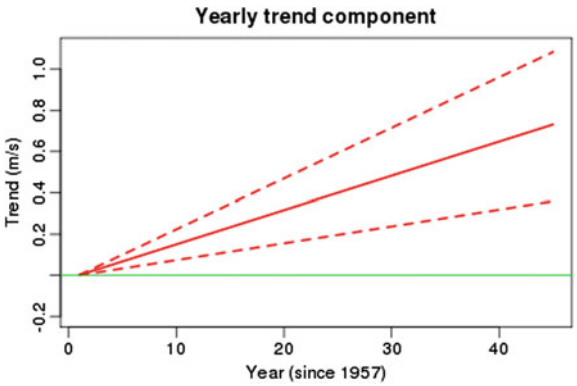

Fig. 6.11 The estimated mean trend for the area north of Island with 90 % credible intervals

6.4 Discussion

The Bayesian hierarchical space-time model applied to monthly maximum wind speeds over an area in the mid-latitude North Atlantic has identified a possible slightly negative trend for the initial area in the North Atlantic, albeit not statistically significant. When significant wave height data were modeled with a similar model for the same area, an increase in monthly maximum significant wave height was discovered, and the results from the analysis of the wind data indicate that this increase is not due to increased wind sea. If the increases in significant wave height are to be explained by increased wind sea, it would necessarily need to be accompanied by an increase in local wind speeds.

The increase in significant wave height could then be explained by increased swell, i.e., remains of wind sea generated by wind forces outside the area and propagated into the area that has been analyzed. This assumption is substantiated by the results obtained when the wind speed model was applied to an area further north. For this area, a significant increase of monthly maximum wind speeds was detected which would possibly lead to increased wind sea in this alternative area. This increased wind sea could then possibly propagate as increased swell to the initial area and explain, at least partly, the observed increase in significant wave height here. It should be noted, however, that only wind speeds have been analyzed and the direction of swell propagation would obviously be highly dependent on wind direction.

The absence of a long-term trend (or possibly a slight decreasing trend) in windiness in one area together with an increase in windiness in an area further north indicate that there might have been a change in the main storm tracks, with storm tracks generally moving more to the north. This would be in agreement with other studies that have described such an effect, i.e., that the storm tracks have experienced a poleward shift as a result of climate change, see e.g., [3, 6, 18]. Such a poleward shift of storm tracks is associated with a poleward shift in surface winds, which would be in agreement with the results presented herein. [1] presents a review of recent studies and states that an observed poleward shift of mid-latitude storms

is the most agreed on result. Hence, it is reassuring that the Bayesian hierarchical space-time model arrives at similar results and is able to pick up this signal in the data.

It is noted that this model only analyses the trend in the monthly maximum wind speed, and this alone might not be a sufficient measure of the wave generating forces. If, for example, the duration of extreme wind speeds increases this would lead to larger waves even without an increase in the wind speed itself. Such effects would not be picked up by the model when applied to monthly maximum wind speeds. Another effect could be the frequencies of strong winds. If there are not sufficiently long calm periods between storms for the sea to quiet down, waves could aggregate to larger heights even without higher wind velocities. Possibly, increasing frequencies and prolonged duration of storms would not necessarily be reflected in the monthly maximum wind speed data and further analyses would be needed to look into this. This is left for further study. Furthermore, the wind direction is important for wave generation, and wind directions have not been analyzed in the present study. A possible extension of the model could be to include wind direction as well as magnitude. It is also assumed that possible effects of changes in fetch due to Arctic ice reduction are negligible.

It has already been emphasized that even though the governing physics is not explicitly included in the model presented in this study, it is undeniably incorporated in the model by way of the data. The Bayesian hierarchical model is a purely probabilistic model and as such it is different from many meteorological and geophysical models based on deterministic relationships such as the Navier-Stokes equations for describing the climate and the atmospheric circulation and for projecting climate change. Physical models remain the primary approach for investigating the impacts of climate change and ensemble studies are carried out in order to quantify uncertainties, where different climate models and small perturbations of the initial conditions give different results. However, it has been acknowledged that there are notable statistical challenges related to climate change projections based on such ensemble studies, see e.g., [4, 7, 10]. The models presented in this paper offer an alternative approach to modeling the impacts of climate change on the wind climate with a more direct approach to modeling of uncertainties, and it should rather be regarded as a complement to the efforts made developing physical models than a competitor.

6.5 Summary and Conclusions

This chapter has presented a Bayesian hierarchical spatiotemporal model for 10-m wind speeds. Overall, the model seems to perform well in capturing the dominating spatial and temporal dependence structures in the wind speed data. Hence, this chapter suggests this modeling framework as an alternative to physical models for analyzing environmental processes such as wind speed in space and time.

A similar model has previously been applied to extreme wave climate over the same area and identified i.a. increasing trends in the monthly maximum significant

wave height. Previous studies have also demonstrated that such increasing trends may have an impact on ship structural loads (see Chap. 7) and that it hence represents an additional hazard to ship operations. The results from the wind speed models do not suggest any corresponding increases in the monthly maximum wind speeds. On the contrary, a slight decreasing trend was estimated although this was not statistically significant. Hence, the results indicate that the roughening of the wave climate could not be explained by increases in locally generated wind sea. Possibly, the increased significant wave height can be explained by increased swell in the area. The monthly maximum wind speed was also analyzed for another ocean area further north and in this area a significant positive trend in the 10-m wind speed was identified. These results agree with various previous studies that suggest that the North Atlantic storm tracks shift polewards due to a warming climate and could also explain, at least partly, an increase in swell in the original area. Thus, the results presented in this paper suggest that the observed increased significant wave height might be mostly due to increased swell.

References

1. Bader, J., Mesquita, M.D.S., Hodges, K.I., Keenlyside, N., Østerhus, S., Miles, M.: A review on Northern Hemisphere sea-ice, storminess and the North Atlantic oscillation: observations and projected changes. Atmos. Res. **101**, 809–834 (2011)
2. Beauchamp, J.J., Olson, J.S.: Corrections for bias in regression estimates after logarithmic transformation. Ecology **54**, 1403–1407 (1973)
3. Bender, F.A.M., Ramanathan, V., Tselioudis, G.: Changes in extratropical storm track cloudiness 1983–2008: observational support for a poleward shift. Clim. Dyn. **38**, 2037–2053 (2012)
4. Collins, M., Chandler, R.E., Cox, P.M., Huthnance, J.M., Rougier, J.: Quantifying future climate change. Nat. Clim. Change **2**, 403–409 (2012)
5. Ferguson, R.: River loads underestimated by rating curves. Water Resour. Res. **22**, 74–76 (1986)
6. Gastineau, G., Soden, B.J.: Model projected changes of extreme wind events in response to global warming. Geophys. Res. Lett. **36**(L10810), 1–5 (2009)
7. Stephenson, D.B., Collins, M., Rougier, J.C., Chandler, R.E.: Statistical problems in the probabilistic prediction of climate change. Environmetrics **23**, 364–372 (2012)
8. Stow, C.A., Reckhow, K.H., Qian, S.S.: A Bayesian approach to retransformation bias in transformed regression. Ecology **87**, 1472–1477 (2006)
9. Talley, L.D., Pickard, G.L., Emery, W.J., Swift, J.H.: Descriptive Physical Oceanography an introduction, 6th edn. Elsevier, Boston (2011)
10. Tebaldi, C., Knutti, R.: The use of the multi-model ensemble in probabilistic climate projections. Philos. Trans. R. Soc. A **365**, 2053–2075 (2007)
11. Uppala, S.M., Kållberg, P.W., Simmons, A.J., Andrae, U., Da Costa Bechtold, V., Fiorino, M., Gibson, J.K., Haseler, J., Hernandez, A., Kelly, G.A., Li, X., Onogi, K., Saarinen, S., Sokka, N., Allan, R.P., Andersson, E., Arpe, K., Balmaseda, M.A., Beljaars, A.C.M., Van de Berg, L., Bidlot, J., Bormann, N., Caires, S., Chevallier, F., Dethof, A., Dragosavac, M., Fisher, M., Fuentes, M., Hagemann, S., Hólm, E., Hoskins, B.J., Isaksen, L., Janssen, P.A.E.M., Jenne, R., McNally, A.P., Mahfouf, J.F., Morcrette, J.J., Rayner, M.A., Saunders, R.W., Simon, P., Sterl, A., Trenberth, K.E., Untch, A., Vasiljevic, D., Vitebro, P., Woolen, J.: The ERA-40 re-analysis. Q. J. R. Meteorol. Soc. **131**, 2961–3012 (2005)
12. Vanem, E., Breivik, O.N.: Bayesian hierarchical modelling of North Atlantic windiness. Nat. Hazard Earth Syst. Sci. **13**, 545–557 (2013)

13. Vanem, E., Huseby, A.B., Natvig, B.: A Bayesian hierarchical spatio-temporal model for significant wave height in the North Atlantic. Stoch. Env. Res. Risk Assess. **26**, 609–632 (2012)
14. Vanem, E., Huseby, A.B., Natvig, B.: Modeling ocean wave climate with a Bayesian hierarchical space-time model and a log-transform of the data. Ocean Dyn. **62**, 355–375 (2012)
15. Vanem, E., Huseby, A.B., Natvig, B.: A stochastic model in space and time for monthly maximum significant wave height. In: Abrahamsen, P., Haugen, R., Kolbjørnsen, O. (eds.) Geostatistics Oslo 2012, pp. 505–517. Springer, Heidelberg (2012)
16. Vanem, E., Huseby, A.B., Natvig, B.: Bayesian hierarchical spatio-temporal modelling of trends and future projections in the ocean wave climate with a CO_2 regression component. Environ. Ecol. Stat. (in press) (2013)
17. Wallcraft, A.J., Kara, A.B., Barron, C.N., Metzger, E.J., Pauley, R.L., Bourassa, M.A.: Comparison of monthly mean 10 m wind speeds from satellites and NWP products over the global ocean. J. Geophys. Res. **114**(D16109), 1–14 (2009)
18. Yin, J.H.: A consistent poleward shift of the storm tracks in simulations of 21st century climate. Geophys. Res. Lett. **32**(L18701), 1–4 (2005)

Chapter 7
Application: Impacts on Ship Structural Loads

In this chapter, it is explored how the estimated long-term trends can be related to the structural loads and response calculations of ships and how load calculations can be updated to take future projections of the ocean wave climate into account. The potential impact of the estimated long-term trends of significant wave height on the wave-induced structural loads of an oil tanker will be discussed and illustrated by an example. For the purpose of this illustration, the estimated linear long-term trends extrapolated from the monthly maximum data and the trends obtained with regression on the B1 scenario will be used, but any estimated trend could be incorporated in the load calculations in a similar way. In short, a joint model for significant wave height and wave period is used, and this is modified to take into account the possible effects of climate change. This leads to a modification of environmental contours specifying the extreme environmental conditions, which again is used to modify the load calculations. An example for a particular oil tanker is presented for illustration. Some parts of this chapter are previously presented in [30, 33].

7.1 Introduction and Background

Extreme environmental conditions impose extreme loads and stresses on marine structures and correspond to failure modes related to, e.g., extreme sagging and hogging conditions. In order to ensure the reliability of marine structures, it is important to make load and response calculations corresponding to the operating conditions that may be encountered throughout its lifetime. In particular, the extreme responses corresponding to the most critical environmental conditions the structure is expected to withstand should be assessed.

Typically, several met-ocean parameters influence the response of a structure and when carrying out load and response calculations of marine structures, a joint environmental model can be utilized. It has been shown that the environmental forces on marine structures may be significantly reduced by accounting for the lack of

E. Vanem, *Bayesian Hierarchical Space-Time Models with Application to Significant Wave Height*, Ocean Engineering & Oceanography 2,
DOI: 10.1007/978-3-642-30253-4_7, © Springer-Verlag Berlin Heidelberg 2013

full correlation of met-ocean parameters, i.e., the extremes of different met-ocean parameters do not normally occur simultaneously. Early joint models were limited to various pairs of environmental parameters such as significant wave height and spectral peak period or significant wave height and current speed, see e.g., [15, 21], but later models extended this approach to include wind, waves, current, and sea water level [5, 6]. Currently, different approaches for joint environmental modeling can be found in the literature, e.g., the Maximum Likelihood Model (MLM) [26], the Conditional Modeling Approach (CMA) [5, 6] and the Nataf model [12, 24]. The modeling of bivariate probability distributions of significant wave height and mean wave period is also discussed in [14], and [27] contains an overview of different methods for bivariate modeling of wave height and period, including the CMA. Multivariate modeling of met-ocean parameters by means of kernel density models are discussed in [1].

Generally, for all approaches both global and event models can be applied. The global approach utilizes all data from a long series of regular observations while the event approach is based on the observations over some threshold level. The global approach includes correlation among observations which in the event approach may be negligible. In this study, the CMA proposed in [5, 6] is adopted. Extensions of this model are discussed in for example [3, 4].

In this chapter, the estimated long-term trends and future projections of the ocean wave climate, as outlined in previous chapters, will be included in load calculations for ships. Hence, the potential impact of changes in future sea states on ship structural loads will be considered, using the CMA and taking due note of inherent uncertainties. As for the long-term trends assumed in this exercise, these refer to the trends in the monthly maxima data, as outlined in previous chapters. However, first a brief introduction of central concepts in probabilistic structural design will be presented.

7.2 Probabilistic Structural Design

In probabilistic structural design, one often defines a performance function $g(\mathbf{X})$ which is dependent on a number of stochastic input variables $\mathbf{X} = (X_1, X_2, \ldots, X_n)^T$. Typically, such a function can be expressed as $g =$ capacity (strength) $-$ demand (stress) so that it identifies the safe and unsafe regions for when the structure fails or not: If $g(\mathbf{X}) > 0$ then the strength is greater than the stress and the structure survives whereas $g(\mathbf{X}) < 0$ means that the stress is greater than the strength and the structure will fail. Hence, the region defined by $g(\mathbf{X}) < 0$ is the failure region of the $\mathbf{X}$-space. $g(\mathbf{X}) = 0$ defines the so-called limit state function and is the boundary between the safe and unsafe regions. Within this framework, the reliability R of a structure is defined as the probability of a performance function $g(\mathbf{X})$ being greater than zero, i.e., (with P_f denoting the probability of failure)

$$R = 1 - P_f = P\left[g(\mathbf{X}) > 0\right] \tag{7.1}$$

Since, g is a function of $\mathbf{X}$ this is equivalent to the probabilities of the random variables $\mathbf{X}$ being in the safe or unsafe regions of the $\mathbf{X}$-space, respectively. Hence, given a joint probability density function (pdf) $f_x(\mathbf{x})$ of the random variables $\mathbf{X}$, the reliability and probability of failure can be evaluated by the integrals

$$R = 1 - P_f = P\left[g(\mathbf{X}) > 0\right] = \int\limits_{g(\mathbf{X})>0} f_x(\mathbf{x})\mathrm{d}\mathbf{x} \tag{7.2}$$

These integrals are normally difficult to solve exactly, and both the joint pdf $f_x(\mathbf{x})$ and the performance function $g(\mathbf{X})$ may be complicated functions. Two commonly used methods to approximate these integrals are the First Order Reliability Method (FORM) and the Second Order Reliability Method (SORM). These methods are closely related to the concept of environmental contours, and the FORM approach will be briefly described in the following. Reference is also give to [16] for a brief description.

7.2.1 First Order Reliability Method (FORM)

The main idea of the FORM is to approximate the failure boundary at the design point (i.e., the point on the failure boundary closest to the origin) by a first order Taylor expansion. In order to alleviate the estimation of the integral, the random input variables $\mathbf{X}$ are often transformed from their original space into the standard normal space, where the transformed random variables $\mathbf{U} = (U_1, U_2, \ldots, U_n)^T$ are independent and standard normally distributed.

The transformation from $\mathbf{X}$ to $\mathbf{U}$ is performed according to the Rosenblatt transformation [28] in Eq. 7.3, where $\Phi(\cdot)$ is the cumulative distribution function of the standard normal distribution, and $F_{\cdot}$ is the cumulative distribution function of the original random variables, respectively.

$$\begin{aligned} U_1 &= \Phi^{-1}\left(F_{X_1}(X_1)\right) \\ U_2 &= \Phi^{-1}\left(F_{X_2|X_1}(X_2)\right) \\ &\vdots \\ U_n &= \Phi^{-1}\left(F_{X_n|X_1,\ldots,X_{n-1}}(X_n)\right) \end{aligned} \tag{7.3}$$

Failure regions in the original space correspond to failure regions in the transformed normal space, defined by the transformed performance function $\tilde{g}(\mathbf{U})$. Hence, the probability integral in 7.2 becomes

$$P_f = P\left[\tilde{g}(\mathbf{U}) < 0\right] = \int\limits_{\tilde{g}(\mathbf{U})<0} \phi_{\mathbf{u}}(\mathbf{u})\mathrm{d}\mathbf{u} \tag{7.4}$$

where $\phi_{\mathbf{u}}(\cdot)$ denotes the standard multivariate normal density function.

Now, in order to calculate this integral in the transformed space, first the point of the minimum distance between the transformed failure boundary, $\tilde{g}(\mathbf{U}) = 0$, and the origin in **U**-space are identified. This point is identified as the *design point* and the distance from this design point to origin is denoted the *reliability index* β_r. Second, the transformed true failure boundary in this point is approximated by a tangent hyperplane; for two-dimensional **U** this hyperplane becomes a tangent line of a circle with radius β_r around origin in **U**-space. This corresponds to a first-order Taylor expansion at the design point (for differentiable $\tilde{g}(\mathbf{U})$). The probability integrals are now reduced to integrating the probability mass on either side of this hyperplane in **U**-space, and due to symmetry in the transformed space, this is simply

$$R = 1 - P_f \approx \Phi(\beta_r) \tag{7.5}$$

Hence, identifying the design point in **U**-space and thereby estimating the reliability index β_r, the reliability and consequently the probability of failure can easily be approximated, using the FORM approach. This method in two dimensions is illustrated in Fig. 7.1. It can easily be seen that due to rotational symmetry, the tangent can be moved along the circle without loss of probability, and hence the two-dimensional problem

$$P_f = \underset{\text{Failure region}}{\iint} \phi_{u_1,u_2}(u_1, u_2)\mathrm{d}u_1\mathrm{d}u_2 \tag{7.6}$$

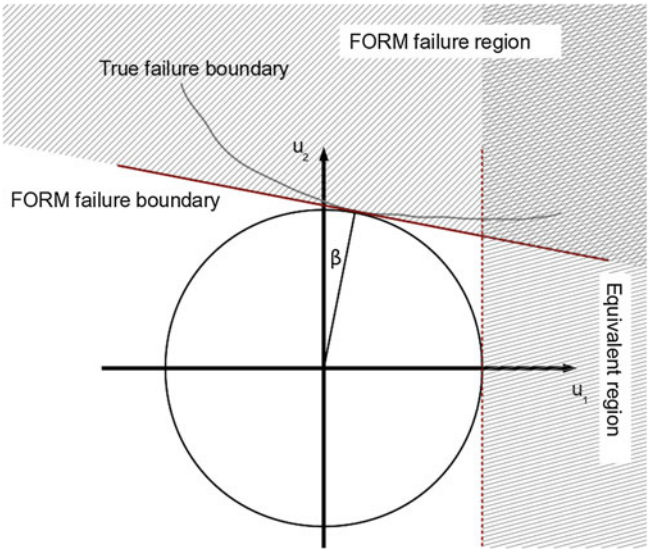

Fig. 7.1 Illustration of the FORM approximation in **U**-space

of finding the probability of being in the FORM failure region in Fig. 7.1 reduces to the one-dimensional problem of finding the probability of **U** being in the equivalent failure region as solved by Eq. 7.5. It is emphasized that the reliability corresponds to the probability of being in the safe region and this is different from the probability of being within the circle with radius β_r. In fact, the reliability will always be greater than the probability of being within the circle defined by β_r.

Note that the approximation in Eq. 7.5 due to the FORM approximation gives an upper boundary for the true failure probability, P_f, if the true transformed failure region is a convex set; in this case, the true failure probability will be overestimated. On the other hand, if the complement of the true failure region is convex, then the FORM approximation gives a lower boundary for the true failure probability.

The inverted procedure, referred to as the Inverse First Order Reliability Method (IFORM), can be used for estimating exceedance regions corresponding to a given failure probability, e.g., the regions corresponding to annual probability of failure of 10^{-2} or 10^{-4}.

The SORM is simply an extension of FORM, where the failure boundary is approximated with the second-order Taylor expansion in the design point to yield a better approximation of the true failure boundary in the transformed space.

7.2.2 Long-Term Response Analysis

In principle, a long-term response analysis requires the full long-term statistics of the relevant random environmental variables, i.e. a continuous long-term description of the environmental loads. In such a full long-term analysis of structural stress, the only approximation is the FORM linearization of the failure boundary. However, normally the long-term behavior of environmental parameters is modeled as a series of piecewise stationary short-term condition processes [22, 29]. Probabilistic response calculations can then be performed for each short-term condition and weighted by the probability distribution of the different conditions in order to establish the long-term response distribution. A further simplification is also often applied, where instead of performing response analysis for all short-term conditions, short-term response analyses are performed for only selected extreme environmental conditions, where the selection has been based on the relevant probability distributions. The highest response level among these extreme environmental conditions can then be applied in the design. In this way, design contours can be used to describe the extreme joint behavior of environmental and structural response variables [19].

7.3 Potential Impact of Climate Change on Ship Structural Loads and Responses

Having identified a trend in the significant wave height data, it would be of great interest to see how such results could be related to the calculation of future environmental loads and responses on ships and other floating structures. For the purpose

of this study, the linear trend estimated from the monthly maximum data without any transformation will be assumed to continue for the next century, and it will be investigated how to relate such a trend to the calculations of ship structural loads and responses. In addition, the trend obtained from the extended model with regression on the B1 emission scenario will be used. This choice of trends to assume is somewhat arbitrary, but the same approach could easily be used on any of the other projected trends as well. The impact of the assumed trend will be illustrated by an example, where various wave induced loads and responses will be calculated for a particular ship taking into account the projected trend in significant wave height over 100 years. The calculated loads will then be compared to results without any trend. It is emphasized that potential influence of such trends on structural design, as was discussed in [9] is out of scope of this present study. The purpose is to demonstrate a case indicating how large the effect of climate change might be and not to give actual design values.

The trend estimated in Chap. 3 corresponds to an addition, 100 years ahead in time, with mean 1.6 m and standard deviation 0.33 or 0.39 m for model alternatives 2 and 5 respectively [31]. It is observed that the estimated trend contribution is symmetric, and the mean and standard deviation of the climatic trend contribution will be denoted as μ_{ct} and σ_{ct}, respectively. For the purpose of illustrating how this would influence ship load calculations, the results with the highest uncertainty will be used, i.e., an additive trend, $T \sim (\mu_{ct}, \sigma_{ct}^2)$ will be assumed, with

$$\mu_{ct} = 1.6\,\text{m} \qquad \sigma_{ct} = 0.39\,\text{m} \tag{7.7}$$

Other future projections were obtained when including a CO_2-regression term in the model, as described in Chap. 5 [32]. Hence, the effect on ship structural response will also be investigated assuming the B1 emission scenario for the extended model. Toward the year 2100, this trend was estimated to have a mean value of 1.9 m with a standard deviation of 0.65 m. Updated response calculations will also be presented for such a trend, i.e., taking into account a climatic trend contribution corresponding to $T \sim (\mu_{B1}, \sigma_{B1}^2)$ with

$$\mu_{B1} = 1.9\,\text{m} \qquad \sigma_{B1} = 0.65\,\text{m} \tag{7.8}$$

These trends were extracted from the corrected ERA-40 data (C-ERA-40) over an area in the North Atlantic. Due to lack of information about wave period in the C-ERA-40 data, the joint distribution of significant wave height and wave period used for load calculations are based on the $\text{ERA}_{\text{Interim}}$ data set [11][1] for a particular location. However, that location is contained within the area considered by the C-ERA-40 data and is assumed representative for the whole area. Furthermore, main features of the C-ERA-40 and $\text{ERA}_{\text{Interim}}$ data sets are similar, and it is assumed that any bias would be similar in the two data sets. The long-term trends obtained in

[1] Website: http://www.ecmwf.int/research/era/do/get/era-interim

the present study are incorporated in the established joint distribution of significant wave height and wave period based on the $\text{ERA}_{\text{Interim}}$ data.

It is noted that the climate trend is estimated from monthly maxima although it is applied to the whole body of the H_s distribution. Thus, the revised H_s distribution is more representative for high values of H_s. When the impact of the trend is explored, extreme loads are considered and this makes these assumptions less troublesome; this simplification is considered acceptable for extremes but neither for fatigue calculations nor specification of operational criteria when lower sea states are of importance.

7.3.1 Joint Model for Significant Wave Height and Wave Period

Information of the distribution of significant wave height alone is normally not sufficient for load and response calculations of floating structures [20]. As a minimum, the joint distribution of significant wave height and wave period is needed. It has previously been proposed to model the marginal distribution of significant wave height, H_s, according to a 3-parameter Weibull distribution and the conditional distribution of the wave period, T, conditional on the significant wave height, as a log-normal distribution [7, 23]. Hence, the joint distribution of significant wave height and wave period will be the product of a Weibull and a log-normal distribution (Eq. 7.9) according to the CMA (for several met-ocean parameters see [5, 6]). Note that the 3-parameter Weibull distribution was first applied to describe significant wave height by [25].

$$f_{H_s,T}(h,t) = f_{H_s}(h) f_{T|H_s}(t|h) \tag{7.9}$$

Furthermore, it is assumed that including the trend in the significant wave height corresponds to a modified marginal distribution for the significant wave height, but that the distribution of wave period, conditional on the significant wave height, remains unchanged. It is noted that even though the conditional distribution is assumed unchanged, the marginal distribution of the wave period will obviously change, so this assumption does not seem too unreasonable.

The 3-parameter Weibull distribution is parametrized by the parameters γ (location), α (scale) and β (shape), as shown in Eq. 7.10. The expressions for the mean and variance of the 3-parameter Weibull distribution is given in Eqs. 7.11 and 7.12 respectively (see e.g., [10]).

$$f(x) = \frac{\beta}{\alpha}\left(\frac{x-\gamma}{\alpha}\right)^{\beta-1} e^{-\left(\frac{x-\gamma}{\alpha}\right)^{\beta}}, x \geq y \tag{7.10}$$

$$E[x] = \gamma + \alpha\Gamma(1+1/\beta) \tag{7.11}$$

$$Var[x] = \alpha^2\left(\Gamma(1+2/\beta) - \Gamma(1+1/\beta)\right) \tag{7.12}$$

It is assumed that the distribution of the significant wave height after the trend has been added can be approximated by a 3-parameter Weibull distribution with the same shape parameter. That is, the trend can be modeled as a modification of the location and scale parameters of the 3-parameter Weibull distribution. A quick simulation study confirms that this is a reasonable approximation and the modified Weibull distribution turns out to be a remarkable good approximation for the distribution of the sum of the fitted distribution and the accumulated trend distribution. Figure 7.2 shows the fitted Weibull distribution together with the correct distribution of the sum of the fitted distribution and the long-term trend as well as the modified Weibull distribution, assuming the accumulated trend from the basic model. As can be seen from the figure, the modified Weibull distribution is a reasonable approximation, and the effect of adding the trend can be seen. With these assumptions, and requiring that the modified distribution should have the correct expectation and variance, the modified parameters due to the long-term trend become

$$\gamma \to \gamma' = \gamma + \mu_{ct} + \Gamma\left(\frac{1}{\beta}+1\right)\left[\alpha - \sqrt{\alpha^2 + \frac{\sigma_{ct}^2}{\Gamma\left(\frac{2}{\beta}+1\right) - \Gamma\left(\frac{1}{\beta}+1\right)^2}}\right] \tag{7.13}$$

$$\alpha \to \alpha' = \sqrt{\alpha^2 + \frac{\sigma_{ct}^2}{\Gamma\left(\frac{2}{\beta}+1\right) - \Gamma\left(\frac{1}{\beta}+1\right)^2}} \tag{7.14}$$

The 3-parameter Weibull distribution was fitted to significant wave height data for one location from the ERA-40_{Interim} data and the estimated parameters together with the modified parameters as a result of adding the accumulated projected long-term trend (over 100 years) are given in Table 7.1. The corresponding mean and standard deviation of the distributions are also given.

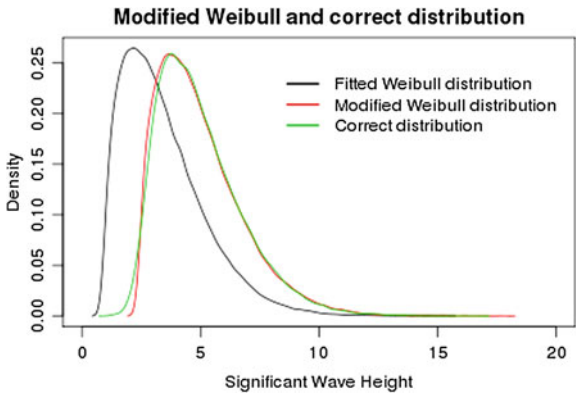

Fig. 7.2 Fitted and modified Weibull density distributions for significant wave height

Table 7.1 Fitted and modified parameters for the 3-parameter Weibull distribution for significant wave height

	α	β	γ	E[h]	sd[h]
Fitted distribution	2.776	1.471	0.8888	3.401	1.737
Modified distribution (Basic model trend)	2.846	1.471	2.393	4.969	1.781
Modified distribution (Regression model / scenario B1)	2.965	1.471	2.613	5.296	1.855

It is observed that the mean of the modified distribution is changed quite drastically, whereas there is only a slight increase in the standard deviation as a result of adding the climatic trend with uncertainties.

The conditional distribution of wave period is modeled as a log-normal distribution, with density function given by Eq. 7.15 and where the parameters are modeled as functions of significant wave height, as shown in Eqs. 7.16–7.17. By assumption, this conditional distribution is not expected to change due to climatic trends, and the parameters a_i and b_i for $i = 1, 2, 3$ are estimated from the data, as shown in Table 7.2. The resulting joint densities of the original and the modified distributions for significant wave height, H_s, and zero-up-crossing period, T_z are illustrated in the contour plots in Fig. 7.3 (on the same scale). Since the conditional distribution of wave period is assumed to remain unaffected by the climatic trend, the estimated parameters will not be modified due to the climatic trend.

$$f_{T|H_s}(t|h) = \frac{1}{t\sigma_t(h)\sqrt{2\pi}} e^{-\frac{(\ln t - \mu_t(h))^2}{2\sigma_t(h)^2}} \tag{7.15}$$

$$\mu_t(h) = E[\ln T_z | H_s = h] = a_1 + a_2 h^{a_3} \tag{7.16}$$

$$\sigma_t(h) = sd[\ln T_z | H_s = h] = b_1 + b_2 e^{b_3 h} \tag{7.17}$$

7.3.2 Environmental Contours

When specifying design criteria as well as carrying out load and response assessment for marine structures, a full long-term load and response analysis can be applied, or alternatively, the environmental contour concept outlined in [16, 34] can be used in conjunction with the Inverse First Order Reliability Method (IFORM). One advantage of establishing environmental contours independent of any structural performance function is that these can then be established without reference to any specific design.

Table 7.2 Fitted parameters pertaining to the conditional log-normal distribution for wave period

	i = 1	i = 2	i = 3
a_i	0.1000	1.489	0.1901
b_i	0.0400	0.1748	−0.2243

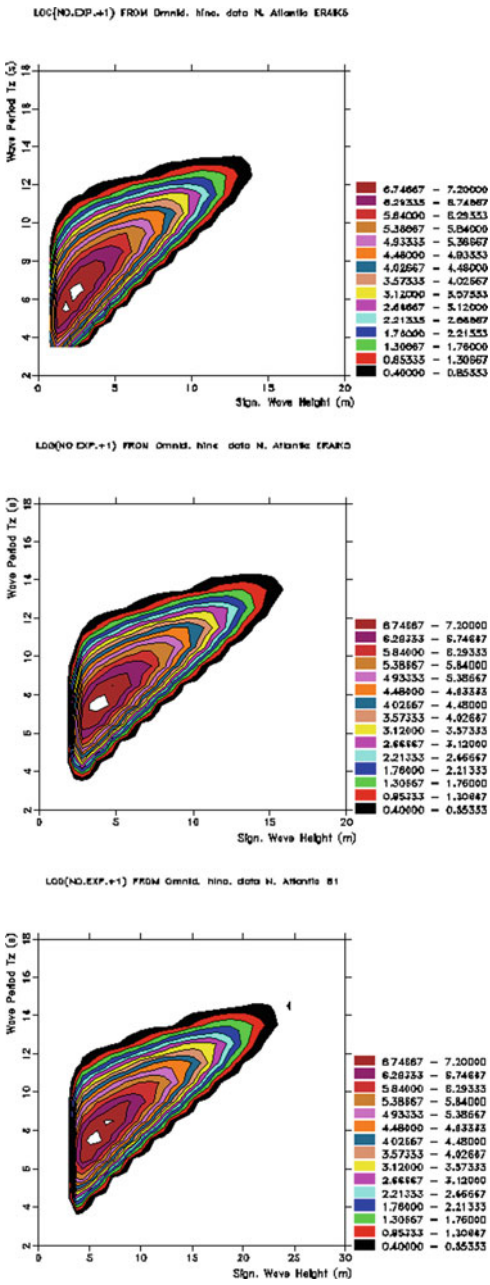

Fig. 7.3 Contour plots of the joint distribution of significant wave height and zero-up-crossing period; Fitted distributions without trend (*top*) and modified distributions with the effect of a climatic trend over 100 years estimated from the basic model (*middle*) and the regression model with the B1 scenario (*bottom*)

The contour lines correspond to a set of design sea states; they apply to all designs and may be used to explore different design alternatives within the resulting design space. Hence, time-consuming response analyses are only required for a limited

set of design sea states for each design proposal, as also pointed out in [2, 22]. An alternative approach combining IFORM with Monte Carlo importance sampling was recently proposed in [29].

The use of environmental contours in conjunction with IFORM is a valid, simplified, and rational method of estimating extreme conditions and is recommended by DNV [13]. The idea is to define contours in the environmental parameter space (usually H_s, T_z) within which extreme responses with a given return period should lie. It requires determination of the joint environmental model of sea state variables of interest. It should be noticed that the contours are found by relating sea state variables to the standard normal variables, an assumption that may affect their accuracy (the transformation by itself is an exact transformation that conserves probability, but tangent lines in the transformed space do not necessarily correspond to straight lines in the original space for such nonlinear transformations). Furthermore, adding the trend introduces a dependency between the sea states at subsequent times, but the effect this might have on the return values have been ignored in this study. Presumably, since the variability of the estimated trend is small in comparison to the variability of sea states, this effect is not very great, and it can be shown, using Jensen's inequality [18], that the resulting design criteria will be conservative.

In short, the environmental contour for an extreme event with return period r, i.e., an event with a probability of p_r of occurrence and corresponding reliability index β_r defined as in Eq. 7.18, is established by varying the standard normal variables U_1 and U_2 along the circle defined by Eq. 7.19. $\Phi(\cdot)$ is the standard normal distribution function.

$$\beta_r = \Phi^{-1}(1 - p_r) \tag{7.18}$$

$$\sqrt{u_1^2 + u_2^2} = \beta_r \tag{7.19}$$

The environmental contours are then found by relating significant wave height (H_s) and the mean wave period (T_z) to the standard normal variables U_1 and U_2 according to the Rosenblatt transformation scheme [28] given in Eq. 7.20, where the F.s refer to the distribution functions of the estimated Weibull and log-normal distributions for significant wave height and mean wave period conditioned on significant wave height. The estimation of design contours for ocean engineering applications is also discussed in for example [19].

$$h_s = F_{H_s}^{-1}(\Phi(u_1)) \qquad t_z = F_{T_z|H_s}^{-1}(\Phi(u_2)) \tag{7.20}$$

Figure 7.4 shows the environmental contour lines of H_s and T_z for the North Atlantic location considered in the present study. The 1, 10, and 25-year return period levels calculated by IFORM are shown in the figures for the fit to the original $\text{ERA}_{\text{Interim}}$ data and for the corrected fits where the two different long-term trends are included. The 3-parameter Weibull distribution for H_s given in Table 7.1 and the conditional log-normal distribution for the T_z have been used in the analysis. As expected, the modification of the distribution for significant wave height moves the

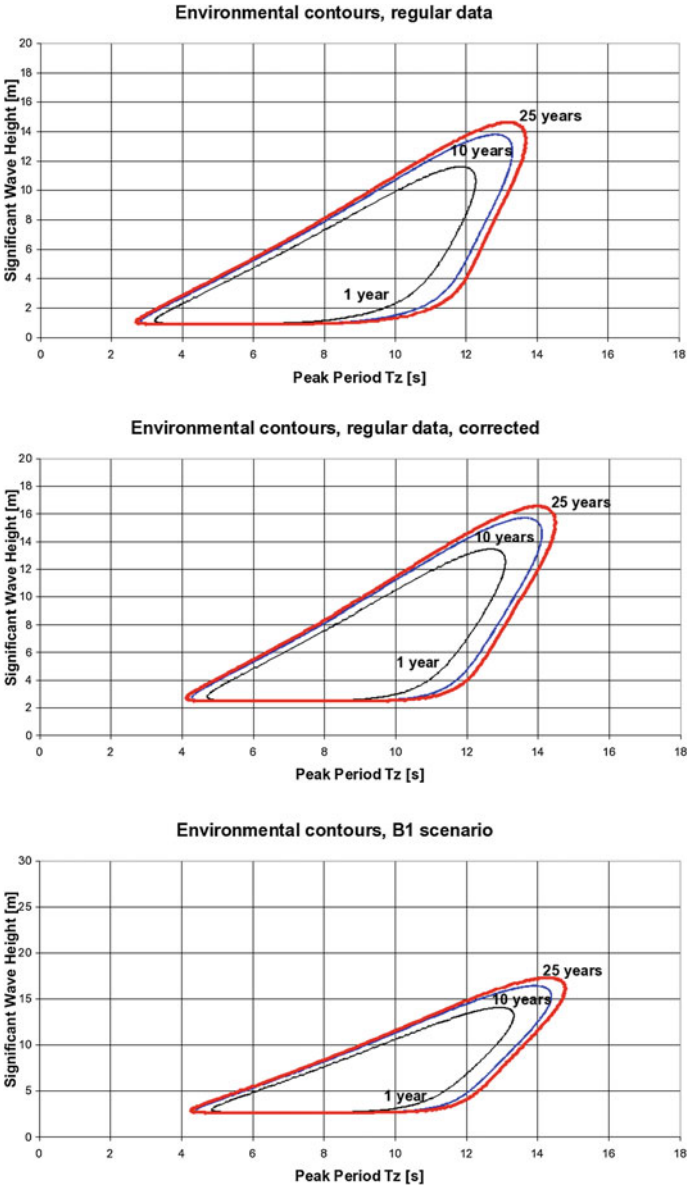

Fig. 7.4 Environmental contour lines for the $\text{ERA}_{\text{Interim}}$ data derived from the original data (*top*) and modified with the climatic trend over 100 years according to the basic model (*middle*) and the extended model with the B1 scenario (*bottom*)

environmental contours to the right. Furthermore, the long-term trend correction has narrowed the contours and increased the maximum 1, 10 and 25-year return H_s and related T_z, see Table 7.3.

Table 7.3 The 1, 10, and 25-year maximum H_s and T_z calculated from the environmental contour (with and without the effects of long-term trends over 100 years)

	$ERA_{Interim}$ data			With trend; basic model			With trend; B1 scenario		
Wave parameter	1-year	10-year	25-year	1-year	10-year	25-year	1-year	10-year	25-year
H_s (m)	11.60	13.80	14.62	13.37	15.63	16.47	14.05	16.40	17.28
$T_z \vert H_s$ (s)	11.86	12.84	13.20	12.66	13.62	13.97	12.95	13.94	14.29

In principle, responses should be calculated for all points along the environmental contours in order to identify the maximum response. However, for the purpose of this study, the (H_s, T_z)-pairs corresponding to the maximum H_s are tacitly assumed to correspond to the extreme response, and the corresponding extreme environmental conditions are the ones shown in Table 7.3. These correspond to the highest values along the vertical axis along the contours.

An alternative approach to establishing environmental contours is proposed in [17], that is somewhat more flexible in how long-term climatic trends can be accounted for in the joint environmental model. However, the resulting environmental contours are very similar to the ones arrived at by the traditional, IFORM-inspired approach adopted in this study.

7.3.3 Illustrative Example: Load Assessment for an Oil Tanker

As an illustrative example, load characteristics will be calculated for an oil tanker of 250 m length and 40 m width with the same characteristics as the one reported in [8]. In this way, the potential impact of the climatic trend on ship structural loads will be investigated.

The 25-year stress amplitudes and response periods for the considered oil tanker have been calculated in the 25-year sea states (H_s, T_z) given in Table 7.3. In order to calculate the responses, a linear transfer function, the same transfer function that was used in the calculations reported in [8], has been assumed. Furthermore, piecewise stationary sea states with 3-h durations have been assumed, and conditioned on the stationary sea states, that is (H_s, T_z), the short-term distributions of sea elevation have been modeled by the Rayleigh distributions. Consequently, a Rayleigh distributed stress process in a short-term sea state has been assumed in the calculations (see [8, 16]). The IFORM method has been used to find the response levels corresponding to the response exceedance probabilities, as outlined in [16]. The Rayleigh distribution is a one-parameter distribution and this is completely specified by calculating the standard deviation of the responses. Hence, the expected extreme responses are the expectations of the corresponding Rayleigh distributions. The response periods, T_r are calculated from the transfer function and the zero-upcrossing periods, T_z.

Table 7.4 includes the results of the analysis for the original joint (H_s, T_z) fit and the modified ones, taking the two alternative 100-year long-term trend estimates into

Table 7.4 25-year extreme load characteristics

	Stress amplitude (MPa)	Response period (s)
Base case	1.0	1.0
Modified fit—Basic model	1.07	1.02
Modified fit—B1 scenario	1.10	1.02

account. The response characteristics obtained using the original (H_s, T_z) fit to the $\text{ERA}_{\text{Interim}}$ data are referred to herein as a Base Case and only relative increases in comparison to the Base Case is given in Table 7.4.

As seen in Table 7.4 incorporation of the long-term trend in the H_s distribution has increased the 25-year stress amplitude and the zero-crossing response period. The 25-year stress amplitude has increased by 7 % if the accumulated trend from the basic model is assumed and by 10 % if the projected trend corresponding to scenario B1 is assumed, both of which is significant. The zero-crossing response periods have increased by 2 %, which might be less serious, due to the estimated long-term trend over 100 years. It is noted that similar calculations have not been done for the A2 scenario, but the effect would presumably be even larger for such a worst-case trend. Furthermore, the potential effect of the modified environmental contours on the structural loads is highly ship-dependent and even though the loads were found to increase significantly for this particular ship, it does not necessarily generalize to all types and sizes of ships. In particular, the effect of the response period is highly structure-dependent.

7.4 Summary and Conclusions

This chapter has described how the estimated long-term trends for significant wave height from the Bayesian hierarchical space-time model outlined in previous chapters can be related to load and response calculations of marine structures. Furthermore, the effect of the estimated trend, extrapolated over 100 years, on the extreme responses for a selected oil tanker was assessed. The results from this crude exercise indicate that the extreme stresses increase quite notably due to climatic trends in the wave climate. The estimated increase of the 25-year extreme stress amplitudes was about 7 and 10 % for two alternative future projections, respectively, and with a 2 % increase in the 25-year extreme response period. Notwithstanding the uncertainties and the assumptions made in this exercise, the results suggest that the effect of climatic trends in the wave climate are not negligible and might have a significant impact on load and response calculations of floating structures. Thus, even though further investigations are needed before firm conclusions can be arrived at, and there are still potential for improvements of the presented model, it is recommended that the effect of climatic change on ship structural responses should be carefully considered in design and reliability calculations of marine structures in the future.

References

1. Athanassoulis, G., Belibassakis, K.: Probabilistic description of metocean parameters by means of kernel density models 1. theoretical backgrounds and first results. Appl. Ocean Res. **24**, 1–20 (2002)
2. Baarholm, G.S., Haver, S., Økland, O.D.: Combining contours of significant wave height and peak period with platform response distributions for predicting design response. Mar. Struct. **23**, 147–163 (2010)
3. Bitner-Gregersen, E.: Joint probabilistic description for combined seas. In: Proceedings of the 24th International Conference on Offshore Mechanics and Arctic Engineering (OMAE 2005). American Society of Mechanical Engineers (ASME) (2005)
4. Bitner-Gregersen, E.: Uncertainties of joint long-term probabilistic modelling of wind sea and swell. In: Proceedings of the 29th International Conference on Ocean, Offshore and Arctic Engineering (OMAE 2010). American Society of Mechanical Engineers (ASME) (2010)
5. Bitner-Gregersen, E., Haver, S.: Joint long term description of environmental parameters for structural response calculation. In: Proceedings of the 2nd International Workshop on Wave Hindcasting and Forecasting (1989)
6. Bitner-Gregersen, E., Haver, S.: Joint environmental model for reliability calculations. In: Proceedings of the 1st International Offshore and Polar Engineering conference (ISOPE 1991). The International Society of Offshore and Polar Engineering (ISOPE) (1991)
7. Bitner-Gregersen, E.M.: Appendix: Joint long term distribution of Hs, Tp. In: Madsen, H.O., Rooney, P., Bitner-Gregersen, E. (eds.) Probabilistic Calculation of Design Criteria for Ultimate Tether Capacity of Snorre TLP. Det Norske Veritas, Report No. 87–31 (1988)
8. Bitner-Gregersen, E.M., Cramer, E.H., Løseth, R.: Uncertainties of load characteristics and fatigue damage of ship structures. Mar. Struct. **8**, 97–117 (1995)
9. Bitner-Gregersen, E.M., Hørte, T., Skjong, R.: Potential impact of climate change on tanker design. In: Proceedings of the 30th International Conference on Ocean, Offshore and Arctic Engineering (OMAE 2011). American Society of Mechanical Engineers (ASME) (2011)
10. Cousineau, D.: Fitting the three-parameter Weibull distribution: Review and evaluation of existing and new methods. IEEE Trans. Dielectr. Electr. Insul. **16**, 281–288 (2009)
11. Dee, D., Uppala, S., Simmons, A., Berrisford, P., Poli, P., Kobayashi, S., Andrae, U., Balmaseda, M., Balsamo, G., Bauer, P., Bechtold, P., Beljaars, A., van de Berg, L., Bidlot, J., Bormann, N., Delsol, C., Dragani, R., Fuentes, M., Geer, A., Haimberger, L., Healy, S., Hersbach, H., Hólm, E., Isaksen, L., Kållberg, P., Köhler, M., MAtricardi, M., McNally, A., Monge-Sanz, B., Morcrette, J.J., Park, B.K., Peubey, C., de Rosnay, P., Tavolato, C., Thépaut, J.N., Vitart, F.: The ERA-Interim reanalysis: configuration and performance of the data assimilation system. Q. J. R. Meteorol. Soc. **137**, 553–597 (2011)
12. Der Kiuregihan, A., Liu, P.L.: Structural reliability under incomplete probability information. J. Eng. Mech. **112**, 85–104 (1986)
13. DNV: Environmental Conditions and Environmental Loads. Det Norske Veritas. DNV-RP-C205 (2010)
14. Ferreira, J., Guedes Soares, C.: Modelling bivariate distributions of significant wave height and mean wave period. Appl. Ocean Res. **24**, 31–45 (2002)
15. Haver, S.: Analysis of uncertainties related to the stochastic modelling of ocean waves. Tech. Rep. UR-80-09, Norges tekniske høgskole (1980)
16. Haver, S., Winterstein, S.: Environmental contour lines: A method for estimating long term extremes by a short term anaysis. Trans. Soc. Nav. Archit. Mar. Eng. **116**, 116–127 (2009)
17. Huseby, A.B., Vanem, E., Natvig, B.: A new approach to environmental contours for ocean engineering applications based on direct Monte Carlo simulations. Ocean Eng. **60**, 124–135 (2013)
18. Jensen, J.: Sur les fonctions convexes et les inégalités entre les valeurs moyennes. Acta Mathematica **30**, 175–193 (1906)

19. Jonathan, P., Ewans, K., Flynn, J.: On the estimation of ocean engineering design contours. In: Proceedings of the 30th International Conference on Offshore Mechanics and Arctic Engineering (OMAE 2011). American Society of Mechanical Engineers (ASME) (2011)
20. Jonathan, P., Flynn, J., Ewans, K.: Joint modelling of wave spectral parameters for extreme sea states. Ocean Eng. **37**, 1070–1080 (2010)
21. Labeyrie, J., Olagnon, M.: Stochastic sensitiveness to combined extreme environmental loads in structural reliability. In: Proceedings of the 12th International Conference on Offshore Mechanics and Arctic Engineering (OMAE 1993). American Society of Mechanical Engineers (ASME) (1993)
22. Leira, B.J.: A comparison of stochastic process models for definition of design contours. Struct. Saf. **30**, 493–505 (2008)
23. Mathisen, J., Bitner-Gregersen, E.: Joint distributions for significant wave height and wave zero-up-crossing period. Appl. Ocean Res. **12**, 93–103 (1990)
24. Nataf, A.: Détermination des distributions dont les marges sont données. Comptes Rendus de l'Académie des Sciences **255**, 42–43 (1962)
25. Nordenstrøm, N.: A method to predict long-term distributions of waves and wave-induced motions and loads on ships and other floating structures. Tech. Rep. 81, Det Norske, Veritas (1973)
26. Prince-Wright, R.: Maximum likelihood models of joint environmental data for TLP design. In: Proceedings of the 14th International Conference on Offshore Mechanics and Arctic Engineering (OMAE 1995). American Society of Mechanical Engineers (ASME) (1995)
27. Repko, A., Van Gelder, P., Voortman, H., Vrijling, J.: Bivariate description of offshore wave conditions with physics-based extreme value statistics. Appl. Ocean Res. **26**, 162–170 (2004)
28. Rosenblatt, M.: Remarks on a multivariate transformation. Ann. Math. Stat. **23**, 470–472 (1952)
29. Sagrilo, L., Næss, A., Doria, A.: On the long-term response of marine structures. Appl. Ocean Res. **33**, 208–214 (2011)
30. Vanem, E., Bitner-Gregersen, E.: Stochastic modelling of long-term trends in the wave climate and its potential impact on ship structural loads. Appl. Ocean Res. **37**, 235–248 (2012)
31. Vanem, E., Huseby, A.B., Natvig, B.: A stochastic model in space and time for monthly maximum significant wave height. In: Abrahamsen, P., Haugen, R., Kolbjørnsen, O. (eds.) Geostatistics Oslo 2012, pp. 505–517. Springer, Heidelberg (2012)
32. Vanem, E., Huseby, A.B., Natvig, B.: Bayesian hierarchical spatio-temporal modelling of trends and future projections in the ocean wave climate with a CO_2 regression component. Environ. Ecol. Stat. (in press) (2013)
33. Vanem, E., Natvig, B., Huseby, A.B., Bitner-Gregersen, E.M.: An illustration of the effect of climate change on the ocean wave climate—a stochastic model. In: Singh, B.R. (ed.) Climate Change—Realities, Impacts Over Ice Cap, Sea Level and Risks, pp. 481–508. InTech, Rijeka (2013)
34. Winterstein, S., Ude, T., Cornell, C., Bjerager, P., Haver, S.: Environmental parameters for extreme response: Inverse FORM with omission factors. In: Proceedings of the 6th International Conference on Structural Safety and Reliability (1993)

Chapter 8
Case Study: Modeling the Effect of Climate Change on the World's Oceans

This chapter analyses the trends and the future projections of significant wave height in several ocean areas at different parts of the world. It uses the same stochastic Bayesian hierarchical space-time model with regression on atmospheric levels of CO_2 in order to estimate the expected long-term trends and make future projections toward the year 2100. The model was initially developed for an area in the North Atlantic Ocean, and has been found to perform reasonably well there, and it will now be investigated how the model performs for other ocean areas and what the effects of climate change may be in these areas according to the model. Eleven new ocean areas have been analyzed with the model, and this chapter presents the results pertaining to the estimated long-term trends and future projections of monthly maximum significant wave height for each of the 12 ocean areas. This chapter is based on results presented in [17].

8.1 Introduction

All the results presented in the previous chapters of this book pertain to a specific area in the North Atlantic Ocean, but in this chapter, it will be investigated how the model performs on 11 alternative areas of the world's oceans. Hence, estimated long-term trends and future projections toward the year 2100, obtained from the Bayesian hierarchical space-time model, will be presented for the following ocean areas:

1. North Atlantic Ocean
2. North East Pacific
3. Gulf of Mexico
4. South Atlantic Ocean
5. North West Pacific
6. Indian Ocean
7. South Pacific Ocean
8. Mid Atlantic Ocean

E. Vanem, *Bayesian Hierarchical Space-Time Models with Application to Significant Wave Height*, Ocean Engineering & Oceanography 2,
DOI: 10.1007/978-3-642-30253-4_8, © Springer-Verlag Berlin Heidelberg 2013

Table 8.1 The different ocean areas selected for study

#	Area description	Longitudes	Latitudes	Grid size
1	North Atlantic Ocean	324–348° E	51–63° N	17 × 9
2	North East Pacific (West coast of USA/Canada)	204–219° E	36–51° N	11 × 11
3	Gulf of Mexico	265.5–274.5° E	22.5–27° N	7 × 4
4	South Atlantic Ocean (West Africa)	336–351° E	27–12° S	11 × 11
5	North West Pacific (Japan)	147–162° E	27–42° N	11 × 11
6	Indian Ocean	60–75° E	0–15° N	11 × 11
7	South Pacific Ocean (Chile)	264–278° E	45–30° S	11 × 11
8	Mid Atlantic Ocean	315–330° E	0–15° N	11 × 11
9	Tasmanian Sea (Eastern Australia)	157.5–172.4° E	42–27° S	11 × 11
10	Mediterranean Sea	16.5–21°E	33–36° N	4 × 3
11	Equatorial Pacific	225–240° E	7.5° S–7.5° N	11 × 11
12	Western Australia	93–108° E	39–24° S	11 × 11

9. Tasmanian Sea
10. Mediterranean Sea
11. Equatorial Pacific
12. Western Australia

It is believed that this will give an indication of how the climate change will influence the wave climate of the world's oceans, even though all future projections are inevitably uncertain.

The same global dataset for significant wave height and atmospheric levels of CO_2 as in previous chapters has been used, and also the same priors, loss functions, model assumptions, and emission scenarios have been employed. It is acknowledged that it might be questionable whether the same priors, for instance, should be used for all ocean areas but it is argued that the amount of data is large enough for this to be of minor importance. The spatial resolution of the data is still 1.5° × 1.5° and monthly maxima have been used for each spatial location. The various ocean areas with corresponding coordinates are summarized in Table 8.1. For most of the areas, a grid of 11 × 11 = 121 points have been selected, but for the Gulf of Mexico and the Mediterranean Sea, such large areas were simply not available and a smaller grid has been used for these areas. It should be observed that ocean area # 1 is identical to the one investigated in previous chapters of this book. The selected ocean areas are indicated on a map in Fig. 8.1.

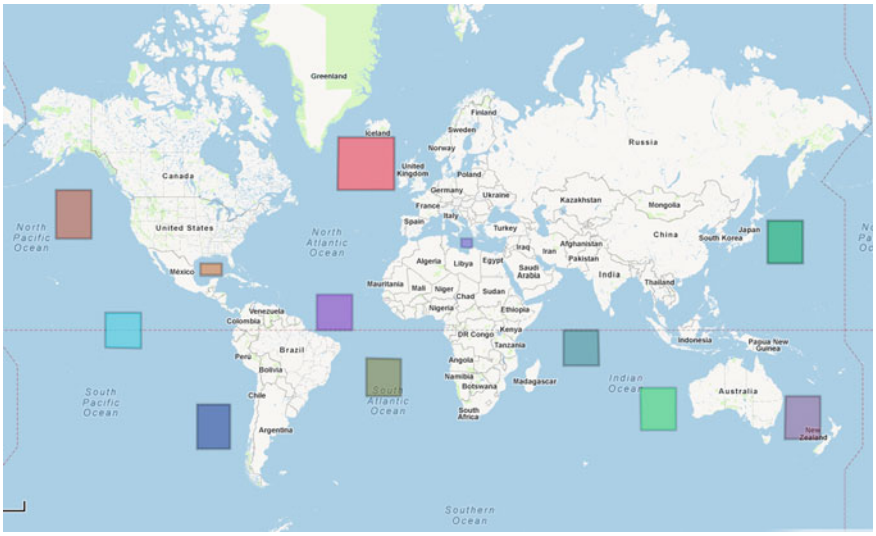

Fig. 8.1 The 12 ocean areas selected for this case study

8.2 Simulation Results for the Various Ocean Areas

The model was simulated using the Gibbs sampler with Metropolis-Hastings steps, as previously [14–16], but the burn-in period was extended to 100,000 samples and the batch size to 20, obtaining 1,000 samples of the posterior parameter vector. Six Metropolis-Hastings steps were performed at each iteration, giving sufficient acceptance rates for all ocean areas. For most areas, the acceptance rate was well above 80 % and the lowest acceptance rate was 35 % for the North Atlantic area.

Trace plots of the posterior marginal distributions suggest that convergence occurred satisfactorily. The main results pertaining to the long-term trends and future projections obtained for the various ocean areas are presented in separate sections below. The posterior mean and standard deviation of the various model parameters are presented in [17] and are not reproduced herein, but it is noted that for the North Atlantic, it is reassuring to observe that the posteriors agree well with the posteriors obtained in [16].

8.2.1 North Atlantic Ocean

The first ocean area that is investigated is the area in the North Atlantic. This is exactly the same area that has been investigated previously, with various models [14–16]. However, a new set of simulations have been run, with slightly different MCMC settings. Nevertheless, the results from these new simulations are directly

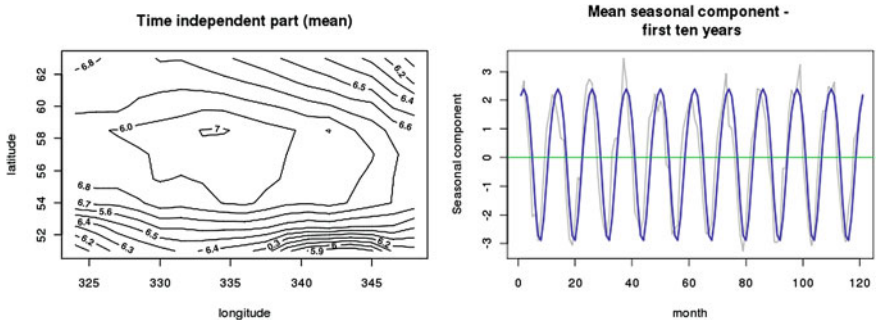

Fig. 8.2 Spatial field and seasonal contribution for the North Atlantic

Table 8.2 Estimated trends and future projections—North Atlantic

	Expectation	90 % Credible interval
Trend (1958–2001)	59 cm	29–87 cm
A2 projections (2001–2100)	5.5 m	2.9–8.2 m
B1 projections (2001–2100)	1.9 m	0.87–3.0 m

comparable to the ones presented in Chap. 5 [16] with a semiannual component, as the same model has been used for the same data, and is included herein for comparison.

The spatial field, $\mu(x)$, varying between 5.8 and 7.0 m and the seasonal component, with contributions oscillating between -2.9 and 2.4 m, are illustrated in Fig. 8.2. The long-term trend does not necessarily start at 0, and for this particular area, the long-term trend starts at 0.53 m. Hence, this contribution could be included in the mean spatial field, so that the adjusted $\mu(x)$ varies between 6.3 and 7.5 m. However, the long-term trend is assumed invariant in space, so the pattern of the adjusted field will be exactly as in Fig. 8.2, only shifted along the z-axis. The short-term dynamic component $\theta(x, t)$ varies between -1.1 and 1.8 m. Overall, these model components seem to perform reasonably well for the North Atlantic Ocean area, and the results are in good agreement to the results presented in [16]. This is of course a requirement, but it also indicates that the Markov chain did converge. The new simulations presented herein have twice as long burn-in period, and it is reassuring to see that this does not influence the results, i.e., it indicates that the samples are from the same posterior distributions; the stationary distributions.

The estimated long-term trends and future projections pertaining to the area in the North Atlantic are illustrated in Fig. 8.3, and the expected trends and future projections along with 90 % credible intervals around the mean are presented in Table 8.2. The trends are adjusted so that they start at 0 m and the future projections are adjusted so that they have a trend of 0 m in 2001. Hence, the future projections are relative to the 2001 situation. This will also be done for all subsequent areas.

It is seen that for this ocean area, the model estimates a significant increasing trend and future increase of significant wave height. Furthermore, the expected trends and

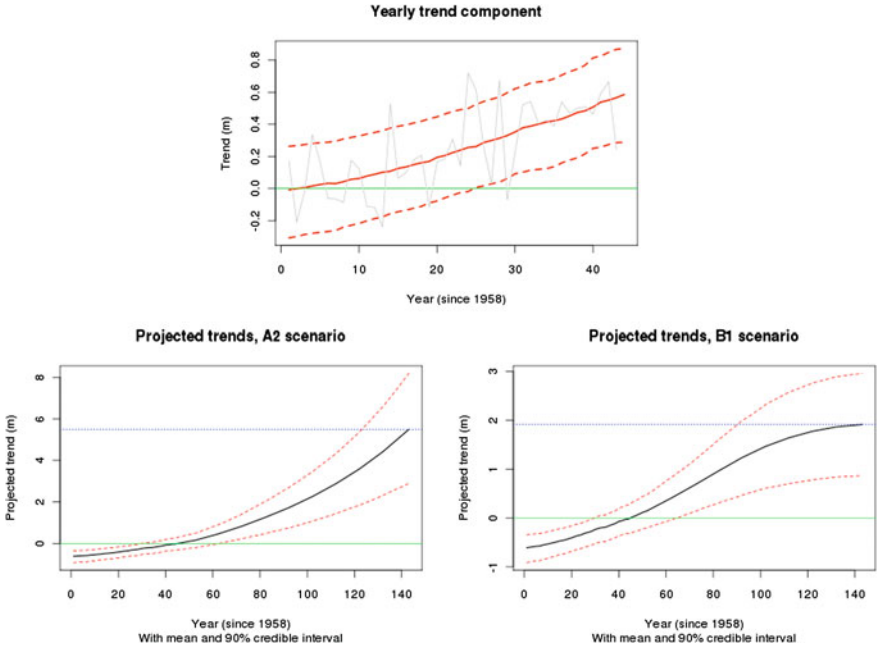

Fig. 8.3 Estimated trend and future projections for the North Atlantic

future projections agree well with the corresponding estimates presented in [16], as indeed it should.

8.2.2 North East Pacific: Western USA/Canada

The spatial field, $\mu(x)$, varying between 1.5 and 3.6 m and the seasonal component, with contributions oscillating between -2.9 and 2.3 m, are illustrated in Fig. 8.4. Adjusted to include the starting value of the trend, the mean adjusted spatial field varies between 4.6 and 6.7 m. The short-term dynamic component $\theta(x, t)$ varies between ± 1.6 m. Overall, these model components seem to perform reasonably well for the North East Pacific Ocean area.

The estimated long-term trends and future projections pertaining to the area in the North East Pacific are illustrated in Fig. 8.5, and the expected trends and future projections along with 90 % credible intervals around the mean are presented in Table 8.3.

It is seen that for this ocean area as well, the model estimates a significant increasing trend and future increase of significant wave height.

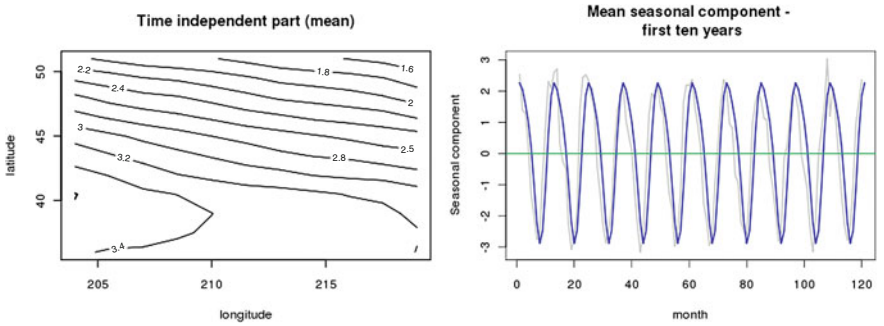

Fig. 8.4 Spatial field and seasonal contribution for the North East Pacific

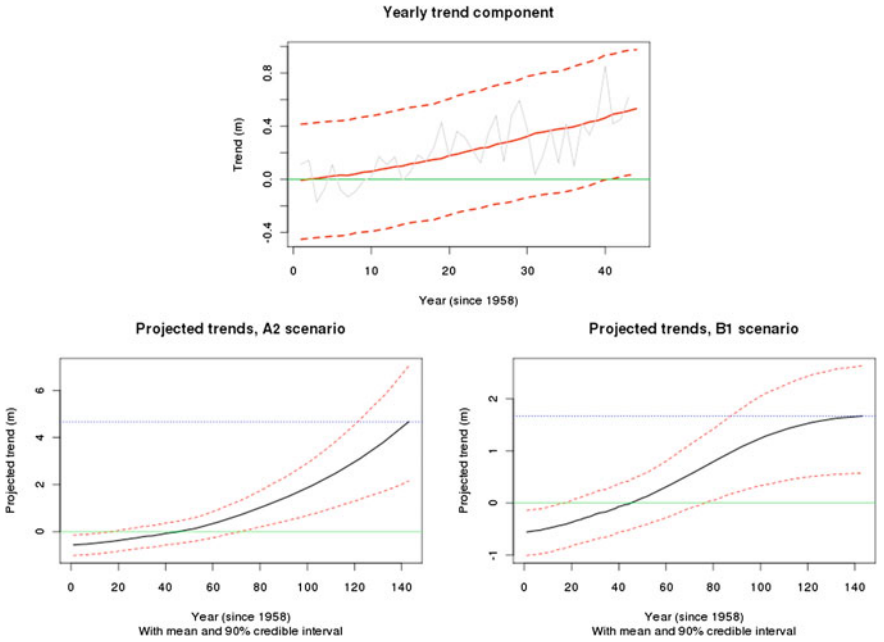

Fig. 8.5 Estimated trend and future projections for the North East Pacific

8.2.3 Gulf of Mexico

The spatial field, $\mu(x)$, varying between 3.2 and 3.6 m and the seasonal component, with contributions oscillating between -1.8 and 0.86 m, are illustrated in Fig. 8.6. The adjusted spatial field ranges between 2.5 and 2.9 m. The short-term dynamic component $\theta(x, t)$ varies between ± 0.6 m. Overall, these model components seem to perform reasonably well also for the Gulf of Mexico, even though for example

Table 8.3 Estimated trends and future projections—North East Pacific

	Expectation	90 % Credible interval
Trend (1958–2001)	53 cm	3.3–97 cm
A2 projections (2001–2100)	4.7 m	2.2–7.0 m
B1 projections (2001–2100)	1.7 m	0.58–2.6 m

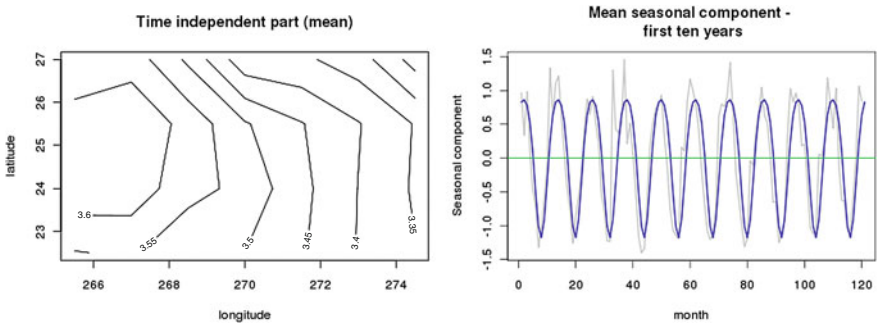

Fig. 8.6 Spatial field and seasonal contribution for the Gulf of Mexico

Table 8.4 Estimated trends and future projections—Gulf of Mexico

	Expectation	90 % Credible interval
Trend (1958–2001)	5.6 cm	−33 to 53 cm
A2 projections (2001–2100)	62 cm	−1.0 to 2.2 m
B1 projections (2001–2100)	20 cm	−54 to 95 cm

the dynamic part $\theta(x, t)$ has become less important than for the North East Pacific Ocean.

The estimated long-term trends and future projections pertaining to the area in the Gulf of Mexico are illustrated in Fig. 8.7, and the expected trends and future projections along with 90 % credible intervals around the mean are presented in Table 8.4.

It is seen that the expected trend is slightly increasing, but the 90 % credible interval of the expected trend and future projections is rather wide and embraces both positive and negative trends. Hence, no significant trend is identified for this ocean area.

8.2.4 South Atlantic Ocean: West Africa

The spatial field, $\mu(x)$, varying between 2.0 and 3.2 m and the seasonal component, with contributions oscillating between −0.47 and 0.49 m, are illustrated in Fig. 8.8.

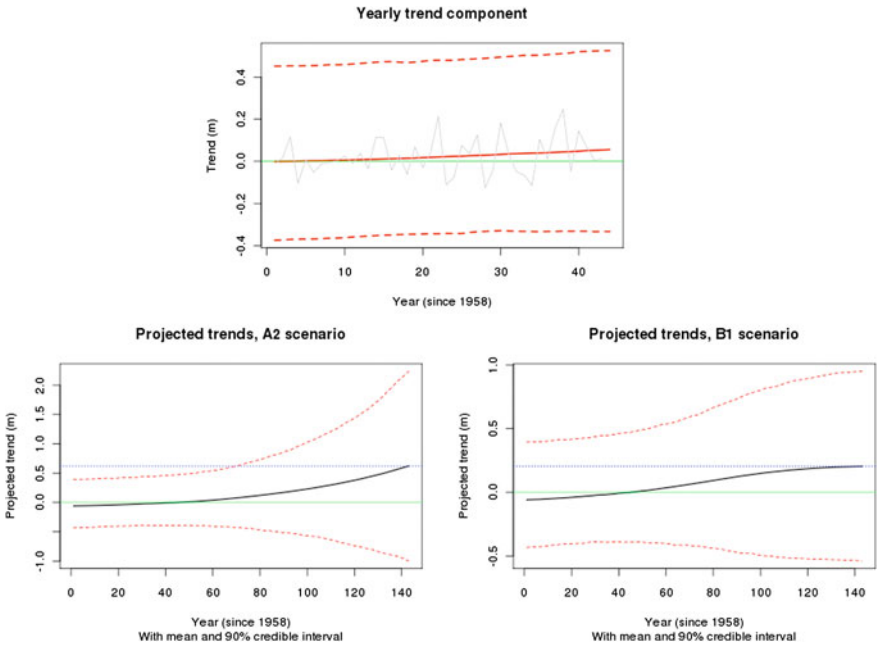

Fig. 8.7 Estimated trend and future projections for the Gulf of Mexico

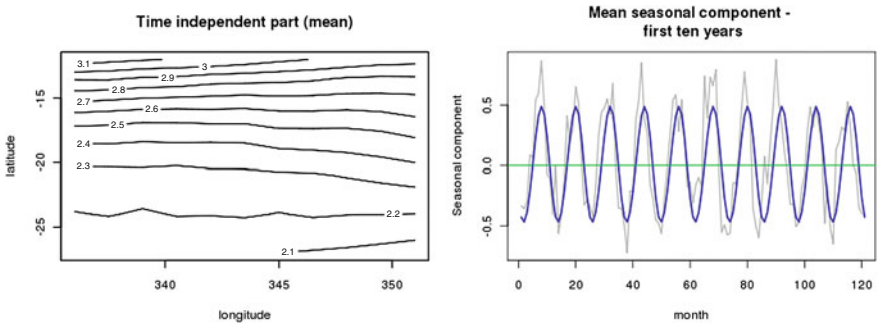

Fig. 8.8 Spatial field and seasonal contribution for the South Atlantic Ocean west of Africa

Adjusted for the starting value of the trend, the spatial field would range between 2.5 and 3.7 m. The short-term dynamic component $\theta(x, t)$ varies between -0.63 and 0.75 m. Overall, these model components seem to perform reasonably well also for the area off West Africa. In particular, it is interesting to see that the model picks up that now the boreal summer season is the roughest season, which makes sense since this area lies on the Southern Hemisphere. For the three previous areas, all of which lie on the Northern Hemisphere, the seasonal contributions were highest during boreal winter.

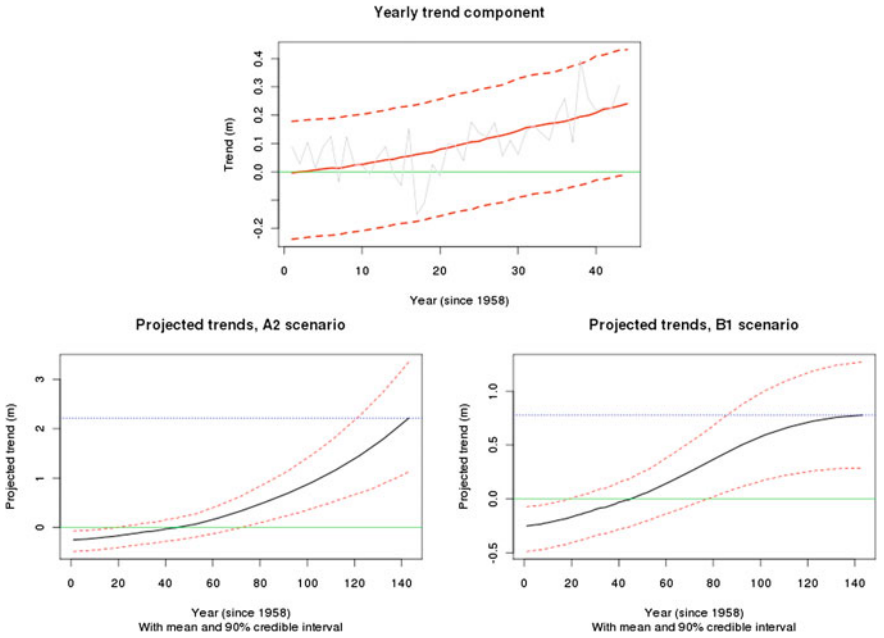

Fig. 8.9 Estimated trend and future projections for the area off West Africa

Table 8.5 Estimated trends and future projections—West Africa

	Expectation	90 % Credible interval
Trend (1958–2001)	24 cm	−1.2 to 43 cm
A2 projections (2001–2100)	2.2 m	1.1 to 3.4 m
B1 projections (2001–2100)	78 cm	29 to 130 cm

The estimated long-term trends and future projections pertaining to the area in the South Atlantic are illustrated in Fig. 8.9, and the expected trends and future projections along with 90 % credible intervals around the mean are presented in Table 8.5.

It is seen that the expected trend is increasing, and most of the 90 % credible interval of the trend is also positive. The expected future projections as well as the complete 90 % credible interval are positive. Hence, a significant increasing trend in monthly maximum significant wave height is predicted for this ocean area toward 2100.

8.2.5 North West Pacific Ocean: Japan

The spatial field, $\mu(x)$, varying between 4.0 and 7.0 m and the seasonal component, with contributions oscillating between −2.2 and 2.0 m, are illustrated in Fig. 8.10. The adjusted spatial field varies spatially between 3.8 and 6.8 m. The short-term

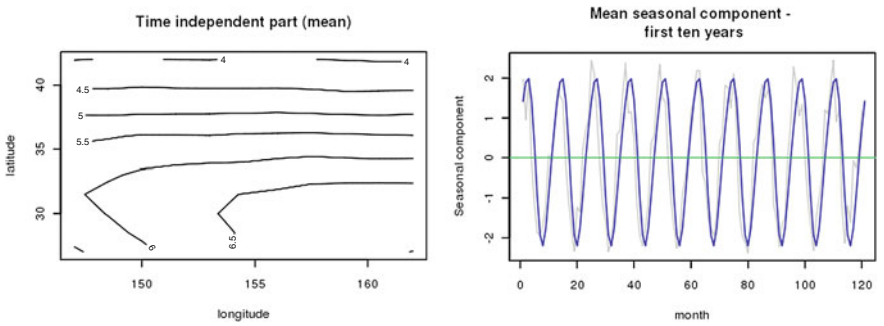

Fig. 8.10 Spatial field and seasonal contribution for the North West Pacific Ocean East of Japan

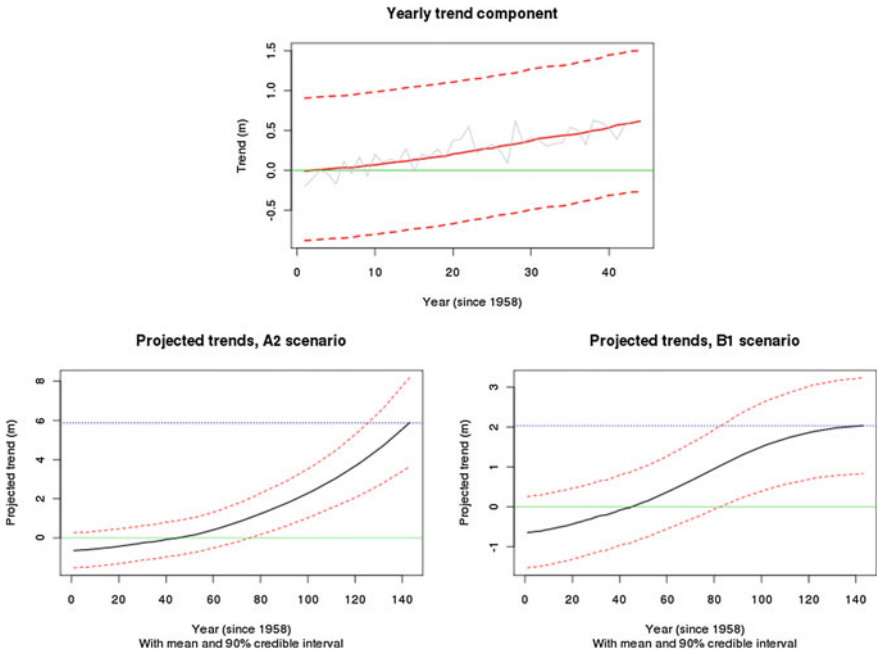

Fig. 8.11 Estimated trend and future projections for the area off Japan

dynamic component $\theta(x, t)$ varies between -1.3 and 1.6 m. Overall, these model components seem to perform reasonably well also for the area off the Japanese coast.

The estimated long-term trends and future projections pertaining to the area in the North West Pacific are illustrated in Fig. 8.11, and the expected trends and future projections along with 90 % credible intervals around the mean are presented in Table 8.6.

Table 8.6 Estimated trends and future projections—North West Pacific

	Expectation	90 % Credible interval
Trend (1958–2001)	62 cm	−27 to 150 cm
A2 projections (2001–2100)	5.9 m	3.6 to 8.2 m
B1 projections (2001–2100)	2.0 m	0.83 to 3.2 m

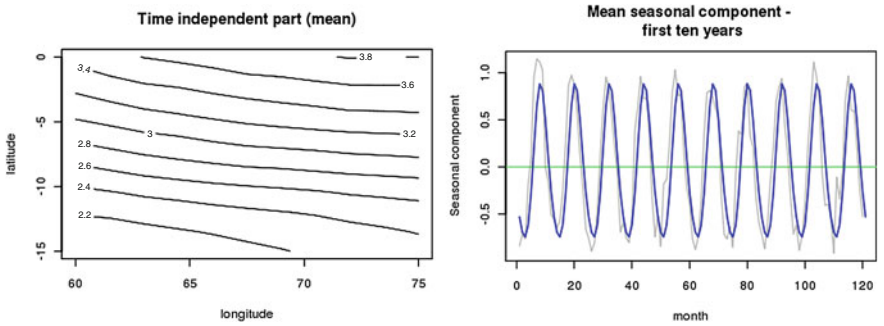

Fig. 8.12 Spatial field and seasonal contribution for the Indian Ocean

Table 8.7 Estimated trends and future projections—Indian Ocean

	Expectation	90 % Credible interval
Trend (1958–2001)	19 cm	6.2–31 cm
A2 projections (2001–2100)	1.8 m	0.91–2.7 m
B1 projections (2001–2100)	62 cm	27–99 cm

The expected trend is increasing, and the whole 90 % credible interval of the future projections is positive. Hence, a significant increasing trend in monthly maximum significant wave height is identified for this ocean area.

8.2.6 Indian Ocean

The spatial field, $\mu(x)$, varying between 2.0 and 3.8 m and the seasonal component, with contributions oscillating from −0.74 to 0.89 m, are illustrated in Fig. 8.12. The adjusted $\mu(x)$ field is shifted to vary between 1.9 and 3.7 m. The short-term dynamic component $\theta(x, t)$ varies between −0.58 and 0.71 m. Overall, these model components seem to perform reasonably well also for this area.

The estimated long-term trends and future projections pertaining to the area in the Indian Ocean are illustrated in Fig. 8.13, and the expected trends and future projections along with 90 % credible intervals around the mean are presented in Table 8.7.

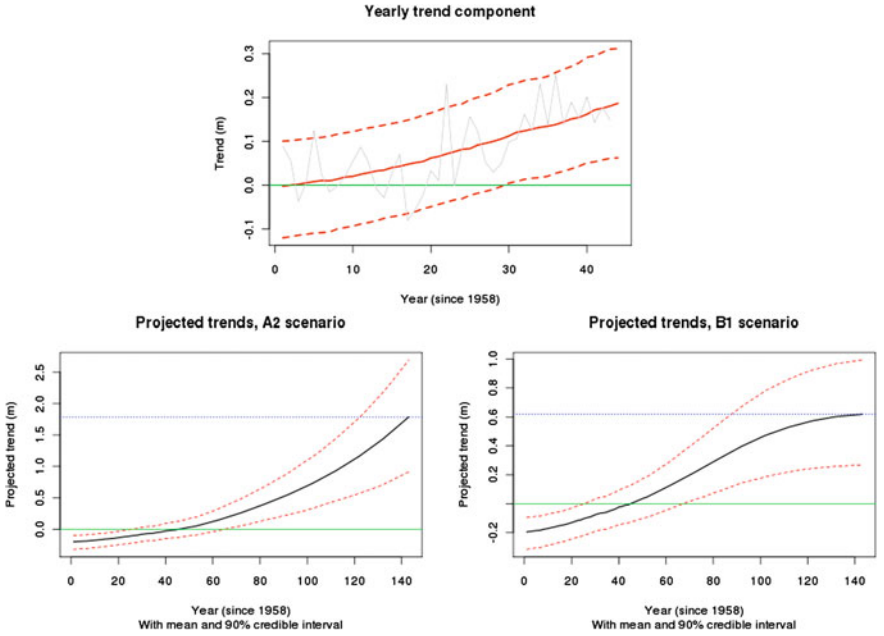

Fig. 8.13 Estimated trend and future projections for the area in the Indian Ocean

The expected trend is increasing, and also the whole 90 % credible interval of the expected trend and future projections toward 2100 is positive. Hence, a significant increasing trend in monthly maximum significant wave height is identified for this ocean area.

8.2.7 South Pacific Ocean: Chile

The spatial field, $\mu(x)$, varying between 4.5 and 7.3 m and the seasonal component, with contributions oscillating from -1.0 to 1.1 m, are illustrated in Fig. 8.14. The adjusted mean spatial field varies between 4.0 and 6.8 m. The short-term dynamic component $\theta(x, t)$ varies between -0.92 and 1.7 m. Overall, these model components seem to perform reasonably well also for this area.

The estimated long-term trends and future projections pertaining to the area in the South Pacific Ocean are illustrated in Fig. 8.15, and the expected trends and future projections along with 90 % credible intervals around the mean are presented in Table 8.8.

The expected trend is increasing, and the whole 90 % credible interval of the expected trend and future projections toward 2100 is positive. Hence, a significant

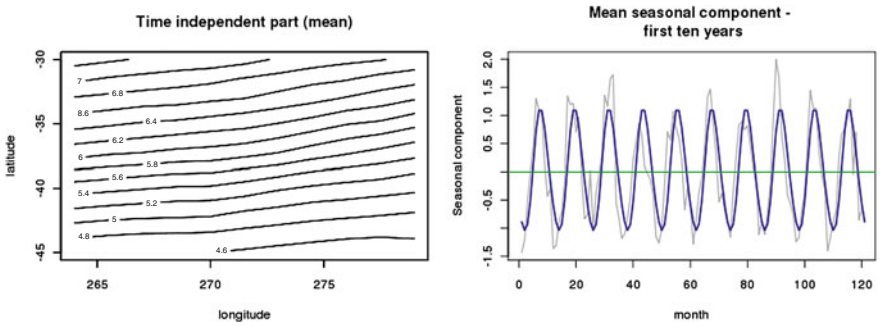

Fig. 8.14 Spatial field and seasonal contribution for the South Pacific Ocean

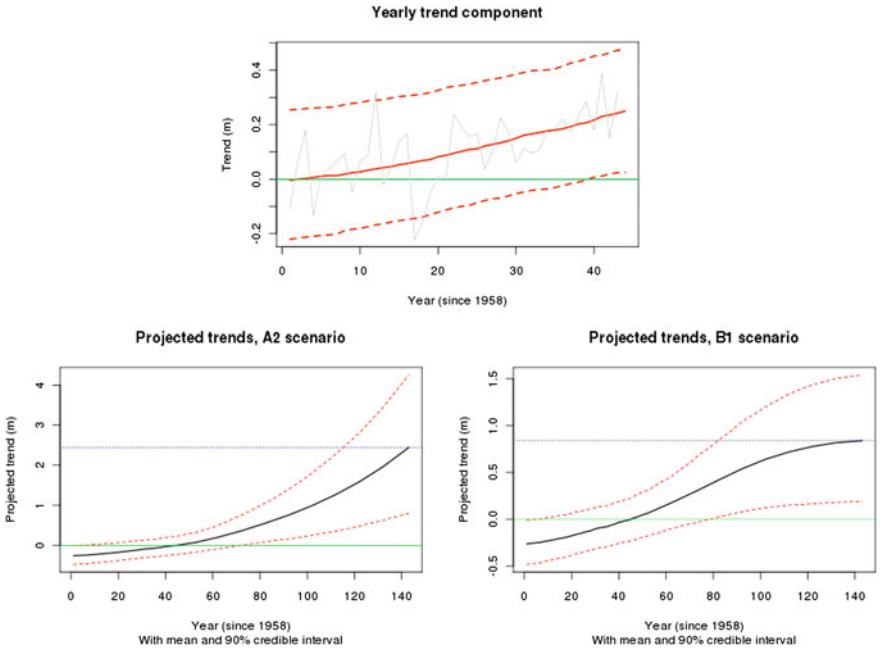

Fig. 8.15 Estimated trend and future projections for the area in the South Pacific Ocean

increasing trend in monthly maximum significant wave height is predicted also for this ocean area.

Table 8.8 Estimated trends and future projections—South Pacific Ocean

	Expectation	90 % Credible interval
Trend (1958–2001)	25 cm	2.5–48 cm
A2 projections (2001–2100)	2.4 m	0.80–4.3 m
B1 projections (2001–2100)	84 cm	19–150 cm

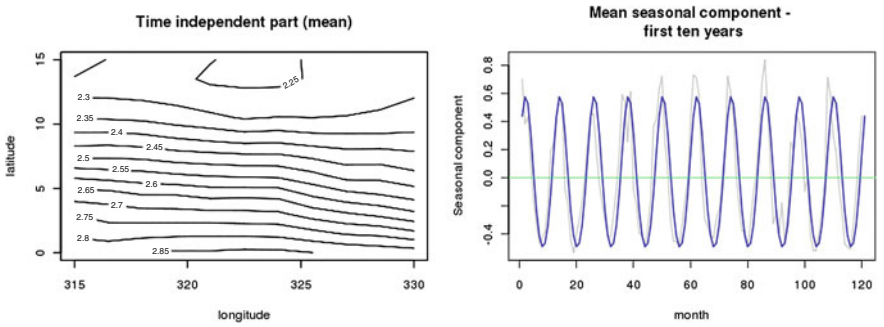

Fig. 8.16 Spatial field and seasonal contribution for the mid Atlantic Ocean

Table 8.9 Estimated trends and future projections—mid Atlantic Ocean

	Expectation	90 % Credible interval
Trend (1958–2001)	24 cm	16–33 cm
A2 projections (2001–2100)	2.3 m	1.6–3.0 m
B1 projections (2001–2100)	80 cm	52–110 cm

8.2.8 Mid Atlantic Ocean

The spatial field, $\mu(x)$, varying between 2.2 and 2.9 m (adjusted field varying between 2.1 and 2.8 m) and the seasonal component, with contributions oscillating between −0.49 and 0.58 m, are illustrated in Fig. 8.16. The short-term dynamic component $\theta(x, t)$ varies between −0.54 and 1.1 m. Overall, these model components seem to perform reasonably well also for this area.

The estimated long-term trends and future projections pertaining to the area in the mid Atlantic Ocean are illustrated in Fig. 8.17, and the expected trends and future projections along with 90 % credible intervals around the mean are presented in Table 8.9.

The expected trend is increasing, and the whole 90 % credible interval of the expected trend and future projections toward 2100 is positive. Hence, a significant increasing trend in monthly maximum significant wave height is predicted also for this ocean area.

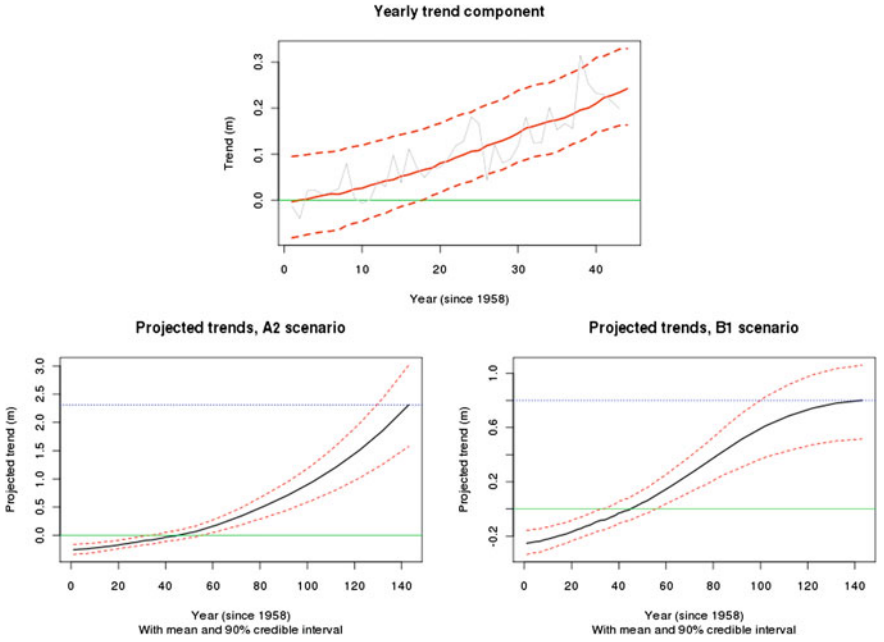

Fig. 8.17 Estimated trend and future projections for the area in the mid Atlantic Ocean

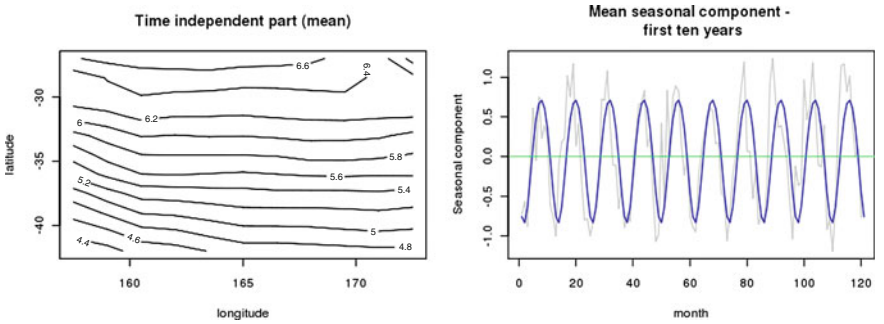

Fig. 8.18 Spatial field and seasonal contribution for the Tasmanian Sea

8.2.9 Tasmanian Sea: Eastern Australia

The spatial field, $\mu(x)$, varying between 4.2 and 6.7 m (adjusted to vary between 3.5 and 6.0 m) and the seasonal component, with contributions oscillating between -0.84 and 0.71 m, are illustrated in Fig. 8.18. The short-term dynamic component $\theta(x, t)$ varies between -0.79 and 1.1 m. Overall, these model components seem to perform reasonably well also for this area.

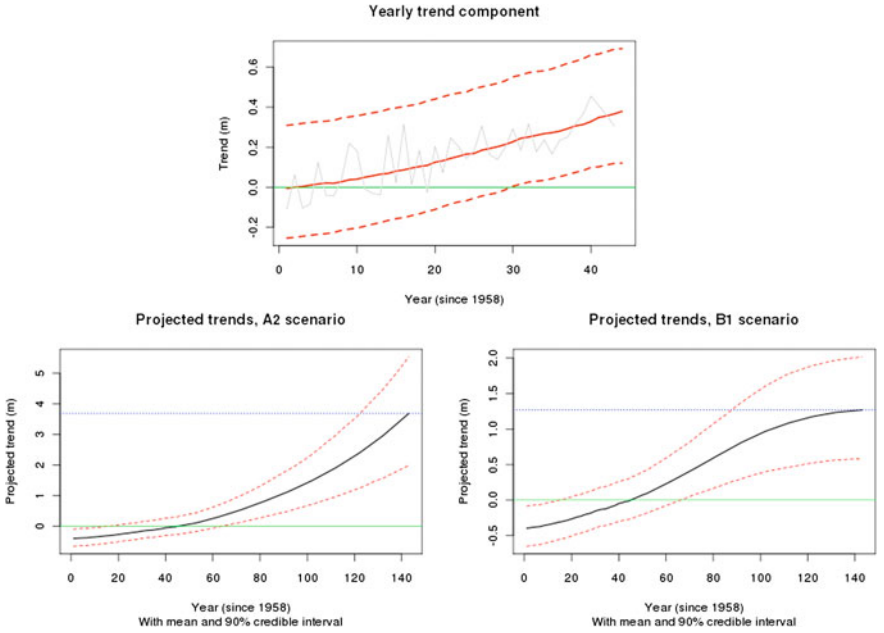

Fig. 8.19 Estimated trend and future projections for the area in the Tasmanian Sea

Table 8.10 Estimated trends and future projections—Tasmanian Sea

	Expectation	90 % Credible interval
Trend (1958–2001)	38 cm	12–69 cm
A2 projections (2001–2100)	3.7 m	2.0–5.5 m
B1 projections (2001–2100)	1.3 m	0.58–2.0 m

The estimated long-term trends and future projections pertaining to the area in the Tasmanian Sea are illustrated in Fig. 8.19, and the expected trends and future projections along with 90 % credible intervals around the mean are presented in Table 8.10.

The expected trend is increasing, and the whole 90 % credible interval of the expected trend and future projections toward 2100 is positive. Hence, a significant increasing trend in monthly maximum significant wave height is predicted also for this ocean area.

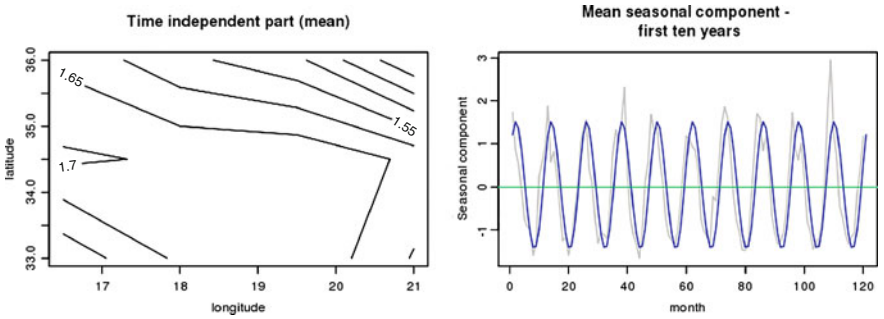

Fig. 8.20 Spatial field and seasonal contribution for the Mediterranean Sea

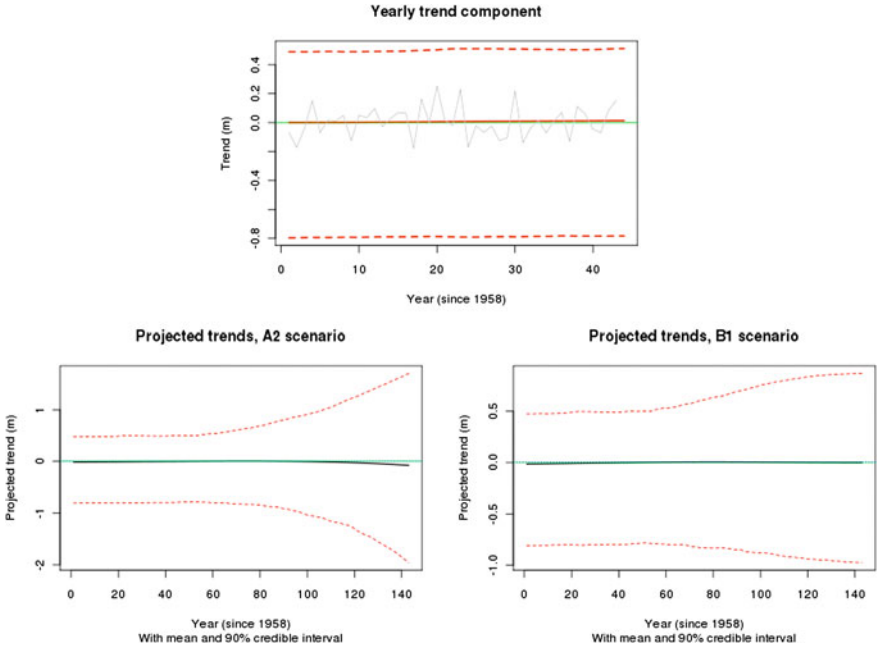

Fig. 8.21 Estimated trend and future projections for the area in the Mediterranean Sea

8.2.10 Mediterranean Sea

The spatial field, $\mu(x)$, varying between 1.4 and 1.7 m and the seasonal component, with contributions oscillating between -0.83 and 0.58 m, are illustrated in Fig. 8.20. The adjusted spatial field varies between 3.0 and 3.3 m. The short-term dynamic component $\theta(x, t)$ varies between -1.4 and 1.5 m. Overall, these model components seem to perform reasonably well also for this area.

Table 8.11 Trends and future projections—Mediterranean Sea

	Expectation	90 % Credible interval
Trend (1958–2001)	1.3 cm	−78 to 51 cm
A2 projections (2001–2100)	−7.7 cm	−2.0 to 1.7 m
B1 projections (2001–2100)	0	−97 to 87 cm

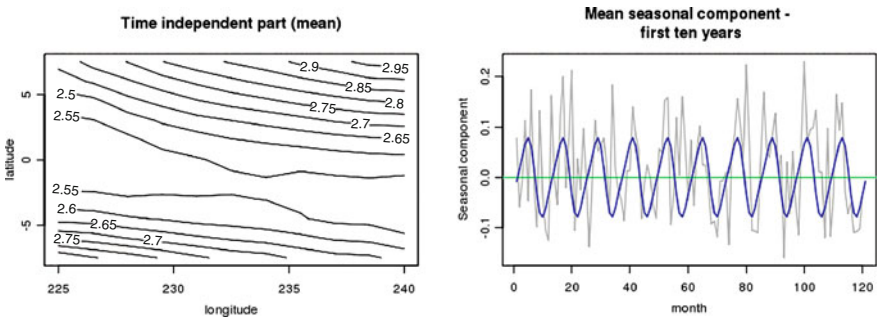

Fig. 8.22 Spatial field and seasonal contribution for the Equatorial Pacific

The estimated long-term trends and future projections pertaining to the area in the Mediterranean Sea are illustrated in Fig. 8.21, and the expected trends and future projections along with 90 % credible intervals around the mean are presented in Table 8.11.

For this particular area, the model has difficulty in detecting a significant trend. The expected future projections are slightly negative but are not significant for either scenario. Hence, for this particular ocean area no trends are identified.

8.2.11 Equatorial Pacific

The spatial field, $\mu(x)$, varying between 2.5 and 3.0 m (adjusted to 2.4 and 2.9 m) and the seasonal component, with expected contributions oscillating between −7.9 and 7.8 cm, are illustrated in Fig. 8.22. The short-term dynamic component $\theta(x, t)$ varies between -0.59 and 0.93 m. Overall, these model components seem to perform reasonably well also for this area. In particular, it is interesting to note that the seasonal variation is almost vanishing for this area; the contribution from the seasonal component is negligible. As this area spans over Equator, this might be as expected, and it is reassuring that the model is able to pick this up.

The estimated long-term trends and future projections pertaining to the area in the Equatorial Pacific are illustrated in Fig. 8.23, and the expected trends and future projections along with 90 % credible intervals around the mean are presented in Table 8.12.

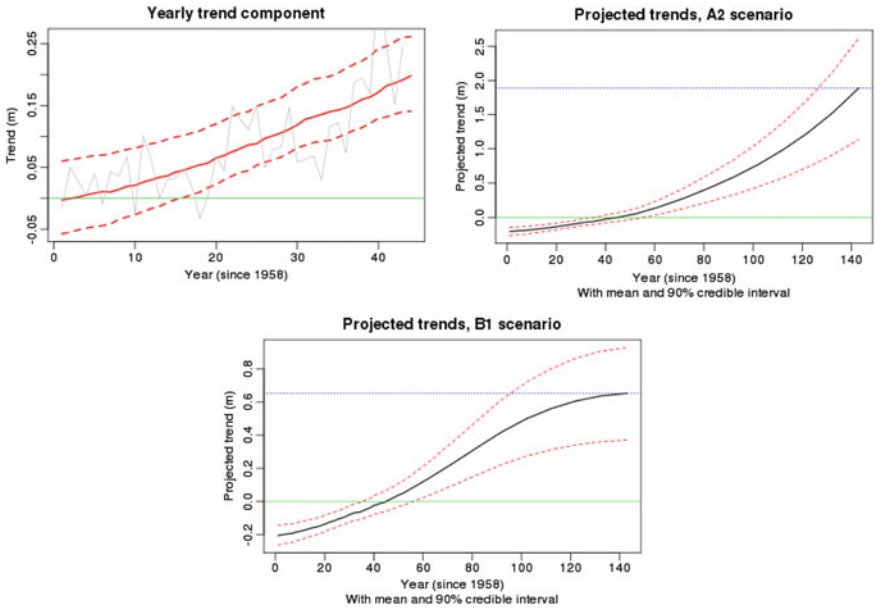

Fig. 8.23 Estimated trend for the area in the Equatorial Pacific

Table 8.12 Estimated trends and future projections—Equatorial Pacific

	Expectation	90 % Credible interval
Trend (1958–2001)	20 cm	14–26 cm
A2 projections (2001–2100)	1.9 m	1.1–2.6 m
B1 projections (2001–2100)	65 cm	37–93 cm

For this area as well, the model estimates a significant increasing trend and future projections, with both expectations and 90 % credible intervals of the mean being strictly positive.

8.2.12 Western Australia

The spatial field, $\mu(x)$, varying between 4.4 and 6.9 m and the seasonal component, with expected contributions oscillating between -1.1 and 1.3 m, are illustrated in Fig. 8.24. The adjusted spatial field varies between 4.0 and 6.5 m. The short-term dynamic component $\theta(x, t)$ varies between -0.78 and 0.98 m. Overall, these model components seem to perform reasonably well also for this area.

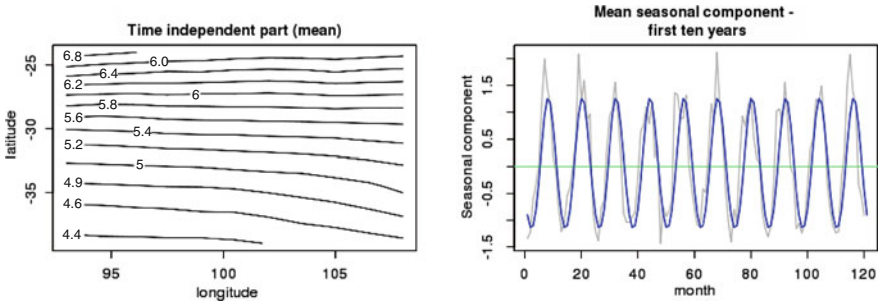

Fig. 8.24 Spatial field and seasonal contribution for Western Australia

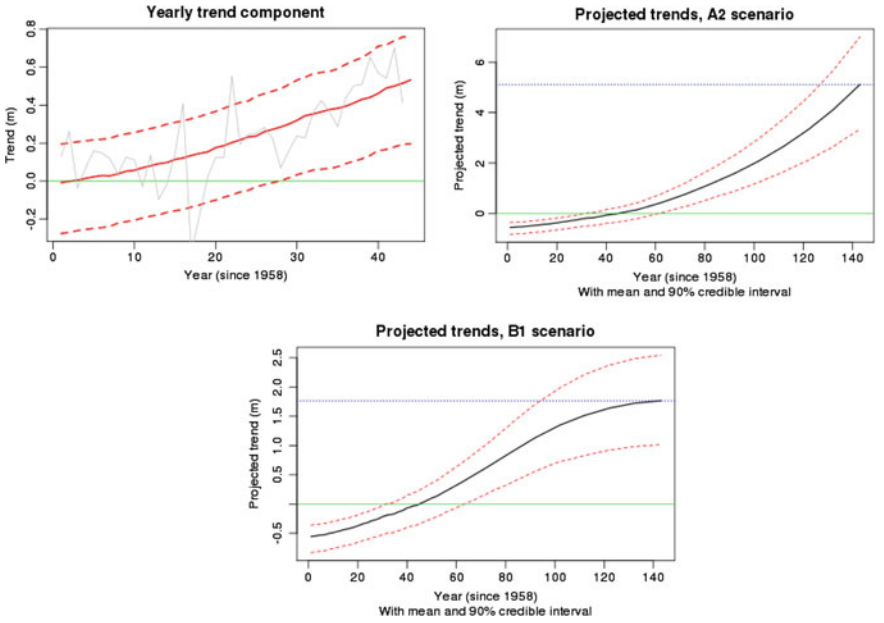

Fig. 8.25 Estimated trend and future projections for the area West of Australia

The estimated long-term trends and future projections pertaining to the area West of Australia are illustrated in Fig. 8.25, and the expected trends and future projections along with 90 % credible intervals around the mean are presented in Table 8.13.

For this area as well, the model estimates a significant increasing trend and future projections, with both expectations and 90 % credible intervals of the mean being strictly positive.

Table 8.13 Estimated trends and future projections—Western Australia

	Expectation	90 % Credible interval
Trend (1958–2001)	53 cm	20–76 cm
A2 projections (2001–2100)	5.1 m	3.3–7.0 m
B1 projections (2001–2100)	1.8 m	1.0–2.5 m

Table 8.14 Standard and weighted prediction losses

Area	NA	NEP	GoM	WAfr	NWP	IO	SP	MA	TS	MS	EP	WAust
L_s	2.544	1.845	0.803	0.630	2.149	0.630	1.029	0.394	1.313	1.383	0.537	1.174
L_w	2.656	1.867	0.815	0.639	2.042	0.655	1.022	0.395	1.297	1.367	0.538	1.178

8.3 Prediction Losses

Even though it is not entirely meaningful to compare the results for different ocean areas, the prediction losses according to the standard and weighted loss functions are calculated in order to get an indication of how well the model performs for the various datasets. Hence, the calculated losses are presented for each ocean area in Table 8.14. The prediction losses correspond to the mean squared prediction error for last time-point, T, with and without a weight introduced to penalize prediction errors for large significant wave heights. Regarding the losses estimated for the North Atlantic Ocean, it is reassuring to observe that the losses in Table 8.14 agree quite well with the losses presented in Chap. 5 [16].

It is emphasized that these losses pertain to different datasets, so they cannot be compared directly; it is merely noted that the losses vary considerably between areas. The losses for the North Atlantic and the North West Pacific are the highest. However, these are also the areas with the most severe wave climate as well as the strongest estimated trends. Therefore, it might not be surprising that these are also associated with the highest prediction losses; it does not necessarily mean that the models perform worst in these areas.

8.4 Discussion

The Bayesian hierarchical space-time model for significant wave height has been applied to several ocean areas throughout the globe, and overall the model seems to perform well. The results seem reasonable and the contributions from the various model components seem to be able to distinguish between the different features pertaining to the various areas.

The time-independent part, $\mu(x)$ gives different patterns of spatial variability for the various ocean areas. For most of the areas, the main variability seems to be in

the north-south direction, which is reasonable, but for some areas, the variability in the east-west direction is found to dominate, most notably in the Gulf of Mexico. The areas with the highest values for this mean spatial field, taking into account the starting value of the long-term trend, are the North Atlantic, South Pacific, North East and North West Pacific and the area West of Australia. These are the areas furthest away from Equator, so this seems reasonable.

The short-term dynamic part with dependencies in both space and time, $\theta(x, t)$, also seems to perform well, and the strongest contributions from this component are found in the North Atlantic, the North East Pacific, the North West Pacific, and in the South Pacific oceans. This may indicate that the model identifies these areas as the stormiest.

It is reassuring to observe that the seasonal model seems to perform well, and it captures the shift of seasonality when going from the Northern to the Southern Hemisphere. For all areas lying to the north of Equator, the boreal winter season corresponds to the highest contribution from this component, whereas the areas south of Equator have a higher contribution during the boreal summer months. The model has difficulty in detecting any seasonal contribution for the Equatorial Pacific area, which is centred around Equator. Hence, the seasonal contribution for this area is mostly noise, and this makes sense. It is the three northernmost areas, the North Atlantic, North East Pacific and North West Pacific Ocean areas that have the highest seasonal variations and this again is reasonable. It is also interesting to note that the annual dominates over the semiannual seasonal contribution for all areas subjected to investigation. The areas where the semiannual contributions are highest are in the North Atlantic, the North East and North West Pacific, and the Gulf of Mexico. However, even in these areas, the annual contributions are much stronger.

With regard to the long-term trends and future projections, significant increasing expected trends were estimated for almost all the areas. The most striking exceptions are the Gulf of Mexico and the Mediterranean Sea. These results might indicate that the trends are very different for these ocean areas, but it might also reflect the limited spatial coverage. As it were, these particular areas have a limited spatial range compared to the other areas, and it might also be that this limitation influences the simulation results. It has been reported previously [14] that there might be some edge effects that has not been taken into account, and hence that a large area is needed for the model to perform well. However, due to the geography, it is not possible to extend these particular ocean areas to contain more grid points.

For all other areas, a significantly increasing trend in monthly maximum significant wave height is estimated, with expected increases toward 2100 varying from 1.8–5.9 m according to the A2 emission scenario and between 62 cm and 2.0 m for the B1 scenario. The largest future increases in the ocean wave climate are projected for the North West Pacific (off the coast of Japan), the North Atlantic, West of Australia, and the North East Pacific.

It is noted that all future projections are associated with high uncertainties, and reservations are made concerning the accuracy of the above results. One critical assumption inherent in the results is that there is a stochastic dependence between the atmospheric level of CO_2 (as a proxy for the level of greenhouse gases and

thereby also for the radiative forcing of the globe) and that this will remain largely unchanged in the future. Furthermore, there might be bias and uncertainty in the input data for significant wave height and CO_2 and all results are conditioned on the input data. Nevertheless, it is believed that the results obtained from the model are interesting, and according to this stochastic model, there will be an increase in the monthly maximum sea states for almost all of the investigated areas.

It would be interesting to compare the projections made from the Bayesian hierarchical space-time model with other projections reported in the literature. However, future projections are highly scenario-dependent and will also be dependent on season and location. Hence, direct comparison might be difficult. Notwithstanding, a brief review of some relevant previous studies is deemed appropriate.

Future projections of the ocean wave climate are investigated in [3], where sea level pressure fields were used as regressors. Results were found to be very dependent on scenario and on season and location, but significant positive trends are predicted in the North Pacific. The relationship between significant wave height and sea level pressure was also utilized in [18], which projected increases in the North East Atlantic for both winter and fall seasons accompanied by decreases in the mid-latitudes of the North Atlantic and increases in the south-west North Atlantic. Projections toward 2080 were also reported in [19] and significant increases were found in areas of the North Pacific and the North Atlantic, by up to 50 cm for the seasonal extremes. Increases were also projected near the Antarctic coast and in the subtropical South Pacific. However, significant decreases were projected for some regions between 40 and 60° south. Projections made in [12] also predict increases in significant wave height by up to 0.4 m over a wide area of the western North Pacific. In [10], projections of the wave climate for the Pacific Ocean are made and it is found that future wave climate changes to lower mean and higher extremes in the middle latitudes and higher mean and maximum wave heights in the high latitudes. Hence, according to this study, the future wave climate will experience both negative and positive changes depending on the region.

Possible changes in future wave climate were also studied in [4], and increases in the extremes were predicted for the eastern North Sea, by 6–8 % and west of the British Isles. South of Iceland, a decrease of 4–6 % was predicted. Buoy data have been analysed in [11] in order to make projections of the wave climate offshore from the U.S. Pacific Northwest. An increase of annual maximum wave height of 0.095 m per year is reported, along with an increase of 0.071 per year for the average of the five highest waves. This would correspond to an increase between 7.1 and 9.5 m for extreme waves over 100 years. This is higher than the projections made in the study presented herein, but since this study is concerned with monthly maxima rather than annual maxima, the results might still be consistent. A recent multimodel ensemble study presented global wave climate projections, and reported that a decreasing trend in annual mean significant wave heights was found for large parts of the globe [7]. This appears to contradict the results presented in this chapter, but it is stressed that projections of extreme sea states were not reported in [7], and decreasing annual means might not necessarily contradict increases in the extremes such as the monthly maxima, see also [10].

A study on the Mediterranean Sea reports that future ocean wave climate will be milder than the present wave climate [9] and that the changes would be larger for the A2 than for the B2 scenario. This actually agrees with the results presented herein, which predicted a slight decrease for the Mediterranean Sea. Wave climate projections are also reported for the Portuguese coast in [1]. The uncertainty of the impact of climate change on future extreme wave conditions in the North Sea is investigated in [5] by running a wave model over an ensemble of different climate change realizations for the 30-year period 2071–2100. The study revealed that there are large uncertainties in the magnitude and the spatial patterns of the climate change signals and indicates that the uncertainties due to different climate models are larger than the uncertainties related to the different scenarios.

Long-term trends in the ocean wave climate off Western Australia were investigated in [2] and they report an increasing trend of 32 cm over a 40-year period from 1970 to 2009. This is slightly less than the long-term trend estimated in the study presented herein, but it is well within the 90 % credible interval. It should also be noted that the areas are not exactly the same but overall the agreement is reasonably good between the two studies.

The model presented in this paper uses the stochastic relationship between levels of CO_2 in the atmosphere and significant wave height. It is acknowledged that this is a simplification, and that there are several mechanisms in between that has not been modeled directly. For example, ocean waves are generated by winds [8], which are again results of air pressure gradients. A more refined model could include several levels of explanatory variables, including wind fields and fields of sea level pressures as well as other relevant meteorological variables. For example, the North Atlantic Oscillation (NAO) index could be a relevant covariate for explaining changes in the wave climate in the North Atlantic Ocean [6, 13, 20]. This has not been tried out to date and remains possible alternatives for further model extensions.

There is a number of factors influencing future projections of ocean wave climate, and future changes are expected to be highly dependent on region, season, percentile of the distribution and adopted forcing scenarios as well as modeling approach, model assumptions, input data etc. Hence, direct comparison may not be feasible in most cases. Nevertheless, most studies seem to agree that there is an expected increasing trend in the ocean wave climate for many areas of the globe even though the uncertainty of any long-term projection remains large.

8.5 Conclusion

This chapter has presented the results obtained from applying the Bayesian hierarchical space-time model to estimate long-term trends and future projections on the ocean wave climate on various ocean areas throughout the globe. Such trends might be a result of global climate change, and a stochastic dependence between significant wave height and levels of CO_2 in the atmosphere has been assumed and exploited.

According to the results obtained from the model, most of the investigated areas, except perhaps two, are expected to experience a trend toward rougher ocean wave

climate toward 2100, with the strongest trends being associated with ocean areas in the North West Pacific (off the coast of Japan), the North Atlantic, West of Australia, and North East Pacific. Qualitatively, the fact that the ocean wave climate is expected to be rougher is in agreement with many previous studies on future wave climate changes, but there is great uncertainty as to how large future changes will be. Nevertheless, it is believed that the results presented herein, estimating future trends in the wave climate pertaining to several ocean areas around the globe, based on a stochastic model with regression on CO_2 levels in the atmosphere, is an important contribution to the scientific discussion and that it might stimulate and motivate further research in this important area, with important implications for maritime and coastal safety.

References

1. Andrade, C., Pires, H., Taborda, R., Freitas, M.: Projecting future changes in wave climate and coastal response in Portugal by the end of the 21st century. J. Coastal Res. SI **50**, 253–257 (2007)
2. Bosserelle, C., Pattiaratchi, C., Haigh, I.: Inter-annual variability and longer-term changes in the wave climate of Western Australia between 1970 and 2009. Ocean Dyn. **62**, 63–76 (2012)
3. Caires, S., Swail, V.R., Wang, X.L.: Projection and analysis of extreme wave climate. J. Clim. **19**, 5581–5605 (2006)
4. Debernard, J.B., Røed, L.P.: Future wind, wave and storm surge climate in the Northern Seas: a revisit. Tellus **60A**, 427–438 (2008)
5. Grabemann, I., Weisse, R.: Climate change impact on extreme wave conditions in the North Sea: an ensemble study. Ocean Dyn. **58**, 199–212 (2008)
6. Greatbatch, R.: The North Atlantic Oscillation. Stoch. Env. Res. Risk Assess. **14**, 213–242 (2000)
7. Hemer, M.A., Fan, Y., Mori, N., Semedo, A., Wang, X.L.: Projected changes in wave climate from a multi-model ensemble. Nat. Clim. Change Advance online publication, 1–6 (2013)
8. Janssen, P.A., Viterbo, P.: Ocean waves and the atmospheric climate. J. Clim. **9**, 5581–5605 (1996)
9. Lionello, P., Cogo, S., Galati, M., Sanna, A.: The Mediterranean surface wave climate inferred from future scenario simulations. Global Planet. Change **63**, 152–162 (2008)
10. Mori, N., Yasuda, T., Mase, H., Tom, T., Oku, Y.: Projection of extreme wave climate change under global warming. Hydrol. Res. Lett. **4**, 15–19 (2010)
11. Ruggiero, P., Komar, P.D., Allan, J.C.: Increasing wave heights and extreme value projections: the wave climate of the U.S. Pacific Northwest. Coast. Eng. **57**, 539–552 (2010)
12. Sasaki, W., Hibiya, T., Kayahara, T.: Interannual variability and future projections of summertime ocean wave heights in the western North Pacific. Ocean Sci. Discuss. **3**, 1637–1651 (2006)
13. Ulbrich, U., Christoph, M.: A shift of the NAO and increasing storm track activity over Europe due to antrophogenic greenhouse gas forcing. Clim. Dyn. **15**, 551–559 (1999)
14. Vanem, E., Huseby, A.B., Natvig, B.: A Bayesian hierarchical spatio-temporal model for significant wave height in the North Atlantic. Stoch. Env. Res. Risk Assess. **26**, 609–632 (2012)
15. Vanem, E., Huseby, A.B., Natvig, B.: Modeling ocean wave climate with a Bayesian hierarchical space-time model and a log-transform of the data. Ocean Dyn. **62**, 355–375 (2012)
16. Vanem, E., Huseby, A.B., Natvig, B.: Bayesian hierarchical spatio-temporal modelling of trends and future projections in the ocean wave climate with a CO_2 regression component. Environmental and Ecological Statistics (in press) (2013)

17. Vanem, E., Natvig, B., Huseby, A.B.: Modelling the effect of climate change on the wave climate of the world's oceans. Ocean Sci. J. **47**, 123–145 (2012)
18. Wang, X.J., Zwiers, F.W., Swail, V.R.: North Atlantic ocean wave climate change scenarios for the twenty-first century. J. Clim. **17**, 2368–2383 (2004)
19. Wang, X.L., Swail, V.R.: Climate change signal and uncertainty in projections of ocean wave heights. Clim. Dyn. **26**, 109–126 (2006)
20. Wanner, H., Brönnimann, S., Casty, C., Gyalistras, D., Luterbacher, J., Schmutz, C., Stephenson, D.B., Xoplaki, E.: North Atlantic Oscillation—consepts and studies. Surv. Geophys. **22**, 321–382 (2001)

Chapter 9
Summary and Conclusions

How to adapt to climate change is one of the most important questions in society today. It is a political question and perhaps a moral question as much as it is a scientific question. Nevertheless, an important prerequisite for making well-founded decisions is a reliable prediction of the future effect of climate change. The stochastic model presented in this monograph aims at contributing to this discussion by providing a model for predicting the effect of climate change on the ocean wave climate. Such an effect could again have practical implications in many areas of society, most notably related to marine and coastal management.

This monograph has presented recent research on the development of stochastic models for significant wave height, an important parameter in the description of the ocean wave climate, and also an important parameter in design of ships and offshore structures. The first chapter gives an introduction to the problem area and discusses why stochastic models for significant wave height are of great interest to the maritime industries. Then, Chap. 2 presents a thorough literature review on stochastic wave models and also includes a review of stochastic models from other areas of applications. A number of different modeling approaches were covered, and the framework of Bayesian hierarchical space-time models was identified as a promising approach for modeling significant wave height in space and time.

Hence, such a model was developed, as outlined in Chap. 3, consisting of different components in space and time; a purely spatial component, a dynamic space-time component, an annual seasonal component, and a long-term trend component. The latter was included in order to identify long-term trends in the data, which may possibly be a result of climate change. Various model alternatives were also tried, where the difference was in how the long-term trend component was modeled. These models were then fitted to spatio-temporal data of significant wave height for an area in the North Atlantic ocean, stemming from the ERA-40 hindcast study, and overall the models seem to perform well. Long-term trends were extracted from the data, which were in reasonable agreement with several previous studies, albeit not all. Finally, estimated linear trends in the data were extrapolated 100 years into the future to provide future projections of significant wave height for the area under

E. Vanem, *Bayesian Hierarchical Space-Time Models with Application to Significant Wave Height*, Ocean Engineering & Oceanography 2,
DOI: 10.1007/978-3-642-30253-4_9, © Springer-Verlag Berlin Heidelberg 2013

consideration. The models were implemented using Markov chain Monte Carlo methods and a Bayesian approach, utilizing prior knowledge by the way of mostly informative prior distributions.

It was observed that the significant wave height data displayed some heteroscedastic features, even after subtracting the seasonal mean. Furthermore, it was observed that there was a stronger trend in the extremes, i.e., monthly maxima, compared to the average conditions. This motivated the introduction of a logarithmic transformation of the data. Hence, a revised model for log-transformed data and the results obtained from fitting the model to log-transformed data were presented in Chap. 4. This model also identifies long-term trends in the data, but the interpretation of the model and its various components are essentially different from the original model. Each model component is now a multiplicative factor rather than an additive term. Hence, the long-term trend is described by a factor which effectively yields a greater trend for extremes compared to non-extremes. Also these models were found to perform reasonably well, even though direct comparison with the results pertaining to the original model was not straightforward.

The effect of including a semiannual seasonal component was also investigated in Chap. 4, but this was found to be insignificant, at least for this particular ocean area, and overall the results were largely unaffected by such an extension. Furthermore, the need to account for re-transformation biases when working with transformed data was discussed, and a bias correction factor was included when needed.

It is acknowledged that merely identifying a linear trend in the data and then extrapolating this trend into the future is somewhat speculative, and it was argued that more reliable projections could be made if the model was extended with sensible covariates. Thus, in Chap. 5, the model was extended with a regression component with atmospheric levels of CO_2 as covariates. Data of historic levels of CO_2 in the atmosphere were obtained, and future projections based on two emissions scenarios were used for model fitting and prediction. The two scenarios represent an extreme scenario, A2, which may be construed as a worst-case scenario, and a more conservative scenario, B1. Consequently, based on these scenarios, future projections of trends in the ocean wave climate were obtained from the extended model.

According to the simulations of the model with the A2 scenario for future CO_2-levels, an expected increase of monthly maximum significant wave height of 5.4 m were estimated for the area in the North Atlantic ocean toward the year 2100. This is quite extreme, but it should be kept in mind that this corresponds to a worst-case scenario. The average monthly maximum significant wave height is about 7.5 m, so this expected increase corresponds to an increase of 72 %. However, the uncertainties are large, with a 90 % credible interval for the expected increase ranging from 2.7 to 8.1 m. For the more conservative scenario, B1, the expected increase in monthly maximum significant wave height is 1.9 m, with a 90 % credible interval ranging from 1.2 to 2.6 m. This corresponds to an increase of about 25 %.

The same modeling framework was applied to monthly maximum wind speeds in the North Atlantic in Chap. 6. It was demonstrated that the estimated increases in the wave climate were not accompanied by a similar trend in the wind climate. On the contrary, the results indicate a possible decreasing trend for the North Atlantic

windiness although very weak and not statistically significant. Accordingly, it is suggested that the observed increase in significant wave height may not be because of increased wind sea, but can possibly be explained by an increase in swell.

In Chap. 7, it is demonstrated how the estimated long-term trends and future projections of significant wave height can be applied to load and response calculations of ships. Hence, the potential impact of changes in future sea states on ship structural loads is considered, using the conditional modeling approach and taking due note of inherent uncertainties. For illustrations, loads characteristics for an example oil tanker were calculated. Based on these calculations, it was found that the estimated linear trends in monthly maximum significant wave height over 100 years corresponds to an increase of the 25-year stress amplitude by 7 % and an increase of 2 % in the zero-crossing response period. Alternatively, using the trends obtained by the extended model and assuming the B1 emission scenario, an increase of 10 % for the 25-year stress amplitude was calculated.

Finally, a case study on how the model estimates long-term trends and makes future projections for various other ocean areas throughout the world is reported. According to the results obtained from the model, increasing trends are expected for the wave climate for 10 of 12 investigated ocean areas and hence, according to the model there will be a rougher wave climate of many of the oceans around the globe. However, as in all future projections, uncertainties are large and reservations should be made regarding the accuracy of the results. Notwithstanding, it is believed that the results obtained by the stochastic model presented in this book are an important contribution to the scientific discussion on the effects of climate change and it is hoped that it might stimulate further research on this important area, with important implications for the safety of life at sea and in coastal areas.

9.1 Open Issues and Suggestions for Further Work

Even though the models presented in this monograph have been found to perform reasonably well overall, and to produce results that agree fairly well with previous studies, some open issues have been identified that may be the focus on further work.

The model has been fitted to data of different temporal resolutions, i.e., using monthly, daily, and six-hourly data, as well as monthly maximum data. However, as it turned out, the model performed poorly on the six-hourly dataset. It did not mix well and, possibly, the Markov chain failed to converge. The reason for this is uncertain. Simulations on the six-hourly dataset were too time consuming for it to be practical to investigate whether a longer burn-in period for the MCMC-simulations would solve the problem, but presumably not. One possible explanation for why the model performs poorly on six-hourly data is that the linear form of the short-term dynamic part $\theta(x, t)$ might not be able to describe possible nonlinear effects at high temporal resolutions. It could be interesting to try to extend the model with nonlinear dynamic components, but this idea has so far not been pursued.

No attempts have been made to control the long-term behavior of the short-term dynamic component $\theta(x, t)$, for example, by imposing restrictions on the vector-autoregressive parameters. This could be introduced in order to make this stationary over long-time periods and hence prevent it from absorbing possible long-term trends in the data. Upon inspection, the long-term effect of $\theta(x, t)$ is found to be negligible, so this is presumably not a serious issue, but it could still be sensible to impose some constraints on the parameters pertaining to this component. Possibly, this could lead to better performance of the model when applied to the full dataset, with temporal resolution of 6 h. It would also be interesting to explore the possible effects of the spatial resolution in the data on future projections and the overall results.

The model was extended with atmospheric CO_2-levels as covariates, but it is acknowledged that making regression directly on the atmospheric CO_2 level is a simplification. The model could be further extended with other meteorological parameters as explanatory variables and include different layers of dependencies. Wave evolution in time and space is mainly a result of wind forcing, and in order to provide long-term predictions related to climate change, evidence of which may yet not be present in the historical data, it may be necessary to include covariates that are closer related to the physics governing the generation of waves. Hence, the inclusion of fields of mean sea level pressure or wind fields in the area as additional covariates is one alternative for further model extensions. In order to make future projections, reasonable projections of such fields would then be needed and there are presently large uncertainties associated with any such projections.

Another alternative could be to include different temporal trends for different seasons. For example, four different temporal trends could be included to allow for different trends in spring, summer, autumn, and winter seasons. It is believed that these trends could be significantly different, and that such a refinement could lead to better model performance. Furthermore, the model could incorporate a temporal trend in the variance (spread) of the data. It is acknowledged that changes in the extreme wave climate can result from a change in the variance even without a significant change in the mean (or indeed, even with an opposite change of the mean). The combined effect of a change in the spread and the mean could be significant and an extended model incorporating a temporal long-term trend in the variance could yield interesting insight. Other possible extension could be to allow the parameter b_0 to vary spatially or to try some other reasonable transformation of the data. Such, and other, model extensions have not been made till date and is left for future work.

Different attempts of model comparison and selection have been tried out, but reliable model selection remains an open issue. Model selection for such complex, hierarchical models are indeed challenging, and there are no standard solutions. For the purpose of this study, two loss functions based on short-term predictive power have been constructed but it is acknowledged that these might not be ideally suited for distinguishing between models with different long-term components. Furthermore, the results are not consistent over all simulations and the loss functions cannot really identify the best models with great confidence. For example, whether the inclusion of a logarithmic transformation of the data represents an improvement or not is inconclusive. On the one hand, the transformation seemed to yield better goodness-

of-fit, whereas it also gave larger losses according to the loss functions. However, for the extended models with CO_2-regression components, model ranking seemed to be rather consistent. Notwithstanding, model selection remains an open issue, and future work could be focused on developing more reliable model selection methods for such complex models.

A logarithmic transformation of the significant wave height data was tried, as reported in Chap. 4. This mended the heteroscedastic features in the data to a large degree, and also estimated higher trends for more severe sea states, but results indicated that the logarithmic transformation might not be the optimal transformation. Hence, one suggestion for further work is to investigate how other nonlinear data transformations perform. Possibly, this would give both better goodness-of-fit and less prediction losses. However, it is not trivial exactly what kind of data transformation would be optimal.

Another issue, even though perhaps not a very serious one, is that the results indicated that there were some edge effects in the spatial field. No particular effort has been placed on how to treat the edge effects in the Markov random field, and possibly, a more explicit modeling of the edges, i.e., grid-points without neighbors in any direction, could improve the results. This is also left for future work and refinement of the model.

Notwithstanding these open issues, the models presented in this monograph are believed to perform reasonably well overall and they seem to be able to capture the variability in space and time of the significant wave height of an area in the North Atlantic Ocean and elsewhere. In particular, long-term trends have been estimated, and realistic future projections of the ocean wave climate toward the year 2100 have been obtained. Even though different model alternatives have been applied, each estimating different long-term trends, all model alternatives are able to detect an increasing trend in the ocean wave climate, and it can be concluded that there are likely to be an effect of climate change on the significant wave height in the North Atlantic Ocean. It is also deemed likely that this effect is not negligible and that the effect on long-term will be large enough to influence the structural loads and responses of ocean-going ships. Thus, even though uncertainties are substantial, it is recommended that the possible effects of climate change are considered in loads calculations of new designs and that potential impact of climate change are taken into account in ship design specifications. Obviously, such effects would also need to be taken into account for other marine structures related to offshore and coastal activities.

It is acknowledged that the models presented herein represent a simplification of reality, as inevitably all models do, and that there is potential for improvements to the models. Nonetheless, it is believed that the presented research is an important contribution to the scientific debate on the effects of climate change, and it is a hope that it can spur further debate and motivate further research into the effects of climate change on the future ocean wave climate.

Appendix A
Markov Chain Monte Carlo Methods

In this appendix, the basics of Markov chain Monte Carlo methods for simulating from statistical distributions will be briefly outlined and the Gibbs sampler and Metropolis-Hastings algorithm will be explained. For further details, reference is made to [1] or similar textbooks.

A.1 Standard Monte Carlo Integration

Classical Monte Carlo integration is a method for solving analytically challenging integrals using Monte Carlo simulation. The basic idea is as follows: Consider an integral on the form

$$I = \int_{\chi} \overline{h}(x)\mathrm{d}x = \int_{\chi} h(x)f(x)\mathrm{d}x = E_f\left[h(x)\right]$$

where $f(x)$ is a density. This is then recognized as the expectancy of $h(x)$ with respect to the density $f(x)$, as shown above. If it is possible to simulate or generate a number of iid $x_i \sim f(x), \quad i = 1, \ldots, m$, then the standard Monte Carlo estimator for the integral I is the empirical average, which converges towards the integral for m sufficiently high:

$$\delta_{MC} = \overline{h}_m = \frac{1}{m}\sum_{j=1}^{m} h(x_j) \longrightarrow I, \quad m \to \infty$$

This technique of estimating the integral I using generation of iid random variables $x_i \sim f(x)$ is referred to as classical Monte Carlo integration. However, the challenge to generate the random variables from $f(x)$ remains, and for some densities direct simulation from f will be difficult. Some alternative methods to direct sampling for simulating from the distribution $f(x)$ are the inversion method, accept–reject sam-

E. Vanem, *Bayesian Hierarchical Space-Time Models with Application to Significant Wave Height*, Ocean Engineering & Oceanography 2,
DOI: 10.1007/978-3-642-30253-4, © Springer-Verlag Berlin Heidelberg 2013

pling and importance sampling, to be briefly outlined in the following, and Markov chain Monte Carlo. The latter approach will be briefly outlined in the subsequent sections.

A.1.1 Inversion Sampling

For densities where the cumulative distribution function $F(x)$ is strictly increasing, one may simulate $X \sim f(x)$ by the inversion method. The algorithm for this simulation is quite simple:

1. Generate random uniform variables on the unit interval $U_i \sim U_{[0,1]}$
2. Then $X = F^{-1}(U) \sim f(x)$ will be a random variable from $f(x)$

The following proof demonstrates that X is indeed a random variable from the distribution $f(x)$, i.e., that $X = F^{-1}(U)$ has cumulative distribution function $F(X)$:

$$P(X < x) = P\left(F^{-1}(U) < x\right) = P(U < F(x)) = F_U(F(x)) = F(x)$$

since the uniform distribution has cumulative distribution function $F_U(x) = x$. However, this method has the weakness that F needs to be invertable, i.e., $F^{-1}(u)$ is required, and it is difficult to generalize to large dimensions.

A.1.2 Accept–Reject Simulation

The accept–reject method simulates candidates y_i for x_i from a proposal distribution $g(x)$ rather than from the target density $f(x)$, and accepts these with a probability that ensures that the accepted samples correspond to the target distribution $f(x)$. The basic idea is that sampling from the proposal distribution may be easier than simulating directly from the target distribution. The requirements on the proposal distribution are simply that $f(x) \leq Mg(x)$ for the whole support of $f(x)$ and some constant M. Generally, the acceptance rate of proposed candidates increases, and thus the efficiency of this method improves, for low values of M. The algorithm for accept–reject sampling is as follows:

1. Generate a candidate from the proposal distribution, i.e., generate $Y_i \sim g(x)$.
2. Accept this candidate with probability $P_{\text{accept}} = \frac{f(x)}{Mg(x)} \leq 1$, i.e., put $X_i = y_i$ with this probability
3. Otherwise, reject the candidate y_i and repeat step 1.

The acceptance step may be implemented by generating a uniform random variable U on the unit interval, and accepting the candidate $x_i = y_i$ if $u < P_{\text{accept}}$. It is noted that the overall rate of accepted candidates is the inverse of the constant M, $P_{\text{accept}} = 1/M$

so it is realized that this method performs best when $g(x)$ is close to $f(x)$. The optimal proposal distribution in terms of efficiency is of course $g(x) = f(x)$ but this is equivalent to direct simulation.

It can be proved that the accepted candidates are indeed distributed as $f(x)$, using Bayes theorem:

$$P(x = y) = P(y|y \text{ accepted}) = \frac{P(y \text{ accepted}|y)P(y)}{\int_\chi P(z \text{ accepted}|z)P(z)\mathrm{d}z}$$

but now, by construction: $P(y \text{ accepted}|y) = P_{\text{accept}} = \frac{f(y)}{Mg(y)}$ and $P(y) = g(y)$, and therefore

$$P(x = y) = \frac{\frac{f(y)}{Mg(y)}g(y)}{\int_\chi \frac{f(z)}{Mg(z)}g(z)\mathrm{d}z} = \frac{f(y)}{\int_\chi f(z)\mathrm{d}z} = f(y)$$

since the integral over a distribution is 1 by definition. With this in mind, it is also straightforward to demonstrate that the ratio of accepted y_is is indeed $1/M$ from the law of total probability:

$$P(\text{accepting } y) = \int_\chi P(\text{accepting } z|z)P(z)\mathrm{d}z = \int_\chi \frac{f(z)}{Mg(z)}g(z)\mathrm{d}z = \frac{1}{M}$$

It can also be shown that the accept–reject method is independent of possible normalizing constants of the target distribution, so that samples of a density $f(x)$ on the form $f(x) = \frac{g(x)}{I}$, where $I = \int g(x)\mathrm{d}x$ can be obtained from sampling from a proposal distribution $h(x)$ so that $g(x) \leq Kh(x)$ for some constant K, and then accepting this proposal with probability $\frac{g(x)}{Kh(x)}$.

A.1.3 Importance Sampling

Another method that allows sampling from an alternative distribution function $g(x)$ other than the target distribution $f(x)$ when estimating Monte Carlo integrals is the method of importance sampling. It is noted that this method may also give higher precision than standard Monte Carlo, i.e., than sampling directly from the target distribution in estimating a Monte Carlo integral, for sensible choices of proposal distributions. Recalling the integral subject to Monte Carlo integration, and rewriting this as:

$$I = \int_\chi h(x)f(x)\mathrm{d}x = \int_\chi \frac{f(x)h(x)}{g(x)}g(x)\mathrm{d}x = E_g\left[\frac{f(x)h(x)}{g(x)}\right]$$

An estimator for this integral can now be based on a simulated sample drawn from $g(x)$, $X_i \sim g(x), i = 1, \ldots, m$ and a weighted average of $h(x_i)$ where the weights corresponds to a correction that is needed since the simulated x_is now are from $g(x)$ instead of $f(x)$:

$$\delta_{IS} = \frac{1}{m}\sum_{j=1}^{m}\frac{f(x_j)h(x_j)}{g(x_j)} = \frac{1}{m}\sum_{j=1}^{m} w_j h(x_j), \quad w_j = \frac{f(x_j)}{g(x_j)}$$

Finally, it is noted that for the importance sampling method to work, appropriate proposal distributions $g(x)$ must be chosen. For example, the weights should be finite and one condition for this is that $f(x) \leq Mg(x)$ for all x within the support of $f(x)$ and some constant M. Furthermore, the variance of the estimator should be finite and an additional condition is that $\text{Var}_f[h(x)] < \infty$. These conditions are rather restrictive, and as a rule of thumb, if $g(x)$ is chosen so that it has heavier tails than $f(x)$, importance sampling works well.

Sequential importance sampling is a generalization of the importance sampling algorithm described above where the proposal distribution is sequentially updated. This may be useful when the parameter of interest changes over time, e.g., when we want to make inference about the variable of an autoregressive model. In this case, within the context of importance sampling, both the target distribution $f(x)$ and the proposal distribution $g(x)$ changes sequentially, and sequential importance sampling is a method to simulate such data, where samples are drawn from a conditional proposal distribution, sequentially updated conditionally on the previous time-step with weights that are sequentially updated as well.

A.2 Monte Carlo Variance

The Monte Carlo estimate converges asymptotically to the true value of the integral of interest as the number of simulations increases. In order to evaluate the precision of the Monte Carlo estimate, the variance of the Monte Carlo estimate compared to the variance of the integral function, $h(x)$ may be investigated. The variance of the Monte Carlo estimate is

$$Var[\bar{h}_m] = Var\left[\frac{1}{m}\sum_{j=1}^{m} h(x_j)\right] = \frac{1}{m^2}Var\left[\sum_{j=1}^{m} h(x_j)\right] = \frac{1}{m}Var_f[h(x)]$$

where $Var_f[h(x)]$ now is the variance of the function $h(x)$ with respect to $f(x)$, since $x_1, \ldots, h_m$ are iid samples from $f(x)$. Therefore, as $m \to \infty$, $Var[\bar{h}_m] \to 0$.

In general, the Monte Carlo variance will increase for dependent samples with a positive correlation structure. If now $\bar{h}_m$ is an estimator based on dependent samples of $f(x)$ the corresponding variance becomes

$$\mathrm{Var}[\bar{h}_m] = \frac{1}{m^2}\mathrm{Var}\left[\sum_{j=1}^{m} h(x_j)\right] = \frac{1}{m^2}\left[\mathrm{mVar}_f[h(x)] + \sum_{i=1}^{m}\sum_{i\neq j} Cov(h(x_i), h(x_j))\right]$$
$$= \frac{1}{m}\mathrm{Var}_f[h(x)]\left[1 + \frac{1}{m}\sum_{i=1}^{m}\sum_{i\neq j}\mathrm{Corr}(h(x_i), h(x_j))\right]$$

Hence, it can be seen that using dependent samples with a positive correlation structure will result in increased variance of the Monte Carlo estimate.

A.3 Markov Chain Monte Carlo

An alternative, useful technique for simulating random variables from a target distribution $f(x)$ is the Markov chain Monte Carlo method. The aim of this method is to construct a Markov chain, $\{X_t\} = X_1 \rightarrow X_2 \rightarrow \ldots \rightarrow X_N$ which has $f(x)$ as its invariant distribution. If the chain in addition is *ergodic*, this distribution will also be the limiting distribution of the chain independent on the starting point, i.e., the distribution of X_t converges to $f(x)$ for t large enough. Then, by allowing the chain to run long enough, the $\{X_t\}$ will represent samples from $f(x)$. Note however, that this will **not** be *independent samples* from $f(x)$. Mathematically, the convergence requirement can be written as:

$$\lim_{k\rightarrow\infty} P(X_k \in A) = \int_A f(x)\mathrm{d}x$$

It is also required that the estimator based on $\{X_t\}$ converges towards the Monte Carlo integral:

$$S_N = \frac{1}{N}\sum_{i=1}^{N} h(x_i) \rightarrow \int_\chi h(x)f(x)\mathrm{d}x = I, \quad N \rightarrow \infty$$

A.3.1 Essential Markov Chain Theory

A Markov chain is a sequence of random variables $\{X_t\}$ where the conditional distribution of X_t given all previous states $x_{t-1}, x_{t-2}, \ldots, x_0$ is the same as the conditional distribution of X_t given the last previous state x_{t-1}, i.e.,:

$$P(x_{k+1} \in A|x_0, x_1, x_2, \ldots, x_k) = P(x_{k+1} \in A|x_k)$$

The chain is stationary or time-homogeneous if the transition kernel does not change over time, i.e., is independent of t so that, for all k:

$$P(x_{k+1} \in A | x_k = x) = P(x_1 \in A | x_0 = x)$$

Furthermore, an invariant distribution π satisfies the following:

$$\pi(y) = \int_{\chi} K(x, y)\pi(x)\mathrm{d}x$$

where $K(x, y)$ is the transition kernel associated with the chain, i.e., in the continuous case $P(X_{k+1} \in A | X_k = x) = \int_A K(x, y)\mathrm{d}y$. χ is the complete state space of the chain. This means that if we are in a state with distribution π, $X_k \sim \pi(x)$, then also the subsequent states will have distribution π, $X_{k+1} \sim \pi(x)$, as shown below:

$$\begin{aligned} P(X_{k+1} \in A) &= \int_{\chi} P(X_{k+1} \in A | X_k = x)\pi(x)\mathrm{d}x = \int_{\chi}\int_{A} K(x, y)\mathrm{d}y\pi(x)\mathrm{d}x \\ &= \int_{A}\int_{\chi} K(x, y)\pi(x)\mathrm{d}x\mathrm{d}y = \int_{A} \pi(y)\mathrm{d}y \\ &\Rightarrow X_{k+1} \sim \pi(x) \end{aligned}$$

If this is satisfied, the chain will stay within the invariant distribution provided that it enters it at some point. However, in order to ensure that the chain surely converges towards this distribution regardless of the starting point of the chain, also referred to as an *ergodic* chain,

$$P(X_k \in A | x_0) \longrightarrow \int_A \pi(x)\mathrm{d}x, \quad k \to \infty$$

some particular conditions must apply. According to Markov chain theory, the following requirements on the random chain need to be satisfied in order for the chain to be ergodic, hence having an invariant or stationary distribution π as its limiting distribution regardless of starting point:

1. *Irreducibility*: A chain is irreducible if all states communicate so that the complete sample space may be visited by the chain, i.e.,

$$\exists\, n : \; P(x_n \in A | x_0 = x) > 0 \quad \forall\, A,\, x$$

2. *Recurrency*: If the average number of visits to an arbitrary set A is infinite, the chain is said to be recurrent. Otherwise, if the average number of visits to A is finite, the chain is transient. A chain is said to be Harris recurrent if the probability of an infinite number of returns to A is 1, and Harris recurrence ensures that the chain has the same limiting distribution for every starting point.
3. *Aperiodicity*: A chain that contains no cycles is said to be aperiodic. An aperiodic chain has period 1.

Under these conditions, the following convergence results hold:

$$P(X_k \in A) \approx \int_A f(x)\mathrm{d}x, \quad \text{for } k \text{ large}$$

$$\frac{1}{N}\sum_{k=1}^{N} h(x_k) \longrightarrow I, \quad \text{for } N \text{ large}$$

and samples from the distribution $f(x)$ can be obtained by running a Markov chain with $f(x)$ as its limiting, invariant distribution.

It is worth noting that even though the invariant distribution π is unique given a transition kernel K, this is not true the other way around. There might be several different transition kernels having the same invariant distribution, and there will hence be different choices of transition kernels to choose from corresponding to varying quality and efficiency of the implementation of the method. In the next sections, two different simulation methods based on Markov chain Monte Carlo will be briefly highlighted: the *Metropolis-Hastings* algorithm and the *Gibbs sampler* which have both been utilized in the simulation of the Bayesian hierarchical space-time model for significant wave height.

A.4 The Metropolis-Hastings Algorithm

The Metropolis-Hastings algorithm simulates random variables from a target distribution $f(x)$ via a conditional proposal distribution $q(y|x)$ by constructing a Markov chain in the following way:

- Given x_t
  1. Generate $Y_t \sim q(y|x_t)$
  2. Take:

$$X_{t+1} = \begin{cases} y_t \text{ with probability } \rho(x, y) = \min\left\{1, \frac{f(y_t)q(x_t|y_t)}{f(x_t)q(y_t|x_t)}\right\} \\ x_t \text{ otherwise} \end{cases}$$

It can be shown that $f(x)$ is the stationary distribution for the resulting Markov chain for almost any conditional proposal distribution $q(y|x)$. Furthermore, it can be shown that the detailed balance criterion is a sufficient criterion for this to be satisfied, i.e., that

$$\pi(x)K(x, y) = \pi(y)K(y, x)$$

and it can easily be shown that the Metropolis-Hastings transition kernel satisfies this criterion. For $y = x$, the detailed balance criterion is obviously satisfied, and for $y \neq x$, the Metropolis-Hastings transition kernel will be $K(x, y) = q(y|x)\rho(x, y)$. Now,

$$
\begin{aligned}
f(x)K(x,y) &= f(x)q(y|x)\rho(x,y) = f(x)q(y|x)\min\left\{1, \frac{f(y)q(x|y)}{f(x)q(y|x)}\right\} \\
&= f(y)q(x|y)\min\left\{\frac{f(x)q(y|x)}{f(y)q(x|y)}, 1\right\} = f(y)q(x|y)\rho(y,x) \\
&= f(y)K(y,x)
\end{aligned}
$$

Thus, there are hardly any restrictions on the proposal distribution $q(y|x)$. Two commonly used alternatives are the independent Metropolis-Hastings algorithm, which is a *global* approach in that the proposal distribution explores the whole support of the target distribution, and the random walk Metropolis-Hastings algorithm, which is a *local* approach in that the proposal distribution only explores states close to the current state of the chain.

A.4.1 Independent Metropolis-Hastings Algorithms

This special case of the general Metropolis-Hastings algorithm uses a proposal distribution independent of X_t, and the Markov chain is constructed by the following algorithm:

- Given x_t

1. Generate $Y_t \sim q(y)$
2. Take:

$$
X_{t+1} = \begin{cases} y_t \text{ with probability } \min\left\{1, \frac{f(y_t)q(x_t)}{f(x_t)q(y_t)}\right\} \\ x_t \text{ otherwise} \end{cases}
$$

It is observed that the acceptance probability in this case can be written as $\rho(x, y) = \min\left\{1, \frac{f(y)/q(y)}{f(x)/q(x)}\right\}$ and thus as a ratio between the target and the proposal distribution (actually, a ratio of a ratio). This is similar to the acceptance–rejection sampling method, but the algorithm is different in that the current value is kept, i.e., $X_{t+1} = X_t$, if the candidate is rejected. Ergodicity is ensured if the proposal distribution satisfies $f(x) \leq Mq(x)$ for all $x \in \text{supp } f$.

A.4.2 Random Walk Metropolis-Hastings Algorithms

A random walk sequence is typically constructed by letting Y_t, and thereby also X_{t+1}, be a perturbation around the previous X_t in the following way:

$$
Y_t = X_t + \epsilon_t, \qquad \varepsilon_t \sim g(\cdot)
$$

where normally $E[\epsilon_t] = 0$. Now, for random walk Metropolis-Hastings $q(y_t|x_t) = g(|y_t - x_t|)$ and typical choices for ϵ_t are uniform, normal or t-distributions:

$$\begin{aligned}&\text{Choice A: } \epsilon_t \sim U_{[-\sigma,\sigma]}\\ &\text{Choice B: } \epsilon_t \sim N(0,\sigma^2)\\ &\text{Choice C: } \quad \epsilon_t \sim \sigma\epsilon_t^0, \quad \epsilon_t^0 \sim t(\nu)\end{aligned}$$

For these choices, and other choices of symmetric functions g, such that $g(-t) = g(t)$, the random walk Metropolis-Hastings algorithm becomes:

- Given x_t

1. Generate $Y_t \sim g(|y - x_t|)$
2. Take:

$$X_{t+1} = \begin{cases} y_t \text{ with probability } \min\left\{1, \frac{f(y_t)}{f(x_t)}\right\} \\ x_t \text{ otherwise}\end{cases}$$

The *mixing properties* of the Markov chain, i.e., how well the chain explores the complete sample space, is determined by the acceptance probability of the candidates. If the acceptance probability is low, the resulting Markov chain will contain frequent sequences of identical states: $X_t = X_{t+1} = X_{t+2} = \ldots$ etc. since rejecting a candidate means that the chain is not allowed to jump to another state and instead takes the current state as the next state.

For the independent Metropolis-Hastings algorithm, where the proposal distribution is global in that its support includes the whole support of the target distribution, the optimal proposal distribution corresponds to maximal acceptance rates. This corresponds to proposal distributions similar to the target distribution, $q \approx f$, and also leads to small correlation between subsequent X_ts.

However, for local proposal distributions such as the random walk Metropolis-Hastings, the optimal acceptance probability should neither be too high nor too low. Low acceptance rates correspond to many subsequent states being identical, but on the other hand, a high acceptance rate corresponds to proposing only small jumps, meaning that it will take a long time to explore the whole state space. The optimal proposal distribution will therefore be a trade-off between creating proposals Y_t that are different from x_t and acceptance of the proposed y_t. As a rule of thumb, the optimum mixing properties of a random walk Metropolis-Hastings algorithm corresponds to acceptance rates around 0.3 (should at least be contained in $\rho \in [0.2, 0.7]$).

A.5 The Slice Sampler

The Slice sampler is another example of a Markov chain Monte Carlo method, but without the use of an accept–reject step. It is based on the fundamental theorem of simulation, i.e., that generation from a distribution with density $f(x)$ is equivalent to uniform generation on the subgraph of f. Realizing that

$$f(x) = \int_0^{f(x)} \mathrm{d}u$$

it is obvious that f appears as the marginal distribution of X of the joint distribution

$$(X, U) \sim U\{(x, u) : x \in \chi,\ 0 \leq u \leq f(x)\}$$

or

$$f(x, u) = I(0 \leq u \leq f(x)) \quad \text{for} \quad x \in \chi$$

Now, the fundamental theorem of simulation states that simulating $X \sim f(x)$ is equivalent to simulating $(X, U) \sim U\{(x, u) : x \in \chi,\ 0 \leq u \leq f(x)\}$. The Slice sampler utilizes this by using a random walk Markov chain with this uniform distribution as its stationary distribution.

A.5.1 2D Slice Sampler

Considering a random variable X, with distribution function $f(x)$ with support χ, and assume we want to simulate samples of X. This can be achieved through the 2D Slice sampler which explores the sample space by, given an initial starting point, iteratively going one step in one direction at a time, i.e., moving from initial point (x, u) to (x', u') by the following two steps, using the conditional distributions of U and X:

$$U|X = x \sim U\{u : 0 \leq u \leq f(x)\}$$
$$X|U = u' \sim U\{x : u' \leq f(x)\}$$

It is easily seen that using the above conditional distributions in a Markov chain indeed yields the correct stationary distribution of the chain. The transition kernel for the move $(x, u) \to (x', u')$ will be the product of kernels for each move $(x, u) \to (x, u')$ and $(x, u') \to (x', u')$:

$$K\left((x, u), (x', u')\right) = K_1\left((x, u), (x, u')\right) K_2\left((x, u'), (x', u')\right) = f(u'|x) f(x'|u')$$
$$= \frac{I(0 \leq u' \leq f(x))}{f(x)} \frac{I(u' \leq f(x'))}{A(u')}$$

where

$$A(u) = \int_{(x:\ u \leq f(x))} \mathrm{d}x = \int_{x \in \chi} I(u \leq f(x)) \mathrm{d}x$$

Now, the distribution function $f(x, u)$ is the invariant or stationary distribution of the chain if

$$f(x', u') = \int_{(x,u)} f(x, u) K\left((x, u), (x', u')\right) \mathrm{d}u\mathrm{d}x$$

which is quite straightforward to demonstrate:

$$\begin{aligned}
&\int_{(x,u)} f(x, u) K\left((x, u), (x', u')\right) \mathrm{d}u\mathrm{d}x \\
&\quad = \int_{((x,u):\, x\in\chi, 0\le u\le f(x))} \frac{I(0 \le u' \le f(x))}{f(x)} \frac{I(u' \le f(x'))}{A(u')} \mathrm{d}x\mathrm{d}u \\
&\quad = \int_{x\in\chi} \frac{I(0 \le u' \le f(x)) I(u' \le f(x'))}{A(u') f(x)} \int_0^{f(x)} \mathrm{d}u \; \mathrm{d}x \\
&\quad = \frac{I(0 \le u' \le f(x'))}{A(u')} \int_{x\in\chi} I(u' \le f(x)) \mathrm{d}x = I(0 \le u' \le f(x')) \\
&\quad = f(x', u')
\end{aligned}$$

Hence, the 2D Slice sampler is defined by the following algorithm, at iteration t:

1. Simulate $u^{t+1} \sim U_{[0, f(x^t)]}$
2. Simulate $x^{t+1} \sim U_{(x:\, u^{t+1} \le f(x^t))}$

The variable U is not really of interest apart from helping to elicit samples of X, and is often referred to as an auxiliary variable. It is also noted that the Slice sampler is valid also if f is an un-normalized density, i.e., the algorithm remains valid if $f(x) = Cf_1(x)$ and $f_1(x)$ is used instead of $f(x)$.

A.5.2 The General Slice Sampler

The general Slice sampler is a generalization of this, where the density $f(x)$ can be decomposed into k positive functions (not necessarily densities) in the following way:

$$f(x) \propto \prod_{i=1}^{k} f_i(x)$$

Now, to sample from $f(x)$, it is realized that each function $f_i(x)$ may be written as an integral, associated with an auxiliary variable w_i:

$$f_i(x) = \int I(0 \le w_i \le f_i(x)) \mathrm{d}w_i$$

and that $f(x)$ will be the marginal density of the joint distribution $(x, w_1, \ldots, w_k) \sim p(x, w_1, \ldots, w_k) \propto \prod_{i=1}^{k} I(0 \le w_i \le f_i(x))$. The corresponding generalization of the Slice sampler algorithm then becomes, at iteration t:

1. Simulate $w_1^{(t+1)} \sim U_{[0, f_1(x^{(t)})]}$

$\vdots$

k. Simulate $w_k^{(t+1)} \sim U_{[0, f_k(x^{(t)})]}$

k + 1. Simulate $x^{(t+1)} \sim U_{A^{(t+1)}}$ with $A^{(t+1)} = \left\{ y : \ w_i^{(t+1)} \leq f_i(y), \ i = 1, \ldots, k \right\}$

A.6 Gibbs Sampling

The Gibbs sampler works according to the same principles as the Slice sampler is based on, i.e., generating samples from the conditional distributions of the target distribution in order to construct a Markov chain with the target density as the invariant distribution. However, instead of utilizing auxiliary variables as in the Slice sampler, the true conditionals are used. In the following section, first the special case of the two-stage Gibbs sampler is presented followed by a generalization to the multi-stage Gibbs sampler in the subsequent section.

A.6.1 The Two-Stage Gibbs Sampler

Consider generation of random variables X and Y from a target density which is the joint density $f(x, y)$ defined on an arbitrary product space $X \times Y$. The two-stage Gibbs sampler then generates a Markov Chain (X_t, Y_t) with the following steps, starting from an initial value x_0 of the variable X, generating for $t = 1, 2, \ldots$:

1. $Y_t \sim f_{Y|X}(\cdot|x_{t-1})$
2. $X_t \sim f_{X|Y}(\cdot|y_t)$

where the marginal $(f_X, \ f_Y)$ and conditional $(f_{X|Y}, \ f_{Y|X})$ distributions associated with the joint distribution are:

$$f_X = \int f(x, y)dy \quad \text{and} \quad f_{Y|X} = \frac{f(x, y)}{f_X(x)}$$
$$f_Y = \int f(x, y)dx \quad \text{and} \quad f_{X|Y} = \frac{f(x, y)}{f_Y(y)}$$

Now, the sequence (X_t, Y_t) is a Markov chain, but also each subsequence (X_t) and (Y_t) is a Markov chain. The transition kernels of the different chains are:

$$\begin{aligned} (X_t, Y_t): &\quad K((x, y), (x', y')) = f_{Y|X}(y'|x) f_{X|Y}(x'|y') \\ (X_t): &\quad K(x, x') = \textstyle\int f_{Y|X}(y|x) f_{X|Y}(x'|y)dy \\ (Y_t): &\quad K(y, y') = \textstyle\int f_{X|Y}(x|y) f_{Y|X}(y'|x)dx \end{aligned}$$

It can easily be demonstrated that the target density $f(x, y)$ is the stationary distribution for the chain (X_t, Y_t), and also that the marginal densities are the stationary distributions for the subchains:

$$\begin{aligned}
&\int_x \int_y f(x, y) K((x, y), (x', y')) dy dx \\
&\quad = \int_x \int_y f(x, y) f_{Y|X}(y'|x) f_{X|Y}(x'|y') dx dy \\
&\quad = f_{X|Y}(x'|y') \int_x f_{Y|X}(y'|x) \int_y f(x, y) dy dx \\
&\quad = f_{X|Y}(x'|y') \int_x f_{Y|X}(y'|x) f_X(x) dx = f_{X|Y}(x'|y') \int_x f(x, y') dx \\
&\quad = f_{X|Y}(x'|y') f_Y(y') = f(x', y')
\end{aligned}$$

and considering the subchain (X_t):

$$\begin{aligned}
\int_x f_X(x) K(x, x') dx &= \int_x f_X(x) \int_y f_{Y|X}(y|x) f_{X|Y}(x'|y) dy dx \\
&= \int_y f_{X|Y}(x'|y) \int_x f_X(x) f_{Y|X}(y|x) dx dy \\
&= \int_y f_{X|Y}(x'|y) \int_x f(x, y) dx dy \\
&= \int_y f_{X|Y}(x'|y) f_Y(y) dy = \int_y f(x', y) dy = f(x')
\end{aligned}$$

The Gibbs sampler thus provides a Markov chain with the target distribution as the invariant distribution and thereby a method for sampling from this distribution. However, note that the chain needs to be investigated for irreducibility, recurrency and aperiodicity on a case by case basis.

A.6.2 Multi-Stage Gibbs Sampler

The multi-stage Gibbs sampler is a generalization of the two-stage Gibbs sampler that allows univariate sampling also for multivariate distributions and problems in high dimensions. Assume that a random variable $X \in \chi$ can be written as a vector $\mathbf{X} = (X_1, \ldots, X_p)$ for some $p > 1$, where now the X_i's may be either uni- or multidimensional. Furthermore, assume that it is possible to simulate from the corresponding conditional densities $f_1, \ldots, f_p$. In other words, it is possible to simulate

$$X_i | x_1, x_2, \ldots, x_{i-1}, x_{i+1}, \ldots, x_p \sim f_i(x_i | x_1, \ldots, x_{i-1}, x_{i+1}, \ldots, x_p) \quad \forall i \in [1, p]$$

Then, the Gibbs sampler for the transition between $\mathbf{X}^{(t)}$ and $\mathbf{X}^{(t+1)}$ is defined by the following algorithm, given $\mathbf{x}^{(t)} = (x_1^{(t)}, \ldots, x_p^{(t)})$:

1. Simulate $X_1^{(t+1)} \sim f_1(x_1 | x_2^{(t)}, \ldots, x_p^{(t)})$
2. Simulate $X_2^{(t+1)} \sim f_2(x_2 | x_1^{(t+1)}, x_3^{(t)}, \ldots, x_p^{(t)})$

   $\vdots$

p. Simulate $X_p^{(t+1)} \sim f_p(x_1^{(t+1)}, \ldots, x_{p-1}^{(t+1)})$

The densities $f_1, \ldots, f_p$ are often referred to as the full conditionals, and these are the only ones used for simulations. Thus, even for high-dimensional problems, the multi-stage Gibbs sampler provides a way to simulate only univariate variables, which may be an advantage in some cases. It is noted that in order for the Gibbs sampler to work, the conditional distributions need to be known and possible to simulate from, and this is not always the case. However, for the Bayesian hierarchical space-time models developed in this book, the various components are specified conditionally and it is quite straightforward to derive the full conditionals, except for a pair of parameters related to the Markov random field. Hence, the Gibbs sampler is an obvious choice for simulating from the model, with additional Metropolis-Hastings steps for simulating from the full conditional of the more problematic parameters.

Reference

1. Robert, C.P., Casella, G.: Monte Carlo Statistical Methods, 2nd edn. Springer, New York (2004)

Appendix B
Extreme Value Modeling

In this appendix, some of the distributions used for modeling extremes will be briefly outlined. Reference is made to textbooks such as [1] for further details, explanations and proofs.

B.1 Generalized Extreme Value Distribution

The generalized extreme value distribution (GEV) is the limit distribution of properly normalized maxima of a sequence of independent and identically distributed random variables. Hence, the GEV distribution is used as an approximation to model maxima of long sequences of random variables. Sometimes, the generalized extreme value distribution is referred to as the Fisher-Tippett distribution.

The generalized extreme value distribution is a family of continuous probability distributions developed to combine the three so-called extreme value distributions: the Gumbel, Fréchet and Weibull families, also referred to as type I, II, and III extreme value distributions. These will be outlined below.

If $X_1, X_2, \ldots, X_n$ is a sequence of independent random variables with a common distribution function, it can be shown that the maximum

$$M_n = \max\{X_1, X_2, \ldots, X_n\}$$

has a generalized extreme value distribution as a limit when $n \to \infty$. This follows from the extremal types theorem (see e.g., [1]), which says that if there exist sequences of constants $\{a_n > 0\}$ and $\{b_n\}$ so that

$$Pr\{(M_n - b_n)/a_n \leq x\} \to G(x) \quad \text{as } n \to \infty$$

for a non-degenerate distribution function G, then G is a member of the generalized extreme value family (if the distribution of the normalized $M_n^* = (M_n - b_n)/a_n$ converges, its limit distribution function will be a member of the GEV family).

E. Vanem, *Bayesian Hierarchical Space-Time Models with Application to Significant Wave Height*, Ocean Engineering & Oceanography 2,
DOI: 10.1007/978-3-642-30253-4, © Springer-Verlag Berlin Heidelberg 2013

Then, it can also be shown that the distribution for M_n as $n \to \infty$ is another member of the same GEV family:

$$\begin{gathered} Pr\{(M_n - b_n)/a_n \leq x\} \approx G(x) \\ \Downarrow \\ Pr\{M_n \leq x\} \approx G\{(x - b_n)/a_n\} = G^*(x) \end{gathered}$$

The cumulative distribution function of the generalized extreme value distribution is:

$$G(x; \mu, \sigma, \xi) = e^{-\left[1+\xi\left(\frac{x-\mu}{\sigma}\right)\right]^{-1/\xi}} \quad \text{for} \quad 1 + \xi(x - \mu)/\sigma > 0$$

Here, $\mu \in \mathbb{R}$ is the location parameter, $\sigma > 0$ is the scale parameter and $\xi \in \mathbb{R}$ is the shape parameter.

The corresponding density function is then:

$$g(x; \mu, \sigma, \xi) = \frac{1}{\sigma}\left[1 + \xi\left(\frac{x-\mu}{\sigma}\right)\right]^{-\frac{1}{\xi}-1} e^{-\left[1+\xi\left(\frac{x-\mu}{\sigma}\right)\right]^{-1/\xi}} \quad \text{for } 1 + \xi(x - \mu)/\sigma > 0$$

Hence, one can model the extremes of a series of independent observations $X_1, X_2, \ldots, X_n$ in the following way: First, block the data into sequences of observations of length n, for some large value of n in order to obtain a series of block maxima, $M_{n,1}, M_{n,2}, \ldots, M_{n,m}$. The M_n's should be GEV distributed, so a GEV distribution can be fitted to these data. The blocks may for example be chosen to represent one year, where n is the number of observations in a year and the block maxima corresponds to annual maxima. Then, estimates of extreme quantiles of the annual maximum distribution can be obtained from setting $G(z_p) = 1 - p$:

$$z_p = \begin{cases} \mu - \frac{\sigma}{\xi}\left[1 - (-\ln(1-p))^{-\xi}\right], & \text{for} \quad \xi \neq 0 \\ \mu - \sigma \ln(-\ln(1-p)) & \text{for} \quad \xi = 0 \end{cases}$$

In other words, the probability of an annual maximum exceeding z_p in any particular year is p, and therefore, this value is expected to be exceeded on average every $1/p$ years. Thus, z_p is referred to as the return level associated with the return period $1/p$ in common terminology.

B.2 Three Families of Extreme Value Distributions

The three special cases of the GEV distribution, for $\xi \to 0$, $\xi > 0$, and $\xi < 0$, correspond to the Gumbel, Fréchet and Weibull families respectively, also referred to as type I, type II, and type III extreme value distributions. These have the following cumulative distribution functions, where $\sigma > 0$ and $\alpha > 0$:

Gumbel distribution or type I extreme value distribution:

$$F(x;\mu,\sigma) = e^{-e^{-(x-\mu)/\sigma}} \qquad \text{for} \quad x \in \mathbb{R}$$

Fréchet distribution or type II extreme value distribution:

$$F(x;\mu,\sigma,\alpha) = \begin{cases} 0 & x \le \mu \\ e^{-((x-\mu)/\sigma)^{-\alpha}} & x > \mu \end{cases}$$

Reversed Weibull distribution or type III extreme value distribution:

$$F(x;\mu,\sigma,\alpha) = \begin{cases} e^{-(-(x-\mu)/\sigma)^{\alpha}} & x < \mu \\ 1 & x \ge \mu \end{cases}$$

The type I extreme value distribution can be linked to types II and III in the following way: If the cumulative distribution function of a random variable X is of type II with $\mu = 0$, i.e., $F(x;0,\sigma,\alpha)$, then the cumulative distribution function of $Y = \ln X$ is of type I, $F(y;\ln\sigma,\frac{1}{\alpha})$. Similarly, if the cumulative distribution function of a random variable X is of type III with $\mu = 0$, i.e., $F(x;0,\sigma,\alpha)$, then the cumulative distribution function of $Y = \ln X$ is of type I, $F(y;-\ln\sigma,\frac{1}{\alpha})$.

B.3 The Generalized Pareto Distribution

The generalized extreme value distribution can be used to model block maxima, but it may be argued that this approach does not utilize all available data. If other data than the block maxima are available, most of the information at hand is actually disregarded in the extreme value analysis. An alternative approach to model extremes is to use threshold models that include all values above a defined threshold, not only the block maxima. The distribution of the excesses above the threshold would consequently have as distribution function a member of the generalized Pareto family of distributions. Let $X_1, X_2, \ldots, X_n$ be a series of independent random variables with common distribution function F and

$$M_n = \max\{X_1, \ldots, X_n\}.$$

Assume F satisfies the extremal types theorem, i.e., if for large n,

$$Pr\{M_n \le x\} \approx G(x) = e^{-\left[1+\xi\left(\frac{x-\mu}{\sigma}\right)\right]^{-1/\xi}}$$

for some $\mu, \sigma > 0$, and ξ. Then, for large enough u, the distribution function of $Y = (X-u)$, conditional on $X > u$, will be approximately

$$H(y) = 1 - \left(1 + \frac{\xi y}{\tilde{\sigma}}\right)^{-1/\xi} \quad \text{for} \quad y > 0 \quad \text{and} \quad (1 + \xi y/\tilde{\sigma}) > 0$$

where

$$\tilde{\sigma} = \sigma + \xi(u - \mu)$$

This family of distributions is called the generalized Pareto family of distributions. In other words, for processes where block maxima have an approximately generalized extreme value distribution G, then the threshold excesses have a corresponding approximate distribution within the generalized Pareto family. The parameters of the generalized Pareto distribution of the threshold excesses are determined by the parameters of the associated generalized extreme value distribution of the block maxima. In particular, the parameter ξ is the same for the two distributions, and $\tilde{\sigma}$ are determined from the parameters of the GEV distribution.

The special case for $\xi = 0$, which could be interpreted as the limit $\xi \to 0$, corresponds to an exponential distribution with parameter $1/\tilde{\sigma}$:

$$H(y) = 1 - e^{-y/\tilde{\sigma}} \quad \text{for} \quad y > 0$$

B.3.1 The Poisson-GPD Model

Threshold models are often used in conjunction with the Poisson process, where the occurrence of an extreme event, i.e., above a certain threshold, is modeled as a Poisson process, and given an extreme event, the threshold exceedance is modeled according to the generalized Pareto distribution. The Poisson-GPD model combines the information of the excess values and the number of exceedances of a fixed threshold u in the following way:

1. Number of exceedences $N \sim Poisson(\lambda)$
2. Conditional on N the excess values $Y_1, \ldots Y_n$ are iid from the Generalized Pareto distribution

There is a close relationship between the GEV and the Poisson-GPD models and this is illustrated by finding the distribution of the maxima of the process described by the Poisson-GPD model (assuming $x > u$):

$$\begin{aligned}
Pr(M_n \leq x) &= Pr(Y_1, \ldots, Y_n \leq x - u) \\
&= Pr(N = 0) + \sum_{n=1}^{\infty} Pr(N = n)\,[Pr(Y_i \leq x - u)]^n \\
&= e^{-\lambda} + \sum_{n=1}^{\infty} \frac{\lambda^n}{n!} e^{-\lambda} \left[1 - (1 + \xi \frac{x-u}{\sigma})^{-1/\xi}\right]^n \\
&= \sum_{n=0}^{\infty} \frac{\left[\lambda\left(1 - (1 + \xi \frac{x-u}{\sigma})^{-1/\xi}\right)\right]^n}{n!} e^{-\lambda} \\
&= \frac{e^{-\lambda}}{e^{-\lambda\left(1-(1+\xi \frac{x-u}{\sigma})^{-1/\xi}\right)}} \sum_{n=0}^{\infty} \frac{\left[\lambda\left(1 - (1 + \xi \frac{x-u}{\sigma})^{-1/\xi}\right)\right]^n}{n!} e^{-\lambda\left(1-(1+\xi \frac{x-u}{\sigma})^{-1/\xi}\right)} \\
&= e^{-\lambda(1+\xi \frac{x-u}{\sigma})^{-1/\xi}}
\end{aligned}$$

This is exactly the GEV distribution and the two approaches give the same distribution for the (block) maxima. The relationship between the parameters of the Poisson-GPD model and the GEV model are

$$\sigma = \psi + \xi(u - \mu)$$
$$\lambda = \left(1 + \xi \frac{u - \mu}{\psi}\right)^{-1/\xi}$$

where ψ is the scale parameter of the GEV-distribution.

This theory is based on an assumption of iid exceedances, and there are generally two types of violations to these assumptions, i.e., different F's (e.g., due to seasonality), and dependence between exceedances.

B.4 Extreme Values of Dependent Sequences

One common assumption for the Poisson process and for extremes to be distributed according to the generalized extreme value distribution, and hence for threshold excesses to be distributed according to the generalized Pareto distribution, is that the underlying process consists of a sequence of independent random events. However, in reality this assumption may not hold true. Considering waves for example, it cannot be assumed that the occurrence of different waves are independent. Surely, during a storm there will be more frequent waves and more extreme waves than in calm weather, so some temporal dependence seems inevitable. Spatial dependencies would also presumably exist. This suggests that modeling extreme waves as Poisson processes or using the generalized extreme value distribution are not ideal approaches and alternative approaches may represent potential for model improvement. In the following, some basics for modeling the maxima of dependent sequences will be outlined.

B.4.1 Maxima of Stationary Dependent Sequences

Even though it may not be assumed that a sequence of events are independent in many cases, it is more likely that long-range independence of extreme events is a valid assumption. That is, two events $X_i > u$ and $X_j > u$ will be approximately independent if the threshold u is high enough and the times t_i and t_j, at which X_i and X_j occur, are far enough apart. If this is the case, only short-range dependencies may be considered. For extreme waves, this could for example be interpreted as dependency between extreme waves during one and the same storm but independence between the occurrence of extreme waves in different storms that are distant in time and space, which may be a reasonable assumption.

If this condition is fulfilled, i.e., that long-range dependencies of extremes are weak, the maxima of the stationary series will approximately follow a distribution within the generalized extreme value family. Moreover, the limiting distribution of maxima of a stationary series where this condition is fulfilled can be related to the limiting distribution of the maxima of a series of independent random variables with the same marginal distribution by an *extremal index* θ, as $n \to \infty$. Therefore, the generalized extreme value distribution can still be used to model block maxima for stationary series, as long as long-term dependencies are weak.

For modeling of threshold exceedances, however, where short-range dependencies could mean that threshold excesses tend to occur in groups, it is not as straightforward. One approach to handle such dependencies of threshold exceedances is to use the method of de-clustering in conjunction with the generalized Pareto distribution:

1. Find an empirical rule to define clusters of exceedances
2. Identify the maximum excess within each cluster
3. Now, assuming cluster maxima to be independent, with conditional excess distribution given by the generalized Pareto distribution
4. Fit the generalized Pareto distribution to the cluster maxima.

For ocean waves, the interpretation of a cluster of exceedances could be extreme waves in one and the same storm, and only the highest wave in a storm is used. Different clusters would be construed as separate storms as long as the temporal and spatial separation is sufficiently large. Hence, if two distinctive storms can be assumed independent, then the different cluster-maxima will be independent and the GPD would be reasonable for adequate clustering of maxima. However, in reality, seasonal effects introduce dependencies between individual storms, and hence between cluster maxima, and such effects might have to be adjusted in order to defend the approximation of the Poisson-GPD model.

B.5 Non-Stationary Generalized Extreme Value Model

In non-stationary processes, where characteristics change systematically over time, the simple assumptions that were made in the derivation of the extreme value characteristics are violated. Non-stationarity may for example be in the form of cyclic variations (e.g., seasonal variation in environmental processes) or as long-term trends (e.g., trends in environmental processes due to climatic changes). The critical assumption is that individual observations are independent and identically distributed, i.e., a constant distribution over time is assumed. However, individual observations of a non-stationary process have distributions that changes in time and therefore, the distributions will not be identical for the different observations. It is therefore questionable whether the use of the GEV distribution is appropriate in modeling the maxima of non-stationary processes.

Notwithstanding, a pragmatic approach is normally adopted, where the standard extreme value models are used as templates that may be enhanced by statistical mod-

eling. Extremes of non-stationary processes will then be modeled using the classical extreme value models as templates, but where the non-stationarity is modeled as non-stationarity in the appropriate distribution parameters. For the GEV family of distributions, the non-stationarity may be modeled in the location, scale, and/or shape parameters. Hence, by substituting $\mu = \mu(t)$, $\sigma = \sigma(t)$ and $\xi = \xi(t)$, the non-stationary generalized extreme value distribution, which can be used for modeling the maximum at time t or the block (annual) maximum in block interval (year) t, will take the following form, with X_t representing the block maximum in block interval t:

$$X_t \sim \text{GEV}\left(\mu(t), \sigma(t), \xi(t)\right)$$

or

$$G(x_t) = e^{-\left[1+\xi(t)\left(\frac{x_t-\mu(t)}{\sigma(t)}\right)\right]^{-1/\xi(t)}} \quad \text{for} \quad 1 + \xi(t)\frac{x_t - \mu(t)}{\sigma(t)} > 0$$

If the extremal behaviour of a series is related to another variable, i.e., a covariate, the extreme value parameters can be written as a function of these covariates and corresponding parameters. A common way to write the non-stationary extreme value parameters is:

$$\theta(t) = h\left(X^T\beta\right)$$

where θ denotes either of the distribution parameters μ, σ or ξ, h is a specified function, β is a vector of parameters and X is a model vector containing the covariates[1].

Reference

1. Coles, S.: An Introduction to Statistical Modeling of Extreme Values. Springer-Verlag, London (2001)

[1] For example: the following model for the location parameter $\mu(t) = \beta_0 + \beta_1 t + \beta_2 t^2$ would have h as the identity function, $X = \begin{bmatrix} 1 \\ t \\ t^2 \end{bmatrix}$ and $\beta = \begin{bmatrix} \beta_0 \\ \beta_1 \\ \beta_2 \end{bmatrix}$ so that

$$\mu(t) = h\left(X^T\beta\right) = \left[1, t, t^2\right]\begin{bmatrix} \beta_0 \\ \beta_1 \\ \beta_2 \end{bmatrix}$$

.

Appendix C
Markov Random Fields

Markov Random Fields are alternatives to geostatistical approaches to modeling spatial stochastic processes and is an example of models defined by conditional probabilities (see e.g. [1]). The main idea is to specify the simultaneous distribution of a vector $\mathbf{Z} = (Z_1, \ldots, Z_n)$, which is normally of high dimension, through the conditional distributions $p(Z_i|Z_j, j \neq i), \forall i$ which are of lower dimensions. Normally, the dependence structure is simplified considerably by assuming dependence only on some neighbours. Defining N_i as the neighborhood of i, a Markov Random Field is defined as

$$P(Z_i|Z_j, j \neq i) = P(Z_i|Z_j, j \in N_i)$$

In order to get a mathematically valid model, there need to be some restrictions on the conditional distributions $p_i(Z_i|Z_j, j \neq i)$ so that there exist a $p(Z_1, \ldots, Z_n)$ such that

$$p_i(Z_i|Z_j, j \neq i) = \frac{p(Z_1, \ldots, Z_n)}{\int_{Z_i} p(Z_1, \ldots, Z_n) dZ_i} = \frac{p(Z_1, \ldots, Z_n)}{p(Z_1, \ldots, Z_{i-1}, Z_{i+1}, \ldots, Z_n)}$$

For example, assuming an auto-normal model

$$p_i(Z_i|Z_j, j \neq i) = N(\mu_i + \sum_{j \in N_i} \beta_{ij}(Z_j - \mu_j), \sigma^2)$$

the joint density becomes

$$p(Z_1, \ldots, Z_n) = \frac{1}{(2\pi\sigma^2)^{n/2}} |B|^{1/2} e^{-\frac{1}{2\sigma^2} \sum_{j,k} (Z_j - \mu_j) b_{jk} (Z_k - \mu_k)}$$

and the following restrictions gives a legal model:

1. $j \in N_i \Leftrightarrow i \in N_j$
2. $\beta_{ij} = \beta_{ji}$ (symmetric)

E. Vanem, *Bayesian Hierarchical Space-Time Models with Application to Significant Wave Height*, Ocean Engineering & Oceanography 2,
DOI: 10.1007/978-3-642-30253-4, © Springer-Verlag Berlin Heidelberg 2013

3. $b_{ij} = \begin{cases} 1 & \text{if } i = j \\ -\beta_{ij} & \text{if } i \in N_j \\ 0 & \text{otherwise} \end{cases}$
4. $B = \{b_{ij}\}$ is positive definite

This means that the joint distribution is normal: $p(Z_1, \ldots, Z_n) = MVN(\mu, \sigma^2 B^{-1})$. The process is homogeneous if the μ_i's and the β_{ij}'s are constant:

$$\mu_i = \mu \ \ \forall i \qquad \text{and}$$
$$\beta_{ij} = \beta \ \ \forall i, j$$

In general, consistency of a given model, $p(Z_i|Z_j, j \neq i)$ can be found by assuming some fixed outcome $\mathbf{Z}^* = (Z_1^*, \ldots, Z_n^*)$ and checking that

$$\begin{aligned} \frac{P(Z_1, \ldots, Z_n)}{P(Z_1^*, \ldots, Z_n^*)} &= \frac{P(Z_1, \ldots, Z_n)}{P(Z_1^*, \ldots, Z_n^*)} \frac{P(Z_1, \ldots, Z_{n-1}, Z_n^*)}{P(Z_1, \ldots, Z_{n-1}, Z_n^*)} = \ldots\ldots \\ &= \ldots\ldots \\ &= \prod_{i=0}^{n-1} \frac{P(Z_1^*, \ldots, Z_i^*, Z_{i+1}, \ldots, Z_n)}{P(Z_1^*, \ldots, Z_{i-1}^*, Z_i^*, Z_{i+1}^*, \ldots, Z_n)} \\ &= \prod_{i=0}^{n-1} \frac{P(Z_{i+1}|Z_1^*, \ldots, Z_i^*, Z_{i+2}, \ldots, Z_n)}{P(Z_{i+1}^*|Z_1^*, \ldots, Z_i^*, Z_{i+2}, \ldots, Z_n)} \end{aligned}$$

$$\Rightarrow \ P(Z_1, \ldots, Z_n) = P(Z_1^*, \ldots, Z_n^*) \prod_{i=0}^{n-1} \frac{P(Z_{i+1}|Z_1^*, \ldots, Z_i^*, Z_{i+2}, \ldots, Z_n)}{P(Z_{i+1}^*|Z_1^*, \ldots, Z_i^*, Z_{i+2}, \ldots, Z_n)}.$$

Restrictions to the possible functions that give legal models are invariance with respect to permutations of variables and invariance with respect to reference state $\mathbf{Z}^*$. There is still a need for the constant $P(Z_1^*, \ldots, Z_n^*)$, which can be obtained by simulation.

C.1 The Hammersley-Clifford Theorem

Assume a Markov random field, $\mathbf{X} = (X_1, \ldots, X_n)$, i.e., a random field with the property $P(x_i|x_j, j \neq i) = P(x_i|x_j, j \in N_i)$, with finite state-space and where all configurations are possible (i.e., $P(X_1, \ldots, X_n) > 0 \ \forall\, x_1, \ldots x_n$). Also assume some reference point $P(0, \ldots, 0) > 0$. Some terminology is needed and a *clique* is defined as a subset of sites such that all members are neighbors. Now, define

$$q(\mathbf{x}) = \log \frac{P(\mathbf{x})}{P(\mathbf{0})} \Rightarrow P(\mathbf{x}) = P(\mathbf{0}) e^{q(\mathbf{x})}$$

and claim that there exist functions $g_i(x_i)$, $g_{ij}(x_i, x_j)$, $g_{ijk}(x_i, x_j, x_k)$, etc. so that

$$q(\mathbf{x}) = \sum_i x_i g_i(x_i) + \sum_{i<j} x_i x_j g_{ij}(x_i, x_j) + \sum_{i<j<k} x_i x_j x_k g_{ijk}(x_i, x_j, x_k) + \ldots + x_1 x_2 \ldots x_n g_{1,2,\ldots,n}(x_1, x_2, \ldots, x_n)$$

Hence, the Hammersley-Clifford theorem for a Markov Random Field becomes:

$g_{ij\ldots s}(x_1, x_2, \ldots, x_s)$ is non-zero if and only if $\{i, j, \ldots, s\}$ forms a clique.

The importance of this theorem is that it enables us to write down the joint probability distribution for any Markov Random Fields, e.g.,:

$$P(\mathbf{x}) = Ce^{q(\mathbf{x})} = Ce^{\sum_i x_i g_i(x_i) + \sum_{i\sim j} x_i x_j g_{ij}(x_i, x_j)}$$

which corresponds to $P(x_i|x_j, j \neq i) = P(x_i|x_j, j \in N_i)$.

C.2 Auto-Models

One particular class of models are so-called auto-models. These have constant g_{ij}-functions and are on the form

$$q(\mathbf{x}) = \sum_i x_i g_i(x_i) + \sum_{i<j} \beta_{ij} x_i x_j$$

where $\beta_{ij} = 0$ if i and j are not neighbours. Some examples of such models are the auto-normal model, the auto-logistic model and the auto-Poisson model as defined below.

– Auto-normal model:

$$p_i(Z_i|Z_j, j \neq i) = N(\mu_i + \sum_{j\in N_i} \beta_{ij}(Z_j - \mu_j), \sigma^2)$$

– Auto-logistic model: For binary data, $Z_i \in \{0, 1\}$,

$$P(Z_i = 1|Z_j, j \neq i) = \frac{e^{\alpha_i + \sum_{j\in N_i} \beta_{ij} Z_j}}{1 + e^{\alpha_i + \sum_{j\in N_i} \beta_{ij} Z_j}}$$

– Auto-Poisson model:

$$Z_i|Z_j, j \neq i \sim Poisson(\mu_i)$$
$$\mu_i = e^{\alpha_i + \sum_{j\in N_i} \beta_{ij} Z_j}$$

It turns out that the auto-Poisson model is not very useful due to some restrictions on the β's (we need $\beta_{ij} < 0$), and a more reasonable model for a counting variable Z could be, with Z_i the count in region i and X_i the intensity in region i:

$$\{X_i\} \text{ an Auto-normal process and}$$
$$Z_i \sim Poisson(e^{X_i})$$

Another example of a particular model is the Potts model, defined by

$$P(\mathbf{x}) \propto e^{\sum_i \alpha_{x_i} + \frac{1}{2}\beta \sum_i \sum_{j \in N_i} I(x_i = x_j)}$$

C.3 Inference in Markov Random Fields

Inference in Markov Random Fields is related to the problem of estimating the model parameters θ given observations x, where we have a model for $\mathbf{X}$:

$$\mathbf{X} \sim P(\mathbf{x}; \theta) = C(\theta) F(\mathbf{x}; \theta)$$

Typically, the joint distribution of X is possible to calculate up to a proportionality constant, but the proportionality constant, which is a function of θ may be difficult to calculate. This makes maximum likelihood difficult; if we are not able to calculate $C(\theta)$, the maximum likelihood estimator is not easily obtained:

$$\widehat{\theta}_{ML} = \arg\max_{\theta} C(\theta) F(\mathbf{x}; \theta)$$

Monte Carlo estimation of $C(\theta)$ is possible, but some alternative approaches have been proposed, to be briefly outlined in the following. The following approaches to parameter estimation of Markov Random Fields are briefly outlined below:

1. Coding methods
2. Pseudo-likelihood
3. Maximum likelihood for Gaussian processes
4. Maximum likelihood in general (Monte Carlo ML)
5. Bayesian methods.

C.3.1 Coding Methods

We consider observations $\mathbf{x}$ on a grid and assume a first-order dependence structure. We can then divide the observations in two parts, one containing the odd points and one with the even points with the two subsets referred to as $\mathbf{x}^1$ and $\mathbf{x}^2$ respectively.

Hence, the joint distribution of $\mathbf{x}$ can be written as

$$P(\mathbf{x};\theta) = p(\mathbf{x}^1|\mathbf{x}^2,\theta)p(\mathbf{x}^2;\theta)$$

It is then suggested to neglect the last term and use $p(\mathbf{x}^1|\mathbf{x}^2,\theta)$ as the likelihood function of the odd points (and similarly for the even points). We also have that given $\mathbf{x}^2$, all the $\mathbf{x}^1$ are independent (and vice verse), and it is possible to write down the joint density for the even (or odd) points. Assuming a first-order Markov Random Field and letting $x_i \in \mathbf{x}^1$ (so that $x_j \in N_i \Rightarrow x_j \in x^2$) we have the conditional distribution for each individual odd point, conditioned on the even points:

$$p(x_i|x_j,\, j \neq i) = p(x_i|\mathbf{x}^2)$$

Now, since all $\mathbf{x}^1$ are independent conditional on $\mathbf{x}^2$, we have an exact expression for the likelihood function of the odd (or even) points

$$\widetilde{L}(\theta) = p(\mathbf{x}^1|\mathbf{x}^2,\theta) = \prod_{i\in I^1} p(x_i|\mathbf{x}^2;\theta)$$

The value of θ that maximizes this expression is an estimator for θ:

$$\widehat{\theta}_{coding} = \arg\max_{\theta} \widetilde{L}(\theta)$$

This is normally easy to calculate, and we may obtain similar estimators based on the odd and even points respectively. However, it is noted that the uncertainty measures obtained from coding methods are unreliable.

C.3.2 Pseudo-Likelihood

In the coding method described above we used

$$P(\mathbf{x};\theta) = p(\mathbf{x}^1|\mathbf{x}^2,\theta)p(\mathbf{x}^2;\theta)$$

and ignored the information in $p(\mathbf{x}^2;\theta)$. This gave two estimators for θ based on either the odd or the even points, conditioned on the others.

$$\widehat{\theta}_{coding} = \arg\max_{\theta} p(\mathbf{x}^1|\mathbf{x}^2;\theta)$$
$$\widehat{\theta}^2_{coding} = \arg\max_{\theta} p(\mathbf{x}^2|\mathbf{x}^1;\theta)$$

The pseudo-likelihood approach extends this method and tries to combine these two estimators to get better estimates by simply multiplying them together:

$$\begin{aligned}\widehat{\theta}_{pseudoL} &= \arg\max_{\theta} p(\mathbf{x}^1|\mathbf{x}^2;\theta)p(\mathbf{x}^2|\mathbf{x}^1;\theta) \\ &= \arg\max_{\theta} \prod_i p(x_i|x_j,\, j \neq i;\theta)\end{aligned}$$

where $\prod_i p(x_i|x_j,\, j \neq i;\theta)$, the product of all one-dimensional conditional distributions, is referred to as the pseudo-likelihood. Maximum pseudo-likelihood estimates are then the values that maximizes this pseudo-likelihood. This is normally easy to compute and is easily generalized to other spatial fields. However, the sampling properties are normally not known and standard approximations for standard errors and likelihood ratio tests for model comparison are not valid for pseudo-likelihoods.

C.3.3 Maximum Likelihood in Gaussian Markov Random Fields

We now assume an auto-normal process:

$$x_i|x_j,\, j \neq i \sim N\left(\widetilde{\mu}_i + \sum_{j\in N_i} \beta_{ij}(x_j - \widetilde{\mu}_j), \sigma_i^2\right)$$

Now, also the full distribution of $\mathbf{X}$ is Gaussian with an explicitly defined normalizing constant. We have

$$\mathbf{X} \sim MVN(\boldsymbol{\mu}, \Sigma) = \frac{1}{(2\pi)^{n/2}|\Sigma|^{1/2}} e^{-\frac{1}{2}(\mathbf{X}-\boldsymbol{\mu})^T\Sigma^{-1}(\mathbf{X}-\mu)}$$

The parameters of this model are $\theta = (\mu_1, \ldots, \mu_n, \{\beta_{ij}\}, \{\sigma_i^2\})$ where we have $\mu = \mu(\theta)$ and $\Sigma = \Sigma(\theta)$. Now, we may write the exact likelihood function $L(\theta) = p(\mathbf{x};\theta)$ where nothing is unknown and this may in principle be optimized with numerical optimization. However, for large datasets (n large) this becomes computationally expensive due to the computation of $\Sigma^{-1}(\mathbf{x} - \boldsymbol{\mu})$ and the determinant $|\Sigma|$.

In order to facilitate the computation of the exact likelihood function, one may introduce the precision matrix as the inverse of the covariance matrix, and this turns out to be sparse. Hence, computing the likelihood becomes easier if modeling through the precision matrix rather than using covariance functions. The fact that the precision matrix is sparse can be demonstrated as follows: First, divide $\mathbf{x}$ into $\mathbf{x}_1$ and everything else, denoted $\mathbf{x}_{-1}$:

$$\mathbf{x} = \begin{pmatrix}\mathbf{x}_1 \\ \mathbf{x}_{-1}\end{pmatrix} \sim MVN\left(\begin{pmatrix}\mu_1 \\ \mu_2\end{pmatrix}, \begin{pmatrix}\Sigma_{11} & \Sigma_{12} \\ \Sigma_{21} & \Sigma_{22}\end{pmatrix}\right)$$

Then, use the general results for the conditional mean and variance for Gaussian processes and compare with the conditional mean and variance from the auto-normal model. First, the mean is:

$$\begin{aligned} E\left[x_1|x_{-1}\right] &= \mu_1 + \Sigma_{12}\Sigma_{22}^{-1}(x_{-1} - \widetilde{\mu}_2) \\ &= \widetilde{\mu}_1 + \sum_{j \in N_1} \beta_{1j}(x_j - \widetilde{\mu}_j) \end{aligned}$$

which gives that $\Sigma_{12}\Sigma_{22}^{-1}$ equals β_{ij} if $j \in N_i$ or else is 0. Hence, we have that

$$\Sigma_{12}\Sigma_{22}^{-1} = \beta_{ij} I(j \in N_i)$$

Furthermore, looking at the variance, we see that

$$\text{Var}\left[x_1|x_{-1}\right] = \Sigma_{11} - \Sigma_{12}\Sigma_{22}^{-1}\Sigma_{21} = \sigma_1^2$$

Now, for a general matrix, we take the inverse and see that this can be written on the following form

$$\begin{pmatrix} \Sigma_{11} & \Sigma_{12} \\ \Sigma_{21} & \Sigma_{22} \end{pmatrix}^{-1} = \begin{bmatrix} (\Sigma_{11} - \Sigma_{12}\Sigma_{22}^{-1}\Sigma_{21})^{-1} & -Q_{11}\Sigma_{12}\Sigma_{22}^{-1} \\ -Q_{22}\Sigma_{21}\Sigma_{11}^{-1} & (\Sigma_{22} - \Sigma_{21}\Sigma_{11}^{-1}\Sigma_{12})^{-1} \end{bmatrix}$$

We now see that the off-diagonal elements are only non-zero for i, j pairs that are neighbors, and the diagonal terms are the inverse of the conditional variances. The non-zero off-diagonal elements are identified to be $-\beta_{ij}$. Hence, if we define the precision matrix as the inverse of the covariance matrix, $Q = \Sigma^{-1}$, then Q will be sparse (containing many zero-elements). How sparse it will be depends on the dependence structure, and the precision matrix will be on the form

$$\begin{aligned} Q &= \Sigma^{-1} \\ &= \begin{bmatrix} \frac{1}{\sigma_1^2} & -\frac{\beta_{12}}{\sigma_1^2} I(1 \sim 2) & \cdots\cdots & & -\frac{\beta_{1n}}{\sigma_1^2} I(1 \sim n) \\ -\frac{\beta_{21}}{\sigma_2^2} I(2 \sim 1) & \frac{1}{\sigma_2^2} & -\frac{\beta_{23}}{\sigma_2^2} I(2 \sim 3) & & \vdots \\ \vdots & & \ddots & & \vdots \\ & -\frac{\beta_{ij}}{\sigma_i^2} I(i \sim j) & \frac{1}{\sigma_i^2} & -\frac{\beta_{ik}}{\sigma_i^2} I(i \sim k) & \\ & & & \ddots & \\ \cdots & \cdots & \cdots & & \frac{1}{\sigma_n^2} \end{bmatrix} \end{aligned}$$

Now, the computational expensive expressions in the likelihood function can be rewritten in terms of the precision matrix, which is sparse:

$$(\mathbf{x} - \mu)^T \Sigma^{-1}(\mathbf{x} - \mu) = (\mathbf{x} - \mu)^T \mathbf{Q}(\mathbf{x} - \mu) = \sum_{i \sim j} (x_i - \mu_i) Q_{ij} (x_j - \mu_j)$$

and $\frac{1}{|\Sigma|} = |\mathbf{Q}|$. The determinant is now of a sparse matrix, which is less computational intensive to compute.

One procedure for calculating the determinant of a matrix $\mathbf{Q}$ is to use the Cholesky decomposition $\mathbf{L}$. The Cholesky decomposition $\mathbf{L}$ is the lower triangular matrix so that

$$\mathbf{Q} = \mathbf{L}\mathbf{L}^T$$

The determinant of $\mathbf{Q}$ may be found by $|\mathbf{Q}| = |\mathbf{L}|^2 = (\prod_i L_{ii})^2$, where the determinant of $\mathbf{L}$ is equal to the square of the product of the diagonal elements of the matrix L since this is a triangular matrix. Hence, it might be possible to optimize the likelihood function expressed in terms of the precision matrix, and given $\mathbf{L}$, simulations from $p(\mathbf{x}; \theta)$ are possible.

C.3.4 General Maximum Likelihood (simulated ML)

Now, assuming a general model, the likelihood function can typically be determined up to a normalizing constant, i.e.,

$$L(\theta) = p(\mathbf{x}; \theta) = C(\theta)F(\mathbf{x}; \theta)$$

where $F(x, \theta)$ is computable, but where $C(\theta) = \frac{1}{\int F(\mathbf{x};\theta)d\mathbf{x}}$ is a function of θ and normally not computable. However, one may assume some specific value θ_0 of θ, and rather consider the ratio $\frac{C(\theta_0)}{C(\theta)}$:

$$\begin{aligned}\frac{C(\theta_0)}{C(\theta)} &= C(\theta_0)\int F(\mathbf{x}; \theta)d\mathbf{x} = C(\theta_0)\int \frac{F(\mathbf{x}; \theta)}{F(\mathbf{x}; \theta_0)}F(\mathbf{x}; \theta_0)d\mathbf{x} \\ &= \int \frac{F(\mathbf{x}; \theta)}{F(\mathbf{x}; \theta_0)}p(\mathbf{x}; \theta_0)d\mathbf{x} = E^{p(\mathbf{x};\theta_0)}\left[\frac{F(\mathbf{x}; \theta)}{F(\mathbf{x}; \theta_0)}\right] \\ &\approx \frac{1}{M}\sum_{m=1}^{M}\frac{F(\mathbf{X}^m; \theta)}{F(\mathbf{X}^m; \theta_0)}\end{aligned}$$

where $\mathbf{X}^1, \ldots, \mathbf{X}^M$ are simulated from $p(\mathbf{x}; \theta_0)$. This can then be used to estimate the likelihood-ratio of θ_0 to θ, where $\mathbf{X}$ denote the actual data that are observed

$$\frac{L(\theta_0)}{L(\theta)} = \frac{C(\theta_0)F(\mathbf{X}; \theta_0)}{C(\theta)F(\mathbf{X}; \theta)} \approx \frac{1}{M}\sum_{m=1}^{M}\frac{F(\mathbf{X}^m; \theta)}{F(\mathbf{X}^m; \theta_0)}\frac{F(\mathbf{X}; \theta_0)}{F(\mathbf{X}; \theta)}$$

Since $F(x; \theta)$ is computable for any θ, this likelihood ratio is possible to compute for all θ and a maximum likelihood estimator may be obtained by numerical optimization (actually, by maximizing $\frac{L(\theta)}{L(\theta_0)}$).

C.3.5 Bayesian Methods

The general idea of Bayesian methods is to introduce a prior distribution on the parameters $\pi(\theta)$ and to make inference from the posterior distribution given observations $\mathbf{X}$

$$\pi(\theta|\mathbf{X}) \propto \pi(\theta)\, p(\mathbf{X};\theta)$$

If now $p(\mathbf{X};\theta)$ is computable, Bayesian analysis can be performed by simulating from $\pi(\theta|\mathbf{X})$, e.g., by MCMC methods (Gibbs sampler, Metropolis-Hastings, etc.). If, on the other hand, simulation from $p(\mathbf{X};\theta)$ is only possible through MCMC, it is still an open question how to best deal with this.

Reference

1. Smith, R.L.: Environmental statistics. University of North Carolina (2001). http://www.stat.unc.edu/postscript/rs/envnotes.pdf. Accessed 25 Aug 2013

Appendix D
Derivation of the Full Conditionals of the Bayesian Hierarchical Space-Time Model for Significant Wave Height

In this appendix, the derivation of the full conditional distributions, needed for the Gibbs sampler, will be outlined. The full conditionals derived in the following pertain to the model alternatives with one temporal noise term, but the full conditionals for the other model alternatives are derived in a similar way. Vectors will be written in bold, and the notation $P(V|\cdot)$ will be used to represent the conditional distribution of V conditioned on all other random quantities, i.e., the full conditionals. How to sample from a multi-normal distribution is outlined in appendix E.

Spatial data will be treated as a vector of size $X = 153 \times 1$, so that for example $\mathbf{Z}_t, \boldsymbol{\theta_t}, \boldsymbol{\mu}$ are all column vectors of size X. For the temporal components without spatial description, e.g., $\boldsymbol{M_t}$ and T_t, a vector of corresponding size may be obtained by multiplication by a vector of ones, $\mathbf{1}$, of size X. In the following, e.g., $\boldsymbol{M_t}$ is assumed to be interpreted as $\mathbf{1}\boldsymbol{M_t}$ in the instances where the $\mathbf{1}$ is not explicitly written. The transpose of a matrix or vector $\mathbf{V}s$ will be denoted $\mathbf{V}'$.

D.1 Conditional Distribution for *H(t)*

Since there are no random noise term in Eq. 3.5, the full conditional distribution of H_t reduces to just a single, fixed value, at each location, x and time, t:

$$P(\boldsymbol{H}_t|\cdot) = \boldsymbol{\mu} + \boldsymbol{\theta_t} + \boldsymbol{M_t} \tag{D.1}$$

Hence, determining $\boldsymbol{\mu}, \boldsymbol{\theta_t}$ and $\boldsymbol{M_t}$ is equivalent to determining $\boldsymbol{H_t} = \boldsymbol{H}(x,t)$ and there is no need to consider these parameters further herein.

E. Vanem, *Bayesian Hierarchical Space-Time Models with Application to Significant Wave Height*, Ocean Engineering & Oceanography 2,
DOI: 10.1007/978-3-642-30253-4, © Springer-Verlag Berlin Heidelberg 2013

D.2 Conditional Distribution for $\boldsymbol{\mu}$

From the model specification, the following conditional distributions are obtained directly for all the parameters with dependence with $\boldsymbol{\mu}$

$$\begin{aligned} \boldsymbol{\mu}|\boldsymbol{\mu_0}, a_\phi, a_\lambda, \sigma_\mu^2 &\sim MVN\left(\boldsymbol{\mu_0}, \sigma_\mu^2 A_{\boldsymbol{\mu}}^{-1}\right) \\ \boldsymbol{Z_t}|\boldsymbol{\mu}, \boldsymbol{\theta_t}, \boldsymbol{M_t}, \sigma_Z^2 &\sim MVN\left(\boldsymbol{\mu} + \boldsymbol{\theta_t} + 1\boldsymbol{M_t}, I\sigma_Z^2\right) \end{aligned} \tag{D.2}$$

where the $X \times X$ precision matrix $\boldsymbol{A_\mu}$ has elements (see e.g., [2])

$$a_{ij} = \begin{cases} 1 & \text{if } i = j \\ -a_\phi & \text{for } i, j \text{ lateral neighbours} \\ -a_\lambda & \text{for } i, j \text{ longitudinal neighbours,} \\ 0 & \text{otherwise} \end{cases} \tag{D.3}$$

$\boldsymbol{I}$ is the identity matrix and $\mathbf{1}$ is a $X \times 1$ vector of ones. $\boldsymbol{A_\mu}$ must be positive definite, and sufficient conditions are that both a_ϕ and a_λ are positive and that $a_\phi + a_\lambda \leq \frac{1}{2}$. (see e.g., [1]).

The interest is in the full conditional $P(\boldsymbol{\mu}|\cdot)$ and by applying Bayes formula and separating out the $\boldsymbol{Z_t}$'s from the remaining parameters, henceforth denoted by $(\cdot)_{-Z}$ the following is obtained

$$P(\boldsymbol{\mu}|\cdot) = P(\boldsymbol{\mu}|\boldsymbol{Z_1}, \ldots, \boldsymbol{Z_T}, (\cdot)_{-\boldsymbol{Z}}) \propto P(\bigcap_{t=1}^{T} \boldsymbol{Z_T}|\boldsymbol{\mu}, (\cdot)_{-\boldsymbol{Z}}) P(\boldsymbol{\mu}|(\cdot)_{-\boldsymbol{Z}})$$

Now, conditioned on the underlying processes, the observations are independent, and the full conditional distribution for $\boldsymbol{\mu}$ is proportional to a product of the known conditional distributions in Eq. D.2

$$\begin{aligned} P(\boldsymbol{\mu}|\cdot) &\propto P(\boldsymbol{\mu}|\boldsymbol{\mu_0}, a_\phi, a_\lambda, \sigma_\mu^2) \prod_{t=1}^{T} P(\boldsymbol{Z}_t|\boldsymbol{\mu}, \boldsymbol{\theta}_t, \boldsymbol{M_t}, \sigma_Z^2) \\ &\propto e^{-\frac{1}{2\sigma_\mu^2}((\boldsymbol{\mu}-\boldsymbol{\mu_0})' \boldsymbol{A_\mu} (\boldsymbol{\mu}-\boldsymbol{\mu_0}))} \\ &\times e^{-\frac{1}{2\sigma_Z^2}(\sum_t (\boldsymbol{Z}_t - \boldsymbol{\mu} - \boldsymbol{\theta}_t - \mathbf{1}\boldsymbol{M_t})' (\boldsymbol{Z}_t - \boldsymbol{\mu} - \boldsymbol{\theta}_t - \mathbf{1}\boldsymbol{M_t}))} \\ &\propto e^{-\frac{1}{2}\left[\boldsymbol{\mu}'\left(\frac{1}{\sigma_\mu^2}\boldsymbol{A_\mu} + \frac{T}{\sigma_Z^2}\boldsymbol{I}\right)\boldsymbol{\mu} - 2\boldsymbol{\mu}'\left(\frac{1}{\sigma_\mu^2}\boldsymbol{A_\mu}\boldsymbol{\mu}_0 + \frac{1}{\sigma_Z^2}\sum_t (\boldsymbol{Z}_t - \boldsymbol{\theta}_t - \mathbf{1}\boldsymbol{M_t})\right)\right]} \end{aligned}$$

which is identified as another multi-normal distribution with the precision matrix between $\boldsymbol{\mu}'$ and $\boldsymbol{\mu}$ and the product of the precision matrix and the expectancy-vector as the factor after $2\boldsymbol{\mu}'$. Thus,

$$\boldsymbol{\mu}|\cdot \sim MVN\left[\left(\frac{1}{\sigma_{\mu}^2}A_{\boldsymbol{\mu}}+\frac{T}{\sigma_Z^2}\boldsymbol{I}\right)^{-1}\left(\frac{1}{\sigma_{\mu}^2}A_{\boldsymbol{\mu}}\boldsymbol{\mu_0}+\frac{1}{\sigma_Z^2}\sum_t(\boldsymbol{Z}_t-\boldsymbol{\theta}_t-\mathbf{1}\boldsymbol{M_t})\right),\left(\frac{1}{\sigma_{\mu}^2}A_{\boldsymbol{\mu}}+\frac{T}{\sigma_Z^2}\boldsymbol{I}\right)^{-1}\right] \tag{D.4}$$

D.3 Conditional Distribution for $\boldsymbol{\theta}(t)$

D.3.1 $P(\boldsymbol{\theta}_t|\cdot)$ for $t = 1, \ldots, T-1$

The hierarchical model gives

$$\begin{aligned}
&\boldsymbol{\theta}_t|b_0,\boldsymbol{\theta}_{t-1},b_N,b_E,b_S,b_W,\sigma_{\theta}^2 \sim MVN\left(\boldsymbol{B\theta}_{t-1},\boldsymbol{I}\sigma_{\theta}^2\right)\\
&\boldsymbol{\theta}_{t+1}|b_0,\boldsymbol{\theta}_t,b_N,b_E,b_S,b_W,\sigma_{\theta}^2 \sim MVN\left(\boldsymbol{B\theta}_t,\boldsymbol{I}\sigma_{\theta}^2\right)\\
&\boldsymbol{Z}_t|\boldsymbol{\mu},\boldsymbol{\theta}_t,\boldsymbol{M_t},\sigma_Z^2 \sim MVN\left(\boldsymbol{\mu}+\boldsymbol{\theta}_t+\mathbf{1}\boldsymbol{M_t},\boldsymbol{I}\sigma_Z^2\right)
\end{aligned} \tag{D.5}$$

where the matrix B is a $X \times X$ matrix with elements

$$b_{ij} = \begin{cases} b_0 & \text{if } i = j\\ b_N & \text{for } j = \text{ neighbours to the North of } i\\ b_E & \text{for } j = \text{ neighbours to the East of } i\\ b_S & \text{for } j = \text{ neighbours to the South of } i\\ b_W & \text{for } j = \text{ neighbours to the West of } i\\ 0 & \text{otherwise}\end{cases} \tag{D.6}$$

Acknowledging that, conditioned on the process $\boldsymbol{\theta}_t$, the processes $\boldsymbol{Z}_t$ and $\boldsymbol{\theta}_{t+1}$ are independent, the full conditional becomes

$$\begin{aligned}
P(\boldsymbol{\theta}_t|\cdot) &\propto P(\boldsymbol{\theta}_t|b_0,\boldsymbol{\theta}_{t-1},b_N,b_E,b_S,b_W,\sigma_{\theta}^2)P(\boldsymbol{\theta}_{t+1}|b_0,\boldsymbol{\theta}_t,b_N,b_E,b_S,b_W,\sigma_{\theta}^2)\\
&\quad\times P(\boldsymbol{Z}_t|\boldsymbol{\mu},\boldsymbol{\theta}_t,\boldsymbol{M_t},\sigma_Z^2)\\
&\propto e^{-\frac{1}{2}\left[\boldsymbol{\theta}_t'\left(\frac{1}{\sigma_{\theta}^2}(\boldsymbol{I}+\boldsymbol{B}'\boldsymbol{B})+\frac{1}{\sigma_Z^2}\boldsymbol{I}\right)\boldsymbol{\theta}_t-2\boldsymbol{\theta}_t'\left(\frac{1}{\sigma_{\theta}^2}(\boldsymbol{B\theta}_{t-1}+\boldsymbol{B}'\boldsymbol{\theta}_{t+1})+\frac{1}{\sigma_Z^2}(\boldsymbol{Z}_t-\boldsymbol{\mu}-\mathbf{1}\boldsymbol{M_t})\right)\right]}
\end{aligned}$$

Hence, by the same argument as above, the full conditional distribution of $\boldsymbol{\theta}_t$, for $t = 1, \ldots, T-1$ is the following multivariate normal distribution:

$$\begin{aligned}
\boldsymbol{\theta}_t|\cdot \sim MVN\Bigg[&\left(\frac{1}{\sigma_{\theta}^2}(\boldsymbol{I}+\boldsymbol{B}'\boldsymbol{B})+\frac{1}{\sigma_Z^2}\boldsymbol{I}\right)^{-1}\left(\frac{1}{\sigma_{\theta}^2}(\boldsymbol{B\theta}_{t-1}+\boldsymbol{B}'\boldsymbol{\theta}_{t+1})+\frac{1}{\sigma_Z^2}(\boldsymbol{Z}_t-\boldsymbol{\mu}-\mathbf{1}\boldsymbol{M_t})\right),\\
&\left(\frac{1}{\sigma_{\theta}^2}(\boldsymbol{I}+\boldsymbol{B}'\boldsymbol{B})+\frac{1}{\sigma_Z^2}\boldsymbol{I}\right)^{-1}\Bigg]
\end{aligned} \tag{D.7}$$

D.3.2 $P(\boldsymbol{\theta}_T|\cdot)$

From the model specification:

$$\begin{aligned}\boldsymbol{\theta}_T|b_0,\boldsymbol{\theta}_{T-1},b_N,b_E,b_S,b_W,\sigma_\theta^2 &\sim MVN\left(\boldsymbol{B}\boldsymbol{\theta}_{T-1},\boldsymbol{I}\sigma_\theta^2\right)\\ \boldsymbol{Z}_T|\boldsymbol{\mu},\boldsymbol{\theta}_T,\boldsymbol{M_t},\sigma_Z^2 &\sim MVN\left(\boldsymbol{\mu}+\boldsymbol{\theta}_T+\mathbf{1}\boldsymbol{M_t},\boldsymbol{I}\sigma_Z^2\right)\end{aligned} \tag{D.8}$$

and parallel to the above,

$$\begin{aligned}P(\boldsymbol{\theta}_T|\cdot) &\propto P(\boldsymbol{\theta}_T|b_0,\boldsymbol{\theta}_{T-1},b_N,b_E,b_S,b_W,\sigma_\theta^2)P(\boldsymbol{Z}_T|\boldsymbol{\mu},\boldsymbol{\theta}_T,\boldsymbol{M_t},\sigma_Z^2)\\ &\propto e^{-\frac{1}{2}\left[\boldsymbol{\theta}_t'\left(\frac{1}{\sigma_\theta^2}\boldsymbol{I}+\frac{1}{\sigma_Z^2}\boldsymbol{I}\right)\boldsymbol{\theta}_t-2\boldsymbol{\theta}_t'\left(\frac{1}{\sigma_\theta^2}\boldsymbol{B}\boldsymbol{\theta}_{T-1}+\frac{1}{\sigma_Z^2}(\boldsymbol{Z}_t-\boldsymbol{\mu}-\mathbf{1}\boldsymbol{M_t})\right)\right]}\end{aligned}$$

Thus, the full conditional for $\boldsymbol{\theta}_T$ becomes

$$\boldsymbol{\theta}_T|\cdot \sim MVN\left[\left(\frac{1}{\sigma_\theta^2}\boldsymbol{I}+\frac{1}{\sigma_Z^2}\boldsymbol{I}\right)^{-1}\left(\frac{1}{\sigma_\theta^2}\boldsymbol{B}\boldsymbol{\theta}_{T-1}+\frac{1}{\sigma_Z^2}(\boldsymbol{Z}_T-\boldsymbol{\mu}-\mathbf{1}M_T)\right),\left(\frac{1}{\sigma_\theta^2}\boldsymbol{I}+\frac{1}{\sigma_Z^2}\boldsymbol{I}\right)^{-1}\right] \tag{D.9}$$

D.3.3 $P(\boldsymbol{\theta_0}|\cdot)$

The model and prior specifications give

$$\begin{aligned}\boldsymbol{\theta}_0|\xi_{\boldsymbol{\theta}_0},\sigma_{\theta_0}^2 &\sim MVN\left(1\xi_{\boldsymbol{\theta}_0},\boldsymbol{I}\sigma_{\theta_0}^2\right)\\ \boldsymbol{\theta}_1|b_0,\boldsymbol{\theta}_0,b_N,b_E,b_S,b_W,\sigma_\theta^2 &\sim MVN\left(\boldsymbol{B}\boldsymbol{\theta}_0,\boldsymbol{I}\sigma_\theta^2\right)\end{aligned} \tag{D.10}$$

and in a similar manner to the above, the following is obtained for the full conditional

$$\begin{aligned}P(\boldsymbol{\theta}_0|\cdot) &\propto P(\boldsymbol{\theta}_0|\xi_{\boldsymbol{\theta}_0},\sigma_{\theta_0}^2)P(\boldsymbol{\theta}_1|b_0,\boldsymbol{\theta}_0,b_N,b_E,b_S,b_W,\sigma_\theta^2)\\ &\propto e^{-\frac{1}{2}\left[\boldsymbol{\theta}_0'\left(\frac{1}{\sigma_\theta^2}\boldsymbol{B}'\boldsymbol{B}+\frac{1}{\sigma_{\theta_0}^2}\boldsymbol{I}\right)\boldsymbol{\theta}_0-2\boldsymbol{\theta}_0'\left(\frac{1}{\sigma_\theta^2}\boldsymbol{B}'\boldsymbol{\theta}_1+\frac{1}{\sigma_{\theta_0}^2}1\xi_{\boldsymbol{\theta}_0}\right)\right]}\end{aligned}$$

Hence, the full conditional for $\boldsymbol{\theta}_0$ becomes

$$\boldsymbol{\theta}_0|\cdot \sim MVN\left[\left(\frac{1}{\sigma_\theta^2}\boldsymbol{B}'\boldsymbol{B}+\frac{1}{\sigma_{\theta_0}^2}\boldsymbol{I}\right)^{-1}\left(\frac{1}{\sigma_\theta^2}\boldsymbol{B}'\boldsymbol{\theta}_1+\frac{1}{\sigma_{\theta_0}^2}1\xi_{\boldsymbol{\theta}_0}\right),\left(\frac{1}{\sigma_\theta^2}\boldsymbol{B}'\boldsymbol{B}+\frac{1}{\sigma_{\theta_0}^2}\boldsymbol{I}\right)^{-1}\right] \tag{D.11}$$

D.4 Conditional Distribution for $\boldsymbol{\mu_0}$

In order to derive the conditional distribution for $\boldsymbol{\mu_0}$, first define the vector $\boldsymbol{\mu_{0L}} = \left(\boldsymbol{\mu}_{0,1}, \boldsymbol{\mu}_{0,2}, \boldsymbol{\mu}_{0,3}, \boldsymbol{\mu}_{0,4}, \boldsymbol{\mu}_{0,5}, \boldsymbol{\mu}_{0,6}\right)'$. The deterministic relation $\boldsymbol{\mu_0} = P\boldsymbol{\mu_{0L}}$, with P the $X \times 6$ trend design matrix with rows $\left(1, m(x), n(x), m(x)^2, n(x)^2, m(x)n(x)\right)$ for $x = 1, \ldots, X = 153$, holds and the model and prior specifications give the conditional distributions in Eq. D.12.

$$\begin{aligned} \boldsymbol{\mu}|\boldsymbol{\mu_{0L}}, a_\phi, a_\lambda, \sigma_\mu^2 &\sim MVN\left(P\boldsymbol{\mu_{0L}}, \sigma_\mu^2 A_{\boldsymbol{\mu}}^{-1}\right) \\ \boldsymbol{\mu_{0L}}|\xi_{\boldsymbol{\mu_0}}, \sigma_{\mu_0}^2 &\sim MVN\left(\xi_{\boldsymbol{\mu_0}}, \boldsymbol{I}\sigma_{\mu_0}^2\right) \end{aligned} \tag{D.12}$$

Bayes formula again gives the full conditionals in a similar manner as above:

$$\begin{aligned} P(\boldsymbol{\mu_{0L}}|\cdot) &\propto P(\boldsymbol{\mu}|\boldsymbol{\mu_{0L}}, a_\phi, a_\lambda, \sigma_\mu^2) P(\boldsymbol{\mu_{0L}}|\xi_{\boldsymbol{\mu_0}}, \sigma_{\mu_0}^2) \\ &\propto e^{-\frac{1}{2}\left[\boldsymbol{\mu_{0L}}'\left(\frac{1}{\sigma_\mu^2} P' A_{\boldsymbol{\mu}} P + \frac{1}{\sigma_{\mu_0}^2}\boldsymbol{I}\right)\boldsymbol{\mu_{0L}} - 2\boldsymbol{\mu_{0L}}'\left(\frac{1}{\sigma_\mu^2} P' A_{\boldsymbol{\mu}}\boldsymbol{\mu} + \frac{1}{\sigma_{\mu_0}^2}\xi_{\boldsymbol{\mu_0}}\right)\right]} \end{aligned}$$

Hence, the full conditional for $\boldsymbol{\mu_0}$ becomes

$$\boldsymbol{\mu_{0L}}|\cdot \sim MVN\left[\left(\frac{1}{\sigma_\mu^2} P' A_{\boldsymbol{\mu}} P + \frac{1}{\sigma_{\mu_0}^2}\boldsymbol{I}\right)^{-1}\left(\frac{1}{\sigma_\mu^2} P' A_{\boldsymbol{\mu}}\boldsymbol{\mu} + \frac{1}{\sigma_{\mu_0}^2}\xi_{\boldsymbol{\mu_0}}\right), \left(\frac{1}{\sigma_\mu^2} P' A_{\boldsymbol{\mu}} P + \frac{1}{\sigma_{\mu_0}^2}\boldsymbol{I}\right)^{-1}\right] \tag{D.13}$$

D.5 Conditional Distribution for $\boldsymbol{b_0}$, $\boldsymbol{b_N}$, $\boldsymbol{b_E}$, $\boldsymbol{b_S}$, and $\boldsymbol{b_W}$

The specification of the model and prior distributions give directly, by defining the vector $\boldsymbol{b} = (b_0, b_N, b_E, b_S, b_W)'$,

$$\begin{aligned} \boldsymbol{\theta}_t|b_0, \boldsymbol{\theta}_{t-1}, b_N, b_E, b_S, b_W, \sigma_\theta^2 &\sim MVN\left(\boldsymbol{B}\boldsymbol{\theta}_{t-1}, \boldsymbol{I}\sigma_\theta^2\right) \\ \boldsymbol{b}|\boldsymbol{\xi_b}, \sigma_b^2 &\sim MVN\left(\boldsymbol{\xi_b}, \boldsymbol{I}\sigma_b^2\right) \end{aligned} \tag{D.14}$$

Conditioned on $\boldsymbol{b}$, $\boldsymbol{\theta}_t$ is only dependent on $\boldsymbol{\theta}_{t-1}$ and the full conditional of $\boldsymbol{b}$ becomes

$$\begin{aligned} P(\boldsymbol{b}|\cdot) &\propto P(\boldsymbol{b}|\boldsymbol{\xi_b}, \sigma_b^2) \prod_{t=1}^{T} P(\boldsymbol{\theta}_t|b_0, \boldsymbol{\theta}_{t-1}, b_N, b_E, b_S, b_W, \sigma_\theta^2) \\ &\propto e^{-\frac{1}{2\sigma_b^2}\left((\boldsymbol{b}-\boldsymbol{\xi_b})'(\boldsymbol{b}-\boldsymbol{\xi_b})\right)} e^{-\frac{1}{2\sigma_\theta^2}\left(\sum_t (\boldsymbol{\theta}_t - \boldsymbol{B}\boldsymbol{\theta}_{t-1})'(\boldsymbol{\theta}_t - \boldsymbol{B}\boldsymbol{\theta}_{t-1})\right)} \end{aligned}$$

In order to rewrite this, we need to find an $X \times 5$-matrix $\mathbf{J}_{\boldsymbol{\theta},t-1}$ so that

$$\mathbf{B}\boldsymbol{\theta}_{t-1} = \mathbf{J}_{\boldsymbol{\theta}_{t-1}}\mathbf{b}$$

Since, $\boldsymbol{B}\boldsymbol{\theta}_{t-1} = b_0\boldsymbol{\theta}_{t-1} + b_N\boldsymbol{\theta}^N_{t-1} + b_E\boldsymbol{\theta}^E_{t-1} + b_S\boldsymbol{\theta}^S_{t-1} + b_W\boldsymbol{\theta}^W_{t-i}$, it is easily seen that, if $\boldsymbol{J}_{\boldsymbol{\theta}_{t-1}}$ is the matrix with rows $\boldsymbol{\theta}_{t-1}$, $\boldsymbol{\theta}^N_{t-1}$, $\boldsymbol{\theta}^E_{t-1}$, $\boldsymbol{\theta}^S_{t-1}$, and $\boldsymbol{\theta}^W_{t-1}$ respectively, the equation above holds, and by defining the $\boldsymbol{J}_D$-matrices, for $D = N, E, S, W$, to be the X x X matrices with ones along the diagonal corresponding to the b_D coefficients in $\boldsymbol{B}$ and zeros elsewhere, then $\boldsymbol{\theta}^D_{t-1} = \boldsymbol{J}_D\boldsymbol{\theta}_{t-1}$ and this can be

$$\boldsymbol{J}_{\boldsymbol{\theta}_{t-1}} = (\boldsymbol{\theta}_{t-1}, \boldsymbol{J}_N\boldsymbol{\theta}_{t-1}, \boldsymbol{J}_E\boldsymbol{\theta}_{t-1}, \boldsymbol{J}_S\boldsymbol{\theta}_{t-1}, \boldsymbol{J}_W\boldsymbol{\theta}_{t-1})$$

where now each of the elements in the vector above is actually an X-dimensional standing vector, defining the rows in the $X \times 5$ dimensional matrix. The full conditional for $\boldsymbol{b}$ can now be written as

$$\begin{aligned} P(\boldsymbol{b}|\cdot) &\propto e^{-\frac{1}{2\sigma^2_b}((\boldsymbol{b}-\boldsymbol{\xi}_{\boldsymbol{b}})'(\boldsymbol{b}-\boldsymbol{\xi}_{\boldsymbol{b}}))} e^{-\frac{1}{2\sigma^2_{\theta}}\left(\sum_t\left(\boldsymbol{\theta}_t-\mathbf{J}_{\boldsymbol{\theta}_{t-1}}\mathbf{b}\right)'\left(\boldsymbol{\theta}_t-\mathbf{J}_{\boldsymbol{\theta}_{t-1}}\mathbf{b}\right)\right)} \\ &\propto e^{-\frac{1}{2}\left[\mathbf{b}'\left(\frac{1}{\sigma^2_b}\boldsymbol{I}+\frac{1}{\sigma^2_{\theta}}\sum_t\mathbf{J}'_{\boldsymbol{\theta}_{t-1}}\mathbf{J}_{\boldsymbol{\theta}_{t-1}}\right)\mathbf{b}-2\mathbf{b}'\left(\frac{1}{\sigma^2_b}\boldsymbol{\xi}_{\boldsymbol{b}}+\frac{1}{\sigma^2_{\theta}}\sum_t\mathbf{J}'_{\boldsymbol{\theta}_{t-1}}\boldsymbol{\theta}_t\right)\right]} \end{aligned}$$

Hence, the full joint conditional for b becomes

$$\mathbf{b}|\cdot \sim MVN\left[\left(\frac{1}{\sigma^2_b}\mathbf{I}+\frac{1}{\sigma^2_{\theta}}\sum_t\mathbf{J}'_{\boldsymbol{\theta}_{t-1}}\mathbf{J}_{\boldsymbol{\theta}_{t-1}}\right)^{-1}\left(\frac{1}{\sigma^2_b}\boldsymbol{\xi}_{\boldsymbol{b}}+\frac{1}{\sigma^2_{\theta}}\sum_t\mathbf{J}'_{\boldsymbol{\theta}_{t-1}}\boldsymbol{\theta}_t\right), \left(\frac{1}{\sigma^2_b}\mathbf{I}+\frac{1}{\sigma^2_{\theta}}\sum_t\mathbf{J}'_{\boldsymbol{\theta}_{t-1}}\mathbf{J}_{\boldsymbol{\theta}_{t-1}}\right)^{-1}\right] \tag{D.15}$$

D.6 Conditional Distribution for $a_{\boldsymbol{\phi}}$ and $a_{\boldsymbol{\lambda}}$

The following is given by the model specification

$$\begin{aligned} \boldsymbol{\mu}|\boldsymbol{\mu}_0, a_{\phi}, a_{\lambda}, \sigma^2_{\mu} &\sim MVN\left(\boldsymbol{\mu}_0, \sigma^2_{\mu}A^{-1}_{\boldsymbol{\mu}}\right) \\ (a_{\phi}, a_{\lambda})|\xi_a, \sigma^2_a &\sim BVN\left(1\xi_a, \mathbf{I}\sigma^2_a\right) \end{aligned} \tag{D.16}$$

which gives the full conditional joint distribution of a_{ϕ} and a_{λ}

$$\begin{aligned} P(a_{\phi}, a_{\lambda}|\cdot) &\propto P(a_{\phi}, a_{\lambda}|\xi_a, \sigma^2_a)P(\boldsymbol{\mu}|\boldsymbol{\mu}_0, a_{\phi}, a_{\lambda}, \sigma^2_{\mu}) \\ &\propto e^{-\frac{1}{2\sigma^2_a}\left[(a_{\phi}-\xi_a)^2+(a_{\lambda}-\xi_a)^2\right]}\frac{1}{|A_{\boldsymbol{\mu}}|^{-1/2}}e^{-\frac{1}{2\sigma^2_{\mu}}(\boldsymbol{\mu}-\boldsymbol{\mu}_0)'A_{\boldsymbol{\mu}}(\boldsymbol{\mu}-\boldsymbol{\mu}_0)} \end{aligned}$$

However, due to the appearance of the determinant $|A_{\boldsymbol{\mu}}|$, which contains a_{ϕ} and a_{λ}, this distribution is difficult to sample from and a Metropolis-Hastings step is introduced. As proposal distribution, the pseudo conditional distribution for $\boldsymbol{\mu}$ is introduced and replaced with the conditional distribution above:

$$P^{pseudo}(\boldsymbol{\mu}|\boldsymbol{\mu}_0, a_\phi, a_\lambda, \sigma_\mu^2) \propto \prod_{i=1}^{X} p(\boldsymbol{\mu}(x_i)|\boldsymbol{\mu}(x_j),\, j \neq i;\, \boldsymbol{\mu}_0, a_\phi, a_\lambda, \sigma_\mu^2)$$

where the $\boldsymbol{\mu}(x_i)$'s, conditional on all other $\boldsymbol{\mu}(x_j)$ are, as specified by the model, univariate normally distributed with expectation

$$\begin{aligned}&\boldsymbol{\mu}_0(x_i) + a_\phi \left(\boldsymbol{\mu}(x_i^N) - \boldsymbol{\mu}_0(x_i^N) + \boldsymbol{\mu}(x_i^S) - \boldsymbol{\mu}_0(x_i^S)\right)\\ &+ a_\lambda \left(\boldsymbol{\mu}(x_i^E) - \boldsymbol{\mu}_0(x_i^E) + \boldsymbol{\mu}(x_i^W) - \boldsymbol{\mu}_0(x_i^W)\right)\end{aligned}$$

and variance σ_μ^2. Now, the following proposal distribution $Q(a_\phi, a_\lambda|\cdot)$ can be used within the Metropolis Hastings step:

$$\begin{aligned}&Q(a_\phi, a_\lambda|\cdot)\\ &\propto e^{-\frac{1}{2}\left(\frac{1}{\sigma_a^2}+\frac{1}{\sigma_\mu^2}\sum_x\left(\boldsymbol{\mu}(x^N)-\boldsymbol{\mu}_0(x^N)+\boldsymbol{\mu}(x^S)-\boldsymbol{\mu}_0(x^S)\right)^2\right)a_\phi^2}\\ &\quad\times e^{a_\phi\left(\frac{1}{\sigma_a^2}\xi_a+\frac{1}{\sigma_\mu^2}\sum_x\left(\boldsymbol{\mu}(x^N)-\boldsymbol{\mu}_0(x^N)+\boldsymbol{\mu}(x^S)-\boldsymbol{\mu}_0(x^S)\right)\left(\boldsymbol{\mu}(x)-\boldsymbol{\mu}_0(x)-a_\lambda\left(\boldsymbol{\mu}(x^E)-\boldsymbol{\mu}_0(x^E)+\boldsymbol{\mu}(x^W)-\boldsymbol{\mu}_0(x^W)\right)\right)\right)}\\ &\quad\times e^{-\frac{1}{2}\left(\frac{1}{\sigma_a^2}+\frac{1}{\sigma_\mu^2}\sum_x\left(\boldsymbol{\mu}(x^E)-\boldsymbol{\mu}_0(x^E)+\boldsymbol{\mu}(x^W)-\boldsymbol{\mu}_0(x^W)\right)^2\right)a_\lambda^2}\\ &\quad\times e^{a_\lambda\left(\frac{1}{\sigma_a^2}\xi_a+\frac{1}{\sigma_\mu^2}\sum_x\left(\boldsymbol{\mu}(x^E)-\boldsymbol{\mu}_0(x^E)+\boldsymbol{\mu}(x^W)-\boldsymbol{\mu}_0(x^W)\right)\left(\boldsymbol{\mu}(x)-\boldsymbol{\mu}_0(x)-a_\phi\left(\boldsymbol{\mu}(x^N)-\boldsymbol{\mu}_0(x^N)+\boldsymbol{\mu}(x^S)-\boldsymbol{\mu}_0(x^S)\right)\right)\right)}\end{aligned}$$

A bivariate normal distribution can be written on the form,

$$f(x, y) \propto e^{-\frac{1}{2}\left[x^2q_x+y^2q_y+2xyq_{xy}-2x(\mu_xq_x+\mu_yq_{xy})-2y(\mu_yq_y+\mu_xq_{xy})\right]}$$

where symmetry requires that $q_{xy} = q_{yx}$. Now, comparing this expression with the expression for the pseudo-distribution above, it is seen that the bivariate pseudo-distribution for a_ϕ and a_λ have the following elements in its precision matrix $Q_{\phi,\lambda}$,

$$\begin{aligned}\tilde{q}_\phi &= \left(\frac{1}{\sigma_a^2} + \frac{1}{\sigma_\mu^2}\sum_x\left(\boldsymbol{\mu}(x^N) - \boldsymbol{\mu}_0(x^N) + \boldsymbol{\mu}(x^S) - \boldsymbol{\mu}_0(x^S)\right)^2\right)\\ \tilde{q}_\lambda &= \left(\frac{1}{\sigma_a^2} + \frac{1}{\sigma_\mu^2}\sum_x\left(\boldsymbol{\mu}(x^E) - \boldsymbol{\mu}_0(x^E) + \boldsymbol{\mu}(x^W) - \boldsymbol{\mu}_0(x^W)\right)^2\right)\\ \tilde{q}_{\phi\lambda} &= \frac{1}{\sigma_\mu^2}\sum_x\left(\boldsymbol{\mu}(x^N) - \boldsymbol{\mu}_0(x^N) + \boldsymbol{\mu}(x^S) - \boldsymbol{\mu}_0(x^S)\right)\left(\boldsymbol{\mu}(x^E) - \boldsymbol{\mu}_0(x^E) + \boldsymbol{\mu}(x^W) - \boldsymbol{\mu}_0(x^W)\right)\end{aligned}$$

and expectations,

$$\begin{aligned}\tilde{\boldsymbol{\mu}}_\phi = \;&\frac{\tilde{q}_\lambda}{\tilde{q}_\phi\tilde{q}_\lambda-\tilde{q}_{\phi\lambda}^2}\left(\frac{1}{\sigma_a^2}\xi_a + \frac{1}{\sigma_\mu^2}\sum_x\left(\boldsymbol{\mu}(x^N) - \boldsymbol{\mu}_0(x^N) + \boldsymbol{\mu}(x^S) - \boldsymbol{\mu}_0(x^S)\right)\left(\boldsymbol{\mu}(x) - \boldsymbol{\mu}_0(x)\right)\right)\\ &-\frac{\tilde{q}_{\phi\lambda}}{\tilde{q}_\phi\tilde{q}_\lambda-\tilde{q}_{\phi\lambda}^2}\left(\frac{1}{\sigma_a^2}\xi_a + \frac{1}{\sigma_\mu^2}\sum_x\left(\boldsymbol{\mu}(x^E) - \boldsymbol{\mu}_0(x^E) + \boldsymbol{\mu}(x^W) - \boldsymbol{\mu}_0(x^W)\right)\left(\boldsymbol{\mu}(x) - \boldsymbol{\mu}_0(x)\right)\right)\end{aligned}$$

$$\tilde{\boldsymbol{\mu}}_\lambda = \frac{\tilde{q}_\phi}{\tilde{q}_\phi\tilde{q}_\lambda - \tilde{q}_{\phi\lambda}^2}\left(\frac{1}{\sigma_a^2}\xi_a + \frac{1}{\sigma_\mu^2}\sum_x \left(\boldsymbol{\mu}(x^E) - \boldsymbol{\mu}_0(x^E) + \boldsymbol{\mu}(x^W) - \boldsymbol{\mu}_0(x^W)\right)\left(\boldsymbol{\mu}(x) - \boldsymbol{\mu}_0(x)\right)\right)$$
$$-\frac{\tilde{q}_{\phi\lambda}}{\tilde{q}_\phi\tilde{q}_\lambda - \tilde{q}_{\phi\lambda}^2}\left(\frac{1}{\sigma_a^2}\xi_a + \frac{1}{\sigma_\mu^2}\sum_x \left(\boldsymbol{\mu}(x^N) - \boldsymbol{\mu}_0(x^N) + \boldsymbol{\mu}(x^S) - \boldsymbol{\mu}_0(x^S)\right)\left(\boldsymbol{\mu}(x) - \boldsymbol{\mu}_0(x)\right)\right).$$

This bivariate normal distribution can now be used as proposal in the Metropolis-Hastings step. When sampling a_ϕ and a_λ, the positive definiteness constraints of A_μ should be kept in mind. Hence, if samples fulfill the conditions (both are positive and the sum not greater than 0.5) they are used in a Metropolis-Hastings step. Otherwise, they will be rejected and new proposals are drawn until a valid pair is obtained. If the proposal has expectations outside the required area, it will be adjusted so that the expectations fulfill the criteria before sampling.

D.7 Conditional Distribution for $\boldsymbol{M_t}$

From the model specification, the following is given for each $t = 1, \ldots, T$

$$\begin{aligned} \boldsymbol{Z}_t|\boldsymbol{\mu}, \boldsymbol{\theta}_t, \boldsymbol{M}_t, \sigma_Z^2 &\sim MVN\left(\boldsymbol{\mu} + \boldsymbol{\theta}_t + \mathbf{1}\boldsymbol{M}_t, \boldsymbol{I}\sigma_Z^2\right) \\ \boldsymbol{M}_t|c, d, \gamma, \eta, \sigma_m^2 &\sim N\left(c\cos(\omega t) + d\sin(\omega t) + \gamma t + \eta t^2, \sigma_m^2\right) \end{aligned} \tag{D.17}$$

and the full conditional becomes, for each t

$$\begin{aligned} P(\boldsymbol{M}_t|\cdot) &\propto P(\boldsymbol{M}_t|c, d, \gamma, \eta, \sigma_m^2)P(\boldsymbol{Z}_t|\boldsymbol{\mu}, \boldsymbol{\theta}_t, \boldsymbol{M}_t, \sigma_Z^2) \\ &\propto e^{-\frac{1}{2}\left[\left(\frac{1}{\sigma_m^2} + \frac{X}{\sigma_Z^2}\right)\boldsymbol{M}_t{}^2 - 2\boldsymbol{M}_t\left(\frac{1}{\sigma_m^2}\left(c\cos(\omega t) + d\sin(\omega t) + \gamma t + \eta t^2\right) + \frac{1}{\sigma_Z^2}1'(\boldsymbol{Z}_t - \boldsymbol{\mu} - \boldsymbol{\theta}_t)\right)\right]} \end{aligned}$$

Hence, the full conditional for $\boldsymbol{M}_t$ for all t is the following univariate normal distribution

$$\begin{aligned} \boldsymbol{M}_t \sim N\Bigg[&\left(\frac{1}{\sigma_m^2} + \frac{X}{\sigma_Z^2}\right)^{-1}\left(\frac{1}{\sigma_m^2}\left(c\cos(\omega t) + d\sin(\omega t) + \gamma t\ + \eta t^2\right)\right. \\ &\left. + \frac{1}{\sigma_Z^2}1'(\boldsymbol{Z}_t - \boldsymbol{\mu} - \boldsymbol{\theta}_t)\right), \left(\frac{1}{\sigma_m^2} + \frac{X}{\sigma_Z^2}\right)^{-1}\Bigg] \end{aligned} \tag{D.18}$$

D.8 Conditional Distribution for c, d, γ, and η

It is assumed that all prior distributions are independent, so the joint prior distribution for c, d, γ, and η can be expressed in terms of a simple 4-dimensional expectation vector and a 4×4 diagonal covariance matrix. By defining the four matrices,

$\boldsymbol{\xi_m} = \begin{bmatrix} \xi_c \\ \xi_d \\ \xi_\gamma \\ \xi_\eta \end{bmatrix}$, $\boldsymbol{\Sigma_m} = \begin{bmatrix} \sigma_c^2 & 0 & 0 & 0 \\ 0 & \sigma_d^2 & 0 & 0 \\ 0 & 0 & \sigma_\gamma^2 & 0 \\ 0 & 0 & 0 & \sigma_\eta^2 \end{bmatrix}$, $\boldsymbol{\beta_m} = \begin{bmatrix} c \\ d \\ \gamma \\ \eta \end{bmatrix}$ and $\boldsymbol{\tau}_t = \begin{bmatrix} \cos(\omega t) \\ \sin(\omega t) \\ t \\ t^2 \end{bmatrix}$, the model specification gives, for $t = 1, \ldots, T$

$$\begin{aligned} \boldsymbol{M}_t | c, d, \gamma, \eta, \sigma_m^2 &\sim N\left(c\cos(\omega t) + d\sin(\omega t) + \gamma t + \eta t^2, \sigma_m^2\right) = N(\boldsymbol{\tau}_t' \boldsymbol{\beta_m}, \sigma_m^2) \\ \boldsymbol{\beta_m} | \xi_c, \xi_d, \xi_\gamma, \xi_\eta, \sigma_c^2, \sigma_d^2, \sigma_\gamma^2, \sigma_\eta^2 &\sim MVN(\boldsymbol{\xi_m}, \boldsymbol{\Sigma_m}) \end{aligned} \tag{D.19}$$

From this, the full conditional for (c, d, γ, η) can easily be derived as follows

$$\begin{aligned} P(c, d, \gamma, \eta | \cdot) &\propto P(c, d, \gamma, \eta | \xi_c, \xi_d, \xi_\gamma, \xi_\eta, \sigma_c^2, \sigma_d^2, \sigma_\gamma^2, \sigma_\eta^2) \prod_{t=1}^{T} P(\boldsymbol{M}_t | c, d, \gamma, \eta, \sigma_m^2) \\ &\propto e^{-\frac{1}{2}\left[\boldsymbol{\beta_m}'\left(\boldsymbol{\Sigma_m}^{-1} + \frac{1}{\sigma_m^2}\sum_t \boldsymbol{\tau}_t \boldsymbol{\tau}_t'\right)\boldsymbol{\beta_m} - 2\boldsymbol{\beta_m}'\left(\boldsymbol{\Sigma_m}^{-1}\boldsymbol{\xi_m} + \frac{1}{\sigma_m^2}\sum_t \boldsymbol{\tau}_t \boldsymbol{M}_t\right)\right]}. \end{aligned}$$

Now, since $\boldsymbol{\Sigma_m}$ is diagonal, its inverse is simply $\boldsymbol{\Sigma_m}^{-1} = \begin{bmatrix} \frac{1}{\sigma_c^2} & 0 & 0 & 0 \\ 0 & \frac{1}{\sigma_d^2} & 0 & 0 \\ 0 & 0 & \frac{1}{\sigma_\gamma^2} & 0 \\ 0 & 0 & 0 & \frac{1}{\sigma_\eta^2} \end{bmatrix}$ and the matrix $\boldsymbol{\tau}_t \boldsymbol{\tau}_t' = \begin{bmatrix} (\cos(\omega t))^2 & \sin(\omega t)\cos(\omega t) & t\cos(\omega t) & t^2\cos(\omega t) \\ \sin(\omega t)\cos(\omega t) & (\sin(\omega t))^2 & t\sin(\omega t) & t^2\sin(\omega t) \\ t\cos(\omega t) & t\sin(\omega t) & t^2 & t^3 \\ t^2\cos(\omega t) & t^2\sin(\omega t) & t^3 & t^4 \end{bmatrix}$ so that the full conditional can be written as, with the precision matrix

$$\boldsymbol{Q_m} = \begin{bmatrix} \frac{1}{\sigma_c^2} + \frac{1}{\sigma_m^2}\sum_t (\cos(\omega t))^2 & \frac{1}{\sigma_m^2}\sum_t \sin(\omega t)\cos(\omega t) & \frac{1}{\sigma_m^2}\sum_t t\cos(\omega t) & \frac{1}{\sigma_m^2}\sum_t t^2\cos(\omega t) \\ \frac{1}{\sigma_m^2}\sum_t \sin(\omega t)\cos(\omega t) & \frac{1}{\sigma_d^2} + \frac{1}{\sigma_m^2}\sum_t (\sin(\omega t))^2 & \frac{1}{\sigma_m^2}\sum_t t\sin(\omega t) & \frac{1}{\sigma_m^2}\sum_t t^2\sin(\omega t) \\ \frac{1}{\sigma_m^2}\sum_t t\cos(\omega t) & \frac{1}{\sigma_m^2}\sum_t t\sin(\omega t) & \frac{1}{\sigma_\gamma^2} + \frac{1}{\sigma_m^2}\sum_t t^2 & \frac{1}{\sigma_m^2}\sum_t t^3 \\ \frac{1}{\sigma_m^2}\sum_t t^2\cos(\omega t) & \frac{1}{\sigma_m^2}\sum_t t^2\sin(\omega t) & \frac{1}{\sigma_m^2}\sum_t t^3 & \frac{1}{\sigma_\eta^2} + \frac{1}{\sigma_m^2}\sum_t t^4 \end{bmatrix}:$$

$$\boldsymbol{\beta_m}|\cdot \sim MVN\left[\boldsymbol{Q_m}^{-1}\begin{bmatrix} \frac{\xi_c}{\sigma_c^2} + \frac{1}{\sigma_m^2}\sum_t \boldsymbol{M}_t\cos(\omega t) \\ \frac{\xi_d}{\sigma_d^2} + \frac{1}{\sigma_m^2}\sum_t \boldsymbol{M}_t\sin(\omega t) \\ \frac{\xi_\gamma}{\sigma_\gamma^2} + \frac{1}{\sigma_m^2}\sum_t \boldsymbol{M}_t t \\ \frac{\xi_\eta}{\sigma_\eta^2} + \frac{1}{\sigma_m^2}\sum_t \boldsymbol{M}_t t^2 \end{bmatrix}, \boldsymbol{Q_m}^{-1}\right] \tag{D.20}$$

D.9 Conditional Distribution for σ_Z^2

From the model and prior specification, the following is given

$$\begin{aligned} \boldsymbol{Z}_t|\boldsymbol{\mu}, \boldsymbol{\theta}_t, \boldsymbol{M}_t, \sigma_Z^2 &\sim MVN\left(\boldsymbol{\mu} + \boldsymbol{\theta}_t + \mathbf{1}\boldsymbol{M}_t, \boldsymbol{I}\sigma_Z^2\right) \\ \sigma_Z^2|\alpha_{\boldsymbol{Z}}, \beta_{\boldsymbol{Z}} &\sim \boldsymbol{IG}(\alpha_{\boldsymbol{Z}}, \beta_{\boldsymbol{Z}}) \end{aligned} \tag{D.21}$$

and parallel to the above, the full conditional distribution becomes

$$\begin{aligned} P(\sigma_Z^2|\cdot) &\propto P(\sigma_Z^2|\alpha_{\boldsymbol{Z}}, \beta_{\boldsymbol{Z}}) \prod_{t=1}^{T} P(\boldsymbol{Z}_t|\boldsymbol{\mu}, \boldsymbol{\theta}_t, \boldsymbol{M}_t, \sigma_Z^2) \\ &\propto \left(\frac{1}{\sigma_Z^2}\right)^{\frac{XT}{2}+\alpha_{\boldsymbol{Z}}+1} e^{-\frac{1}{\sigma_Z^2}\left(\beta_{\boldsymbol{Z}}+\frac{1}{2}\sum_t(\boldsymbol{Z}_t-\boldsymbol{\mu}-\boldsymbol{\theta}_t-\mathbf{1}\boldsymbol{M}_t)'(\boldsymbol{Z}_t-\boldsymbol{\mu}-\boldsymbol{\theta}_t-\mathbf{1}\boldsymbol{M}_t)\right)} \end{aligned}$$

In other words, the full conditional distribution for σ_Z^2 becomes another inverse gamma distribution with updated parameters, i.e.,

$$\sigma_Z^2|\cdot \sim \boldsymbol{IG}\left(\alpha_{\boldsymbol{Z}} + \frac{XT}{2}, \beta_{\boldsymbol{Z}} + \frac{1}{2}\sum_t (\boldsymbol{Z}_t - \boldsymbol{\mu} - \boldsymbol{\theta}_t - \mathbf{1}\boldsymbol{M}_t)'(\boldsymbol{Z}_t - \boldsymbol{\mu} - \boldsymbol{\theta}_t - \mathbf{1}\boldsymbol{M}_t)\right) \tag{D.22}$$

D.10 Conditional Distribution for $\sigma_{\boldsymbol{\mu}}^2$

Similarly, the model and prior specification gives

$$\begin{aligned} \boldsymbol{\mu}|\boldsymbol{\mu_0}, a_\phi, a_\lambda, \sigma_\mu^2 &\sim MVN\left(\boldsymbol{\mu_0}, \sigma_\mu^2 A_{\boldsymbol{\mu}}^{-1}\right) \\ \sigma_\mu^2|\alpha_{\boldsymbol{\mu}}, \beta_{\boldsymbol{\mu}} &\sim \boldsymbol{IG}\left(\alpha_{\boldsymbol{\mu}}, \beta_{\boldsymbol{\mu}}\right) \end{aligned} \tag{D.23}$$

which gives the following full conditional distribution for σ_μ^2

$$\begin{aligned} P(\sigma_\mu^2|\cdot) &\propto P(\sigma_\mu^2|\alpha_{\boldsymbol{\mu}}, \beta_{\boldsymbol{\mu}}) P(\boldsymbol{\mu}|\boldsymbol{\mu_0}, a_\phi, a_\lambda, \sigma_\mu^2) \\ &\propto \left(\frac{1}{\sigma_\mu^2}\right)^{\alpha_{\boldsymbol{\mu}}+\frac{X}{2}+1} e^{-\frac{1}{\sigma_\mu^2}\left(\beta_{\boldsymbol{\mu}}+\frac{1}{2}(\boldsymbol{\mu}-\boldsymbol{\mu_0})'A_{\boldsymbol{\mu}}(\boldsymbol{\mu}-\boldsymbol{\mu_0})\right)} \end{aligned}$$

Hence, the full conditional distribution of σ_μ^2 is inverse gamma as follows

$$\sigma_\mu^2|\cdot \sim \boldsymbol{IG}\left(\alpha_{\boldsymbol{\mu}} + \frac{X}{2}, \beta_{\boldsymbol{\mu}} + \frac{1}{2}(\boldsymbol{\mu} - \boldsymbol{\mu_0})'A_{\boldsymbol{\mu}}(\boldsymbol{\mu} - \boldsymbol{\mu_0})\right) \tag{D.24}$$

D.11 Conditional Distribution for σ_{θ}^2

From the model and prior specification, the following is given for $t = 1, \ldots, T$

$$\begin{aligned} \boldsymbol{\theta}_t | b_0, \boldsymbol{\theta}_{t-1}, b_N, b_E, b_S, b_W, \sigma_{\theta}^2 &\sim MVN\left(\boldsymbol{B}\boldsymbol{\theta}_{t-1}, \boldsymbol{I}\sigma_{\theta}^2\right) \\ \sigma_{\theta}^2 | \alpha_{\boldsymbol{\theta}}, \beta_{\boldsymbol{\theta}} &\sim \boldsymbol{IG}(\alpha_{\boldsymbol{\theta}}, \beta_{\boldsymbol{\theta}}) \end{aligned} \tag{D.25}$$

Now,

$$\begin{aligned} P(\sigma_{\theta}^2|\cdot) = P(\sigma_{\theta}^2|\boldsymbol{\theta}_T, \ldots, \boldsymbol{\theta}_1, (\cdot)_{-\boldsymbol{\theta}}) &\propto P(\boldsymbol{\theta}_T, \ldots, \boldsymbol{\theta}_1|\sigma_{\theta}^2, (\cdot)_{-\boldsymbol{\theta}}) P(\sigma_{\theta}^2|(\cdot)_{-\boldsymbol{\theta}}) \\ &\propto P(\sigma_{\theta}^2|(\cdot)_{-\boldsymbol{\theta}}) \prod_{t=1}^{T} P(\boldsymbol{\theta}_t|\boldsymbol{\theta}_{t-1}, \sigma_{\theta}^2, (\cdot)_{-\boldsymbol{\theta}}) \end{aligned}$$

since, conditionally on $\boldsymbol{\theta}_{t-1}$, $\boldsymbol{\theta}_t$ is independent of all previous $\boldsymbol{\theta}_s$. Consequently

$$P(\sigma_{\theta}^2|\cdot) \propto \left(\frac{1}{\sigma_{\theta}^2}\right)^{\alpha_{\boldsymbol{\theta}} + \frac{XT}{2} + 1} e^{-\frac{1}{\sigma_{\theta}^2}\left(\beta_{\boldsymbol{\theta}} + \frac{1}{2}\sum_t (\boldsymbol{\theta}_t - \boldsymbol{B}\boldsymbol{\theta}_{t-1})'(\boldsymbol{\theta}_t - \boldsymbol{B}\boldsymbol{\theta}_{t-1})\right)}$$

and,

$$\sigma_{\theta}^2|\cdot \sim \boldsymbol{IG}\left(\alpha_{\boldsymbol{\theta}} + \frac{XT}{2}, \beta_{\boldsymbol{\theta}} + \frac{1}{2}\sum_t (\boldsymbol{\theta}_t - \boldsymbol{B}\boldsymbol{\theta}_{t-1})'(\boldsymbol{\theta}_t - \boldsymbol{B}\boldsymbol{\theta}_{t-1})\right) \tag{D.26}$$

D.12 Conditional Distribution for $\sigma_{\boldsymbol{m}}^2$

The following is specified by the model, for all $t = 1, \ldots, T$,

$$\begin{aligned} \boldsymbol{M}_t | c, d, \gamma, \eta, \sigma_m^2 &\sim N\left(c\cos(\omega t) + d\sin(\omega t) + \gamma t + \eta t^2, \sigma_m^2\right) \\ \sigma_m^2 | \alpha_m, \beta_m &\sim \boldsymbol{IG}(\alpha_m, \beta_m) \end{aligned} \tag{D.27}$$

The full conditional then becomes

$$\begin{aligned} P(\sigma_m^2|\cdot) &\propto P(\sigma_m^2|\alpha_m, \beta_m) \prod_{t=1}^{T} P(\boldsymbol{M}_t|c, d, \gamma, \eta, \sigma_m^2) \\ &\propto \left(\frac{1}{\sigma_m^2}\right)^{\alpha_m + \frac{T}{2} + 1} e^{-\frac{1}{\sigma_m^2}\left(\beta_m + \frac{1}{2}\sum_t (\boldsymbol{M}_t - c\cos(\omega t) - d\sin(\omega t) - \gamma t - \eta t^2)^2\right)} \end{aligned}$$

Thus,

$$\sigma_m^2|\cdot \sim \boldsymbol{IG}\left(\alpha_m + \frac{T}{2}, \beta_m + \frac{1}{2}\sum_t \left(\boldsymbol{M}_t - c\cos(\omega t) - d\sin(\omega t) - \gamma t - \eta t^2\right)^2\right) \quad \text{(D.28)}$$

References

1. Besag, J., Kooperberg, C.: On conditional and intrinsic autoregression. Biometrika **82**, 733–746 (1995)

2. Smith, R.L.: Environmental statistics. University of North Carolina (2001). http://www.stat.unc.edu/postscript/rs/envnotes.pdf. Accessed 21 Oct 2010

Appendix E
Sampling from a Multi-normal Distribution

Many of the full conditional distributions used in this study are multi-normal, and there is a need to draw samples from such distributions. In the following, a brief outline of how to obtain samples from a multi-normal distribution based on a number of independent samples from a standard normal distribution is presented.

Assume the interest is in sampling from a n-dimensional multi-normal distribution with mean vector $\boldsymbol{\mu}$ and covariance matrix $\boldsymbol{\Sigma} = \boldsymbol{Q}^{-1}$. $\boldsymbol{Q}$ is then the $n \times n$ precision matrix.

$$\boldsymbol{X} \sim MVN(\mu, \boldsymbol{Q}^{-1})$$

Cholesky-decomposition of the precision matrix yields

$$\boldsymbol{Q} = \boldsymbol{L}\boldsymbol{L}'$$

where $\boldsymbol{L}$ is a lower triangular matrix with strictly positive diagonal elements and $\boldsymbol{L}'$ denotes the transpose of $\boldsymbol{L}$.

By expressing the mean vector by some vector a multiplied with the covariance matrix in the following way

$$\boldsymbol{Q}^{-1}\boldsymbol{a} = \boldsymbol{\mu} \Leftrightarrow \boldsymbol{a} = \boldsymbol{Q}\boldsymbol{\mu} = \boldsymbol{L}\boldsymbol{L}'\boldsymbol{\mu}$$

and then setting

$$\boldsymbol{L}'\boldsymbol{\mu} = \boldsymbol{b} \Leftrightarrow \boldsymbol{\mu} = \left(\boldsymbol{L}'\right)^{-1}\boldsymbol{b}$$

with

$$\boldsymbol{L}\boldsymbol{b} = \boldsymbol{L}\boldsymbol{L}'\boldsymbol{\mu} = \boldsymbol{a} \Leftrightarrow \boldsymbol{b} = \boldsymbol{L}^{-1}\boldsymbol{a}$$

and letting

$$\boldsymbol{Y} \sim MVN(0, \boldsymbol{I}),$$

it can easily be verified that

E. Vanem, *Bayesian Hierarchical Space-Time Models with Application to Significant Wave Height*, Ocean Engineering & Oceanography 2,
DOI: 10.1007/978-3-642-30253-4, © Springer-Verlag Berlin Heidelberg 2013

$$\boldsymbol{X} = \left(\boldsymbol{L}'\right)^{-1}(\boldsymbol{b} + \boldsymbol{Y})$$

are indeed samples from the distribution $\boldsymbol{X} \sim MVN(\boldsymbol{\mu}, \boldsymbol{Q}^{-1})$. Hence, sampling from $\boldsymbol{X}$ is achieved by determining $\boldsymbol{L}$ and and $\boldsymbol{b}$ as outlined above.

To verify that the samples stem from the correct distribution, observe that, keeping in mind that the multi-normal distribution is completely specified by its mean vector and covariance matrix,

$$\begin{aligned} E\boldsymbol{X} &= \left(\boldsymbol{L}'\right)^{-1}\boldsymbol{b} = \boldsymbol{\mu} \\ \mathrm{Cov}\boldsymbol{X} &= \left(\boldsymbol{L}'\right)^{-1}\boldsymbol{L}^{-1} = \left(\boldsymbol{L}\boldsymbol{L}'\right)^{-1} = \boldsymbol{Q}^{-1} \end{aligned}$$

As a special case for $n = 1$, a sample from an arbitrary normal distribution, say $x \sim N(\mu, \sigma^2)$ can be obtained from a sample from the standard normal distribution $y \sim N(0, 1)$ by

$$x = \mu + \sigma y$$

This technique will be used extensively when sampling the various full conditionals derived in appendix D.

E.1 Sampling from a Bivariate Normal Distribution

In order to sample from a bivariate normal distribution with means μ_1 and μ_2, standard deviations σ_1 and σ_2, and correlation ρ, the following technique has been employed.

1. Generate two uncorrelated standard normal variables z_1 and z_2.
2. Generate a correlated pair y_1 and y_2 from the desired bi-normal distribution by setting

$$\begin{aligned} y_1 &= \mu_1 + \sigma_1 z_1 \\ y_2 &= \mu_2 + \sigma_2\left[z_1\rho + z_2\sqrt{1-\rho^2}\right] \end{aligned}$$